SENSITIVITY ANALYSIS WITH RESPECT TO ELASTIC BOUNDARY CONDITIONS AND LASER SPATIAL VARIABLES WITHIN EXPERIMENTAL SPATIAL DYNAMIC MODELING

by

Gerhardus Venter

Thesis submitted to the Faculty of
Virginia Polytechnic Institute and State University
in partial fulfillment of the requirements for the degree of

MASTER OF SCIENCE

in

Mechanical Engineering

APPROVED:

R. L. West, Chairman

C.E. Knight

L.D. Mitchell

May, 1995

Blacksburg, Virginia

SENSITIVITY ANALYSIS WITH RESPECT TO ELASTIC BOUNDARY CONDITIONS AND LASER SPATIAL VARIABLES WITHIN EXPERIMENTAL SPATIAL DYNAMIC MODELING

by

Gerhardus Venter

Committee Chairman: R.L. West
Mechanical Engineering

(ABSTRACT)

Experimental spatial dynamics modeling is a new method used to obtain a dynamic model of a harmonically excited vibrating structure. The continuous three-dimensional, complexed-valued velocity field of the structure is solved from a weighted least-squares finite element formulation, making use of high spatial density data obtained from a scanning laser Doppler vibrometer.

Analytical expressions for the first- and second-order error sensitivity of the obtained model with respect to model parameters of the finite element model are developed. A frequency response analysis, resulting in a pseudo-dynamic stiffness matrix and the direct method of differentiation are used to obtain the required sensitivities. These sensitivities may be used to update the parameters to obtain a more accurate model, and also to yield a signal-to-noise level for which the data must be obtained.

Analytical expressions are also developed for the first-order error sensitivity of the obtained model with respect to the spatial variables (position and orientation) of the laser. A parametric representation of both the laser beam as well as the surface of the structure is used. A variation in the spatial variables of the laser leads to a shift in the measured velocity, compared to the analytical model. The influence of changes in the spatial variables on the accuracy of the model is thus crucial. Once again, the results obtained may also be used to yield a signal-to-noise level for which the data must be obtained.

The formulations developed are examined by making use of a theoretical model of a beam structure with out-of-plane harmonic excitation.

Where can I go from your Spirit?
Where can I flee from your
presence?
If I go up to the heavens, you are
there;
if I make my bed in the depths,
you are there.
If I rise on the wings of the dawn,
if I settle on the far side of the sea,
even there your hand will guide me,
your right hand will hold me fast.

PSALM 139: 7 - 10

Dedication

Dedicated to Sanet.

Acknowledgments

I acknowledge my advisor, Bob West, for all his time and effort to help make this thesis possible. Without his understanding and knowledge it would have been impossible to complete this work. I am also thankful for the willingness of my other committee members , Dr. L.D. Mitchell and Dr. C.E. Knight, to serve on my committee.

My parents deserve my deepest appreciation and gratitude for all their love and support.

Lastly, I have to thank my wife Sanet, her love and patience have given new meaning to my life. All the sacrifices she had to make in order for me to complete this work, have not gone by unnoticed.

TABLE OF CONTENTS

LIST OF FIGURES

LIST OF TABLES

NOMENCLATURE

Mathematical symbols

$[\ ]$	Matrix
$\{\ \}$	Vector
$[\ ]^{-1}$	Inverse of a matrix
$[\ ]^{T}$	Transpose of a matrix
$\rightarrow$	Vector (function format)
—	Nodal point values
$\cdot$, $\cdot\cdot$	Time differentiation (First and second order)
', '', '''	Spatial differentiation (First, Second and third order)

Latin symbols

A, A_e	Cross sectional area of an element
a, v, u	Nodal acceleration, velocity and displacement vectors
$A(x,t)$, $A(x,\omega,t)$	Dynamic acceleration response
$\mathbf{A}_x$, $\mathbf{A}_y$, $\mathbf{A}_z$	Temporary matrices defined for rotations about the x, y and z axes of the laser respectively
B	Strain-displacement vector, Curvature-displacement matrix
C_1, C_2, C_3, C_4	Constants of integration (Spatial part)
D	Amplitude of dynamic displacement response (Temporal part), Constant in equation describing a plane in three-dimensional space
D	Pseudo-dynamic stiffness matrix
D_1, D_2	Constants of integration (Temporal part)
$\mathbf{D}_c$	Moment-curvature matrix
E	Stress-strain matrix

E	Young's modulus of material
$El.dof$	Degrees of freedom of the system
$(error)_i$	Error function of *i-th* scanning position
$\hat{e}_x$, $\hat{e}_y$, $\hat{e}_z$	Unit vector in the *x*, *y* and *z* direction respectively
$\mathbf{F}$	Nodal force vector
$F(x,t)$, $F(x,\omega,t)$	Harmonic forcing function
$f(x,t)$	Amplitude of harmonic forcing function
h	Step size for numerical differentiation
I	Moment of inertia about bending axis of structure
l, m, n	Direction cosines
$\hat{i}$, $\hat{j}$, $\hat{k}$	Unit vectors in the x, y and z directions
$\mathbf{J}$	Jacobian matrix
$\lvert\mathbf{J}\rvert$	Determinant of the Jacobian matrix
$\mathbf{k}$	Submatrix of global stiffness matrix
K_A, K_T, K_R	Elastic boundary stiffness for axial, transverse and rotational degrees of freedom
L, L_e	Length of an element
$\overline{Laser_x}$, $\overline{Laser_y}$, $\overline{Laser_z}$	Orientation vectors of the laser
$\mathbf{M}$, $\mathbf{C}$, $\mathbf{K}$	Mass, Damping and stiffness matrices
$\overline{m}_{Residual}$	Sample mean of residuals
$m(x)$	Mass per unit length
$\mathbf{N}$	Vector of finite element basis functions
$\vec{N}$	Normal of a surface
$\mathbf{R}$, $\mathbf{R}_o$, $\mathbf{R}_d$	End point, origin and direction of the laser beam
$(Residual)_i$	Residual of dynamic displacement response
$s^2_{Residual}$	Sample variance of residuals
t	Time, thickness, parameter of parametric equations
$\mathbf{T}_S$	Transformation matrix between rectangular and spherical laser coordinate systems
$\mathbf{T}_R$	Transformation matrix between laser and structural rectangular coordinate systems
$T(\omega,t)$	Temporal part of the differential equation of motion

u, v, w	Displacement degrees of freedom in the x, y and z directions respectively
$u(\omega,x)$	Amplitude of dynamic displacement response
$U(x,t)$, $U(x,\omega,t)$	Dynamic displacement response
$\tilde{V}_{Li}$	Projection of the structure's velocity on the laser beam
$v(\omega,x)$	Amplitude of the dynamic displacement response
$V(x,t)$, $V(x,\omega,t)$	Dynamic velocity response
X, Y, Z	X, y and z axes of a rectangular coordinate system
x, y, z	Coordinates in rectangular coordinate system
X	Displacement in the x-direction (two degree of freedom system)
$X(\omega,x)$	Spatial part of the differential equation of motion
z	Explicit part of the derivative of a constraint function with respect to a design variable

Greek symbols

α	Plate element length in x-direction
$\overline{\alpha}$	Mass proportional damping constant
β	Constant used in differential equation of motion, Angle between the measured and modeled velocity fields, Plate element length in y-direction
$\overline{\beta}$	Stiffness proportional damping constant
$Cos\theta_x$, $Cos\theta_y$, $Cos\theta_z$	Direction cosines of the laser beam
χ, γ	Generic sensitivity variables
$\delta_x, \delta_y, \delta_z$	Rotations about the x, y and z axes of the laser
ε	Axial strain
ϕ	Phase angle
$\mathbf{\Gamma}$	Inverse of the Jacobian matrix
γ	Shear strain, Aspect ratio of element
η_x, η_y, η_z	Direction cosines of the laser beam
$\boldsymbol{\lambda}$	Adjoined vector
ν	Poisson's ratio

θ	Rotational degree of freedom
θ_{Lx}, θ_{Ly}	Deflection angles of the laser beam
ρ	Mass density of the material
σ	Axial stress
τ	Shear stress
ω	Forcing frequency
ω_n	Natural frequency
ξ, η, ζ	Local coordinates of the element
ζ	Viscous damping factor

Subscripts

0	Specific point at which function is approximated
I, II	Submatrix components of global stiffness matrix
i, j	Generic indices - generally used to give components of a vector
L	Laser coordinate system
o	Origin of the laser
S	Structural coordinate system
x, y, z	Components in the *x, y and z* directions

Chapter 1
Introduction

1.1 General overview of the thesis and problem domain

In a very competitive world where lighter, stronger and cheaper designs are sought after, it is no longer acceptable to find poor, approximate results to complicated structural vibration problems.

Many physical phenomena may be described by the laws of physics, often in terms of differential equations. Vibrations of continuous structures are no exception and the resulting governing equations are of the partial differential type. In general, it is not possible to find a closed-form solution of a differential equation defined over a region with arbitrary shape, material and loading conditions. However, high-speed digital computers have made it possible to find accurate numerical approximations to these governing equations.

When making use of computer-based dynamic models to solve for the dynamic response of a structure, experimental testing must be incorporated into the design process in order to achieve and validate the best designs. Experimental testing is a key part of the design process, not only because it may be used to validate and update the computer model, but also because it will likely result in a better understanding of the actual vibration problem.

For the same system it is possible to construct a number of mathematical models describing the vibrational response. One of the most widely used methods, is the method of modal analysis where the structure is reduced to a number of equivalent spring, mass and damper systems. The modal analysis method characterizes the structure in terms of the modal parameters of natural frequencies, mode shapes and modal damping ratios. Experimental modal analysis typically makes use of data obtained from surface-mounted accelerometers. This method of obtaining data, places a practical restriction on the number of spatial data points used to model the structure, but covers many frequency components. Unfortunately the modal parameters are not easily related to parameters

related to the design of the structure.

The need to find accurate approximations of complex systems together with the development in computer technology, have led to new methods of dynamic modeling and analysis. The most prominent being the finite element method. The finite element method makes use of a spatial formulation, incorporating the shape, size, material and loading as well as boundary conditions of the structure.

A relatively new procedure that incorporates both experimental testing and the finite element method is known as experimental spatial dynamics modeling (ESDM). Experimental spatial dynamics modeling is the process of constructing a dynamic model by making use of high spatial density data obtained from a laser Doppler vibrometer (LDV). This may be achieved by using a statistical least squares discrete finite element formulation to model the continuous, three-dimensional complexed-valued velocity field. Both non-parametric as well as parametric models may be constructed for the dynamic response of the system, each model having it's own advantages, disadvantages and specific uses.

The research goal of this thesis is twofold:

1. *Evaluate the error sensitivity of the ESDM formulation to finite element model parameters*
2. *Evaluate the error sensitivity of the ESDM formulation to the spatial variables of position and orientation of the laser*

Evaluation of the influence of the model parameters, as well as the spatial variables (position and orientation) of the laser, on the accuracy of the obtained model is very important. The influence of the model parameters may be used, not only to update the estimates of the parameters themselves, but also to determine a signal-to-noise level for which the experimental data must be acquired. On the other hand the spatial position and orientation of the laser is important due to the fact that uncertainties in these variables may lead to misinterpretation of the experimental data. A variation in the position of the laser will lead to a shift in the measured velocity field. This is due, primarily, to the fact that the measured velocity is assigned to a different position on the structure than where it was actually measured. A variation in the orientation of the laser may also lead to shifting the position of the acquired data as well as in incorrect values of the measured velocities due to a projection error of the actual velocity.

1.2 Solution concepts and hypothesis statement of the research

Experimental spatial dynamics modeling will be used to construct a model for the continuous, three-dimensional, complex-valued velocity field of a vibrating structure. The influence of the model parameters of the parametric model as well as the influence of the spatial position and orientation of the laser on this constructed model, will be evaluated. These influences may be evaluated a number of different ways including:

Inspection of graphs: Graphs of the error function (difference between the modeled and the actual velocity fields) versus the model parameters may be constructed, enabling the user to visually evaluate the influence of the different variables on the accuracy of the model. This provides a qualitative evaluation of the sensitivity of the error to the specified model parameters and spatial position and orientation of the laser. This visualization method has the disadvantage that it is not possible to form a quantitative relationship between changes in the error function due to changes in the independent variables.

The visualization of the gradients of the error function becomes especially difficult with an increasing number of model parameters.

Analysis of variances: This is a statistical method which quantifies the changes in the variances of the error function due to changes in the specific parameters. This approach quantifies the uncertainty in the error function due to the effect of the model parameters and the spatial position and orientation of the laser, by making use of sampling techniques. Unfortunately, analysis of variances alone does not seek to obtain a direct functional relationship between changes in the error function and changes in the specific variables.

Calculation of gradients: By calculating the gradients of the error function with respect to the specific model parameters, it is possible to find a direct, quantitative, functional relationship between changes in the error function due to changes in the specific variables.

The hypothesis statement for the research is thus:

By calculation of the gradients of the error function with respect to model parameters of the finite element model, as well as with respect to the spatial variables of the laser, the influence of these variables on the accuracy of the obtained model may be evaluated.

1.3 Objectives of the research

From the research goal and hypothesis statement the research objectives may be summarized as follows:

1. Formulate an error function which incorporates a numerical solution for the dynamic response of the structure, consistent with high spatial density laser measurements
2. Calculate the gradient of the error function with respect to the model parameters of the parametric model
3. Calculate the gradient of the error function with respect to the spatial position and orientation of the laser

1.4 Scope of the research

The broad scope of this research lies within the general framework of ESDM. As such this research seeks to develop an element of technology within the ESDM framework.

The vibrating structure will be modeled by means of the finite element method in order to obtain the mass and stiffness matrices of the structure. The elements used will be limited to straight, one-dimensional beam elements and flat, Kirchoff plate elements which model out-of-plane bending in two-dimensional plate structures.

Normal-mode-type response will be considered. Normal mode response in this study is limited to considering a model with little or no damping. This means only the real part of the generalized complex dynamic response will be used. It is understood that the

data acquired with the laser, for the dynamic response of the structure, is real but composed of real and imaginary coefficients of the response in the phase plane. However, for the structures under consideration in this study the phase response are typically 0 or 180 degrees relative to the force, depending on the excitation frequency and the natural frequencies of the structure.

The analytical expressions for the gradients of the error function with respect to the model parameters of the parametric model as well as with respect to the spatial position and orientation of the laser will be determined. In the case of the gradients of the error function with respect to the model parameters, first- and second-order derivatives will be calculated. For the gradients of the error function with respect to the spatial position and orientation of the laser, only first-order derivatives will be calculated.

1.5 Summary and outline of the thesis

The body of the thesis is divided into nine chapters which may be summarized as follows in order to provide an overview of the material covered:

Chapter 1	-	An introduction and short overview of the thesis
Chapter 2	-	The literature research
Chapter 3	-	Experimental spatial dynamics modeling formulation
Chapter 4	-	Dynamic response using a frequency response formulation
Chapter 5	-	Sensitivity of the error function with respect to finite element model parameters
Chapter 6	-	Parametric representation of the laser beam and the surface of the structure and the Ray-Patch intersection formulation used
Chapter 7	-	Sensitivity of the error function with respect to the spatial variables of position and orientation of the laser
Chapter 8	-	Results obtained from the research
Chapter 9	-	Summary, conclusions and recommendations

Chapter 2
Literature Search

A literature search was performed in order to identify obstacles that might be encountered and directions to follow in achieving the research goals and objectives. The representation of the surface of the structure, methods of solving for the dynamic response from the finite element equations as well as different methods of evaluating derivatives were analyzed.

2.1 Representation of the surface of the structure

The representation of the surface of the structure is an important part of the research, since it has a significant influence on the gradients when considering curved surfaces. In general, the surface of a structure is curved and this curvature is accounted for in the finite element formulation, by one of two methods:

1. Approximation of the curvature by a number of flat (or straight) elements
2. Making use of curved elements

Various formulations for curved elements are available and are generally more complex than the formulations used for flat elements. One such possibility is the generalized shell elements (Cook, Malkus and Plesha 1989). These elements have been among the most difficult to devise and are formulated by making use of a classical shell theory.

Another well known approach to formulate curved surfaces in computer graphics and geometric modeling is obtained by making use of the B-Splines surface formulations (Bartels, Beatty and Barsky 1987). Curved elements are typically obtained by making use of cubic B-Spline shape functions. A quadrilateral element formulated in this way, has

higher order continuity across element boundaries which results in a smoother dynamic response model.

The representation of the surface in this research, however, is limited to approximations making use of straight beam elements and straight sided, flat plate elements. In both these formulations a sub-parametric formulation will be used (Reddy 1993). In sub-parametric formulations, the geometry is represented by lower order shape functions than those used to represent the dependent variable (dynamic response in this research). For the beam element, the geometry will be represented by making use of linear Lagrangian shape functions, while bi-linear Lagrangian shape functions will be used for the plate elements.

2.2 Gradients of the error function with respect to finite element model parameters

It can be shown that the only terms in the error function containing finite element model parameters, are the steady state amplitude components of the modeled velocity field. This velocity field, in turn, may be written in terms of the modeled dynamic displacement response. Thus, in order to evaluate the gradients of the error function with respect to finite element model parameters, it is necessary to find the gradients of the steady state dynamic displacement response with respect to these model parameters.

The dynamic response may be solved from the semi-discrete finite element formulation (this is a discrete representation of the spatial part and a continuous representation of the temporal part of the differential equation):

$$\mathbf{M}\cdot\mathbf{a}+\mathbf{C}\cdot\mathbf{v}+\mathbf{K}\cdot\mathbf{u}=\mathbf{F} \qquad \text{. . . (2.1)}$$

by making use of one of two different methods:

1. Time-history analysis (Cook, Malkus and Plesha 1989)
2. Frequency response analysis (Meirovitch 1986)

In time-history analysis several different techniques are used which may be summarized into two major groups. The first group is comprised by methods known as modal methods. While the second group is comprised by the so called direct integration or step-by-step methods. The modal methods employ a modal summation technique in order to obtain the dynamic response of the system. The direct integration techniques, on the other hand, make use of numerical integration of a prescribed order. Both methods yield the dynamic response of the system in the time domain.

Modal summation yields the response in terms of the modal parameters of natural frequency, mode shapes and modal damping. The response is, thus, given as an implicit function of finite element model parameters and the calculation of the gradients of the response with respect to these model parameters is, thus, not easily accomplished. The direct integration methods yields the response at discrete time steps and no functional relationship between the steady-state response amplitude and the finite element model parameters may be found.

The data acquired from the LDV is in the time domain but is represented by a frequency-domain model (Montgomery 1994). A frequency response analysis will, thus, be best suited for obtaining the steady-state response of the structure, as the frequency is known from the experimental data. The frequency analysis also yields the response as an explicit function of finite element model parameters, which enables the direct calculation of the gradients of the response with respect to model parameters.

A frequency response analysis may be obtained by making use of a direct stiffness matrix formulation (Meirovitch 1986 or Zienkiewicz and Taylor 1989) in order to develop a pseudo-dynamic stiffness matrix incorporating the mass, damping and stiffness matrices into a single matrix, **D**. This pseudo-dynamic stiffness matrix is a function of the excitation frequency and may be written as:

$$\mathbf{D}(\omega) = -\omega^2 \cdot \mathbf{M} + i\omega \cdot \mathbf{C} + \mathbf{K} \qquad \text{. . . (2.2)}$$

The pseudo-dynamic stiffness formulation reduces the frequency response analysis to the form shown in *Equation 2.3* where **u** is the vector of dynamic nodal displacements and **F** is the vector of dynamic nodal forces:

$$\mathbf{D} \cdot \mathbf{u} = \mathbf{F} \qquad \ldots \textbf{(2.3)}$$

Differentiating *Equation 2.3* with respect to a model parameter, say χ, yields:

$$\mathbf{D} \cdot \frac{d\mathbf{u}}{d\chi} = \frac{d\mathbf{F}}{d\chi} - \frac{d\mathbf{D}}{d\chi} \cdot \mathbf{u} \qquad \ldots \textbf{(2.4)}$$

Equation 2.4 falls into an area of structural optimization, generally known as design sensitivity analysis (Arora 1989). Design sensitivity analysis involves the evaluation of the sensitivity of a constraint function, limiting a static displacement and/or stress component, with respect to a design variable. A typical inequality constraint function, dependent on only one design variable, say χ, may be written as:

$$g(\mathbf{u}, \chi) \geq 0 \qquad \ldots \textbf{(2.5)}$$

By making use of the chain rule of differentiation, the derivative of the constraint function with respect to the design variable, may be written as (Haftka and Gürdal 1993)

$$\frac{dg}{d\chi} = \frac{\partial g}{\partial \chi} + \mathbf{z}^T \cdot \frac{d\mathbf{u}}{d\chi} \qquad \ldots \textbf{(2.6)}$$

where the vector $\mathbf{z}^T$ has the following components:

$$z_i = \frac{\partial g}{\partial u_i} \qquad \ldots \textbf{(2.7)}$$

The right-hand side of *Equation 2.6* may be explained as the summation of the explicit part of the derivative and the implicit part through the dependence on **u**. The explicit part is usually equal to zero or easy to calculate, while the implicit part may be obtained from *Equation 2.4*. *Equation 2.4* is normally evaluated by one of two methods.

The first is the direct method which involves the direct evaluation of $\frac{d\mathbf{u}}{d\chi}$ from *Equation 2.4*, while the other is known as the adjoined method (Haftka and Gürdal 1993).

In the adjoined method, *Equation 2.4* is pre-multiplied by $\mathbf{z}^T \cdot \mathbf{D}^{-1}$ and the solution to $\mathbf{z}^T \cdot \frac{d\mathbf{u}}{d\chi}$ is then found by making use of an adjoined vector, $\boldsymbol{\lambda}$. The adjoined vector is defined as the solution of:

$$\mathbf{D} \cdot \boldsymbol{\lambda} = \mathbf{z} \cdot \qquad \text{. . . (2.8)}$$

Although the adjoined method is normally preferred due to better efficiency, it is not of any use in the context of this research. This is due to the fact that the adjoined method directly evaluates the $\mathbf{z}^T \cdot \frac{d\mathbf{u}}{d\chi}$ term without the calculation of the sensitivity of the required structural response, $\frac{d\mathbf{u}}{d\chi}$.

In this research, $\frac{d\mathbf{u}}{d\chi}$ will be solved directly from *Equation 2.4*. The design variable will be replaced by a parametric model parameter, enabling the calculation of the sensitivity of the dynamic response with respect to a parametric model parameter by making use of the direct method of differentiation.

2.3 Gradient of the error function with respect to the spatial position and orientation of the laser

In order to formulate the error function in terms of the spatial position and orientation of the laser, it is necessary to find the scanning position of the laser beam on the structure in terms of these spatial variables. This may be accomplished by:

1. Making use of direct geometrical relationships
2. Making use of the Ray-Patch intersection formulation

Making use of direct geometrical relationships to find the scanning position as a function of the spatial variables of the laser, is a very tedious operation, especially in three-dimensional space (Ellis and Gulick 1986). Furthermore, this method does not lend itself to generalization and new relationships must be developed for each new scanning position as well as for every new structure. This makes it almost impossible to develop a general procedure that makes use of this method in order to evaluate the scanning position for different structures and positions and orientations of the laser.

The Ray-Patch intersection formulation (Glassner 1989) makes use of vector notation and parametric equations to model the laser beam and the surface of the structure. The use of this formulation simplifies the geometric relationships greatly. Furthermore, a general procedure, making use of this formulation, may be developed rather easily in order to find scanning positions for different structures and positions and orientations of the laser.

2.4 Numerical evaluation of derivatives

The derivative of a function may be calculated numerically by means of a finite difference approximation. These approximations are derived from a Taylor series expansion of a function about a specific point. The simplest of these approximations is the forward-difference method, which is a first-order method (first-order accuracy) and may be written as (Burden and Faires 1989):

$$f'(x_0) = \frac{f(x_0 + h) - f(x_0)}{h} - \frac{h}{2} f''(\xi) \quad \text{with} \quad x_0 < \xi < (x_0 + h)$$

$$f'(x_0) \approx \frac{f(x_0 + h) - f(x_0)}{h} \qquad \text{. . . (2.9)}$$

where the step size, h, is larger than zero. When the step size, h, is smaller than zero, *Equation 2.9* is also known as the backward-difference method. The backward-difference method still has a first-order convergence rate.

The central-difference method is also often used. This is a second-order method which may be written as (Burden and Faires 1989):

$$f'(x_0) = \frac{f(x_0 + h) - f(x_0 - h)}{2h} - \frac{h^2}{6} f'''(\xi) \quad \text{with} \quad (x_0 - h) < \xi < (x_0 + h)$$

$$f'(x_0) \approx \frac{f(x_0 + h) - f(x_0 - h)}{2h}$$

. . . **(2.10)**

It is a simple process to incorporate these finite difference approximations into a computer program evaluating the derivatives of a function, which makes them very popular, even though they might be computationally intensive. Unfortunately, these approximations may exhibit accuracy problems due to the fact that these methods represent a linear approximation to the gradient about the specific point of interest.

From *Equations 2.9 and 2.10*, it seems as if a smaller step size, *h*, will lead to a better approximation and more accurate results. However, this is, in general, not true due to the fact that the approximations have two different types of error associated with them. These errors may be summarized as follows:

1. **Truncation error:** Error due to the neglected higher order terms of the Taylor series expansion of the function
2. **Condition error:** Difference between the exact and the numerical function evaluation. This is usually due to round-off errors in the evaluation process.

Clearly the truncation error will become smaller with a smaller step size. The condition error, on the other hand, will become larger with smaller step sizes and might become significant for extremely small step sizes or for ill-conditioned systems. This leads to the so called 'step size dilemma' (Haftka and Gürdal 1993). A small step size is needed to reduce the truncation error, but this leads to larger condition errors. In some cases no step size may be found which would yield accurate results. As an approximation method,

numerical differentiation is, thus, unstable due to the fact that the small values of the step size needed to reduce the truncation error causes the condition error to grow (Burden and Faires 1989).

Higher order finite-difference algorithms with higher accuracy are available, for example five point formulas with fourth-order accuracy (Burden and Faires 1989). However, due to the high computational cost associated with these formulas, they are rarely used in cases where the cost of each function evaluation is high.

2.5 Analytical evaluation of derivatives

When the error function is explicitly known in terms of the model parameters or spatial position and orientation of the laser, the required gradients may be determined analytically. Although it is generally more tedious to determine analytical expressions for the gradients, compared to the numerical methods, many advantages are gained when this method is used. Three of the most important advantages are:

1. An exact solution is obtained
2. This solution is a continuous expression defined over the whole domain of the problem
3. This solution makes use of the continuous, three-dimensional, complexed-valued velocity field obtained from the ESDM formulation

By making use of the chain rule of differentiation (Ellis and Gulick 1986) it is possible to write the gradients as an expansion of partial derivatives. This simplifies the evaluation process.

2.6 Summary

From the literature search it is evident that a frequency response analysis, resulting in a pseudo-dynamic stiffness formulation, is a good choice for solving the dynamic response of the structure in the context of this research. This is due to the fact that a frequency response analysis directly relates the laser measurement to the predicted

response of the parametric model. This process also preserves the error structure between the measured and predicted response, yielding a straight forward statistical analysis. Furthermore, it also enables the use of the direct method of differentiation, as well as the calculation of the response without the necessity to determine the eigenvalues and eigenvectors of the system, or the sensitivities of these eigenvalues and eigenvectors.

The Ray-Patch intersection formulation will be used to find the scanning position of the laser on the structure. This procedure may be generalized and incorporated into a computer program.

Due to the accuracy problems associated with the numerical evaluation of the gradients and the inherent instability of the method, the gradients will be evaluated analytically. This will make full use of the continuous three-dimensional complexed-valued velocity field obtained from the ESDM formulation.

Chapter 3
Experimental Spatial Dynamics Modeling Formulation

ESDM is used to construct a model of the continuous three-dimensional complex-valued velocity field of a vibrating structure. The method makes use of a weighted least squares discrete finite element formulation. High spatial density data, obtained from a scanning LDV, will be used to solve for this continuous, three-dimensional, complex-valued velocity field.

The basic ESDM formulation will be derived in this chapter. This will be done without an in-depth discussion of the statistical detail associated with the method.

3.1 Experimental Spatial Dynamics Modeling

In this section the basic concepts of ESDM will be summarized. This will be done by means of the flow chart shown in *Figure 3.1*.

Experimental sampling of both the surface shape and surface velocity of a vibrating structure is the starting point of the ESDM concept. The measurements are obtained from positionally registered scanning LDV's. Actual three-dimensional shape models and dynamic response models of the vibrating structure may be formed from the acquired high spatial density geometrical and velocity data. These shape and dynamic response models may then be investigated by means of scientific visualization techniques.

As stated earlier, the scope of this research lies within the general framework of ESDM. More specifically, the dynamic response model will be considered. A conventional finite element model will be used to obtain a parametric representation of the structure. The area of interest of this research, within the global framework of ESDM is highlighted in *Figure 3.1* by means of the darker flow lines.

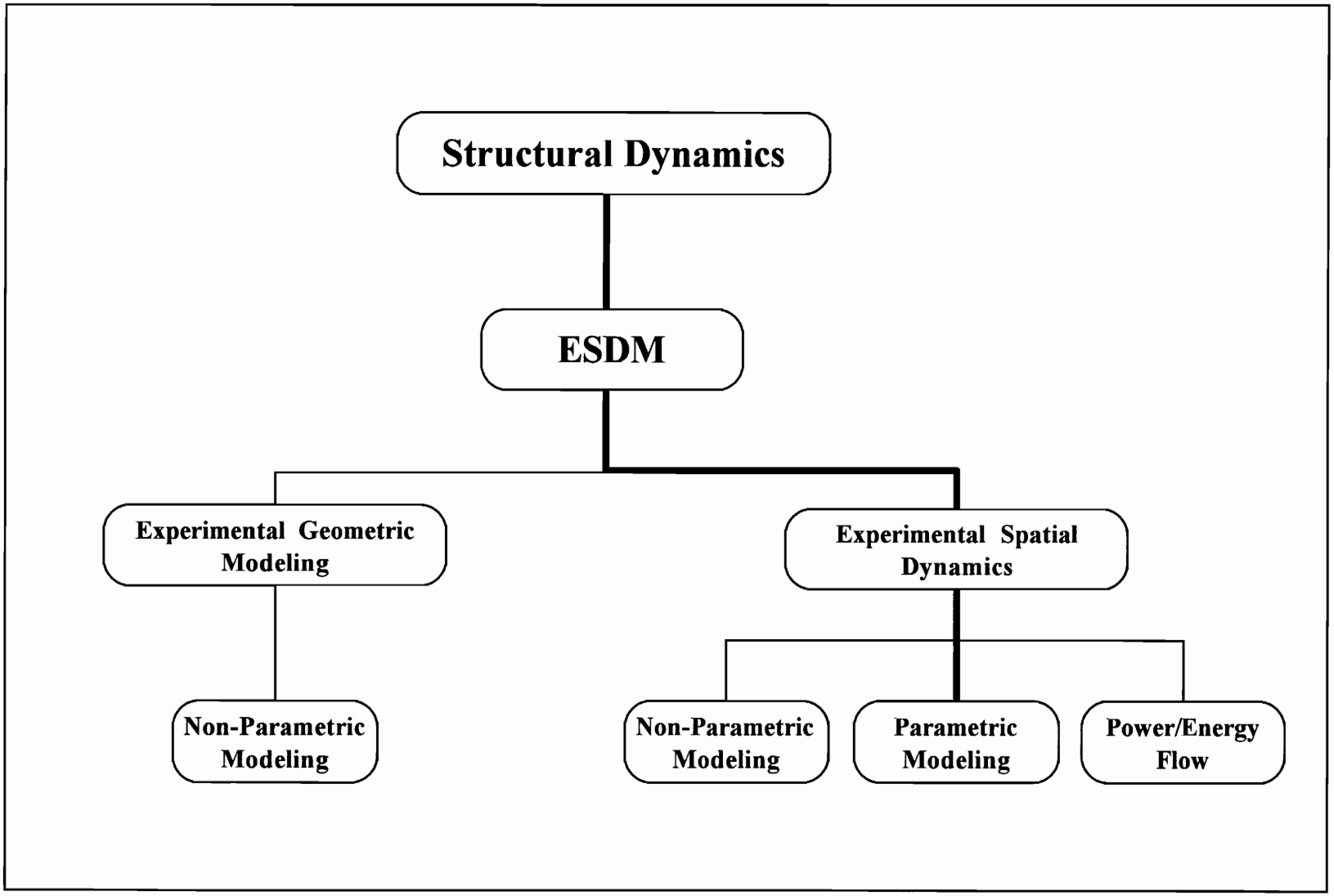

Figure 3.1: Overview of Experimental Spatial Dynamics Modeling

3.2 The dynamic displacement field

Since the actual velocity field of a vibrating structure is to be determined, it is important to investigate the velocity response of a structure and the mathematical representation thereof. The velocity field will be obtained from the dynamic displacement response of the structure. The dynamic displacement response will, thus, be studied first before looking at the actual velocity field.

The classical closed-form solution for the transverse dynamic response of a vibrating beam or plate structure, excited by a harmonic forcing function, is a partial differential equation. The partial differential equation describing the forced, transverse vibration of an Euler-Bernoulli beam may be written as (Meirovitch 1986):

$$\frac{\partial^2}{\partial x^2}\left[EI(x)\cdot\frac{\partial^2 U(x,\omega,t)}{\partial x^2}\right]+m(x)\cdot\frac{\partial^2 U(x,\omega,t)}{\partial t^2}=F(x,\omega,t) \qquad \text{. . . (3.1)}$$

The vibration of linear structures, as is the case with the Euler-Bernoulli beam described in *Equation 3.1*, have the following properties (Meirovitch 1986):

1. When no excitation force is applied, the structure will vibrate at it's natural frequencies
2. When an excitation force is applied, the structure will vibrate at the excitation frequency

Furthermore, the forcing function as well as the solution, are separable into spatial and temporal components. For the homogeneous case (no excitation) or for the case where the harmonic forcing function is represented by forces and/or couples applied at the end points of the structure, the general solution to *Equation 3.1* may be expressed as a product of the spatial and temporal components as (McCallion 1973):

$$U(x,\omega,t)=X(x,\omega)\cdot T(t,\omega) \qquad \text{. . . (3.2)}$$

Upon substitution of *Equation 3.2* into *Equation 3.1*, the partial differential equation of *Equation 3.1* may be divided into two ordinary differential equations, which may be written as:

$$\frac{\partial^4 X(x,\omega)}{\partial x^4} - \beta^4 \cdot X(x,\omega) = 0 \qquad \frac{\partial^2 T(t,\omega)}{\partial t^2} + \omega^2 \cdot T(t,\omega) = 0$$

with

$$\beta^4 = \frac{\omega^2 \cdot m(x)}{EI(x)}$$

. . . **(3.3)**

where the circular frequency of vibration, ω, depends on the frequency of the excitation.

The solutions of these two ordinary partial differential equations may be written in terms of the constants of integration as:

$$X(x,\omega) = C_1 \cdot Sin(\beta x) + C_2 \cdot Cos(\beta x) + C_3 \cdot Sinh(\beta x) + C_4 \cdot Cosh(\beta x)$$

$$T(t,\omega) = D_1 \cdot e^{i\omega t} + D_2 \cdot e^{-i\omega t}$$

$$= D \cdot Cos(\omega t - \phi)$$

. . . **(3.4)**

where the constants of integration C_1, C_2, C_3 and C_4 are obtained from the boundary conditions, which include the end forces and/or couples if present. The constants D_1 and D_2 (or D and ϕ) are obtained from the initial conditions. The final form of *Equation 3.4* yields the real part of the solution. By taking the product of the two solutions shown in *Equation 3.4*, according to *Equation 3.2*, the total solution of the displacement field may, after some algebraic manipulation, be written as:

$$U(x,\omega,t) = u(\omega,x) \cdot Cos(\omega t - \phi)$$

. . . **(3.5)**

The complex nature of the dynamic response, relative to the excitation, is represented in the phase plane by the phase angle ϕ (*Figure 3.2*).

This solution is a special case of the general dynamic response of a structure excited by a harmonic forcing function. The harmonic forcing function and dynamic displacement response for a general three-dimensional structure are also separable into spatial and temporal components (Meirovitch 1986) and may be written in vector-form as:

$$\vec{F}(x,y,z,\omega,t) = \vec{f}(x,y,z,\omega)\cdot e^{i\omega t}$$

$$\vec{U}(x,y,z,\omega,t) = \vec{u}(x,y,z\omega)\cdot e^{i(\omega t-\phi)}$$

. . . **(3.6)**

This general form of the dynamic displacement response will be used in the development of the velocity field.

3.3 Dynamic velocity field

The velocity field may be obtained from the displacement field by taking the first derivative of the displacement field with respect to time. Similarly the acceleration field may be obtained from the velocity field by taking the first derivative of the velocity field with respect to time. If the general form of the displacement field as shown in *Equation 3.6* is used, the velocity and acceleration fields may be written as:

$$\vec{V}(x,y,z,\omega,t) = \frac{\partial \vec{U}}{\partial t} = i\cdot\omega\cdot\vec{u}(x,y,z,\omega)\cdot e^{i(\omega t-\phi)} = i\cdot\omega\cdot\vec{U}(x,y,z,\omega,t)$$

$$\vec{A}(x,y,z,\omega,t) = \frac{\partial \vec{V}}{\partial t} = -\omega^2\cdot\vec{u}(x,y,z,\omega)\cdot e^{i(\omega t-\phi)} = -\omega^2\cdot\vec{U}(x,y,z,\omega,t)$$

. . . **(3.7)**

Furthermore, if the fact that i may be written in terms of the phase angle as $i = e^{i\pi/2}$ and -1 as $-1 = e^{i\pi}$ are taken into account, it is clear that the velocity leads the

displacement by the phase angle $\pi/2$ and is a factor ω larger. The acceleration, on the other hand, leads the displacement by the phase angle π and is a factor ω^2 larger.

The relationship between the displacement, velocity, acceleration and the forcing function may also be written in terms of the natural frequency and the viscous damping factor as (Meirovitch 1986):

$$\vec{A}(x,y,z,\omega,t)+2\zeta\omega_n\cdot\vec{V}(x,y,z,\omega,t)+\omega_n{}^2\cdot\vec{U}(x,y,z,\omega,t)=f_o\cdot Cos(\omega t) \quad \text{. . . (3.8)}$$

By making use of *Equations 3.7 and 3.8*, the relationship between the displacement, velocity, acceleration fields and the forcing function may be represented schematically in the phase plane as shown in *Figure 3.2*.

As stated in the scope of the research, only normal mode type response will be considered, which implies little or no damping in the numerical model. From *Figure 3.2* it is clear that the value of the phase angle, ϕ, will be equal to either 0 or 180 degrees for the case where the damping is zero or very small.

Since a certain amount of damping will always be present in the actual model, the damping term will be included in the derivation of the gradients of the error function in order to keep the method as general as possible. Small and/or proportional damping may then be represented by the derived formulation.

If the relationship of *Equation 3.7* and the representation of i in terms of the phase angle are taken into account, the velocity field may be written as:

$$\vec{V}(x,y,z,w,t)=\omega\cdot\vec{u}(x,y,z,\omega)\cdot e^{i(\omega t-\phi+\frac{\pi}{2})}$$

$$=\vec{v}(x,y,z,\omega)\cdot e^{i(\omega t-\phi+\frac{\pi}{2})} \quad \text{. . . (3.9)}$$

From *Equation 3.9*, the amplitude of the steady state velocity field may be written in terms of the forcing frequency and the amplitude of the steady state displacement field as:

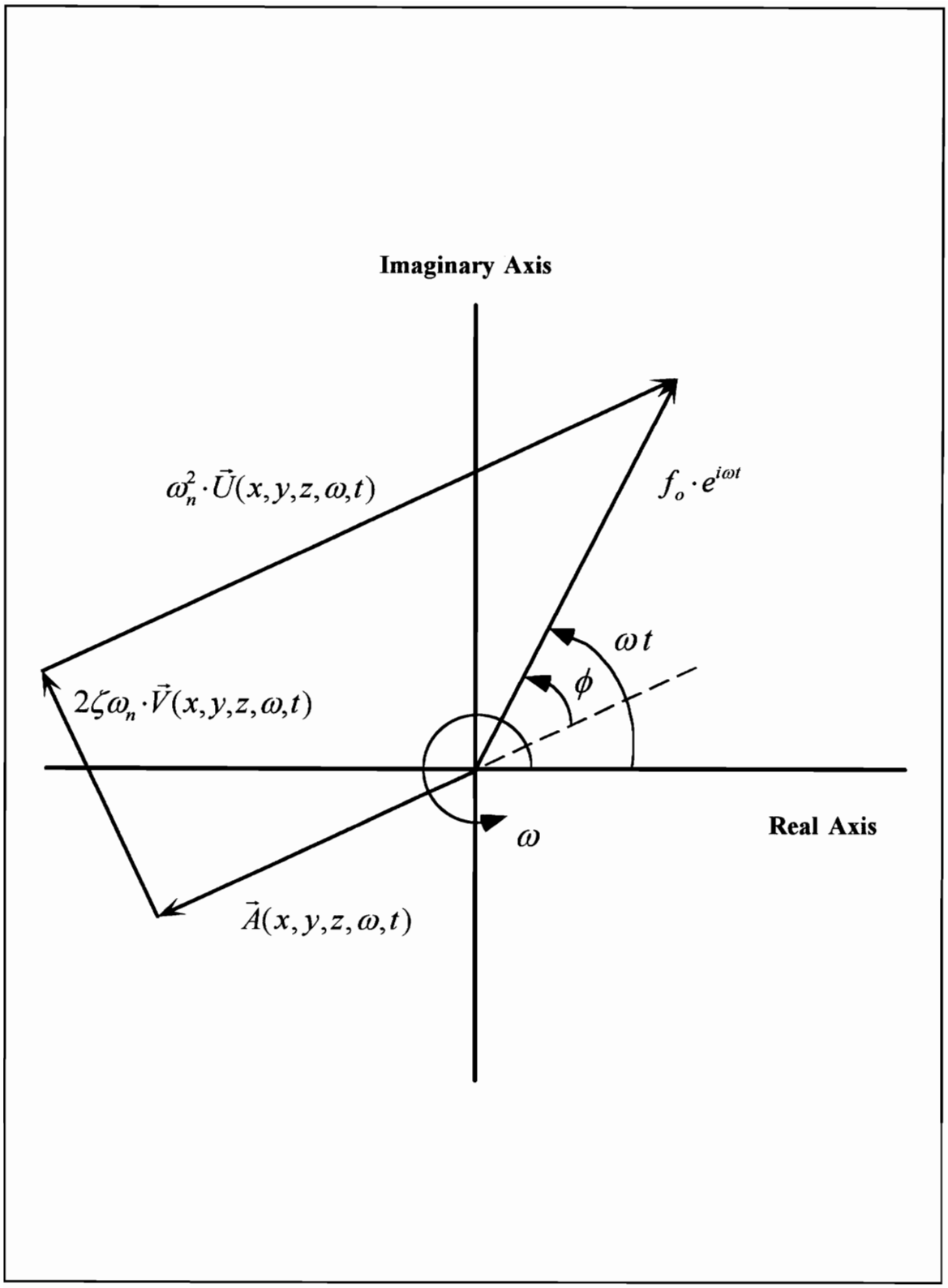

Figure 3.2: Complex nature of the dynamic response relative to the excitation

$$\vec{v}(x, y, z, \omega) = \omega \cdot \vec{u}(x, y, z, \omega)$$

. . . **(3.10)**

Equation 3.11 may now be obtained from *Equation 3.10* by writing the real-valued amplitude of the velocity field in component form as follows:

$$\vec{v}(x_i, y_i, z_i, \omega) = \vec{v}_x(x_i, y_i, z_i, \omega) \cdot \hat{i} + \vec{v}_y(x_i, y_i, z_i, \omega) \cdot \hat{j} + \vec{v}_z(x_i, y_i, z_i, \omega) \cdot \hat{k}$$

$$= \omega \cdot (\vec{u}_x(x_i, y_i, z_i, \omega) \cdot \hat{i} + \vec{u}_y(x_i, y_i, z_i, \omega) \cdot \hat{j} + \vec{u}_z(x_i, y_i, z_i, \omega) \cdot \hat{k})$$

. . . **(3.11)**

The vector component form of the amplitude of the steady-state velocity field will be used in the formulation of the ESDM error function.

3.4 Error function

An error function, yielding the residual between the components of the modeled velocity field and the LDV measured velocity field, may be derived from the dot product of the modeled velocity vector and the measured velocity vector. The continuous three-dimensional, complex-valued, velocity field will then be solved from the high spatial density data obtained from the LDV by performing a least squares multiple regression incorporating these residuals.

The dot product of the modeled velocity field at any point x_i, y_i and z_i on the structure and the measured velocity vector along the line of sight of the laser beam may be written as:

$$\vec{v}(x_i, y_i, z_i, \omega) \cdot \vec{V}_{Li} = |\vec{v}(x_i, y_i, z_i, \omega)| |\vec{V}_{Li}| Cos\beta_i$$

. . . **(3.12)**

Equation 3.12 may be expanded into vector component form, as shown in *Equation 3.13*:

$$\vec{v}_x(x_i, y_i, z_i, \omega) \cdot \vec{V}_{Lxi} + \vec{v}_y(x_i, y_i, z_i, \omega) \cdot \vec{V}_{Lyi} + \vec{v}_z(x_i, y_i, z_i, \omega) \cdot \vec{V}_{Lzi}$$

$$= \left|\vec{v}(x_i, y_i, z_i, \omega)\right| \left|\vec{V}_{Li}\right| Cos\beta_i \quad \text{. . . (3.13)}$$

From *Figure 3.3*, the following relationship between the modeled velocity vector, the projection of the structure's velocity on the laser beam ($\widetilde{V}_{Li}$) and the angle between the modeled and measured velocity vectors, at each measuring point, may be written as:

$$\widetilde{V}_{Li} = \left|\vec{v}(x_i, y_i, z_i, \omega)\right| \cdot Cos\beta_i \quad \text{. . . (3.14)}$$

Furthermore, the components of the *i-th* measured velocity vector can be written as

$$\vec{V}_{Lxi} = \left|\vec{V}_{Li}\right| \cdot Cos\theta_{xi} \qquad \vec{V}_{Lyi} = \left|\vec{V}_{Li}\right| \cdot Cos\theta_{yi} \qquad \vec{V}_{Lzi} = \left|\vec{V}_{Li}\right| \cdot Cos\theta_{zi} \quad \text{. . . (3.15)}$$

where the $Cos\theta_{xi}$, $Cos\theta_{yi}$ and $Cos\theta_{zi}$ terms represent the direction cosines of the laser beam with respect to the *x*, *y* and *z* axes of the structural coordinate system.

Upon substitution of *Equations 3.15 and 3.14* into *Equation 3.13* and dividing both sides of the resulting equation by $\left|\vec{V}_{Li}\right|$, *Equation 3.16* is obtained:

$$\vec{v}_x(x_i, y_i, z_i, \omega) \cdot Cos\theta_{xi} + \vec{v}_y(x_i, y_i, z_i, \omega) \cdot Cos\theta_{yi} + \vec{v}_z(x_i, y_i, z_i, \omega) \cdot Cos\theta_{zi} = \widetilde{V}_{Li} \quad \text{. . . (3.16)}$$

The left-hand side of *Equation 3.16* represents the projection of the modeled velocity field onto the laser beam direction, while the right-hand side represents the value as measured by the LDV along the line-of-sight of the laser beam. *Equation 3.16* will only be satisfied if there is no difference between the modeled and the measured velocity vectors. In general, this will not be true and an error function may be written as:

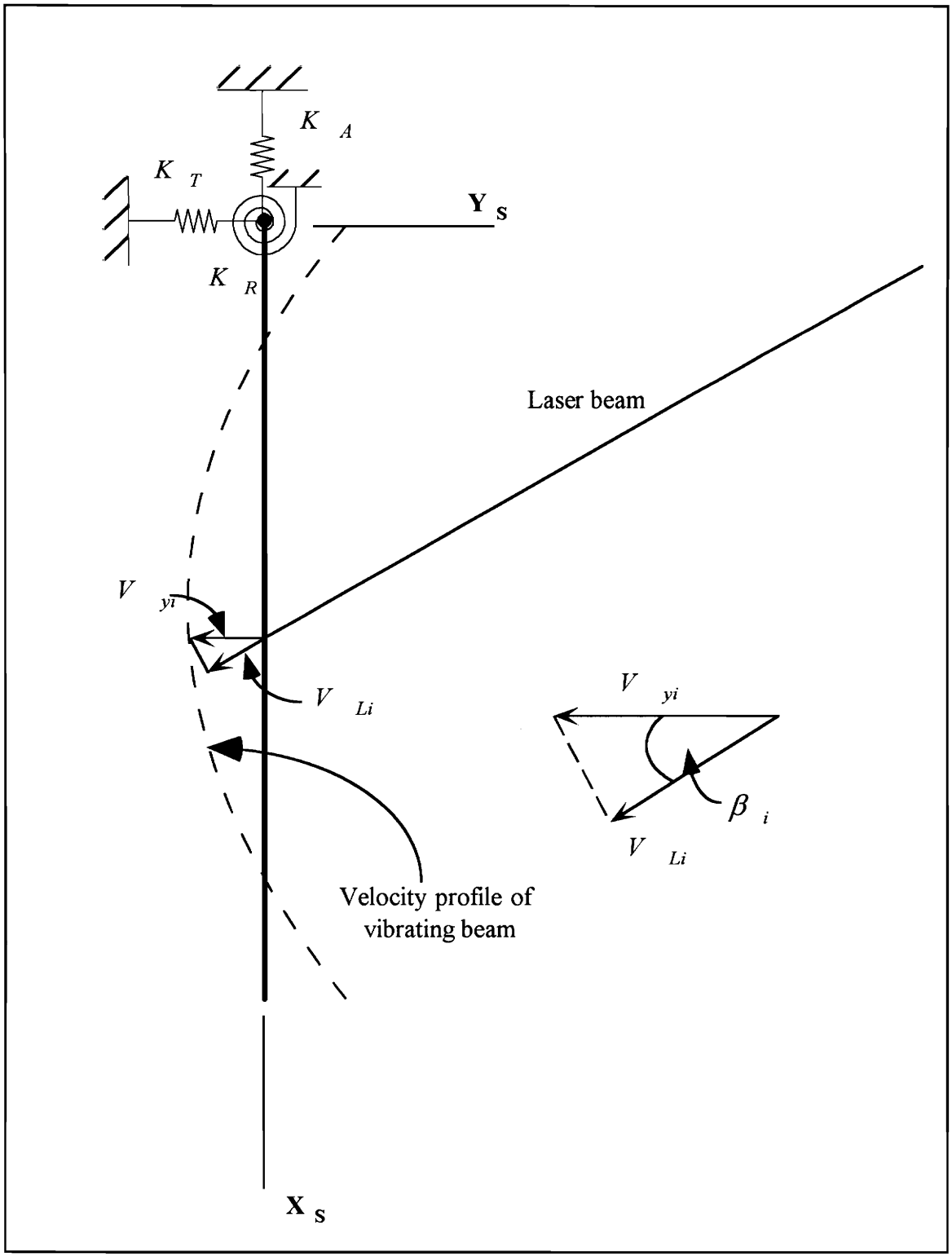

Figure 3.3: Relationship between the structure's velocity vector (V_{Li}) and the modeled velocity vector (V_{yi}) for the two-dimensional case

$$error_i = \vec{v}_x(x_i, y_i, z_i, \omega) \cdot \eta_{xi} + \vec{v}_y(x_i, y_i, z_i, \omega) \cdot \eta_{yi} + \vec{v}_z(x_i, y_i, z_i, \omega) \cdot \eta_{zi} - \tilde{V}_{Li} \quad \text{. . . (3.17)}$$

where the direction cosines are represented by the η_{xi}, η_{yi} and η_{zi} terms.

3.5 Finite element representation of the velocity field

By making use of the finite element formulation, an approximate solution to the velocity field may be obtained. The finite element method will be used to find the mass and stiffness matrices of the structure by approximation of the spatial component of the governing partial differential equation (*Equation 3.1* for Euler-Bernoulli beams). This semi-discrete formulation of the partial differential equation may be written in matrix form in terms of the mass, damping and stiffness matrices as:

$$\mathbf{M} \cdot \ddot{\mathbf{d}} + \mathbf{C} \cdot \dot{\mathbf{d}} + \mathbf{K} \cdot \mathbf{d} = \mathbf{F} \quad \text{. . . (3.18)}$$

The mass and stiffness matrices will be obtained directly from the finite element method, while Rayleigh damping ($\mathbf{C} = \overline{\alpha} \cdot \mathbf{M} + \overline{\beta} \cdot \mathbf{K}$) (Cook, Malkus and Plesha 1989) will be used to form a proportional damping matrix. *Equation 3.18* represents a linear system of ordinary differential equations that must be solved simultaneously in order to find a solution for the nodal values of the dynamic displacement response. In this research, the equations will be solved by making use of a frequency response analysis, resulting in a pseudo-dynamic stiffness formulation.

By making use of the finite element basis functions, the continuous displacement field may be calculated over the whole region of the structure. Furthermore, making use of *Equation 3.10*, the approximate velocity field may be obtained from the approximate displacement field, in terms of the finite element basis functions. The components of this continuous velocity field may be written in terms of the finite element basis functions as

$$v_{xi} = \sum_{j=1}^{El.dof} (N_j(\xi_i, \eta_i, \zeta_i) \cdot \bar{v}_{xj})$$

$$v_{yi} = \sum_{j=1}^{El.dof} (N_j(\xi_i, \eta_i, \zeta_i) \cdot \bar{v}_{yj})$$

$$v_{zi} = \sum_{j=1}^{El.dof} (N_j(\xi_i, \eta_i, \zeta_i) \cdot \bar{v}_{zj})$$

. . . (3.19)

where the variables $\bar{v}_{xj}$, $\bar{v}_{yj}$ and $\bar{v}_{zj}$ represent the nodal values of the velocity field, obtained from the nodal values of the displacement field, using *Equation 3.10*. The process of obtaining this continuous velocity field from the nodal values of the displacement field, may be summarized as follows:

1. Identify the element that contains the specific laser measurement
2. Map the global x, y and z coordinates to the local ξ, η and ζ coordinates of the element (in this research this will be done by making use of a sub-parametric formulation)
3. Use *Equation 3.18* to solve for the components of the velocity field at the specific point on the specific element

This approximate solution of the velocity field is used to construct the discrete error function, derived from the finite element formulation. The components of the modeled velocity field in *Equation 3.17* will now be replaced by the approximate field solution of *Equation 3.19*, evaluated at specific points on the structure to obtain:

$$error_i = v_{xi} \cdot \eta_{xi} + v_{yi} \cdot \eta_{yi} + v_{zi} \cdot \eta_{zi} - \tilde{V}_{Li}$$

. . . (3.20)

A solution to the actual velocity field, over the domain of the structure, will be found by solving a system of linear equations. The actual solution will minimize the square root of *Equation 3.20*, summed over all the laser measurements.

3.6 Relation of the error function to the research

As shown in *Equation 3.10*, the velocity components contained in the error function, *Equation 3.20*, may be written in terms of the displacement response of the structure. This dynamic displacement response of the structure is obtained from the solution of the semi-discrete formulation, *Equation 3.18*, which is obtained by means of the finite element method. The components of the dynamic response of the structure are the only terms included in the error function which are obtained from, and, thus, are dependent on the parameters of the finite element formulation.

In order to evaluate the gradients of the error function with respect to finite element model parameters, the gradients of the dynamic displacement response with respect to these model parameters must be evaluated.

On the other hand, the spatial variables of the laser have an influence on both the velocity components as well as the direction cosines contained in the error function. In order to evaluate the gradients of the error function with respect to these variables, the gradients of the velocity components as well as of the direction cosines with respect to the spatial variables of the laser must be found.

In order to evaluate the above derivatives, it is first of all necessary to solve for the dynamic response of the structure from the semi-discrete formulation shown in *Equation 3.18*. This will be done by making use of a frequency response analysis using a pseudo-dynamic stiffness formulation which will be derived in the next chapter.

Chapter 4

Dynamic Response using a Frequency Response Formulation

The components of the modeled dynamic response, as needed in the ESDM formulation, will be calculated from a finite element model of the structure. As stated in the literature search, it is not practical (within the context of this research) to solve for the dynamic response from the finite element formulation, by making use of a time-history analysis. Instead, the dynamic response will be solved for using a frequency response analysis, which will be incorporated into the specific problem by making use of a pseudo-dynamic stiffness formulation.

In this chapter, a frequency response formulation will be derived, the different finite elements used in the research will be discussed and lastly a test case will be evaluated. The purpose of the test case is to compare the results obtained from the frequency response, pseudo-dynamic stiffness formulation to that obtained from a closed-form solution in order to establish the validity of the method.

4.1 Frequency response formulation

The dynamic displacement response of a structure, excited by a harmonic forcing function, may be written in terms of a frequency response formulation (Meirovitch 1986 or Zienkiewicz and Taylor 1989). The use of this frequency response formulation has many advantages. The most important of these advantages, within the context of this research, may be summarized as:

1. The dynamic response can be calculated without the evaluation of eigenvalues and eigenvectors
2. The dynamic response can be solved from a set of linear equations, similar to that of the static case. This means that existing, linear solvers may be used which are normally very efficient
3. The direct method of differentiation can be used in order to evaluate the sensitivity of the error function with respect to finite element model parameters

The frequency response formulation will first be derived for a two degree of freedom mass, spring and damper system. Once this basic formulation is derived it can be generalized for a multi-degree of freedom system by making use of matrix notation.

The two degree of freedom system shown in *Figure 4.1*, has the following mass, damping and stiffness matrices:

$$\mathbf{M} = \begin{bmatrix} m_1 & 0 \\ 0 & m_2 \end{bmatrix} \qquad \mathbf{C} = \begin{bmatrix} c_1 + c_2 & -c_2 \\ -c_2 & c_2 + c_3 \end{bmatrix} \qquad \mathbf{K} = \begin{bmatrix} k_1 + k_2 & -k_2 \\ -k_2 & k_2 + k_3 \end{bmatrix} \quad \text{. . . (4.1)}$$

The differential equations of motion for this system may be written as:

$$\begin{aligned} m_{11}\ddot{x}_1 + m_{12}\ddot{x}_2 + c_{11}\dot{x}_1 + c_{12}\dot{x}_2 + k_{11}x_1 + k_{12}x_2 &= F_1(t) \\ m_{21}\ddot{x}_1 + m_{22}\ddot{x}_2 + c_{21}\dot{x}_1 + c_{22}\dot{x}_2 + k_{21}x_1 + k_{22}x_2 &= F_2(t) \end{aligned} \quad \text{. . . (4.2)}$$

The harmonic forcing function in *Equation 4.2*, may be written in complex form in terms of the amplitude and the forcing frequency as shown in *Equation 4.3*:

$$F_1(t) = F_1 e^{i\omega t} \qquad F_2(t) = F_2 e^{i\omega t} \quad \text{. . . (4.3)}$$

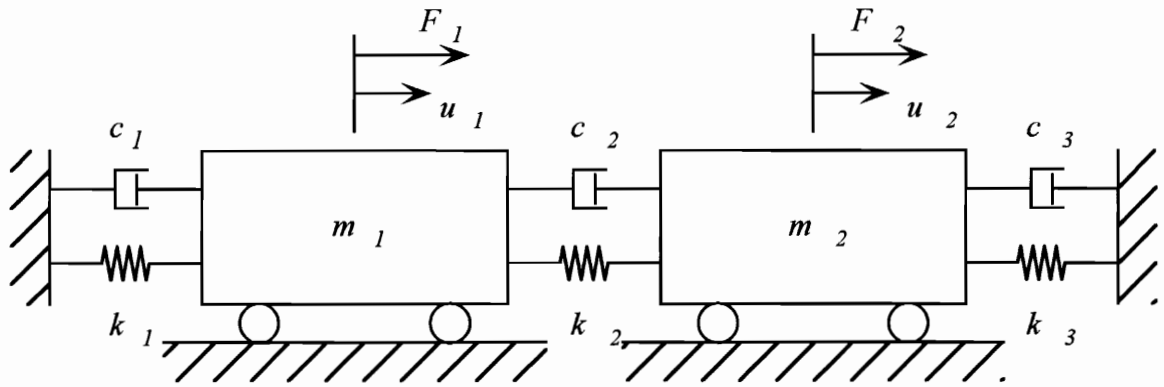

Figure 4.1: Two-degree-of-freedom mass, spring and damper system.

For linear structures, the steady-state dynamic displacement response due to a harmonic forcing function (Meirovitch 1986), is also a harmonic function. The dynamic displacement response of the system may, thus, be written as a complex function in terms of the forcing frequency and the amplitude of the displacement as (*Chapter 3*):

$$x_1(t) = X_1 e^{i(\omega t - \phi)} \qquad x_2(t) = X_2 e^{i(\omega t - \phi)}$$

. . . **(4.4)**

For the normal-mode-type response with very little, or no proportional damping, the phase angle will always be equal to 0 or 180 degrees (*Figure 3.1*) and may, thus, be omitted from *Equation 4.4* to obtain:

$$x_1(t) = X_1 e^{i\omega t} \qquad x_2(t) = X_2 e^{i\omega t}$$

. . . **(4.5)**

Upon substitution of *Equations 4.3 and 4.5* into *Equation 4.2* and dividing throughout by $e^{i\omega t}$, the resulting set of equations, yielding the steady-state dynamic displacement response, may be written in matrix form as in *Equation 4.6*:

$$\left(\begin{bmatrix} k_{11} & k_{12} \\ k_{12} & k_{22} \end{bmatrix} - \omega^2 \begin{bmatrix} m_{11} & m_{12} \\ m_{12} & m_{22} \end{bmatrix} + i\omega \begin{bmatrix} c_{11} & c_{12} \\ c_{12} & c_{22} \end{bmatrix} \right) \begin{bmatrix} X_1 \\ X_2 \end{bmatrix} = \begin{bmatrix} F_1 \\ F_2 \end{bmatrix}$$

. . . **(4.6)**

By defining the mass, stiffness and damping matrices and the nodal displacement and force vectors as

$$\mathbf{M} = \begin{bmatrix} m_1 & 0 \\ 0 & m_2 \end{bmatrix} \qquad \mathbf{C} = \begin{bmatrix} c_1 + c_2 & -c_2 \\ -c_2 & c_2 + c_3 \end{bmatrix} \qquad \mathbf{K} = \begin{bmatrix} k_1 + k_2 & -k_2 \\ -k_2 & k_2 + k_3 \end{bmatrix}$$

$$\mathbf{X} = \begin{Bmatrix} X_1 \\ X_2 \end{Bmatrix} \qquad \mathbf{F} = \begin{Bmatrix} F_1 \\ F_2 \end{Bmatrix}$$

Equation 4.6 can be written in matrix from as:

$$\left(\mathbf{K} - \omega^2 \cdot \mathbf{M} + i\omega \cdot \mathbf{C}\right) \cdot \mathbf{X} = \mathbf{F} \quad \text{. . . (4.7)}$$

In the context of the finite element method the damping will be represented by Rayleigh damping. The damping matrix in *Equation 4.7* may then be obtained from:

$$\mathbf{C} = \overline{\alpha} \cdot \mathbf{M} + \overline{\beta} \cdot \mathbf{K} \quad \text{. . . (4.8)}$$

where $\overline{\alpha}$ and $\overline{\beta}$ are respectively known as the mass and the stiffness proportional damping constants. These constants are determined by choosing the fractions of critical damping at two different frequencies and solving for $\overline{\alpha}$ and $\overline{\beta}$ simultaneously from *Equation 4.9* (Cook, Malkus and Plesha 1989).

$$\overline{\alpha} = 2(\xi_2 \cdot \omega_2 - \xi_1 \cdot \omega_1) / (\omega_2^2 - \omega_1^2)$$

$$\overline{\beta} = 2 \cdot \omega_1 \cdot \omega_2 (\xi_1 \cdot \omega_2 - \xi_2 \cdot \omega_1) / (\omega_2^2 - \omega_1^2) \quad \text{. . . (4.9)}$$

The stiffness, mass and damping matrices of *Equation 4.7*, can now be incorporated into a single matrix as follows:

$$\mathbf{D} = \mathbf{K} - \omega^2 \cdot \mathbf{M} + i\omega \cdot \mathbf{C} \quad \text{. . . (4.10)}$$

The matrix **D** of *Equation 4.10* is known as the pseudo-dynamic stiffness matrix. In this research the stiffness and mass matrices of *Equation 4.10*, will be written in terms of the spatial variables of the structure as obtained from the finite element method. The structural damping may be determined from the finite element method, but is most often obtained by making use of Rayleigh damping of the form shown in *Equation 4.8* (Cook, Malkus and Plesha 1989). The damping term will, however, not be used in this research

and is included only to keep the method general. Future researchers may decide upon a representation of the structure's damping that fits into the general framework of their research.

By expanding the matrix equations of *Equations 4.7 and 4.10*, *Equation 4.11* is obtained, which is valid for a n degree of freedom system.

$$\underset{n\times n}{\mathbf{D}}\cdot\underset{n\times 1}{\mathbf{X}}=\underset{n\times 1}{\mathbf{F}} \qquad \text{. . . (4.11)}$$

4.2 Element formulations used in the research

The stiffness, mass and damping matrices obtained from the finite element method, depend on the formulation of the specific element used to represent the structure. In this research two different types of elements will be considered:

1. Straight, one-dimensional beam elements with three degrees of freedom per node
2. Flat, straight-sided, Kirchoff plate elements with five degrees of freedom per node

These elements will now be discussed separately.

4.2.1 Beam element

A schematic representation of the beam element used, with it's degrees of freedom

$$Dof=\{u_1,w_1,\theta_1,u_2,w_2,\theta_2\}$$

is shown in *Figure 4.2*. This element is generally known as a plane frame element and the element matrices are obtained from a simple matrix summation of the linear rod and beam element matrices. These matrices will now be discussed separately.

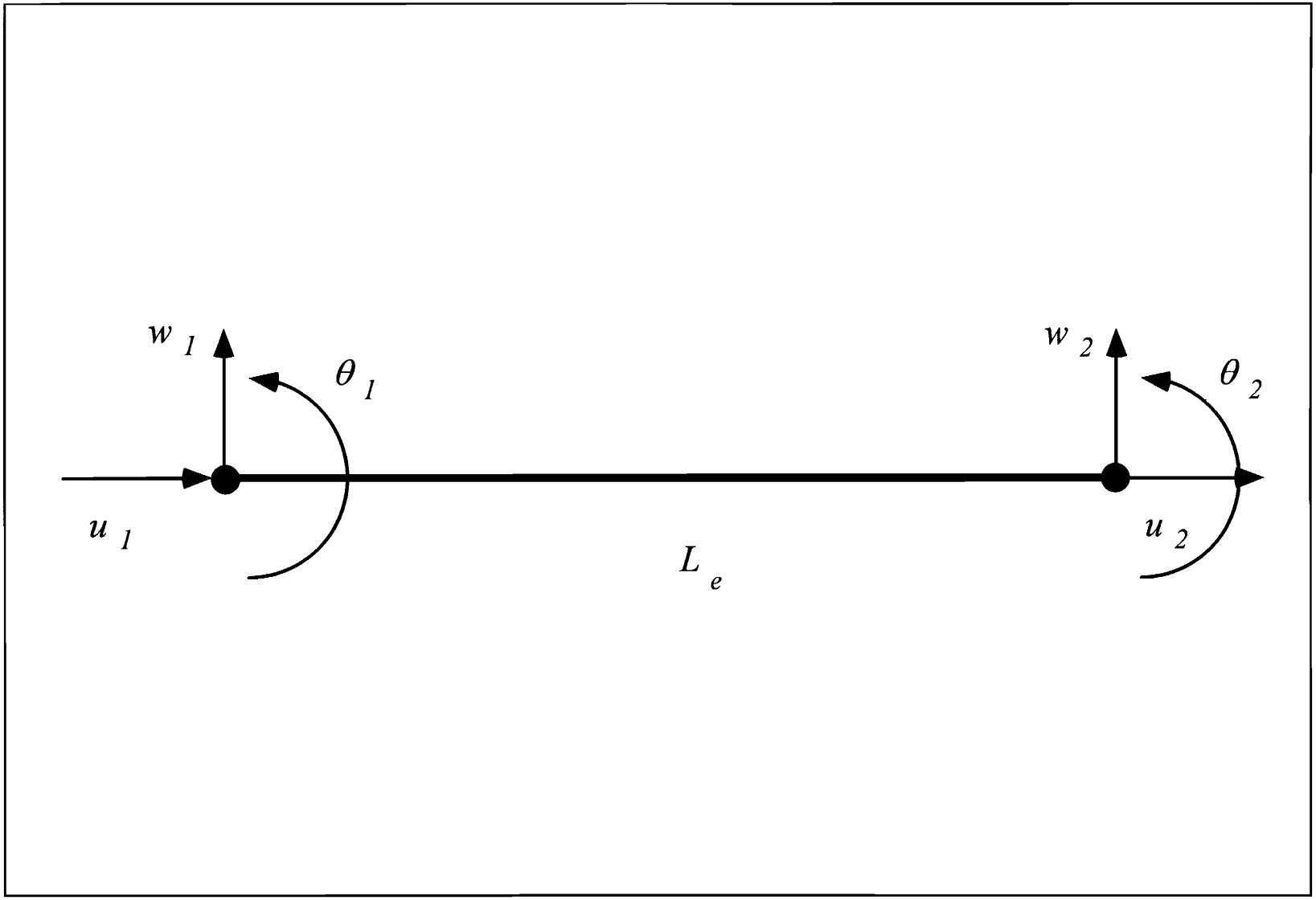

Figure 4.2: Modified beam element with three degrees of freedom per node

Linear rod element: This element is based on a linear axial displacement field which may be written as (Cook, Malkus and Plesha 1989):

$$\phi(x) = a_1 + a_2 \cdot x$$

. . . **(4.12)**

This displacement field may be written in terms of the nodal displacements and the shape functions for the element as

$$u(\xi) = \mathbf{N}^T \cdot \begin{Bmatrix} u_1 \\ u_2 \end{Bmatrix}$$

. . . **(4.13)**

where the linear Lagranian shape functions are defined in terms of the local coordinate, ξ, of the element as:

$$\mathbf{N}_{LinearRod} = \begin{bmatrix} \frac{1-\xi}{2} \\ \frac{1+\xi}{2} \end{bmatrix} \quad \text{with } -1 \le \xi \le 1$$

. . . **(4.14)**

The element stiffness matrix may be obtained by writing the potential energy stored in the element in terms of the assumed strain-displacement and stress-strain relationships as well as the specific shape functions for the element, in order to obtain:

$$\mathbf{K} = \int_{-1}^{1} \left(\mathbf{B}^T \cdot AE \cdot \mathbf{B} \right) \cdot \frac{dx}{d\xi} \cdot d\xi \text{ with } B_i = \frac{\partial N_i(\xi)}{\partial \xi} \cdot \frac{\partial \xi}{\partial x}$$

. . . **(4.15)**

B is known as the strain-displacement vector while AE is obtained from the stress-strain relationship. *Equation 4.16* shows the resulting element stiffness matrix for an element along the x-axis. The matrix is expanded to a six by six matrix in order to accommodate the degrees of freedom of the beam element in the matrix summation used

to construct the stiffness matrix of the plane frame element.

$$\mathbf{K}_{LinearRod} = \frac{AE}{L}\begin{bmatrix} 1 & 0 & 0 & -1 & 0 & 0 \\ 0 & 0 & 0 & 0 & 0 & 0 \\ 0 & 0 & 0 & 0 & 0 & 0 \\ -1 & 0 & 0 & 1 & 0 & 0 \\ 0 & 0 & 0 & 0 & 0 & 0 \\ 0 & 0 & 0 & 0 & 0 & 0 \end{bmatrix}$$

. . . **(4.16)**

Beam element: For the beam element a cubic, transverse displacement field of the form (Cook, Malkus and Plesha 1989)

$$\phi(x) = a_1 + a_2 \cdot x + a_3 \cdot x^2 + a_4 \cdot x^3$$

. . . **(4.17)**

will be assumed. This displacement field may be written in terms of the nodal displacements and rotations, as well as the shape functions, as:

$$w(\xi) = \mathbf{N}^T \cdot \begin{Bmatrix} w_1 \\ \theta_1 \\ w_2 \\ \theta_2 \end{Bmatrix}$$

. . . **(4.18)**

where the cubic Hermetian shape functions, defined in terms of the local coordinate of the element, ξ, and the element length, L_e, are given by:

$$\mathbf{N}_{Beam} = \begin{bmatrix} \frac{2-3\xi+\xi^3}{4} \\ \frac{L_e(1-\xi-\xi^2+\xi^3)}{8} \\ \frac{2+3\xi-\xi^3}{4} \\ \frac{L_e(-1-\xi+\xi^2+\xi^3)}{8} \end{bmatrix} \qquad \text{with } -1 \le \xi \le 1$$

. . . **(4.19)**

The stiffness matrix for the beam element are obtained by writing the potential energy stored in the element in terms of the assumed curvature-displacement and momentum-curvature relationships, yielding:

$$\mathbf{K} = \int_{-1}^{1} \left(\mathbf{B}^T \cdot EI \cdot \mathbf{B}\right) \cdot \frac{dx}{d\xi} \cdot d\xi \text{ with } B_i = \frac{\partial}{\partial \xi} \cdot \left(\frac{\partial N_i(\xi)}{\partial \xi} \cdot \frac{\partial \xi}{\partial x} \right) \cdot \frac{\partial \xi}{\partial x}$$

. . . **(4.20)**

In this case **B** is defined as the curvature-displacement vector and *EI* is obtained from the stress-strain relationship.

The resulting stiffness matrix for a beam element along the *x*-axis, is shown in *Equation 4.21.* Once again the matrix is expanded in order to accommodate the degrees of freedom of the linear rod element in the matrix summation used to obtain the stiffness matrix of the plane frame element.

$$\mathbf{K}_{Beam} = \frac{EI}{L^3} \begin{bmatrix} 0 & 0 & 0 & 0 & 0 & 0 \\ 0 & 12 & 6L & 0 & -12 & 6L \\ 0 & 6L & 4L^2 & 0 & -6L & 2L^2 \\ 0 & 0 & 0 & 0 & 0 & 0 \\ 0 & -12 & -6L & 0 & 12 & -6L \\ 0 & 6L & 2L^2 & 0 & -6L & 4L^2 \end{bmatrix}$$

. . . **(4.21)**

The stiffness matrix of the plane frame element is obtained from *Equations 4.16 and 4.21* as shown in *Equation 4.22.*

$$\mathbf{K}_{Total} = \mathbf{K}_{LinearRod} + \mathbf{K}_{Beam} \qquad \text{. . . (4.22)}$$

Furthermore, a lumped-mass matrix, with no mass on the rotational degrees of freedom (this is consistent with Euler-Bernoulli beam theory (Meirovitch 1986)), will be used for this element. The element mass matrix will be formed from a matrix summation of the rod and beam element matrices. A general scheme for obtaining the final six by six lumped mass matrix in terms of the mass density, ρ, element length, L_e, and element area, A_e, may be written as:

$$M_{11} = M_{22} = M_{44} = M_{55} = \frac{1}{2} \cdot \rho \cdot L_e \cdot A_e$$

$$\text{all other} \quad M_{ij} = 0 \qquad i, j \in [1,6] \qquad \text{. . . (4.23)}$$

4.2.2 Plate element

The plate element used in this study is shown in *Figure 4.3*. This element has five degrees of freedom per node as follows

$$Dof = \{u_1, v_1, w_1, \theta_{x1}, \theta_{z1}, u_2, v_2, w_2, \theta_{x2}, \theta_{z2}, u_3, v_3, w_3, \theta_{x3}, \theta_{z3}, u_4, v_4, w_4, \theta_{x4}, \theta_{z4}\}$$

and consist of a combination of a bi-linear plane stress element (Cook, Malkus and Plesha 1989) and a Kirchoff plate element (Haug, Choi and Komkov 1986). The element stiffness matrix will again be constructed from a matrix summation of the stiffness matrices of the plane stress and the Kirchoff plate elements. The plane stress and Kirchoff plate elements will now be discussed separately.

Plane-Stress element: This element is based on an assumed bi-linear, in-plane displacement field which may be written as:

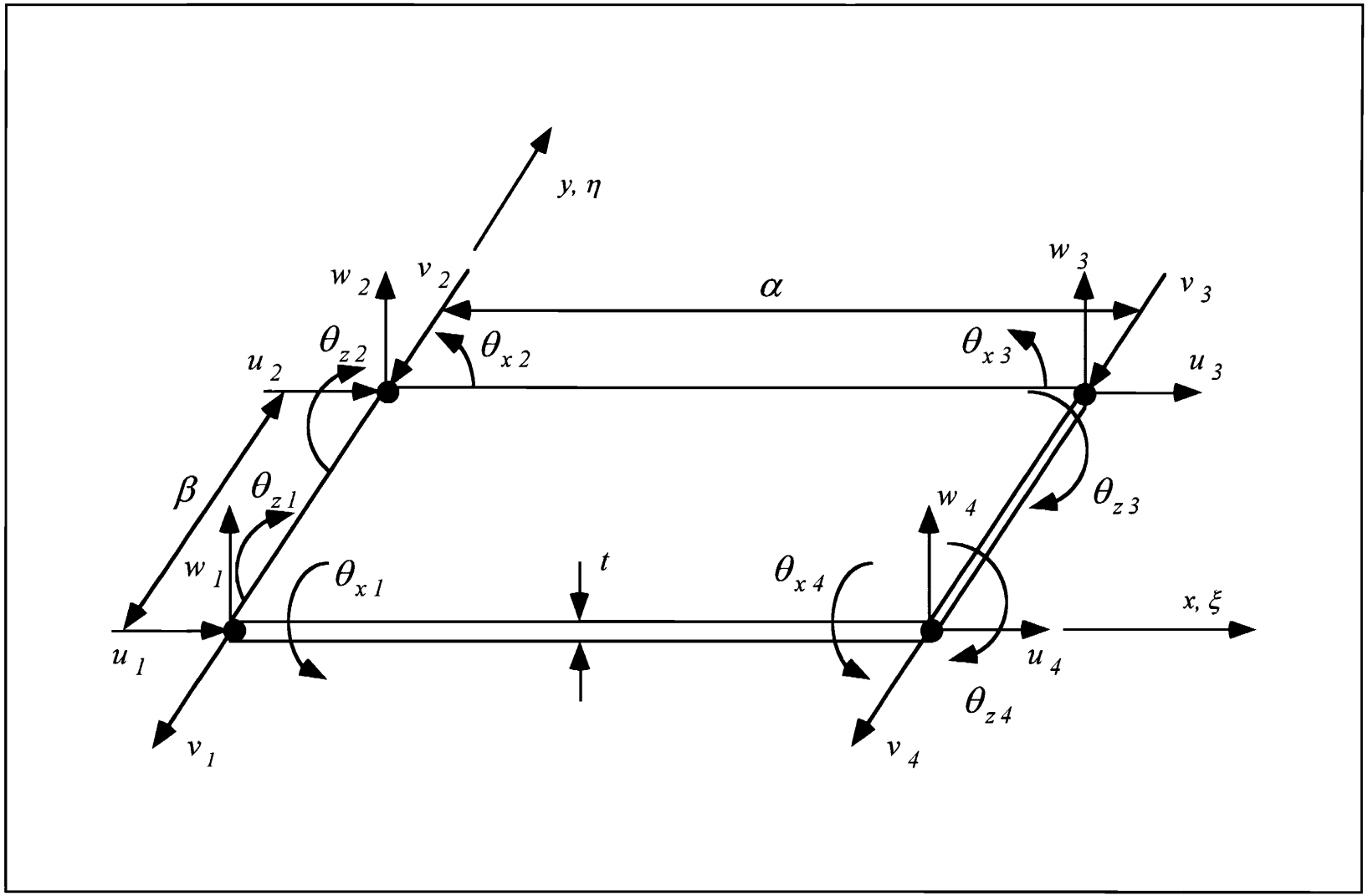

Figure 4.3: Modified plate element with five degrees of freedom per node

$$\phi(x,y) = a_1 + a_2 \cdot x + a_3 \cdot x \cdot y + a_4 \cdot y$$

. . . **(4.24)**

This displacement field may be written in terms of the nodal displacements and the shape functions as:

$$\begin{Bmatrix} u(\xi,\eta) \\ v(\xi,\eta) \end{Bmatrix} = \mathbf{N}^T \cdot \begin{Bmatrix} u_1 \\ v_1 \\ u_2 \\ \vdots \\ v_4 \end{Bmatrix}$$

. . . **(4.25)**

The bi-linear Lagranian shape functions for this element are defined in terms of the local coordinates of the element, ξ and η (*Figure 4.3*), and may be written as:

$$\mathbf{N}^T_{PlaneStress} = \begin{bmatrix} (\xi-1)(\eta-1) \\ (1-\xi)\eta \\ \xi\eta \\ (1-\eta)\xi \end{bmatrix} \quad with \quad 0 \le \xi, \eta \le 1$$

. . . **(4.26)**

As in the case for the one-dimensional rod element, the stiffness matrix for this plane stress element may be obtained by writing the potential energy stored in the element in terms of the assumed strain-displacement and stress-strain relationships. For the two-dimensional plane stress element, the assumed strain-displacement and stress-strain relationships may be written in matrix form as:

$$\begin{Bmatrix} \varepsilon_x \\ \varepsilon_y \\ \gamma_{xy} \end{Bmatrix} = \underset{3\times 8}{\mathbf{B}} \cdot \begin{Bmatrix} u_1 \\ v_1 \\ u_2 \\ \vdots \\ v_4 \end{Bmatrix} \qquad \begin{Bmatrix} \sigma_x \\ \sigma_y \\ \tau_{xy} \end{Bmatrix} = \underset{3\times 3}{\mathbf{E}} \cdot \begin{Bmatrix} \varepsilon_x \\ \varepsilon_y \\ \gamma_{xy} \end{Bmatrix}$$

. . . **(4.27)**

where the strain-displacement matrix, **B**, and the stress strain matrix, **E**, is defined for the plane stress element as shown in *Equation 4.28*.

$$\underset{3\times 8}{\mathbf{B}} = \begin{bmatrix} \frac{\partial N_1}{\partial x} & 0 & \frac{\partial N_2}{\partial x} & 0 & \cdots \\ 0 & \frac{\partial N_1}{\partial y} & 0 & \frac{\partial N_2}{\partial y} & \cdots \\ \frac{\partial N_1}{\partial y} & \frac{\partial N_1}{\partial x} & \frac{\partial N_2}{\partial y} & \frac{\partial N_2}{\partial x} & \cdots \end{bmatrix} \qquad \underset{3\times 3}{\mathbf{E}} = \frac{E}{1-\nu^2} \begin{bmatrix} 1 & \nu & 0 \\ \nu & 1 & 0 \\ 0 & 0 & \frac{1-\nu}{2} \end{bmatrix}$$

. . . **(4.28)**

The stiffness matrix may be defined in the local coordinates of the element, in terms of the strain-displacement matrix and the stress-strain matrices (*Equation 4.28*), the element thickness, t, and the determinant of the Jacobian matrix ,$|\mathbf{J}|$, as:

$$\mathbf{K} = \int_0^1 \int_0^1 \left(\mathbf{B}^T \cdot \mathbf{E} \cdot \mathbf{B}\right) \cdot t \cdot |\mathbf{J}| \cdot d\xi \cdot d\eta$$

. . . **(4.29)**

Evaluation of *Equation 4.29* for a rectangular element with sides along the x and y-axes respectively, yields the following stiffness matrix for the plane-stress element:

$$\mathbf{K}_{PlaneStress} = \frac{E \cdot t}{24 \cdot \alpha \cdot \beta \cdot (\nu^2 - 1)} \cdot \begin{bmatrix} \mathbf{k}_{I,I} & \mathbf{k}_{II,I} \\ \mathbf{k}_{II,I} & \mathbf{k}_{II,II} \end{bmatrix}$$

. . . **(4.30)**

E is the Young's Modulus, t the thickness and ν the Poisson's ratio of the element, while α and β is the length of the element along the x and y-axes respectively (*Figure 4.3*). The submatrices $\mathbf{k}_{I,I}$, $\mathbf{k}_{II,I}$ and $\mathbf{k}_{II,II}$ are shown in *Figures 4.4*. As before these matrices are expanded to accommodate the degrees of freedom of the Kirchoff plate element during the matrix summation required to obtain the combined element.

Kirchoff plate element: This element is based on an assumed cubic, transverse displacement field which may be written as:

$$\phi(x,y) = 1 + a_1 \cdot x + a_2 \cdot y + a_3 \cdot x^2 + a_4 \cdot x \cdot y + a_5 \cdot y^2 + a_6 \cdot x^3 + a_7 \cdot x^2 \cdot y + a_8 \cdot x \cdot y^2 + a_9 \cdot y^3 + a_{10} \cdot x^3 \cdot y + a_{11} \cdot x \cdot y^3 \quad \text{. . . (4.31)}$$

This displacement field may be written in terms of the nodal displacements and the shape functions as:

$$w(\xi,\eta) = \mathbf{N}^T \cdot \begin{Bmatrix} w_1 \\ \theta_{x1} \\ \theta_{z1} \\ \vdots \\ \theta_{z4} \end{Bmatrix} \quad \text{. . . (4.32)}$$

As for the beam element, Hermitian shape functions will be used. These shape functions may be written in terms of the local coordinates of the element, ξ and η, and the element length, α and β, along the x and y-axes respectively as (*Figure 4.3*):

$$\mathbf{k}_{I,I} = \begin{bmatrix} 4(-\alpha^2 - 2\beta^2 + \alpha^2\nu) & & & & & & & & \\ -3\alpha\beta(\nu+1) & 4(-2\alpha^2 - \beta^2 + \beta^2\nu) & & & & & & & \\ 0 & 0 & 0 & & & & & & \\ 0 & 0 & 0 & 0 & & & & & \\ 0 & 0 & 0 & 0 & 0 & & & & \\ 4(\alpha^2 - \beta^2 - \alpha^2\nu) & -3\alpha\beta(3\nu-1) & 0 & 0 & 0 & 4(-\alpha^2 - 2\beta^2 + \alpha^2\nu) & & & \\ 3\alpha\beta(3\nu-1) & 2(4\alpha^2 - \beta^2 + \beta^2\nu) & 0 & 0 & 0 & 3\alpha\beta(\nu+1) & 4(-2\alpha^2 - \beta^2 + \beta^2\nu) & & \\ 0 & 0 & 0 & 0 & 0 & 0 & 0 & 0 & \\ 0 & 0 & 0 & 0 & 0 & 0 & 0 & 0 & 0 \\ 0 & 0 & 0 & 0 & 0 & 0 & 0 & 0 & 0 \end{bmatrix}$$

Symmetric

$$\mathbf{k}_{II,I} = \begin{bmatrix} 2(\alpha^2 + 2\beta^2 - \alpha^2\nu) & 3\alpha\beta(\nu+1) & 0 & 0 & 0 & 2(-\alpha^2 + 4\beta^2 + \alpha^2\nu) & -3\alpha\beta(3\nu-1) & 0 & 0 & 0 \\ 3\alpha\beta(\nu+1) & 2(2\alpha^2 + \beta^2 - \beta^2\nu) & 0 & 0 & 0 & 3\alpha\beta(3\nu-1) & 4(-\alpha^2 + \beta^2 - \beta^2\nu) & 0 & 0 & 0 \\ 0 & 0 & 0 & 0 & 0 & 0 & 0 & 0 & 0 & 0 \\ 0 & 0 & 0 & 0 & 0 & 0 & 0 & 0 & 0 & 0 \\ 0 & 0 & 0 & 0 & 0 & 0 & 0 & 0 & 0 & 0 \\ 2(-\alpha^2 + 4\beta^2 + \alpha^2\nu) & 3\alpha\beta(3\nu-1) & 0 & 0 & 0 & 2(\alpha^2 + 2\beta^2 - \alpha^2\nu) & -3\alpha\beta(\nu+1) & 0 & 0 & 0 \\ 3\alpha\beta(3\nu-1) & 4(-\alpha^2 + \beta^2 - \beta^2\nu) & 0 & 0 & 0 & -3\alpha\beta(\nu+1) & 2(2\alpha^2 + \beta^2 - \beta^2\nu) & 0 & 0 & 0 \\ 0 & 0 & 0 & 0 & 0 & 0 & 0 & 0 & 0 & 0 \\ 0 & 0 & 0 & 0 & 0 & 0 & 0 & 0 & 0 & 0 \\ 0 & 0 & 0 & 0 & 0 & 0 & 0 & 0 & 0 & 0 \end{bmatrix}$$

$$\mathbf{k}_{II,II} = \begin{bmatrix} 4(-\alpha^2 - 2\beta^2 + \alpha^2\nu) & & & & & & & & \\ -3\alpha\beta(\nu+1) & 4(-2\alpha^2 - \beta^2 + \beta^2\nu) & & & & & & & \\ 0 & 0 & 0 & & & & & & \\ 0 & 0 & 0 & 0 & & & & & \\ 0 & 0 & 0 & 0 & 0 & & & & \\ 4(\alpha^2 - \beta^2 - \alpha^2\nu) & -3\alpha\beta(3\nu-1) & 0 & 0 & 0 & 4(-\alpha^2 - 2\beta^2 + \alpha^2\nu) & & & \\ 3\alpha\beta(3\nu-1) & 2(4\alpha^2 - \beta^2 + \beta^2\nu) & 0 & 0 & 0 & 3\alpha\beta(\nu+1) & 4(-2\alpha^2 - \beta^2 + \beta^2\nu) & & \\ 0 & 0 & 0 & 0 & 0 & 0 & 0 & 0 & \\ 0 & 0 & 0 & 0 & 0 & 0 & 0 & 0 & 0 \\ 0 & 0 & 0 & 0 & 0 & 0 & 0 & 0 & 0 \end{bmatrix}$$

Symmetric

Figure 4.4: Submatrices for the rectangular plane-stress element

$$\mathbf{N}_{Plate}^{T} = \begin{bmatrix} 1-\xi\eta-(3-2\xi)\xi^2(1-\eta)-(1-\xi)(3-2\eta)\eta^2 \\ (1-\xi)\eta(1-\eta)^2\beta \\ -\xi(1-\xi)^2(1-\eta)\alpha \\ (1-\xi)(3-2\eta)\eta^2+\xi(1-\xi)(1-2\xi)\eta \\ -(1-\xi)(1-\eta)\eta^2\beta \\ -\xi(1-\xi)^2\eta\alpha \\ (3-2\xi)\xi^2\eta-\xi\eta(1-\eta)(1-2\eta) \\ -\xi(1-\eta)\eta^2\beta \\ (1-\xi)\xi^2\eta\alpha \\ (3-2\xi)\xi^2(1-\eta)+\xi\eta(1-\eta)(1-2\eta) \\ \xi\eta(1-\eta)^2\beta \\ (1-\xi)\xi^2(1-\eta)\alpha \end{bmatrix} \quad \text{with} \quad 0 \le \xi, \eta \le 1$$

. . . (4.33)

As for the beam element the element stiffness matrix may be obtained from the assumed curvature-displacement and moment-curvature relationships. These relationships yield a curvature-displacement (**B**) and a moment-curvature ($\mathbf{D}_c$) matrix (similar to the plane-stress element). The resulting definition of the stiffness matrix from these relationships, may be written in terms of the local coordinates of the element , the element thickness, t, and the determinant of the Jacobian matrix, $|\mathbf{J}|$, as:

$$\mathbf{K} = \int_0^1 \int_0^1 \left(\mathbf{B}^T \cdot \mathbf{D}_c \cdot \mathbf{B}\right) \cdot t \cdot |\mathbf{J}| \cdot d\xi \cdot d\eta$$

. . . (4.34)

Evaluation of *Equation 4.34* yields the element stiffness matrix for the Kirchoff plate element. Only rectangular elements (*Figure 4.3*) will be considered in this research and the stiffness matrix for a rectangular element may be written as

$$\mathbf{K}_{Plate} = \frac{E \cdot t^3}{12 \cdot \alpha \cdot \beta \cdot (\nu^2 - 1)} \cdot \begin{bmatrix} \mathbf{k}_{I,I} & \mathbf{k}_{II,I} \\ \mathbf{k}_{II,I} & \mathbf{k}_{II,II} \end{bmatrix}$$

. . . (4.35)

where the submatrices for the rectangular element (already expanded as before) are shown in *Figure 4.5* with γ representing the aspect ratio of the rectangular element (i.e. β/α). The element stiffness matrix for a rectangular element may then be obtained from a simple matrix summation of the plane-stress and Kirchoff plate element matrices as follows:

$$\mathbf{K}_{Total} = \mathbf{K}_{PlaneStress} + \mathbf{K}_{Plate} \qquad \ldots \textbf{(4.36)}$$

For this element a consistent mass matrix will be used. The mass matrix for each of the two elements (plane-stress element and Kirchoff plate element) may be obtained by making use of the appropriate shape functions in evaluating *Equation 4.37*. The element mass matrices are shown in *Figures 4.6 and 4.7* respectively.

$$\mathbf{M} = \int_0^1 \int_0^1 \rho \cdot \mathbf{N}^T \cdot \mathbf{N} \cdot t \cdot |\mathbf{J}| \cdot d\xi \cdot d\eta \qquad \ldots \textbf{(4.37)}$$

Once again the total mass matrix for the combined element may be obtained from a matrix summation of the plane-stress and the Kirchoff plate elements, as shown in *Equation 4.38*:

$$\mathbf{M}_{Total} = \mathbf{M}_{PlaneStress} + \mathbf{M}_{Plate} \qquad \ldots \textbf{(4.38)}$$

4.3 Test case

Since the components of the modeled, steady-state velocity terms in the error function will be determined from the frequency response formulation, the accuracy and validity of the method within the context of this research is important. In order to validate the use of the frequency response formulation, a test case with a closed-form solution will be set up and evaluated. The results obtained from both the beam as well as the plate elements will then be compared to the results obtained from the closed-form solution.

$$\mathbf{k}_{I,I} = \begin{bmatrix}
0 & & & & & & & & & \\
0 & 0 & & & & & & & & \\
0 & 0 & 4(\gamma^2+\gamma^{-2})+\tfrac{1}{5}(14-4\nu) & & & & & & & \\
0 & 0 & \left[2\gamma^{-2}+\tfrac{1}{5}(1+4\nu)\right]\beta & \left[\tfrac{4}{3}\gamma^{-2}+\tfrac{4}{15}(1-\nu)\right]\beta^2 & & & & & & \\
0 & 0 & -\left[2\gamma^2+\tfrac{1}{5}(1+4\nu)\right]\alpha & -\nu\alpha\beta & \left[\tfrac{4}{3}\gamma^2+\tfrac{4}{15}(1-\nu)\right]\alpha^2 & & & & & \\
0 & 0 & 0 & 0 & 0 & 0 & & & & \\
0 & 0 & 0 & 0 & 0 & 0 & 0 & & & \\
0 & 0 & 2(\gamma^2-2\gamma^{-2})-\tfrac{1}{5}(14-4\nu) & -\left[2\gamma^{-2}+\tfrac{1}{5}(1-\nu)\right]\beta & \left[-\gamma^2+\tfrac{1}{5}(1+4\nu)\right]\alpha & 0 & 0 & 4(\gamma^2+\gamma^{-2})+\tfrac{1}{5}(14-4\nu) & & \\
0 & 0 & \left[2\gamma^{-2}+\tfrac{1}{5}(1-\nu)\right]\beta & \left[\tfrac{2}{3}\gamma^{-2}-\tfrac{1}{15}(1-\nu)\right]\beta^2 & 0 & 0 & 0 & -\left[2\gamma^{-2}+\tfrac{1}{5}(1+4\nu)\right]\beta & \left[\tfrac{4}{3}\gamma^{-2}+\tfrac{4}{15}(1-\nu)\right]\beta^2 & \\
0 & 0 & \left[-\gamma^2+\tfrac{1}{5}(1+4\nu)\right]\alpha & 0 & \left[\tfrac{2}{3}\gamma^2-\tfrac{4}{15}(1-\nu)\right]\alpha^2 & 0 & 0 & -\left[2\gamma^2+\tfrac{1}{5}(1+4\nu)\right]\alpha & \nu\alpha\beta & \left[\tfrac{4}{3}\gamma^2+\tfrac{4}{15}(1-\nu)\right]\alpha^2
\end{bmatrix}$$

Symmetric

$$\mathbf{k}_{II,I} = \begin{bmatrix}
0 & 0 & 0 & 0 & 0 & 0 & 0 & 0 & 0 & 0 \\
0 & 0 & 0 & 0 & 0 & 0 & 0 & 0 & 0 & 0 \\
0 & 0 & -2(\gamma^2+\gamma^{-2})+\tfrac{1}{5}(14-4\nu) & \left[-\gamma^{-2}+\tfrac{1}{5}(1-\nu)\right]\beta & \left[\gamma^2-\tfrac{1}{5}(1-\nu)\right]\alpha & 0 & 0 & -2(2\gamma^2-\gamma^{-2})-\tfrac{1}{5}(14-4\nu) & \left[-\gamma^{-2}+\tfrac{1}{5}(1+4\nu)\right]\beta & \left[2\gamma^2+\tfrac{1}{5}(1-\nu)\right]\alpha \\
0 & 0 & \left[\gamma^{-2}-\tfrac{1}{5}(1-\nu)\right]\beta & \left[\tfrac{1}{3}\gamma^{-2}+\tfrac{1}{15}(1-\nu)\right]\beta^2 & 0 & 0 & 0 & \left[-\gamma^{-2}+\tfrac{1}{5}(1+4\nu)\right]\beta & \left[\tfrac{2}{3}\gamma^{-2}-\tfrac{4}{15}(1-\nu)\right]\beta^2 & 0 \\
0 & 0 & \left[-\gamma^2+\tfrac{1}{5}(1-\nu)\right]\alpha & 0 & \left[\tfrac{1}{3}\gamma^2+\tfrac{1}{15}(1-\nu)\right]\alpha^2 & 0 & 0 & -\left[2\gamma^2+\tfrac{1}{5}(1-\nu)\right]\alpha & 0 & \left[\tfrac{2}{3}\gamma^2-\tfrac{1}{15}(1-\nu)\right]\alpha^2 \\
0 & 0 & 0 & 0 & 0 & 0 & 0 & 0 & 0 & 0 \\
0 & 0 & 0 & 0 & 0 & 0 & 0 & 0 & 0 & 0 \\
0 & 0 & -2(2\gamma^2-\gamma^{-2})-\tfrac{1}{5}(14-4\nu) & \left[\gamma^{-2}-\tfrac{1}{5}(1+4\nu)\right]\beta & \left[2\gamma^2+\tfrac{1}{5}(1-\nu)\right]\alpha & 0 & 0 & -2(\gamma^2+\gamma^{-2})+\tfrac{1}{5}(14-4\nu) & \left[\gamma^{-2}-\tfrac{1}{5}(1-\nu)\right]\beta & \left[\gamma^2-\tfrac{1}{5}(1-\nu)\right]\alpha \\
0 & 0 & \left[\gamma^{-2}-\tfrac{1}{5}(1+4\nu)\right]\beta & \left[\tfrac{2}{3}\gamma^{-2}-\tfrac{4}{15}(1-\nu)\right]\beta^2 & 0 & 0 & 0 & \left[-\gamma^{-2}+\tfrac{1}{5}(1-\nu)\right]\beta & \left[\tfrac{1}{3}\gamma^{-2}+\tfrac{1}{15}(1-\nu)\right]\beta^2 & 0 \\
0 & 0 & -2\left[\gamma^2+\tfrac{1}{5}(1-\nu)\right]\alpha & 0 & \left[\tfrac{2}{3}\gamma^2-\tfrac{1}{15}(1-\nu)\right]\alpha^2 & 0 & 0 & \left[-\gamma^{-2}+\tfrac{1}{5}(1-\nu)\right]\alpha & 0 & \left[\tfrac{1}{3}\gamma^2+\tfrac{1}{15}(1-\nu)\right]\alpha^2
\end{bmatrix}$$

$$\mathbf{k}_{II,II} = \begin{bmatrix}
0 & & & & & & & & & \\
0 & 0 & & & & & & & & \\
0 & 0 & 4(\gamma^2+\gamma^{-2})+\tfrac{1}{5}(14-4\nu) & & & & & & & \\
0 & 0 & -\left[2\gamma^{-2}+\tfrac{1}{5}(1+4\nu)\right]\beta & \left[\tfrac{4}{3}\gamma^{-2}+\tfrac{4}{15}(1-\nu)\right]\beta^2 & & & & & & \\
0 & 0 & \left[2\gamma^2+\tfrac{1}{5}(1+4\nu)\right]\alpha & -\nu\alpha\beta & \left[\tfrac{4}{3}\gamma^2+\tfrac{4}{15}(1-\nu)\right]\alpha^2 & & & & & \\
0 & 0 & 0 & 0 & 0 & 0 & & & & \\
0 & 0 & 0 & 0 & 0 & 0 & 0 & & & \\
0 & 0 & 2(\gamma^2-2\gamma^{-2})-\tfrac{1}{5}(14-4\nu) & \left[2\gamma^{-2}+\tfrac{1}{5}(1-\nu)\right]\beta & \left[\gamma^2-\tfrac{1}{5}(1+4\nu)\right]\alpha & 0 & 0 & 4(\gamma^2+\gamma^{-2})+\tfrac{1}{5}(14-4\nu) & & \\
0 & 0 & -\left[2\gamma^{-2}+\tfrac{1}{5}(1-\nu)\right]\beta & \left[\tfrac{2}{3}\gamma^{-2}-\tfrac{1}{15}(1-\nu)\right]\beta^2 & 0 & 0 & 0 & \left[2\gamma^{-2}+\tfrac{1}{5}(1+4\nu)\right]\beta & \left[\tfrac{4}{3}\gamma^{-2}+\tfrac{4}{15}(1-\nu)\right]\beta^2 & \\
0 & 0 & \left[\gamma^2-\tfrac{1}{5}(1+4\nu)\right]\alpha & 0 & \left[\tfrac{2}{3}\gamma^2-\tfrac{4}{15}(1-\nu)\right]\alpha^2 & 0 & 0 & \left[2\gamma^2+\tfrac{1}{5}(1+4\nu)\right]\alpha & \nu\alpha\beta & \left[\tfrac{4}{3}\gamma^2+\tfrac{4}{15}(1-\nu)\right]\alpha^2
\end{bmatrix}$$

Symmetric

Figure 4.5: Submatrices for the rectangular Kirchoff plate element

$$\mathbf{M}_{PlaneStress} = \frac{\alpha \cdot \beta \cdot \rho \cdot t}{36}$$

$$\begin{bmatrix}
4 & & & & & & & & & & & & & & & & & & & \\
0 & 4 & & & & & & & & & & & & & & & & & & \\
0 & 0 & 0 & & & & & & & & & & & & & & & & & \\
0 & 0 & 0 & 0 & & & & & & & & & & & & & & & & \\
0 & 0 & 0 & 0 & 0 & & & & & & & & & & & & & & & \\
2 & 0 & 0 & 0 & 0 & 4 & & & & & & & & & & & & & & \\
0 & 2 & 0 & 0 & 0 & 0 & 4 & & & & & & & & & & & & & \\
0 & 0 & 0 & 0 & 0 & 0 & 0 & 0 & & & & & & & & & & & & \\
0 & 0 & 0 & 0 & 0 & 0 & 0 & 0 & 0 & & & & & & & & & & & \\
0 & 0 & 0 & 0 & 0 & 0 & 0 & 0 & 0 & 0 & & & & & & & & & & \\
1 & 0 & 0 & 0 & 0 & 2 & 0 & 0 & 0 & 0 & 4 & & & & & & & & & \\
0 & 1 & 0 & 0 & 0 & 0 & 2 & 0 & 0 & 0 & 0 & 4 & & & & & & & & \\
0 & 0 & 0 & 0 & 0 & 0 & 0 & 0 & 0 & 0 & 0 & 0 & 0 & & & & & & & \\
0 & 0 & 0 & 0 & 0 & 0 & 0 & 0 & 0 & 0 & 0 & 0 & 0 & 0 & & & & & & \\
0 & 0 & 0 & 0 & 0 & 0 & 0 & 0 & 0 & 0 & 0 & 0 & 0 & 0 & 0 & & & & & \\
2 & 0 & 0 & 0 & 0 & 1 & 0 & 0 & 0 & 0 & 2 & 0 & 0 & 0 & 0 & 4 & & & & \\
1 & 2 & 0 & 0 & 0 & 0 & 1 & 0 & 0 & 0 & 0 & 2 & 0 & 0 & 0 & 0 & 4 & & & \\
0 & 0 & 0 & 0 & 0 & 0 & 0 & 0 & 0 & 0 & 0 & 0 & 0 & 0 & 0 & 0 & 0 & 0 & & \\
0 & 0 & 0 & 0 & 0 & 0 & 0 & 0 & 0 & 0 & 0 & 0 & 0 & 0 & 0 & 0 & 0 & 0 & 0 & \\
0 & 0 & 0 & 0 & 0 & 0 & 0 & 0 & 0 & 0 & 0 & 0 & 0 & 0 & 0 & 0 & 0 & 0 & 0 & 0
\end{bmatrix}$$

Symmetric

Figure 4.6: Mass matrix for the rectangular plane-stress element

$$\mathbf{M}_{Plate} = \frac{\alpha \cdot \beta \cdot \rho \cdot t}{176400}$$

$$\begin{bmatrix}
0 & & & & & & & & & & & & & & & & & & & \\
0 & 0 & & & & & & & & & & & & & & & & & & \\
0 & 0 & 24178 & & & & & & & & & & & & & & & & & \\
0 & 0 & 3227\beta & 560\beta^2 & & & & & & & & & & & & & & & & \\
0 & 0 & -3227\alpha & -441\alpha\beta & 560\alpha^2 & & & & & & & & & & & & & & & \\
0 & 0 & 0 & 0 & 0 & 0 & & & & & & & & & & & & & & \\
0 & 0 & 0 & 0 & 0 & 0 & 0 & & & & & & & & & & & & & \\
0 & 0 & 8582 & 1918\beta & -1393\alpha & 0 & 0 & 24178 & & & & & & & & & & & & \\
0 & 0 & -1918\beta & -420\beta^2 & 294\alpha\beta & 0 & 0 & -3227\beta & 560\beta^2 & & & & & & & & & & & \\
0 & 0 & -1393\alpha & -294\alpha\beta & 280\alpha^2 & 0 & 0 & -3227\alpha & 441\alpha\beta & 560\alpha^2 & & & & & & & & & & \\
0 & 0 & 0 & 0 & 0 & 0 & 0 & 0 & 0 & 0 & 0 & & & & & & & & & \\
0 & 0 & 0 & 0 & 0 & 0 & 0 & 0 & 0 & 0 & 0 & 0 & & & & & & & & \\
0 & 0 & 2758 & 812\beta & -812\alpha & 0 & 0 & 8582 & -1393\beta & -1918\alpha & 0 & 0 & 24178 & & & & & & & \\
0 & 0 & -812\beta & -210\beta^2 & 196\alpha\beta & 0 & 0 & -1393\beta & 280\beta^2 & 294\alpha\beta & 0 & 0 & -3227\beta & 560\beta^2 & & & & & & \\
0 & 0 & -812\alpha & -196\alpha\beta & -210\alpha^2 & 0 & 0 & -1918\alpha & -294\alpha\beta & -420\alpha^2 & 0 & 0 & 3227\alpha & -441\alpha\beta & 560\alpha^2 & & & & & \\
0 & 0 & 0 & 0 & 0 & 0 & 0 & 0 & 0 & 0 & 0 & 0 & 0 & 0 & 0 & 0 & & & & \\
0 & 0 & 0 & 0 & 0 & 0 & 0 & 0 & 0 & 0 & 0 & 0 & 0 & 0 & 0 & 0 & 0 & & & \\
0 & 0 & 8582 & 1393\beta & -1918\alpha & 0 & 0 & 2758 & -812\beta & -812\alpha & 0 & 0 & 8582 & -1918\beta & 1393\alpha & 0 & 0 & 24178 & & \\
0 & 0 & 1393\beta & 280\beta^2 & -294\alpha\beta & 0 & 0 & 812\beta & -210\beta^2 & -196\alpha\beta & 0 & 0 & 1918\beta & -420\beta^2 & 294\alpha\beta & 0 & 0 & 3227\beta & 560\beta^2 & \\
0 & 0 & 1918\alpha & 294\alpha\beta & -420\alpha^2 & 0 & 0 & 812\alpha & -196\alpha\beta & -210\alpha^2 & 0 & 0 & 1393\alpha & -294\alpha\beta & 210\alpha^2 & 0 & 0 & 3227\alpha & 441\alpha\beta & 560\alpha^2
\end{bmatrix}$$

Symmetric

Figure 4.7: Consistent mass matrix for the Kirchoff plate element

A cantilevered beam, rigidly fixed at the left end will be considered. The beam will be excited at the free end by a transverse, harmonic, forcing function and a schematic representation of the setup is shown in *Figure 4.8*. A 304 stainless steel beam will be used and the following geometry, material properties and excitation force is applicable:

Dimensions:	Length	=	1.3716	m
	Width	=	0.0762	m
	Thickness	=	0.00635	m
Material:	ν	=	0.27	
	E	=	196	GPa
	ρ	=	7905	kg/m^3
Load:	f_0	=	5	N
	ω	=	0.1	rad/s

4.3.1 Closed-form solution

The partial differential equation describing the vibration of a beam may be written as (Meirovitch 1986):

$$EI\frac{\partial^4 W(x,t)}{\partial x^4}+m(x)\cdot\frac{\partial^2 W(x,t)}{\partial t^2}=F(x,t) \qquad \text{. . . (4.39)}$$

Clough and Penzien (1975) derived the following fourth-order, ordinary differential equation which may be solved for the transverse, steady-state response of a vibrating beam subjected to a prescribed, transverse, harmonic forcing function:

$$w^{iv}(x)-\frac{m(x)\cdot\omega^2}{EI}\cdot w(x)=0 \qquad \text{. . . (4.40)}$$

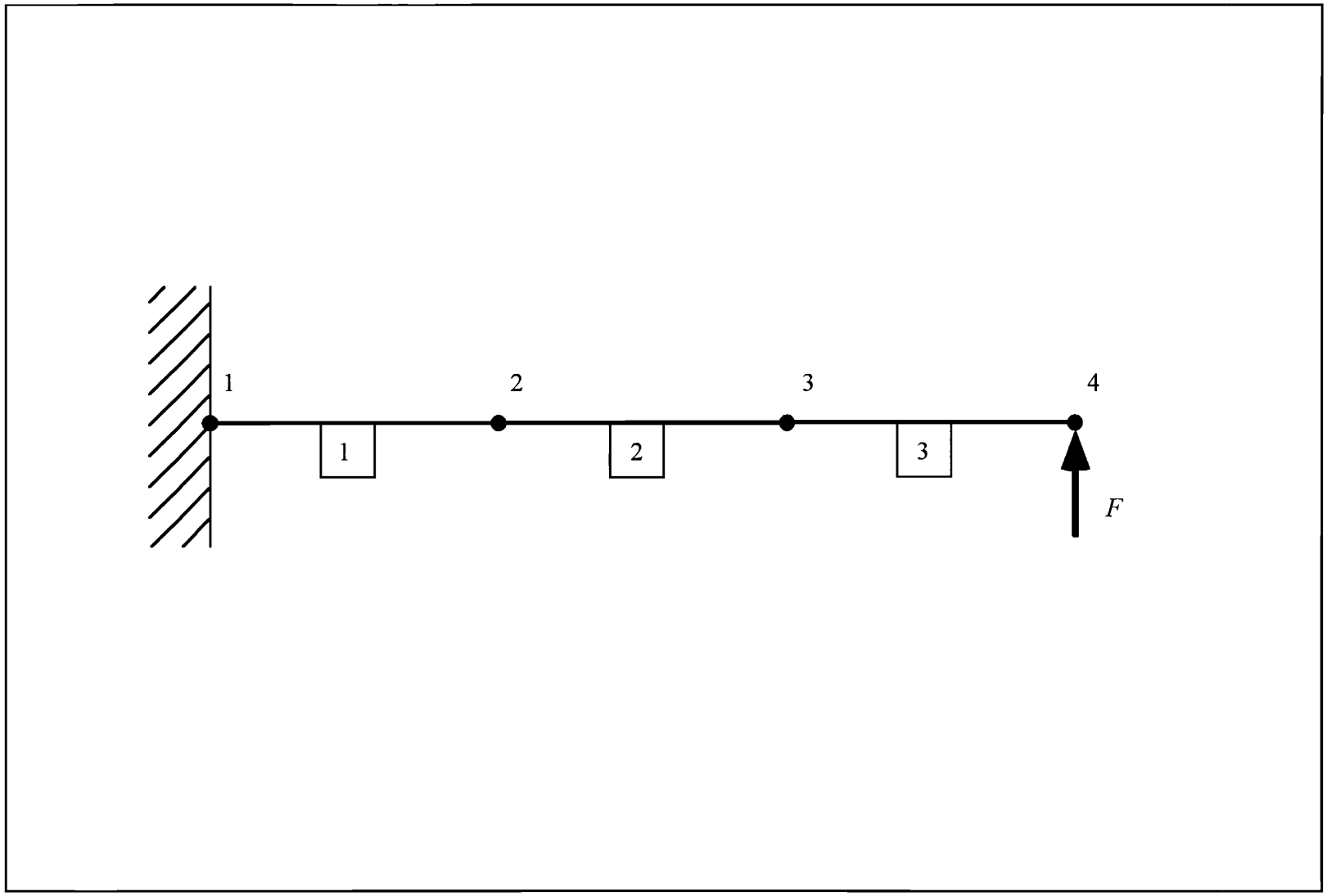

Figure 4.8: Schematic representation of the test case

In order to find a solution to *Equation 4.40*, four boundary conditions are needed. For this specific test case, these boundary conditions are given by:

- **Displacement at $x = 0$:** $w(0) = 0$
- **Slope at $x = 0$:** $w'(0) = 0$
- **Moment at $x = L$:** $EI\,w''(L) = 0$
- **Shear force at $x = L$:** $w'''(L) = -\frac{F_o}{EI}$

By making use of *Equation 4.40* and the above boundary conditions, the closed-form solution was obtained using the mathematical software package, Mathematica (Version 2.2). The obtained solution may be written as:

$$w(x) = \frac{3.91185}{e^{\beta \cdot x}} - 2.92967 e^{\beta \cdot x} - 0.982186 Cos[\beta \cdot x] + 6.84152 Sin[\beta \cdot x]$$

with

$$\beta^4 = \frac{m(x) \cdot \omega^2}{EI} = (0.104669)^4$$

. . . **(4.41)**

The total solution, as a function of time and position, may then be written as:

$$W(x,t) = w(x) \cdot Sin\,\omega t$$

. . . **(4.42)**

4.3.2 Finite element model

Two models of the structure were considered. The first model was obtained by making use of three beam elements yielding a model with nine degrees of freedom. The second model was formed by making use of three plate elements, yielding a model with thirty degrees of freedom.

Both of these models were created and solved by making use of subroutines developed within the mathematical software package, Mathematica (Version 2.2).

4.3.3 Results

The transverse steady-state displacement response as calculated from the closed-form solution, the beam element model as well as the plate element model are listed in *Table 4.1* at the node points of the elements. The dynamic response is constant over the width of the beam.

Table 4.1: Transverse steady-state displacement response (w) for the test case

***X*-Position along the length of the beam [m]**	**Transverse displacement (Exact solution) [m]**	**Transverse displacement (Beam Elements) [m]**	**Transverse displacements (Plate Elements) [m]**
0	0	0	0
0.4572	0.0019994	0.0019993	0.00199898
0.9144	0.0069978	0.0069978	0.00699698
1.3716	0.0134957	0.0134957	0.01349449

The solutions obtained from the three formulations are shown graphically in *Figure 4.9*. Since the difference between the results obtained from the three models are so small that it can not be identified in *Figure 4.9*, the difference were also quantified numerically. The residual for the approximate results, obtained from the beam and plate element models, were defined as the difference in the value of the transverse displacement response obtained from the approximate and the exact solutions. For the plate element model this may be written as:

$$(Residual)_i = w_{(plate)i} - w_{(exact)i} \quad \text{. . . (4.43)}$$

Scatter plots of the residuals for the beam and plate element models are shown in *Figures 4.10 and 4.11* respectively. The mean and the variance of the residuals, as well

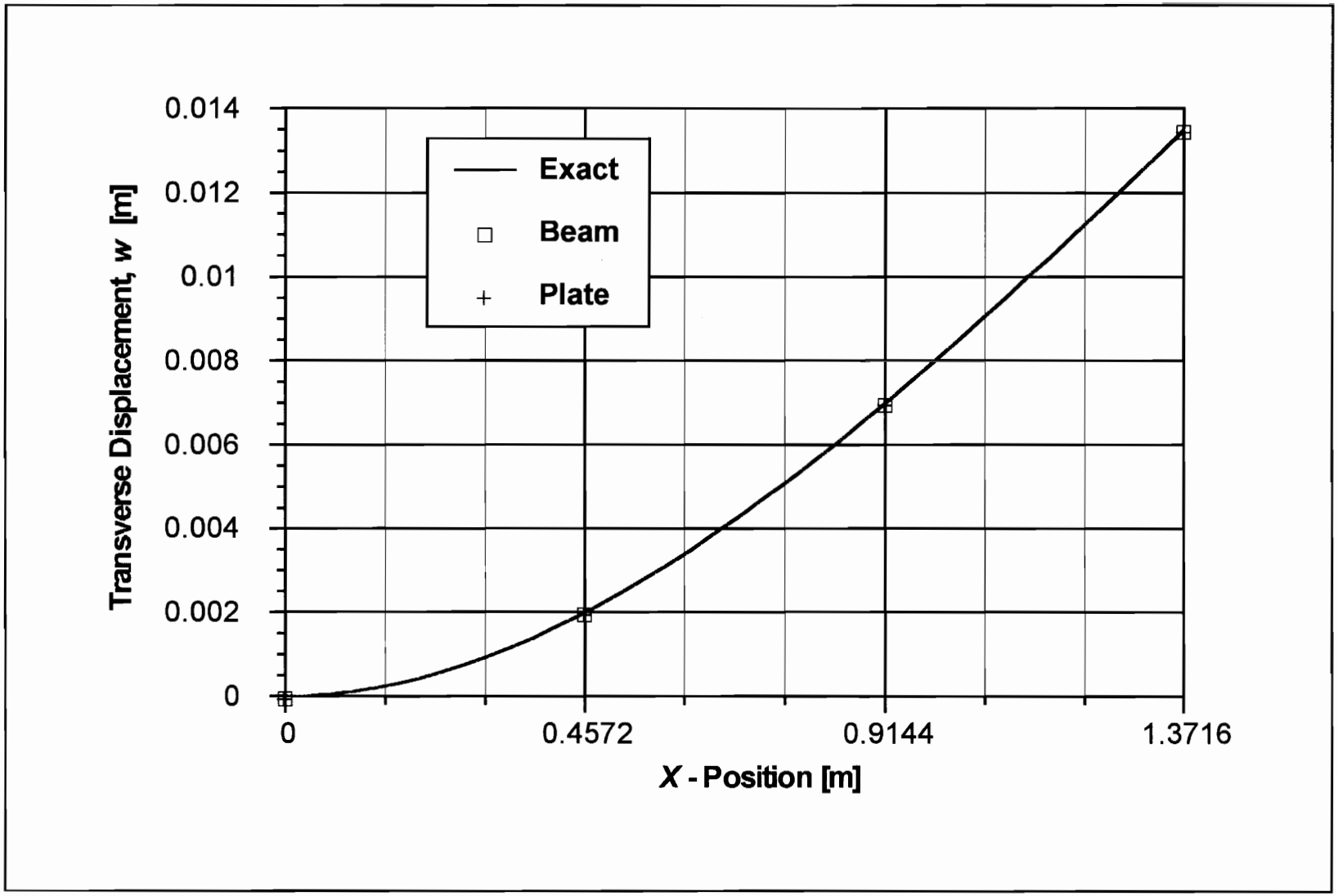

Figure 4.9: Dynamic displacement response obtained from the exact solution, the beam element approximation and the plate element approximation

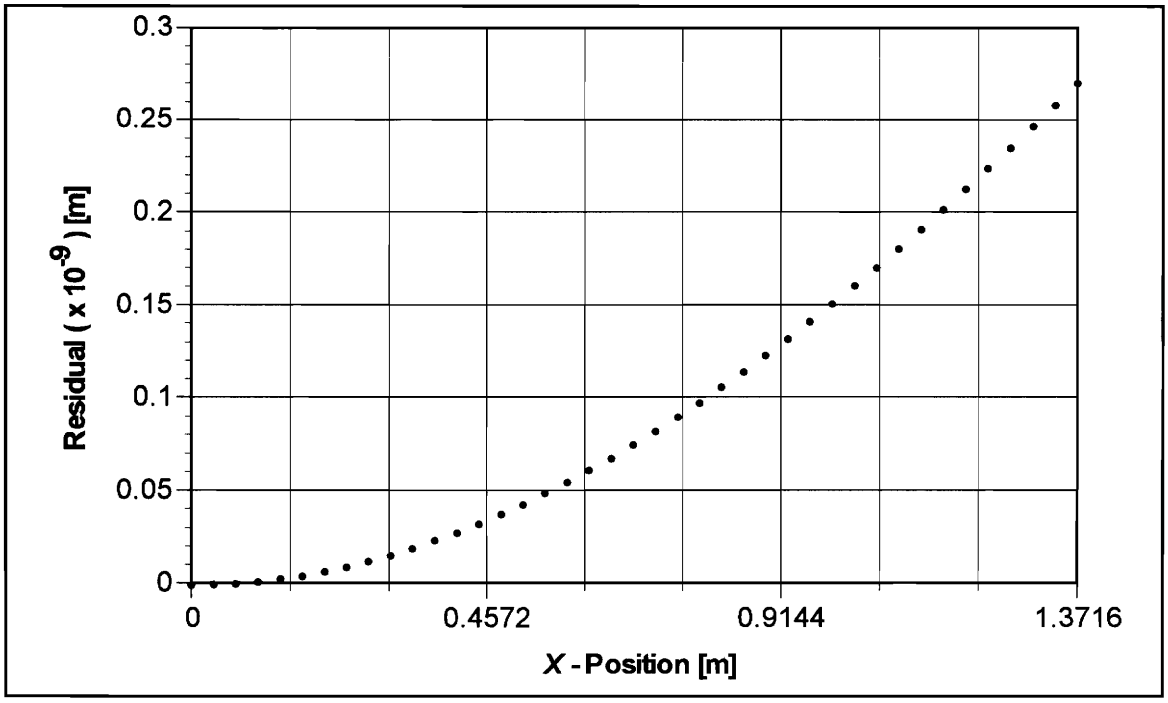

Figure 4.10: Residual of the beam element approximation

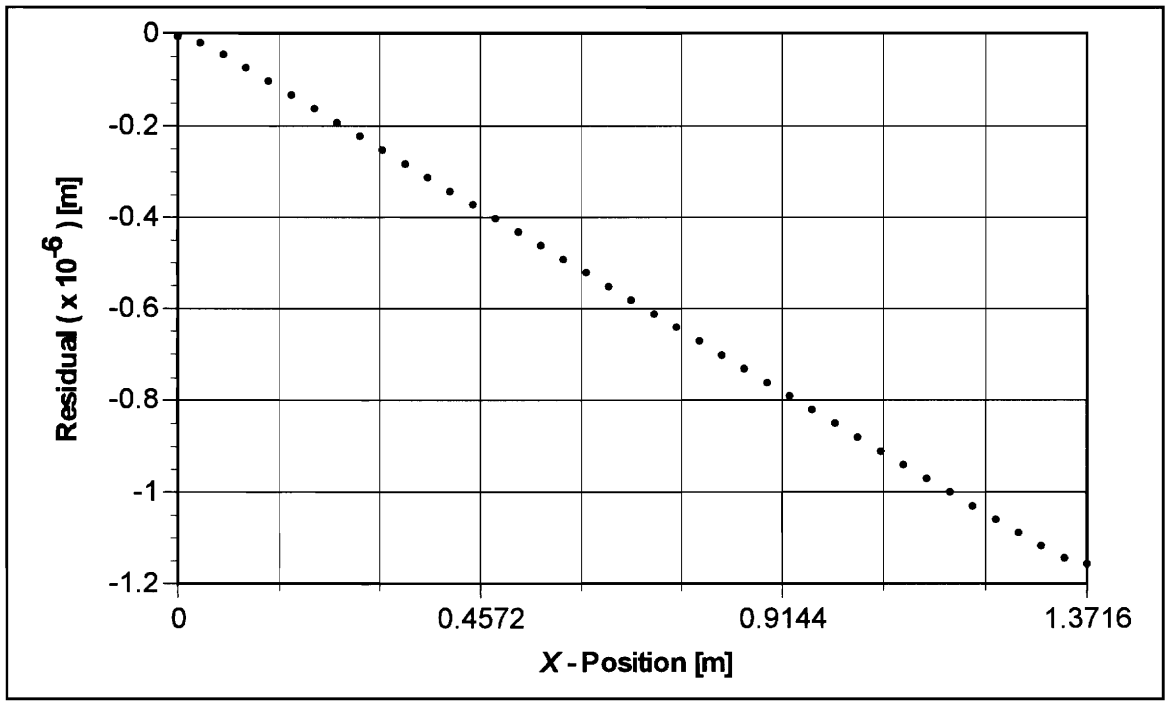

Figure 4.11: Residual of the plate element approximation

as the signal-to-noise ratio (*S/N*) may be defined as shown in *Equation 4.44* (Ott 1993). The definitions used in *Equation 4.44* for the mean and the variance are that of the sample mean and the sample variance.

$$Mean = \overline{m}_{Residual} = \frac{1}{n} \cdot \left(\sum_{i=1}^{n} (Residual)_i \right)$$

$$Variance = s^2{}_{Residual} = \frac{1}{n-1} \cdot \left(\sum_{i=1}^{n} \left((Residual)_i^2 \right) - \frac{\left(\sum_{i=1}^{n} (Residual)_i \right)^2}{n} \right)$$

$$\text{Signal - to - noise ratio} = \frac{S}{N} = \frac{w_{\max}}{\sqrt{s^2{}_{Residuals}}}$$

. . . **(4.44)**

where n is the number of sampling points considered.

The mean and the variance of the residuals as well as the signal-to-noise ratio for the beam and the plate element solutions are shown in *Table 4.2*. In order to ensure a normal distribution of the data, the residuals were calculated at forty evenly spaced data points (Ott 1993).

Table 4.2: Mean, variance and signal-to-noise ratios for the beam and plate element approximations

	Mean	**Variance**	**Signal-to-noise**
Beam	$9.89442\ 10^{-11}$	$7.17853\ 10^{-21}$	$1.59286\ 10^{8}$
Plate	$-5.89471\ 10^{-7}$	$1.20951\ 10^{-13}$	38805.1

Although both models give very good approximations, the beam element model, consisting of three elements, were found to be more accurate that the plate element model with the same number of elements. The beam element model shows a smaller mean and variance of the residuals and a higher signal-to-noise ratio. The residuals of both models

are clearly biased (residuals not randomly scattered about zero), but this should be expected due to the inherent differences between the two approximate and the exact solution. These differences consists mainly of the different material properties used to calculate the approximate results.

Since the results obtained from the frequency response analysis are very accurate compared to the results obtained from the closed-form solution of the problem, the pseudo-dynamic stiffness matrix is shown to be both valid and accurate for this problem. The problem that will be considered in the research is also a beam problem and the frequency response formulation is, thus, shown to be a good choice for calculating the steady-state dynamic response within the context of this research.

Chapter 5

Sensitivity of the error function with respect to the elastic boundary conditions of the numerical model

The pseudo-dynamic stiffness formulation, together with the direct method of differentiation enable the calculation of the sensitivity of the error function with respect to any finite element model parameter. In this chapter, however, it will be shown how the sensitivity of the error function with respect to the elastic boundary conditions may be evaluated.

5.1 Fundamentals of the approach

The influence on the accuracy of a model, obtained through ESDM, due to changes in the elastic boundary conditions will be evaluated. This will be accomplished by calculating the sensitivity of the error function with respect to the elastic boundary conditions contained in the numerical model.

5.1.1 Underlying motivation and fundamental philosophy for the approach

The sensitivity of the error function with respect to the elastic boundary conditions must be evaluated. The ESDM error function, consistent with a finite element formulation evaluated for a given measurement on the structure, is given by *Equation 3.20* and may be rewritten as:

$$error_i = v_{xi} \cdot \eta_{xi} + v_{yi} \cdot \eta_{yi} + v_{zi} \cdot \eta_{zi} - \tilde{V}_{Li} \qquad \text{. . . (5.1)}$$

The velocity components contained in *Equation 5.1* may be obtained from the dynamic displacement response of a structure as shown in *Equation 3.10*. For steady-

state type response, the spatial relationship between the amplitudes of the steady-state velocity and displacement may be written in general as:

$$\overline{v}(x,y,z) = \omega \cdot \overline{u}(x,y,z)$$

$$= \omega \cdot \left(u_x(x,y,z) \cdot \hat{i} + u_y(x,y,z) \cdot \hat{j} + u_z(x,y,z) \cdot \hat{k} \right)$$

. . . **(5.2)**

Upon substitution of *Equation 5.2* into *Equation 5.1* and taking the first-order derivative with respect to a finite element model parameter, say χ, *Equation 5.3* is obtained as follows:

$$\frac{\partial (error_i)}{\partial \chi} = \omega \cdot \frac{\partial u_{xi}}{\partial \chi} \cdot \eta_{xi} + \omega \cdot \frac{\partial u_{yi}}{\partial \chi} \cdot \eta_{yi} + \omega \cdot \frac{\partial u_{zi}}{\partial \chi} \cdot \eta_{zi}$$

. . . **(5.3)**

By taking the derivative of *Equation 5.3* with respect to another finite element model parameter, say γ, the second-order relationship of *Equation 5.4* is obtained:

$$\frac{\partial^2 (error_i)}{\partial \chi \partial \gamma} = \omega \cdot \frac{\partial^2 u_{xi}}{\partial \chi \partial \gamma} \cdot \eta_{xi} + \omega \cdot \frac{\partial^2 u_{yi}}{\partial \chi \partial \gamma} \cdot \eta_{yi} + \omega \cdot \frac{\partial^2 u_{zi}}{\partial \chi \partial \gamma} \cdot \eta_{zi}$$

. . . **(5.4)**

The forcing frequency (ω) and the direction cosines of the laser in the structural coordinate system are not dependent on the finite element model parameters. Thus, in order to obtain the sensitivities of the error function with respect to the elastic boundary conditions, it is first of all necessary to calculate the derivatives of the steady-state displacement response with respect to the same boundary conditions. The derivatives of the steady-state dynamic displacement response may be obtained from the direct method of differentiation. However, in order to enable the use of the direct method of differentiation, the steady-state dynamic response must be solved from the frequency response formulation.

5.1.2 Method of solving the problem

The method of solving the problem, may be divided into four basic steps. These steps may in turn be summarized conceptually as follows:

1. Find a semi-discrete formulation for the steady-state dynamic response of the system by making use of the finite element formulation
2. Solve for the steady-state dynamic displacement response from the semi-discrete formulation (this is a discrete representation of the spatial part and a continuous representation of the temporal part of the differential equation) by making use of the frequency response formulation
3. Obtain the first- and-second order derivatives of the displacement response with respect to the elastic boundary conditions by making use of the direct method of differentiation
4. Obtain the sensitivity of the error function with respect to the elastic boundary conditions by making use of *Equations 5.3 and 5.4*.

5.2 Resulting formulation

The resulting mathematical formulation for obtaining the goals of this part of the research will now be developed. This includes the solution of the steady-state dynamic displacement response from the semi-discrete formulation by means of the frequency response formulation as well as the calculation of the first- and second-order derivatives of this response by means of the direct method of differentiation.

5.2.1 Goals and criteria used to evaluate the success of the method

The goal of this part of the research, as stated in *Chapter 1*, is to evaluate the sensitivity of the accuracy of a model, obtained from the ESDM formulation, to finite element model parameters. Calculating these sensitivities, also yields the sensitivity of the dynamic response with respect to the same finite element model parameters.

Specifically the first- and second-order sensitivities of the error function with respect to the elastic boundary conditions of the numerical model must be evaluated.

Furthermore, these sensitivities must be obtained by means of an analytical evaluation of the derivatives involved. This will be accomplished by making use of a frequency response formulation as well as the direct method of differentiation. The frequency response formulation will be used to obtain the steady-state dynamic response from the semi-discrete formulation, while the direct method of differentiation will be used to obtain the analytical derivatives of the response.

5.2.2 Fundamental assumptions or limitations to be applied to the method

The assumptions and limitations to be applied, may be divided into three areas within the problem formulation.

5.2.2.1 Beam elements

The beam element used is an Euler-Bernoulli beam element. The Euler-Bernoulli beam theory is applicable to beams with small deformations where shear deformations are neglected. Small deformations are normally considered to be deformations which have a magnitude of less than a few tens of the thickness of the beam. Due to the length of the beam considered in the example problems of this thesis, this upper limit on the magnitude of the deformations is violated. However, the Euler-Bernoulli beam theory is still valid due to the small strains caused by the observed deformations. The assumptions for Euler-Bernoulli beam theory (Cook and Young 1985 and Meirovitch 1986) may be summarized as follows:

1. Points on the mid surface of the beam (neutral axis) translate only in the transverse (out-of-plane) direction
2. Straight lines normal to the mid surface before loading, remain straight and normal to the mid surface after loading (thus transverse shear deformation is assumed to be zero)
3. Rotational inertia is negligible small due to the fact that the rotation is assumed to be insignificant compared to the transverse displacement

5.2.2.2 Plate elements

The plate element used is a Kirchoff plate element. Kirchoff plate theory is applicable to thin plates where the transverse shear deformation is neglected. The assumptions and limitations for this theory are the same as for the Euler-Bernoulli beam theory, with the only difference being the fact that the theory is now applicable to two-dimensional space.

5.2.2.3 Frequency response analysis

This formulation is applicable to systems where the forcing functions can be represented by periodic functions, such as a Fourier series representation (Zienkiewicz and Taylor 1989). The forcing function and the dynamic displacement response may be written in the following form:

$$F(x,t) = f(x) \cdot e^{t(\alpha_1 + i\alpha_2)}$$

$$U(x,t) = u(x) \cdot e^{t(\alpha_1 + i\alpha_2)} \qquad \text{. . . (5.5)}$$

The dynamic displacement response has the same general form as the forcing function, due to the fact that linear systems are considered. The fact that only periodic forcing functions may be considered is not much of a limitation since most forcing functions may be written as periodic functions by making use of the Fourier series approximation.

5.2.3 Mathematical formulation

As stated earlier, the derivatives of the dynamic displacement response with respect to the elastic boundary conditions have to be found before the sensitivities of the error function with respect to the same variables may be evaluated. The dynamic displacement response will be calculated from the frequency response formulation which results in a pseudo-dynamic stiffness matrix yielding *Equations 5.6 and 5.7*.

$$\mathbf{D} \cdot \mathbf{u} = \mathbf{F} \qquad \text{. . . (5.6)}$$

where

$$\mathbf{D} = \mathbf{K} - \omega \cdot \mathbf{M} + i\omega \cdot \mathbf{C} \qquad \text{. . . (5.7)}$$

The pseudo-dynamic stiffness matrix of the system, as well as the system mass and damping matrices, are constructed using the direct stiffness method based on *Equation 5.7*. The system matrices are assembled as if there were no constraints acting on the structure. The elastic boundary conditions will then be incorporated into the model by adding the appropriate boundary condition model, which includes the stiffness parameters. In this study these stiffness variables include the axial stiffness, K_A, transverse stiffness, K_T, and rotational stiffness, K_R. These boundary stiffnesses are parameters to a new boundary condition model which relates the elastic boundary conditions to the appropriate degrees of freedom of the unconstrained, global stiffness matrix. For example, for a cantilevered beam with elastic boundary conditions at the left end (*Figure 5.1*), the matrix shown in *Equation 5.8* must be assembled into the global stiffness matrix. For this system, the boundary condition model given by *Equation 5.8* must be added to the degrees of freedom of the first node of the structure. The matrix summations, necessary to obtain the global stiffness and mass matrices, are shown schematically in *Figure 5.1*.

$$\mathbf{K}_{boundary} = \begin{bmatrix} K_A & 0 & 0 \\ 0 & K_T & 0 \\ 0 & 0 & K_R \end{bmatrix}; \; Dof = \{u_i, w_i, \theta_i\} \qquad \text{. . . (5.8)}$$

If the same structure as shown in *Figure 5.1*, is now modeled by means of plate elements (*Figure 5.2*), there are two nodes at the left end of the structure. For the plate element model, the matrix shown in *Equation 5.9* must be assembled (in a similar way as was done for the beam element model) into the global stiffness matrix at the degrees of freedom for each of these two nodes:

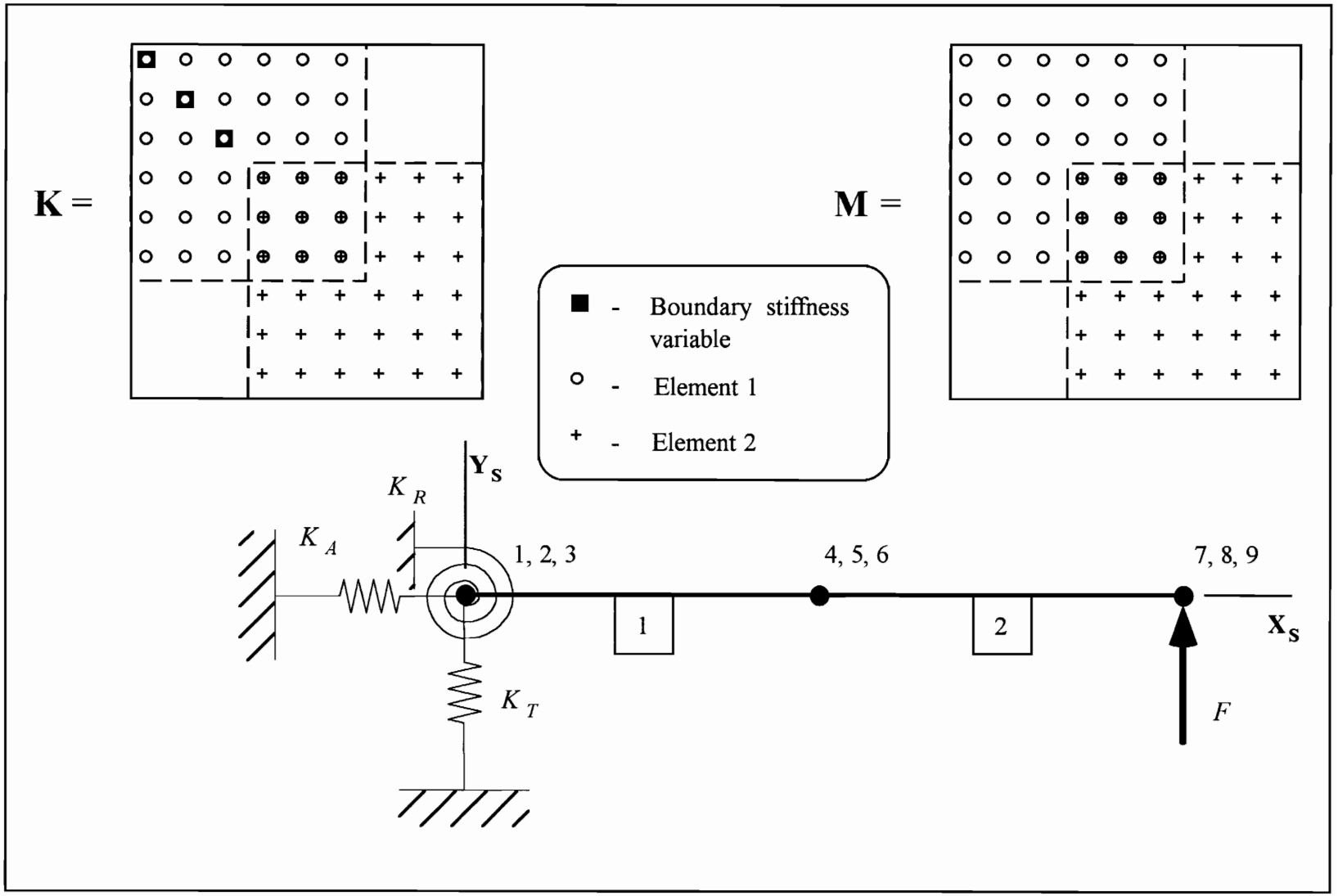

Figure 5.1: Nine degrees of freedom beam model with elastic boundary conditions

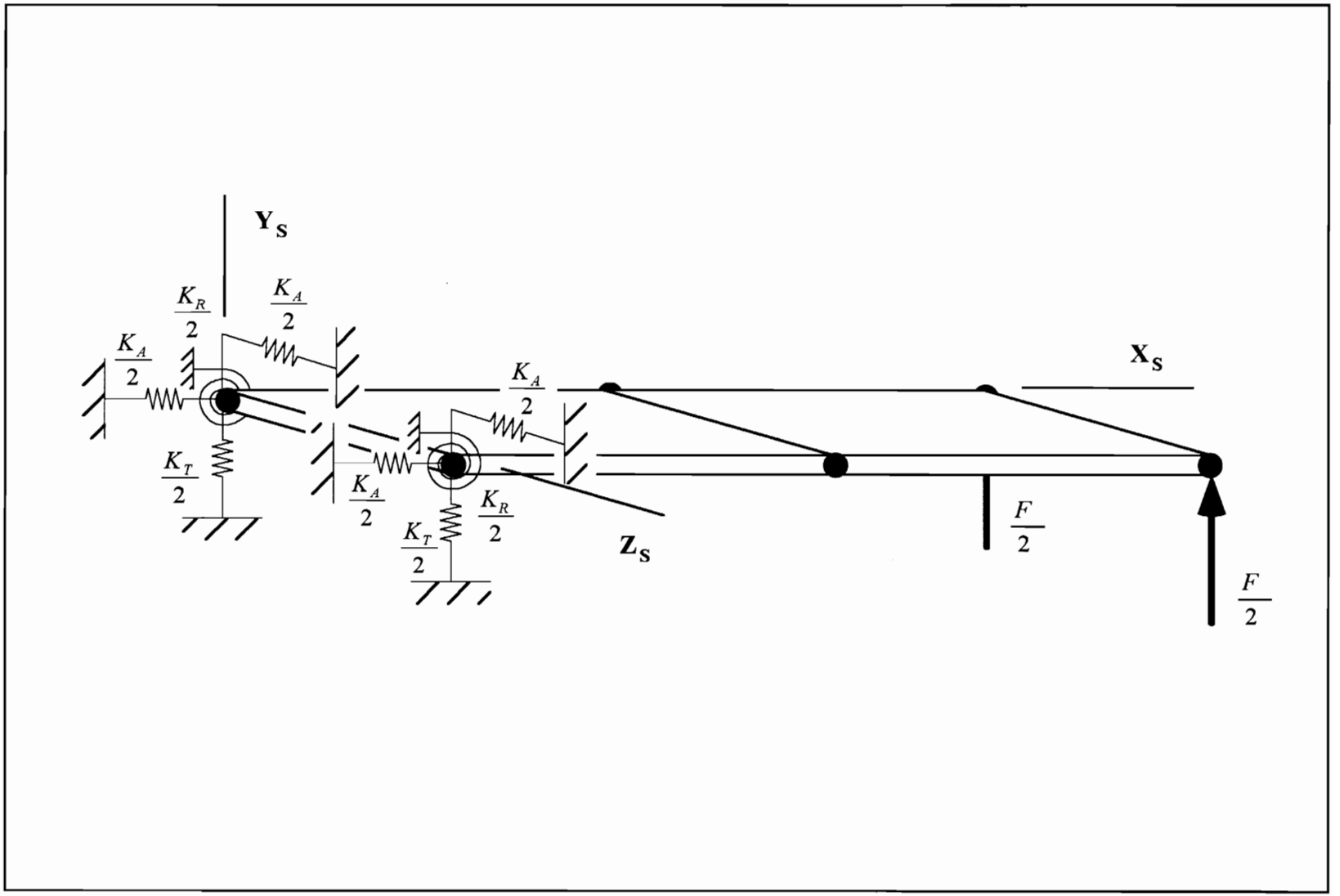

Figure 5.2: Plate element model with elastic boundary conditions

$$\mathbf{K}_{boundary} = \frac{1}{2}\begin{bmatrix} K_A & 0 & 0 & 0 & 0 \\ 0 & K_A & 0 & 0 & 0 \\ 0 & 0 & K_T & 0 & 0 \\ 0 & 0 & 0 & 0 & 0 \\ 0 & 0 & 0 & 0 & K_R \end{bmatrix} \quad Dof = \{u_i, v_i, w_i, \theta_{xi}, \theta_{zi}\}$$

. . . **(5.9)**

The factor of one half in *Equation 5.9* is due to the fact that the boundary stiffness is divided between the two nodes of the plate element at the end point of the structure. The zero entry on the diagonal is due to the fact that the elastic boundary conditions of the structure is assumed to place no restriction on rotations about the x-axis. Lastly, the stiffness of the boundary in the plane of the structure (directions corresponding to the displacements u_i and v_i) are assumed to be equal.

The method allows the addition of lumped parameters (for example discrete dampers) to the mass and damping matrices, by making use of the same principles as used for the stiffness matrix. In this study, however, the mass matrices will be constructed exactly the same way as for a structure with no boundary conditions, thus ignoring the mass of the elastic boundary conditions. Furthermore, in the scope of this research, no damping will be considered and the damping matrix will thus be set equal to zero. This is not a limitation to the method, as this method will allow both lumped and distributed as well as viscous and structural damping models. This is, however, a limitation in the scope of this portion of the thesis.

With the stiffness, mass and damping matrices known, the pseudo-dynamic stiffness matrix may be obtained from *Equation 5.7*. The steady-state dynamic displacement response may then be solved from *Equation 5.6* using this frequency response formulation.

The next step of the method is to calculate the first- and second-order derivatives of the steady-state dynamic displacement response by means of the direct method of differentiation as shown in *Equations 5.10 and 5.11* (Haftka and Gürdal 1993):

$$\frac{\partial \mathbf{u}}{\partial \chi} = \mathbf{D}^{-1}\left(\frac{\partial \mathbf{F}}{\partial \chi} - \frac{\partial \mathbf{D}}{\partial \chi} \cdot \mathbf{u}\right)$$

. . . **(5.10)**

$$\frac{\partial^2 \mathbf{u}}{\partial \chi \partial \gamma} = \mathbf{D}^{-1}\left(\frac{\partial^2 \mathbf{F}}{\partial \chi \partial \gamma} - \frac{\partial^2 \mathbf{D}}{\partial \chi \partial \gamma}\cdot \mathbf{u} - \frac{\partial \mathbf{D}}{\partial \chi}\cdot\frac{\partial \mathbf{u}}{\partial \gamma} - \frac{\partial \mathbf{D}}{\partial \chi}\cdot\frac{\partial \mathbf{u}}{\partial \gamma}\right)$$

. . . **(5.11)**

The force vector is currently assumed to be independent of the elastic boundary conditions and the derivatives of the force vector with respect to these variables will be equal to zero.

5.2.4 Summary of resulting equations

The general form of *Equations 5.3, 5.4, 5.10 and 5.11* may be modified to obtain the sensitivities of the error function with respect to the elastic boundary conditions. This modification consists of a variable substitution as well as recognizing the fact that the forcing function is currently assumed to be independent of the elastic boundary variables. With these modifications, *Equation 5.3* yields the sensitivity of the error function in terms of the elastic boundary conditions as:

$$\frac{\partial(error_i)}{\partial K_A} = \omega\cdot\frac{\partial u_{xi}}{\partial K_A}\cdot\eta_{xi} + \omega\cdot\frac{\partial u_{yi}}{\partial K_A}\cdot\eta_{yi} + \omega\cdot\frac{\partial u_{zi}}{\partial K_A}\cdot\eta_{zi}$$

$$\frac{\partial(error_i)}{\partial K_T} = \omega\cdot\frac{\partial u_{xi}}{\partial K_T}\cdot\eta_{xi} + \omega\cdot\frac{\partial u_{yi}}{\partial K_T}\cdot\eta_{yi} + \omega\cdot\frac{\partial u_{zi}}{\partial K_T}\cdot\eta_{zi}$$

$$\frac{\partial(error_i)}{\partial K_R} = \omega\cdot\frac{\partial u_{xi}}{\partial K_R}\cdot\eta_{xi} + \omega\cdot\frac{\partial u_{yi}}{\partial K_R}\cdot\eta_{yi} + \omega\cdot\frac{\partial u_{zi}}{\partial K_R}\cdot\eta_{zi}$$

. . . **(5.12)**

Equation 5.10, on the other hand, yields the required derivatives of the steady-state dynamic displacement response as:

$$\frac{\partial \mathbf{u}}{\partial K_A} = \mathbf{D}^{-1} \cdot \frac{\partial \mathbf{D}}{\partial K_A} \cdot \mathbf{u}$$

$$\frac{\partial \mathbf{u}}{\partial K_T} = \mathbf{D}^{-1} \cdot \frac{\partial \mathbf{D}}{\partial K_T} \cdot \mathbf{u}$$

$$\frac{\partial \mathbf{u}}{\partial K_R} = \mathbf{D}^{-1} \cdot \frac{\partial \mathbf{D}}{\partial K_R} \cdot \mathbf{u}$$

. . . **(5.13)**

The derivative of the pseudo-dynamic stiffness matrix, **D**, with respect to the elastic boundary stiffness variable K_A, may be written as:

$$\frac{\partial \mathbf{D}}{\partial K_A} = \frac{\partial \mathbf{K}}{\partial K_A} - \omega \cdot \frac{\partial \mathbf{M}}{\partial K_A} + i\omega \cdot \frac{\partial \mathbf{C}}{\partial K_A}$$

. . . **(5.14)**

The boundary condition model are incorporated into the pseudo-dynamic stiffness matrix through the addition of the two diagonal submatrices of *Equations 5.8 and 5.9* to the global stiffness matrices of the beam and plate element models respectively. Due to the fact that the boundary condition model contains only stiffness elements, the mass and damping matrices are not effected by the boundary condition model and *Equation 5.14* reduces to:

$$\frac{\partial \mathbf{D}}{\partial K_A} = \frac{\partial \mathbf{K}}{\partial K_A}$$

. . . **(5.15)**

The derivative with respect to the elastic boundary conditions for all the entries of **D**, except for those obtained from *Equations 5.8 and 5.9*, will, thus, be equal to zero. The sensitivity of *Equation 5.8* (beam element model) with respect to the elastic boundary variables may be written as

$$\frac{dK_{Boundary}}{dK_A} = \begin{bmatrix} 1 & 0 & 0 \\ 0 & 0 & 0 \\ 0 & 0 & 0 \end{bmatrix}$$

$$\frac{dK_{Boundary}}{dK_T} = \begin{bmatrix} 0 & 0 & 0 \\ 0 & 1 & 0 \\ 0 & 0 & 0 \end{bmatrix}$$

$$\frac{dK_{Boundary}}{dK_R} = \begin{bmatrix} 0 & 0 & 0 \\ 0 & 0 & 0 \\ 0 & 0 & 1 \end{bmatrix}$$

. . . **(5.16)**

with similar relationships for *Equation 5.10*, the plate element model submatrix.

Lastly, the nodal displacement vector, **u**, will be evaluated from the frequency response formulation (*Equation 5.6*) by making use of a linear solver.

5.3 Test case

Once the dynamic displacement response is solved from the pseudo-dynamic stiffness formulation, the calculation of the sensitivities of the error function with respect to the elastic boundary conditions is rather trivial. The validity of the elastic boundary variables within the frequency response formulation is critical to the success of the evaluation of these derivatives. In order to establish the validity of the elastic boundary condition variables within the frequency response formulation, a test problem will be evaluated. For the test problem, the sensitivity of the error function with respect to the stiffness variable K_R, will also be evaluated as a representative case to show the evaluation of the sensitivities.

For the test case a cantilevered beam with a harmonic forcing function at the free end will be considered. The setup of the test case is basically the same as the test case used in *Chapter 4*. The same structure and loading conditions will be considered, but the

fixed boundary conditions will be replaced by elastic boundary conditions. The dimensions and material properties of the structure as well as the loading condition may be summarized as:

Dimensions:	Length	=	1.3716	m
	Width	=	0.0762	m
	Thickness	=	0.00635	m
Material:	ν	=	0.27	
	E	=	196	GPa
	ρ	=	7905	kg/m^3
Load:	f_0	=	5	N
	ω	=	0.1	rad/s

The experimental setup is the same as the schematic setup shown in *Figures 5.1 and 5.2* for the beam and the plate element models respectively. For the test case, however, three elements instead of two will be used to model the structure. Three elements were chosen due to the fact that the results were found to be well converged as well as to compare the results with those obtained from *Chapter 4*. Two problems with different elastic boundary conditions, will be evaluated which may be stated as:

Problem 1 For the first problem, boundary conditions with very high stiffness values will be used. High boundary stiffness values are assigned as an approximation to fixed boundary conditions. The results obtained from this problem will then be compared to the exact results for the test case with fixed boundary conditions, as obtained in *Chapter 4*.

The numerical values for these elastic boundary conditions will be taken as:

$K_A = 1\text{x}10^{12}$	N/m
$K_T = 1\text{x}10^{12}$	N/m
$K_R = 1\text{x}10^{12}$	N/rad

Problem 2 For the second problem, typical elastic boundary conditions at the left end of the beam will be considered. Boundary stiffness values will be calculated for a support, consisting of a circular aluminum rod. The rod will have the following dimensions and material conditions:

Length	=	0.30	m
Diameter	=	0.01	m
Young's Modulus	=	69	GPa

From the equations for a cantilevered beam (Cook and Young 1985) the stiffness values were calculated to be:

$$K_A = \frac{3EI}{L^3} = 3.763366\text{x}10^3 \quad \text{N/m}$$

$$K_T = \frac{AE}{L} = 18.06416\text{x}10^6 \quad \text{N/m}$$

$$K_R = \frac{2EI}{L^2} = 752.6732 \quad \text{N.m/rad}$$

Figure 5.3 gives a schematic representation of the experimental setup, with the position and orientation of the laser shown. The position and orientation of the laser will be used in the calculation of the error sensitivity later in the example problem.

5.3.1 Results

The results obtained from the exact solution (fixed boundary conditions - *Chapter 4*), Problem 1 and Problem 2 are listed in *Table 5.1*. The dynamic response is constant over the width of the beam. The results are also shown graphically in *Figure 5.4*.

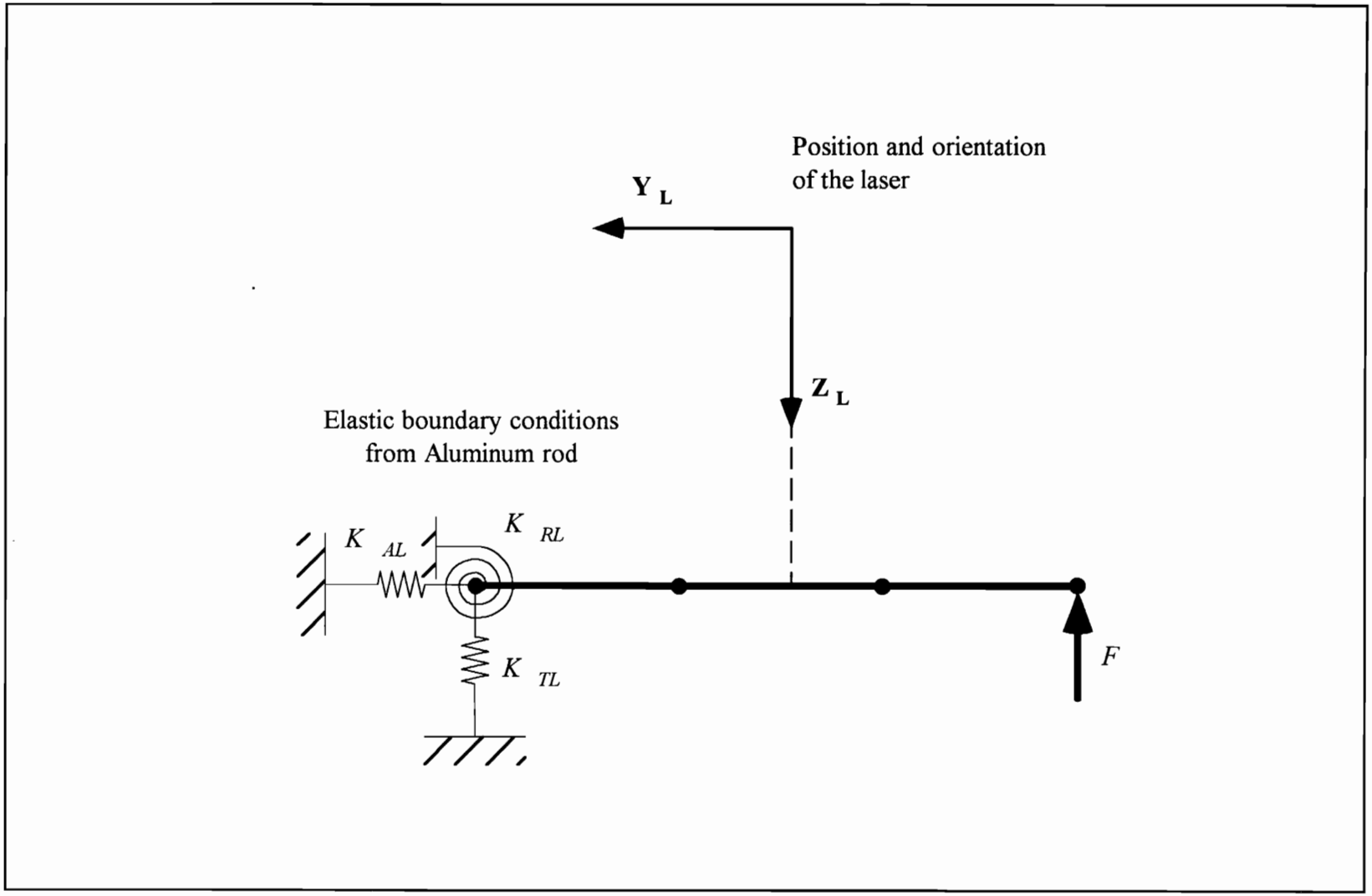

Figure 5.3: Experimental setup used for evaluating the sensitivity of the error function with respect to K_{RL}

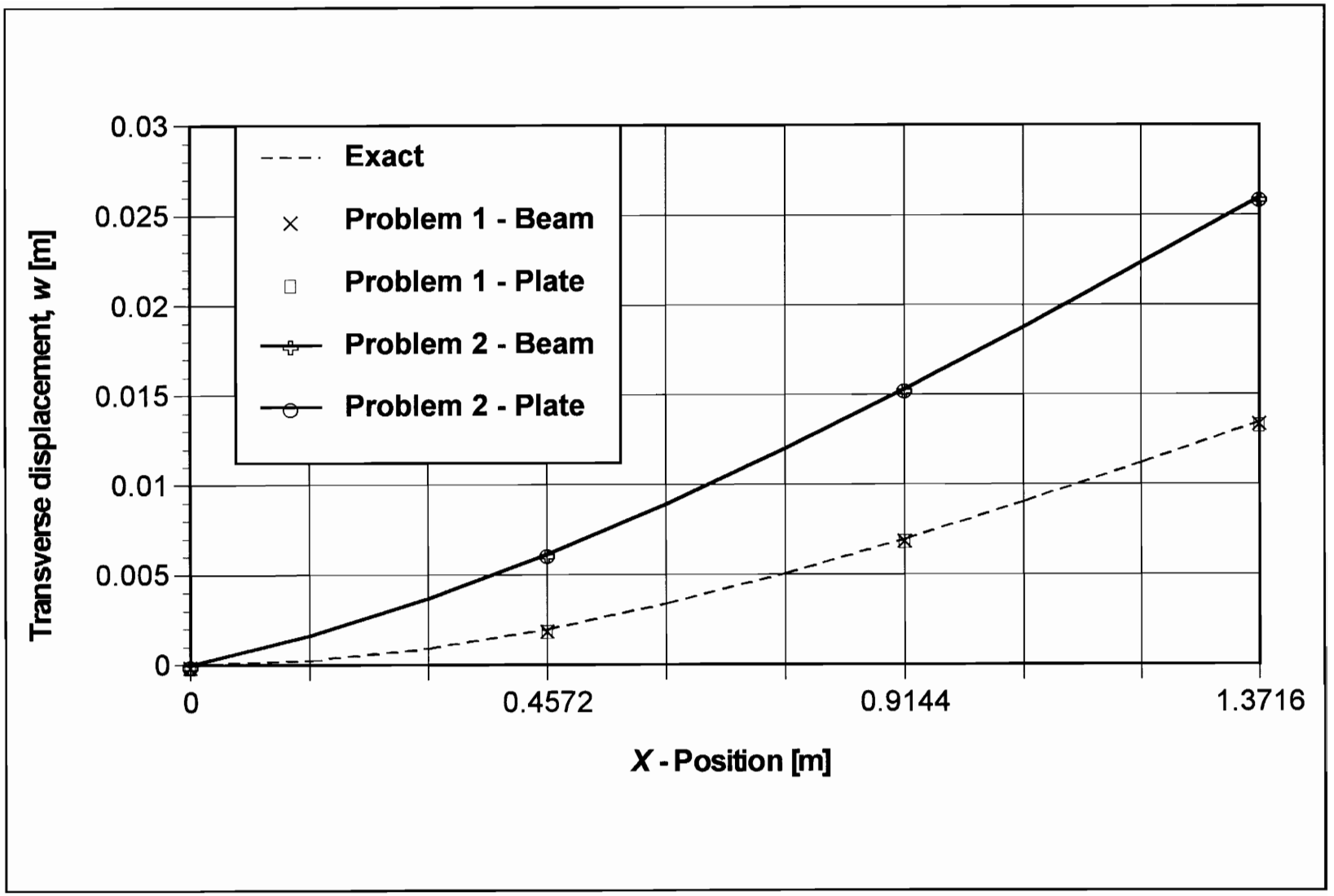

Figure 5.4: Steady-state transverse displacement response for the test case.

Table 5.1: Displacement response for the test case - Problem 1 and Problem 2

X-Position along beam length [m]	Exact Transverse displacement [m]	Problem 1 Transverse displacement [m]		Problem 2 Transverse displacement [m]	
		Beam	Plate	Beam	Plate
0	0	5.0002E-12	2.5001E-12	2.7682E-7	1.32875E-6
0.4572	0.0019994	0.0019993	0.00199898	0.0061659	0.00616652
0.9144	0.0069978	0.0069978	0.00699698	0.0153307	0.0153308
1.3716	0.0134957	0.0134957	0.0134945	0.025995	0.0259947

As expected the results for Problem 1 (high elastic boundary stiffness) and the exact solution are very close (no difference in the first seven significant figures). Also, it was found that the residuals, the mean and the variance of the residuals, as well as the signal-to-noise ratio for the results obtained from Problem 1 are not significantly different from those obtained in *Chapter 4*. The values used for the elastic boundary conditions were, thus, high enough to give a good approximation of fixed boundary conditions. Furthermore, it is clear that the use of the boundary stiffness variables are valid within the pseudo-dynamic stiffness formulation. The models gave very close answers and the difference are most probably due to inherit differences between the two approximations. One of the major differences is the fact that the plate element model take the Poisson's ratio into account while the beam element model does not.

It should be noted that there is a limit on the magnitude of the values assigned to the elastic boundary conditions. If the values are too large, the resulting pseudo-dynamic stiffness matrix becomes ill-conditioned. This ill-conditioning may lead to numerical difficulties when solving the system of equations, yielding large inaccuracies in the results. This is however not a limitation due to the fact that the case of very high boundary stiffnesses may be solved by making use of conventional, prescribed displacement boundary conditions.

The effect of the elastic boundary conditions on the response can clearly be seen in the response as obtained from Problem 2. The response has the same tendency over the length of the beam as the response obtained from Problem 1, with three major differences.

Firstly, the response at x equal to zero is not exactly equal to zero. Secondly, the gradient of the response at x equal to zero is no longer zero, which is a consequence of the elastic rotational stiffness of the boundary. Lastly, the response as obtained from Problem 2 is larger in magnitude than that obtained from Problem 1. The difference in the magnitude of the response is largely due to the non-zero slope at $x = 0$.

The results of Problem 1 compare well with the exact solution while the results of Problem 2 show a response curve as could be expected with both models yielding results with no significant difference. The validity of the elastic boundary conditions within the frequency response formulation is, thus, proved.

5.3.2 Sensitivity calculation

In order to show the calculation of the sensitivities, the sensitivity of the beam element model with respect to the rotational boundary stiffness variable, K_R, will be evaluated as a representative case. The same beam element model (as previously used in the test case) with three elements will be used due to the fact that the procedure of calculating the sensitivities are well illustrated.

For the beam element model of the test case, *Equation 5.12* reduces to:

$$\frac{\partial(error_i)}{\partial K_R} = \omega \cdot \frac{\partial u_{yi}}{\partial K_R} \cdot \eta_{yi} \qquad \text{. . . (5.17)}$$

due to the fact that:

$$u_{xi} = u_{zi} = 0$$

If the laser is now positioned directly above the midpoint of the beam such that the z-axis of the laser is pointing directly downwards (*Figure 5.3*) the direction cosines of the laser beam, at the node points are given by:

$$\eta_{yi} = \{0.985619, 0.998371, 0.998371, 0.985619\}$$

The derivative of the nodal point dynamic response vector with respect to K_R may then be obtained as shown in *Figure 5.5*. Lastly, the forcing frequency is know from the problem statement to be equal to 0.1 rad/s.

The sensitivity of the error function with respect to K_R at the node points of the structure are shown graphically in *Figure 5.6* and the results are summarized in *Table 5.2*.

Table 5.2: Sensitivity of the error function with respect to K_R

X-Position along the length of the beam [m]	$\frac{\partial (error)_i}{\partial K_R}$ **- Beam element model [(m.s^{-1})/(N/m)]**
0	-3.78287E-16
0.4572	-8.79570E-8
0.9144	-1.75917E-7
1.3716	-2.60506E-7

In order to verify the results obtained, the derivative of the displacement response with respect to K_R will be verified. It is not necessary to verify the sensitivity of the error function with respect to K_R due to the fact that the other terms in *Equation 5.17* (the frequency of the forcing function and the direction cosines) are known constants. A first-order Taylor series approximation of the displacement field about a specific point with respect to a change in K_R may be written as:

$$\left(u_{yi}\right)_{approx} = u_{y0i} + \Delta K_R \cdot \frac{\partial u_{yi}}{\partial K_R} \qquad \text{. . . (5.18)}$$

For a 10% change in the value of K_R *Equation 5.18* yields:

$$\left(u_{yi}\right)_{approx} = \{2.76823\text{E}-7, 0.00574925, 0.0144974, 0.024745\}$$

$$\frac{\partial \mathbf{u}}{\partial K_R} = -\mathbf{D} \cdot \frac{\partial \mathbf{D}}{\partial K_R} \cdot \mathbf{u}$$

$$= \begin{bmatrix} 2.074E8 & & & & & & & & & & & \\ 0 & 1.810E7 & & & & & & & & & & \\ 0 & 9147.23 & 3540.75 & & & & & & & & & \\ -2.074E8 & 0 & 0 & 4.14E8 & & & & & & & & \\ 0 & -40014.1 & -9147.23 & 0 & 80028.3 & & & & & & & \\ 0 & 9147.23 & 1394.04 & 0 & 0 & 5576.15 & & & & & & \\ 0 & 0 & 0 & -2.07E8 & 0 & 0 & 4.15E8 & & & & & \\ 0 & 0 & 0 & 0 & -40014.1 & -9147.23 & 0 & 80028.3 & & & & \\ 0 & 0 & 0 & 0 & 9147.23 & 1394.04 & 0 & 0 & 5576.15 & & & \\ 0 & 0 & 0 & 0 & 0 & 0 & -2.07E-8 & 0 & 0 & 2.07E8 & & \\ 0 & 0 & 0 & 0 & 0 & 0 & 0 & -40014.1 & -9147.23 & 0 & 40014.1 & \\ 0 & 0 & 0 & 0 & 0 & 0 & 0 & 9147.23 & 1394.04 & 0 & -9147.23 & 2788.08 \end{bmatrix}^{-1} \cdot \begin{bmatrix} 0 & & & & & & & & & & & \\ 0 & 0 & & & & & & & & & & \\ 0 & 0 & 1 & & & & & & & & & \\ 0 & 0 & 0 & 0 & & & & & & & & \\ 0 & 0 & 0 & 0 & 0 & & & & & & & \\ 0 & 0 & 0 & 0 & 0 & 0 & & & & & & \\ 0 & 0 & 0 & 0 & 0 & 0 & 0 & & & & & \\ 0 & 0 & 0 & 0 & 0 & 0 & 0 & 0 & & & & \\ 0 & 0 & 0 & 0 & 0 & 0 & 0 & 0 & 0 & & & \\ 0 & 0 & 0 & 0 & 0 & 0 & 0 & 0 & 0 & 0 & & \\ 0 & 0 & 0 & 0 & 0 & 0 & 0 & 0 & 0 & 0 & 0 & \\ 0 & 0 & 0 & 0 & 0 & 0 & 0 & 0 & 0 & 0 & 0 & 0 \end{bmatrix} \cdot \begin{Bmatrix} 0 \\ 2.76E-7 \\ 0.009112 \\ 0 \\ 0.006166 \\ 0.017312 \\ 0 \\ 0.015331 \\ 0.022232 \\ 0 \\ 0.025995 \\ 0.023872 \end{Bmatrix}$$

$$= \{-2.41155E\text{-}14,\ -5.53552E\text{-}6,\ -11.0712E\text{-}6,\ -16.6069E\text{-}6\}^{T}$$

Figure 5.5: Evaluation of the sensitivity of the displacement response with respect to K_R

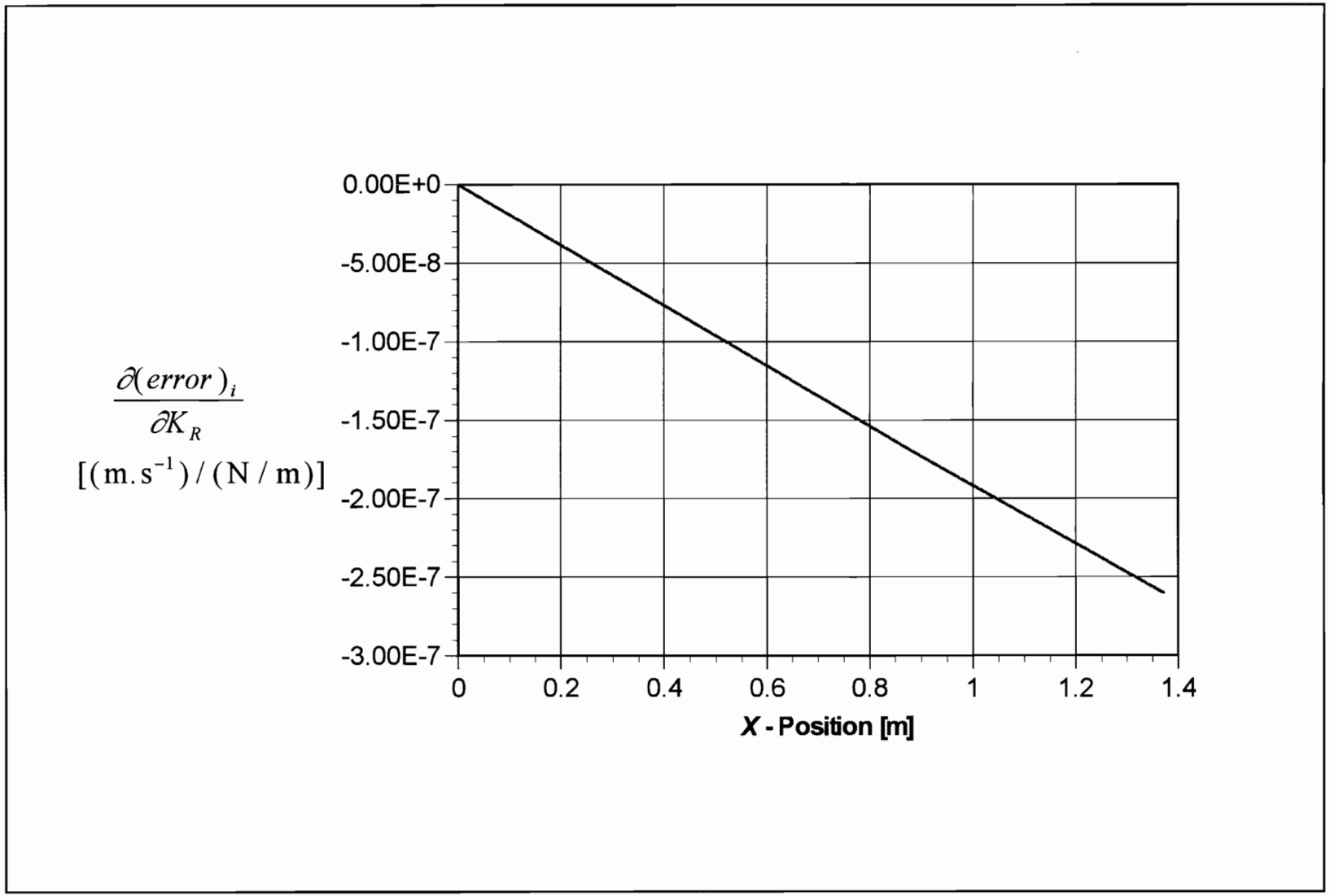

Figure 5.6: Sensitivity of the error function with respect to K_R

Reevaluating the nodal point dynamic response from the frequency response analysis with the new value of K_R (10% bigger) yields:

$$u_{yi} = \{2.76823\text{E}-7, 0.00578713, 0.0145731, 0.0248587\}$$

The maximum difference between the approximate and the exact results is thus 0.65%, showing the validity and correctness of the derivative of the displacement response with respect to K_R.

Chapter 6

Parametric representation of the laser beam and the surface of the structure and the Ray-Patch intersection formulation used

A key part in finding the sensitivity of the error function with respect to the spatial variables of the laser, is to find the scanning position of the laser beam on the surface of the structure as a function of the spatial variables of the laser. This will be achieved by making use of a parametric representation of the laser beam and the surface, as well as by making use of a Ray-Patch intersection formulation.

6.1 Spatial variables of the laser

The first step in the development of the formulation will be to establish the spatial variables of the laser and the notation used for each of these variables. A typical experimental setup, as used to gather data by means of a scanning LDV within ESDM, will be used to define the spatial variables of the laser. Such an experimental setup is shown schematically in *Figure 6.1*.

The spatial variables of the laser, describing the position and orientation of the laser, consist of six variables, which may be divided into two groups consisting of three variables each, as follows:

1. Spatial variables of position
2. Spatial variables of orientation

The spatial variables of position are the x, y and z components of the origin of the laser in the rectangular structural coordinate system and are denoted by x_{Lo}, y_{Lo} and z_{Lo} as shown in *Figure 6.1*. The spatial variables of orientation consist of the three vectors along the axis of the rectangular coordinate system located at the origin of the laser. These three

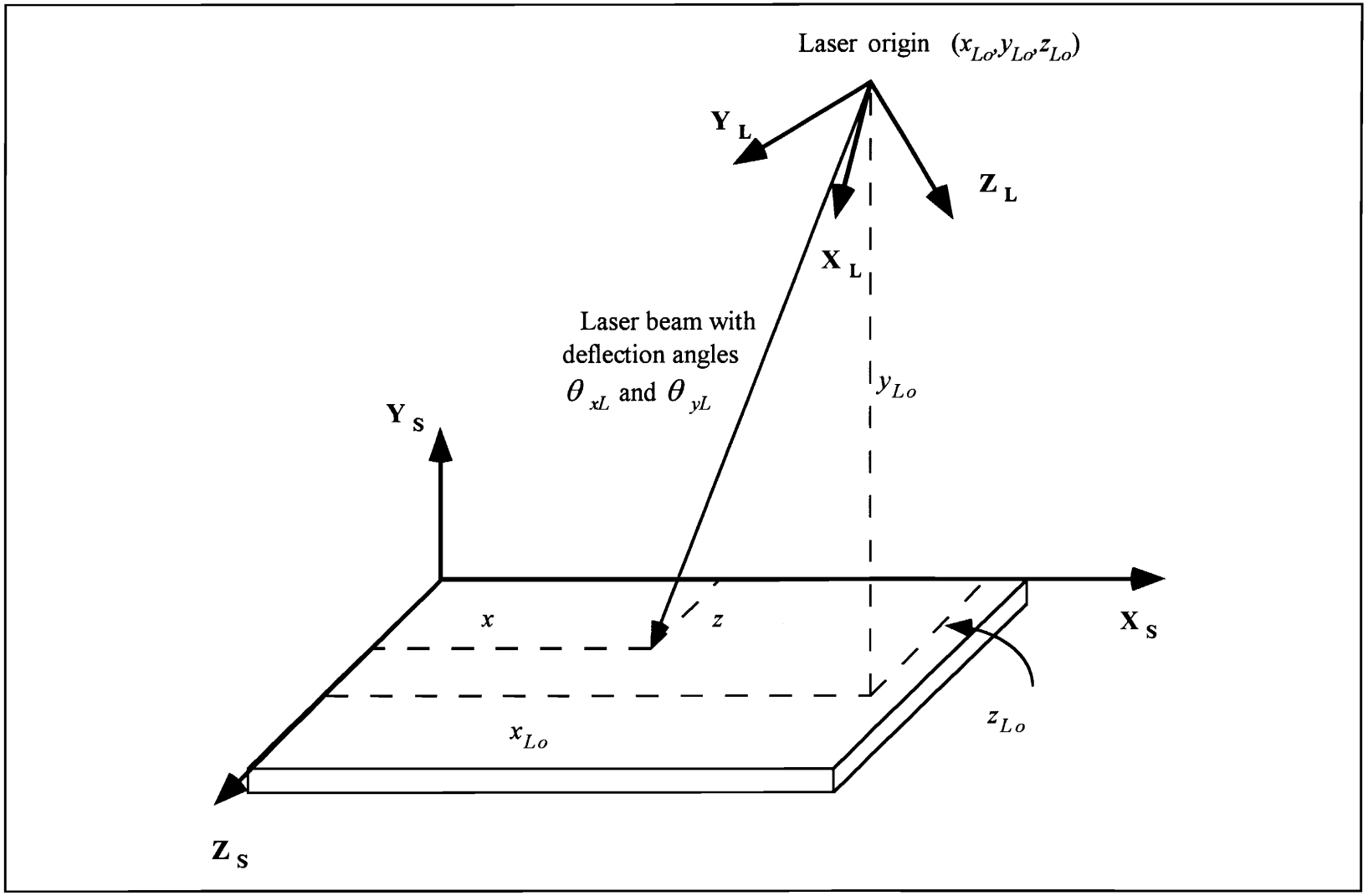

Figure 6.1: Experimental setup showing the structural and laser coordinate systems

vectors are not independent of each other since only two are necessary to define the orientation of the laser uniquely. These vectors will be denoted by $\overline{Laser_x}$, $\overline{Laser_y}$ and $\overline{Laser_z}$ and must be defined in the structural coordinate system. Changes in these vectors will be represented by rotations about each of the three axes of the rectangular laser coordinate system defined at the origin of the laser. These rotations are independent of each other and will be represented by the symbols δ_x, δ_y and δ_z, for rotations about the x, y and z axes respectively.

Figure 6.1 also illustrates some other important concepts that will be used in this chapter. It is important to note that the rectangular structural and laser coordinate systems are in general not aligned. Furthermore, the laser beam is defined in a pseudo-spherical coordinate system located at the origin of the laser, by means of the two deflection angles, θ_{Lx} and θ_{Ly}, and the length of the beam. These two angles are used to deflect the laser beam in such a way as to scan the surface of the structure.

6.2 Ray-Patch intersection formulation

The Ray-Patch intersection formulation yields the intersection between a straight line and a surface patch in three-dimensional space. This intersection is found by making use of parametric representations of the laser beam and the surface of the structure. In this thesis the scope of the work will be limited to reducing the three-dimensional surface patch to a bi-linear surface patch in three-dimensional space.

6.2.1 Parametric representation of a straight line in three-dimensional space

The origin and direction cosines of a line in three-dimensional space may be written in vector notation as:

$$\mathbf{R}_o = \{x_{Lo}, y_{Lo}, z_{Lo}\} \qquad \mathbf{R}_d = \{\eta_x, \eta_y, \eta_z\} \qquad \text{. . . (6.1)}$$

where x_{Lo}, y_{Lo} and z_{Lo} represent the origin of the laser in three-dimensional space, while η_x, η_y and η_z represent the direction cosines of the laser beam in the structural coordinate system.

The origin and direction of the straight line (*Equation 6.1*) may be used to form parametric equations for the line (Zill 1992). These parametric equations represent the laser beam from the point $\mathbf{R}_o$, parallel to the direction vector $\mathbf{R}_d$, as follows:

$$x = x_{Lo} + \eta_x \cdot t \qquad y = y_{Lo} + \eta_y \cdot t \qquad z = z_{Lo} + \eta_z \cdot t \qquad \text{. . . (6.2)}$$

Any position along the length of the laser beam may, thus, be written in terms of the parameter t. The value of t varies from $t = 0$ at point $\mathbf{R}_o$, to infinity as the length of the beam tends to infinity in the direction of the vector $\mathbf{R}_d$. The Ray-Patch intersection formulation may be developed from these parametric equations for a straight line from a point in three-dimensional space parallel, to a direction vector.

Making use of vector notation, the parametric equations of *Equation 6.2* may be combined into a single equation as:

$$\mathbf{R}(t) = \mathbf{R}_o + \mathbf{R}_d \cdot t$$

$$\mathbf{R}(t) = (x_{Lo} + \eta_x \cdot t) \cdot \hat{i} + (y_{Lo} + \eta_y \cdot t) \cdot \hat{j} + (z_{Lo} + \eta_z \cdot t) \cdot \hat{k} \qquad \text{. . . (6.3)}$$

6.2.2 Parametric representation of a surface in three-dimensional space

The equation for the bi-linear surface patch in three-dimensional space, can be described by the normal to the surface, $\vec{N}$. The normal to the surface can be written in terms of the direction cosines of the normal vector as shown in *Equation 6.4*.

$$\vec{N} = n_x \cdot \hat{i} + n_y \cdot \hat{j} + n_z \cdot \hat{k} \qquad \text{. . . (6.4)}$$

The bi-linear surface can be written as (Zill 1992):

$$n_x \cdot x + n_y \cdot y + n_z \cdot z + D = 0 \quad \text{. . . (6.5)}$$

where the variable D is a constant.

If the parametric equations of *Equation 6.3* are substituted into *Equation 6.5*, the parametric equation of *Equation 6.6* is obtained:

$$n_x \cdot (x_{Lo} + \eta_x \cdot t) + n_y \cdot (y_{Lo} + \eta_y \cdot t) + n_z \cdot (z_{Lo} + \eta_z \cdot t) + D = 0 \quad \text{. . . (6.6)}$$

The value of the parameter t, corresponding to the point of intersection between the ray and the surface, may then be solved from *Equation 6.6* in order to obtain:

$$t = \frac{-(n_x \cdot x_{Lo} + n_y \cdot y_{Lo} + n_z \cdot z_{Lo} + D)}{n_x \cdot \eta_x + n_y \cdot \eta_y + n_z \cdot \eta_z} \quad \text{. . . (6.7)}$$

Equation 6.7 may also be written in vector notation as:

$$t = -\frac{(\vec{N} \cdot \mathbf{R}_o + D)}{\vec{N} \cdot \mathbf{R}_d} \quad \text{. . . (6.8)}$$

From *Equations 6.3 and 6.8*, the point of intersection between the line and the plane may then be solved to obtain:

$$\mathbf{r} = \{x, y, z\}$$

$$= \{x_{Lo} + \eta_x \cdot t, y_{Lo} + \eta_y \cdot t, z_{Lo} + \eta_z \cdot t\} \quad \text{. . . (6.9)}$$

From *Equation 6.9*, the scanning position of the laser beam on the surface of the structure may, thus, be solved in terms of the spatial variables of the laser, x_{Lo}, y_{Lo}, z_{Lo}, δ_x, δ_y and δ_z.

6.3 Scanning position in terms of the spatial position of the laser

The Ray-Patch intersection formulation will now be used to obtain the scanning position of the laser beam on the surface of the structure in terms of the spatial position of the laser. Parametric equations will be developed for the laser beam while the surface of the structure will be represented by the equation for a bi-linear surface patch in three-dimensional space as shown in *Equation 6.5*.

A unit vector parallel to the laser beam will be used to obtain the direction cosines of the laser beam in the structural coordinate system. However, the laser beam is specified in the spherical laser coordinate system by means of its length and the two deflection angles, θ_{Lx} and θ_{Ly}. The unit vector must thus be transformed from the spherical laser coordinate system to the rectangular structural coordinate system, which will involve two separate vector transformations. The unit vector must first be transformed from the spherical to the rectangular laser coordinate system and then from the rectangular laser coordinate system to the rectangular structural coordinate system.

The spherical to rectangular laser coordinate transformation will be accomplished by making use of a spherical to rectangular transformation matrix. The laser spherical coordinate system is somewhat different than the spherical coordinate system normally defined in mathematics. Both these coordinate systems are shown schematically in *Figure 6.2*. From *Figure 6.2* the relationship between the rectangular and spherical laser coordinate systems may be obtained, yielding the transformation matrix between the two coordinate systems as:

$$\begin{Bmatrix} x_L \\ y_L \\ z_L \end{Bmatrix} = \mathbf{T}_S \qquad \text{with} \qquad \mathbf{T}_S = \rho \cdot \begin{Bmatrix} Sin(\theta_{Ly}) \cdot Cos(\theta_{Lx}) \\ -Sin(\theta_{Lx}) \\ Cos(\theta_{Lx}) \cdot Cos(\theta_{Ly}) \end{Bmatrix} \qquad \text{. . . (6.10)}$$

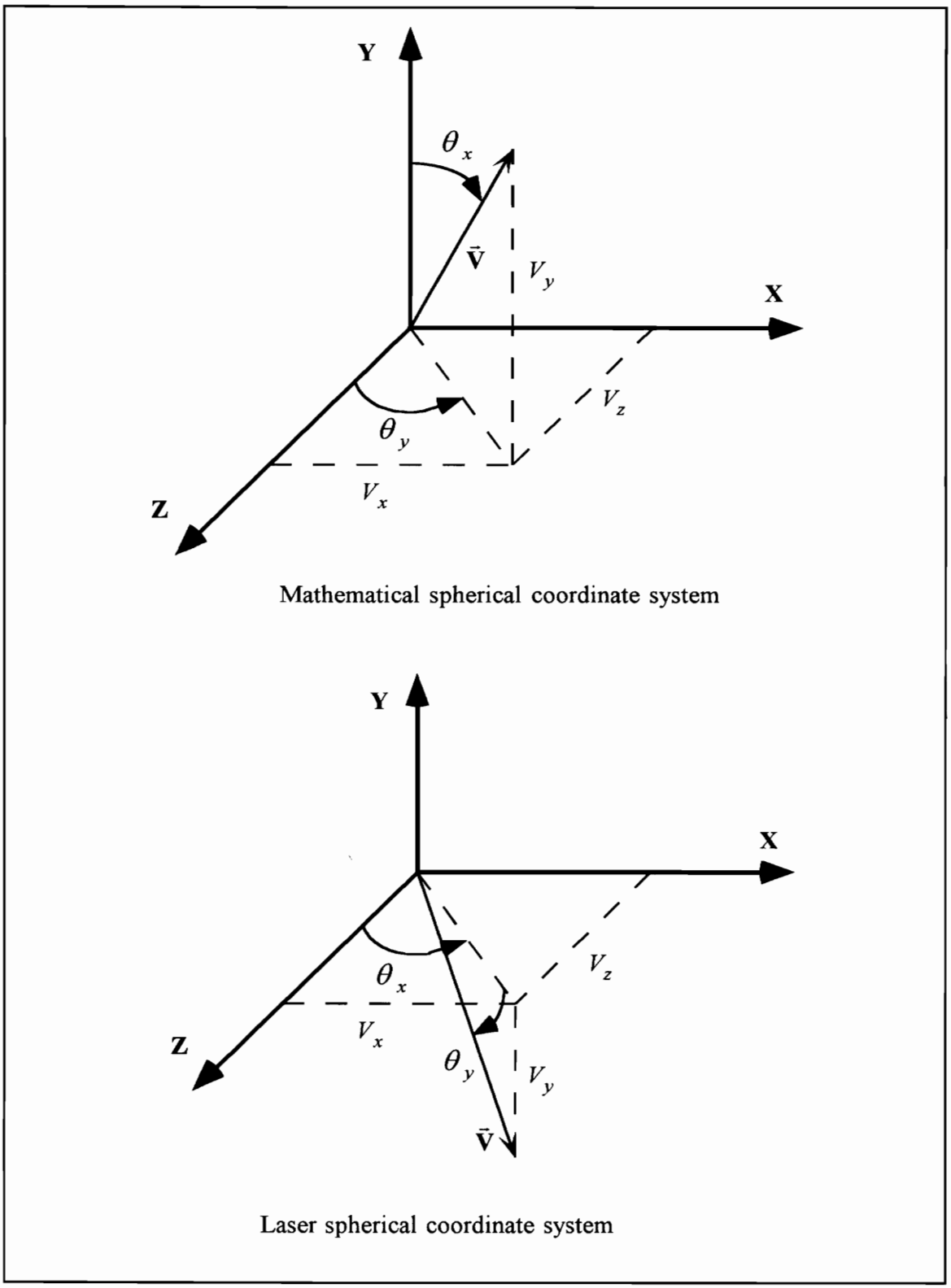

Figure 6.2: Spherical coordinate systems

For the unit vector used, the length of the vector, ρ, in *Equation 6.10* is equal to one. By making use of *Equation 6.10*, the unit vector parallel to laser beam may be obtained in the rectangular laser coordinate system. Since the rectangular laser and structural coordinate systems are, in general, not aligned (*Figure 6.1*), the next step is to transform the unit vector from the rectangular laser coordinate system to the rectangular structural coordinate system. The relationships between the coordinates of a vector in two, unaligned rectangular coordinate systems, with the same origin, is shown schematically in *Figure 6.3*. From the relationship shown in *Figure 6.3*, the transformation of a vector from the laser coordinate system (x_L, y_L and z_L components) to the structural coordinate system (x, y and z components) may be written in matrix form as:

$$\begin{Bmatrix} x_L \\ y_L \\ z_L \end{Bmatrix} = \mathbf{T}_R \cdot \begin{Bmatrix} x \\ y \\ z \end{Bmatrix} \qquad \text{with} \qquad \mathbf{T}_R = \begin{bmatrix} l_1 & m_1 & n_1 \\ l_2 & m_2 & n_2 \\ l_3 & m_3 & n_3 \end{bmatrix} \qquad \text{. . . (6.11)}$$

The matrix $\mathbf{T}_R$ is composed of the direction cosines of the axes of the laser coordinate system with respect to the axes of the structural coordinate system as shown in *Figure 6.3*. Matrix $\mathbf{T}_R$ is an orthogonal matrix ($\mathbf{T}_R^{-1} = \mathbf{T}_R^T$) and the inverse relationship of *Equation 6.11* may thus be written as:

$$\begin{Bmatrix} x \\ y \\ z \end{Bmatrix} = \mathbf{T}_R^T \cdot \begin{Bmatrix} x_L \\ y_L \\ z_L \end{Bmatrix} \qquad \text{. . . (6.12)}$$

Introducing the convention that the top surface of the structure is located parallel to the x-z plane at $y = 0$ (this convention will hold for all surfaces considered in this research), the scanning position of the laser beam on the structure may be solved in terms of the spatial variables of the laser from the Ray-Patch intersection formulation (*Equations 6.8 and 6.9*) as follows

$$\mathbf{r}_{ScanningPosition} = \{x_{Lo} + \eta_x \cdot t, y_{Lo} + \eta_y \cdot t, z_{Lo} + \eta_z \cdot t\} \qquad \text{. . . (6.13)}$$

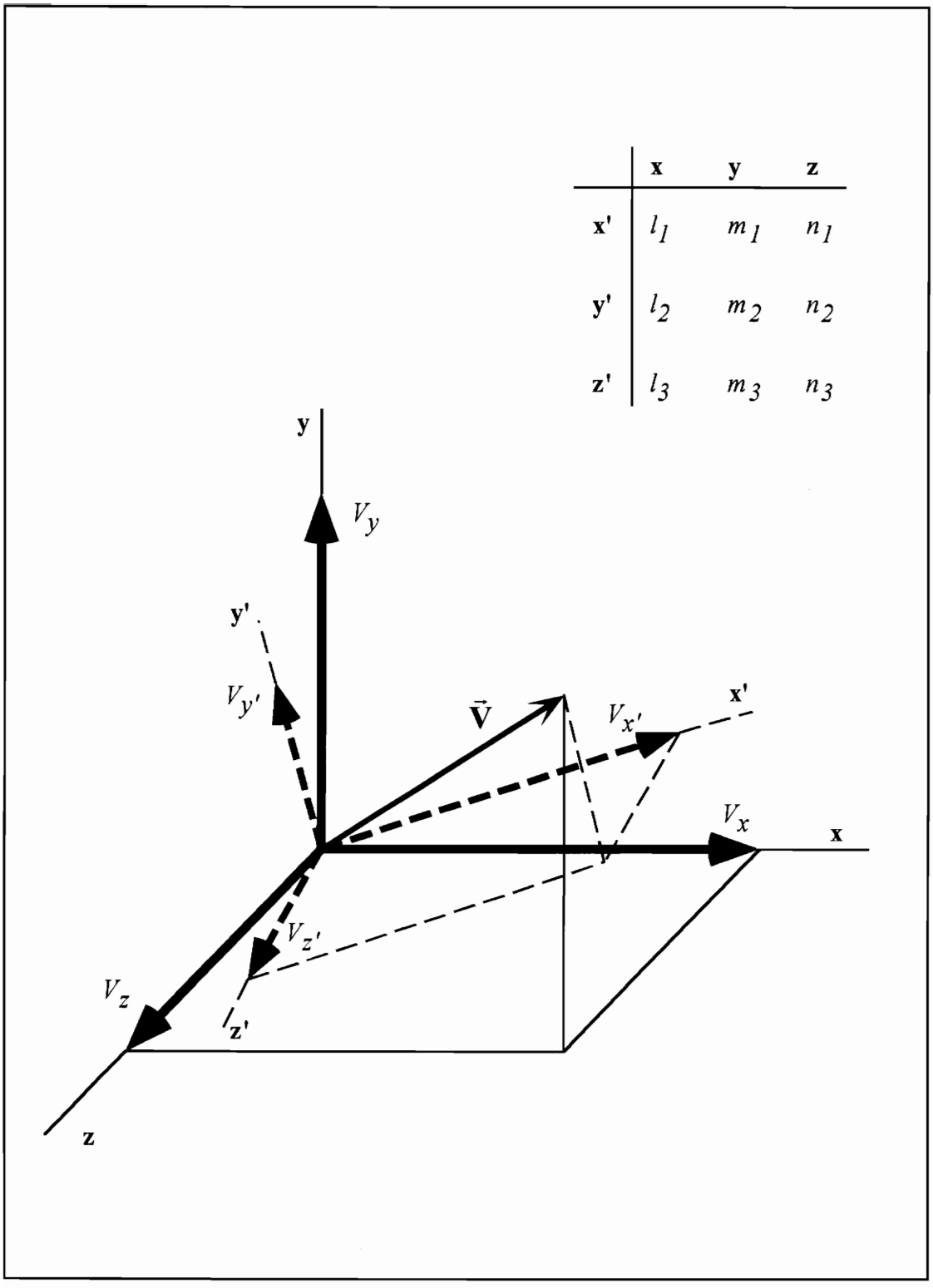

Figure 6.3: Rotational transformation between two rectangular, three-dimensional coordinate systems

with the parametric variable, t, given as:

$$t = -\frac{(\vec{N} \cdot \mathbf{R}_o + D)}{\vec{N} \cdot \mathbf{R}_d} \quad \text{. . . (6.14)}$$

The origin of the laser $\mathbf{R}_o$ and the direction of the laser, $\mathbf{R}_d$, are given by

$$\mathbf{R}_o = \{x_{Lo}, y_{Lo}, z_{Lo}\} \qquad \mathbf{R}_d = \{\eta_x, \eta_y, \eta_z\} = \mathbf{T}_R^T \cdot \mathbf{T}_S \quad \text{. . . (6.15)}$$

while the normal to the surface patch may be written as:

$$\vec{N} = \{0, 1, 0\} \quad \text{. . . (6.16)}$$

6.4 Scanning position in terms of the spatial orientation of the laser

As stated earlier, changes in the orientation variables of the laser will be represented by rotations about each of the axes of the laser. In order to find the scanning position of the laser beam on the surface of the structure in terms of these rotations, it is necessary to work with only one variable at a time. The derivation will be performed for rotations about the z axis of the rectangular laser coordinate system, but the method is the same for rotations about the other two axes.

In order to develop the method, a temporary rectangular coordinate system will be defined at the origin of the laser. This coordinate system will be defined in such a way as to be precisely aligned with the structural coordinate system. The first step in developing the formulation is to write the unit vectors defining the axes of the temporary coordinate system in terms of the orientation variable in question. For rotations about the z-axis (the temporary coordinate system with rotations about the z-axis is shown schematically in *Figure 6.4*) the direction vectors may be written as:

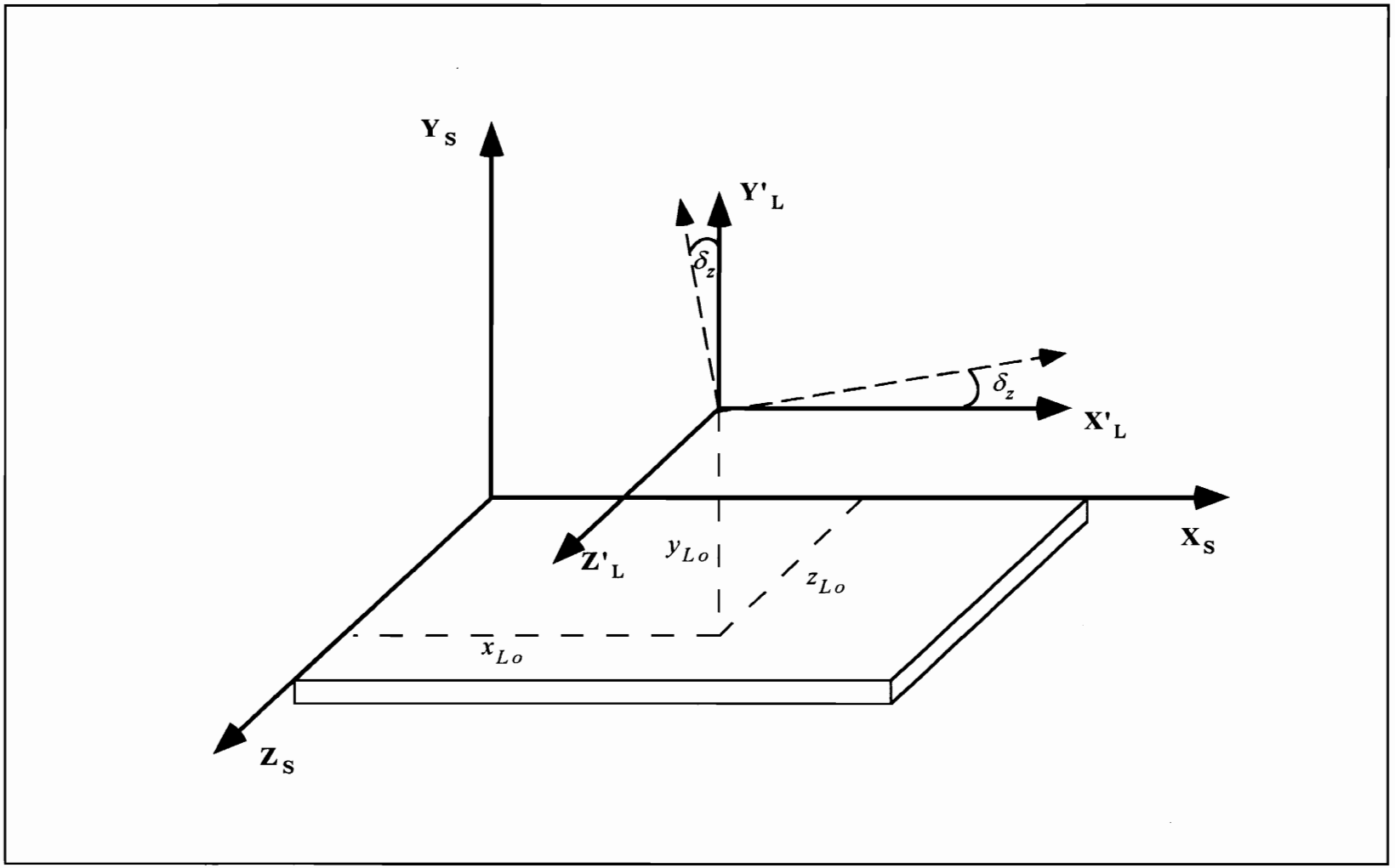

Figure 6.4: Temporary coordinate system with rotations (δ_z) about the **Z'$_L$**-axis

$$\mathbf{A}_z = \begin{bmatrix} Cos(\delta_z) & -Sin(\delta_z) & 0 \\ Sin(\delta_z) & Cos(\delta_z) & 0 \\ 0 & 0 & 1 \end{bmatrix}$$

. . . **(6.17)**

It will be noted that the matrix $\mathbf{A}_z$ yields the unit vectors defining the axis of the structural coordinate system if the rotation is taken to be zero.

Making use of the three-dimensional transformation matrix between the rectangular laser coordinate system and the rectangular structural coordinate system (as well as the temporary coordinate system in this case, since they are precisely aligned), *Equation 6.11*, these direction vectors may be transformed to the actual orientation of the rectangular laser coordinate system as follows:

$$\overline{\mathbf{T}}_R = \mathbf{T}_R \cdot \mathbf{A}^T$$

. . . **(6.18)**

In effect, the unit vectors along the laser rectangular coordinate system is, thus, known in terms of the rotations about each of the three axes of the laser. The scanning position will once again be solved from the Ray-Patch intersection formulation, in the same way as described in *Section 6.2*. The only difference being the use of the matrix $\overline{\mathbf{T}}_R$ (*Equation 6.18*) instead of $\mathbf{T}_R$ (*Equation 6.11*) as the transformation matrix between the rectangular structural and laser coordinate systems. The resulting equations from the Ray-Patch intersection formulation for rotations about the *z*-axis can then be written as follows:

$$\mathbf{r}_{ScanningPosition} = \{x_{Lo} + \eta_x \cdot t, y_{Lo} + \eta_y \cdot t, z_{Lo} + \eta_z \cdot t\}$$

. . . **(6.19)**

with the parametric variable, t, given as:

$$t = -\frac{(\vec{N} \cdot \mathbf{R}_o + D)}{\vec{N} \cdot \mathbf{R}_d}$$

. . . **(6.20)**

The origin of the laser $\mathbf{R}_o$ and the direction of the laser, $\mathbf{R}_d$, are given by

$$\mathbf{R}_o = \{x_{Lo}, y_{Lo}, z_{Lo}\} \qquad \mathbf{R}_d = \{\eta_x, \eta_y, \eta_z\} = \mathbf{T}_R^T \cdot \mathbf{A}_z \cdot \mathbf{T}_S \quad \text{. . . (6.21)}$$

while the normal to the surface patch may be written as:

$$\vec{N} = \{0, 1, 0\} \quad \text{. . . (6.22)}$$

6.5 Test case

A test case will be used to show the process of calculating the scanning position as a function of the spatial variables of the laser. The scanning position is defined as the coordinates, in the structural coordinate system, where the laser beam hits the structure. As a test case, a 0.5 by 0.5 meter square plate will be evaluated. In order to simplify the algebra involved, for better illustration of the method, the plate will be modeled by one element only. The method will be the same as in the general case (multiple elements) except for the fact that it will no longer be necessary to identify the specific element containing the point of intersection. Furthermore, the laser will be positioned in such a way that the scanning position, as well as the influence of the spatial variables on the scanning position, may easily be calculated from simple geometrical relationships. The results obtained from this geometrical relationships will then be used to verify the results obtained from the Ray-Patch intersection formulation.

6.5.1 Setup of the test case

The experimental setup is shown schematically in *Figure 6.5*. The laser will be located 2.5 meters directly above the midpoint of the plate at:

$$\{x_{Lo}, y_{Lo}, z_{Lo}\} = \{0.25, 2.5, 0.25\} \quad [\text{m}]$$

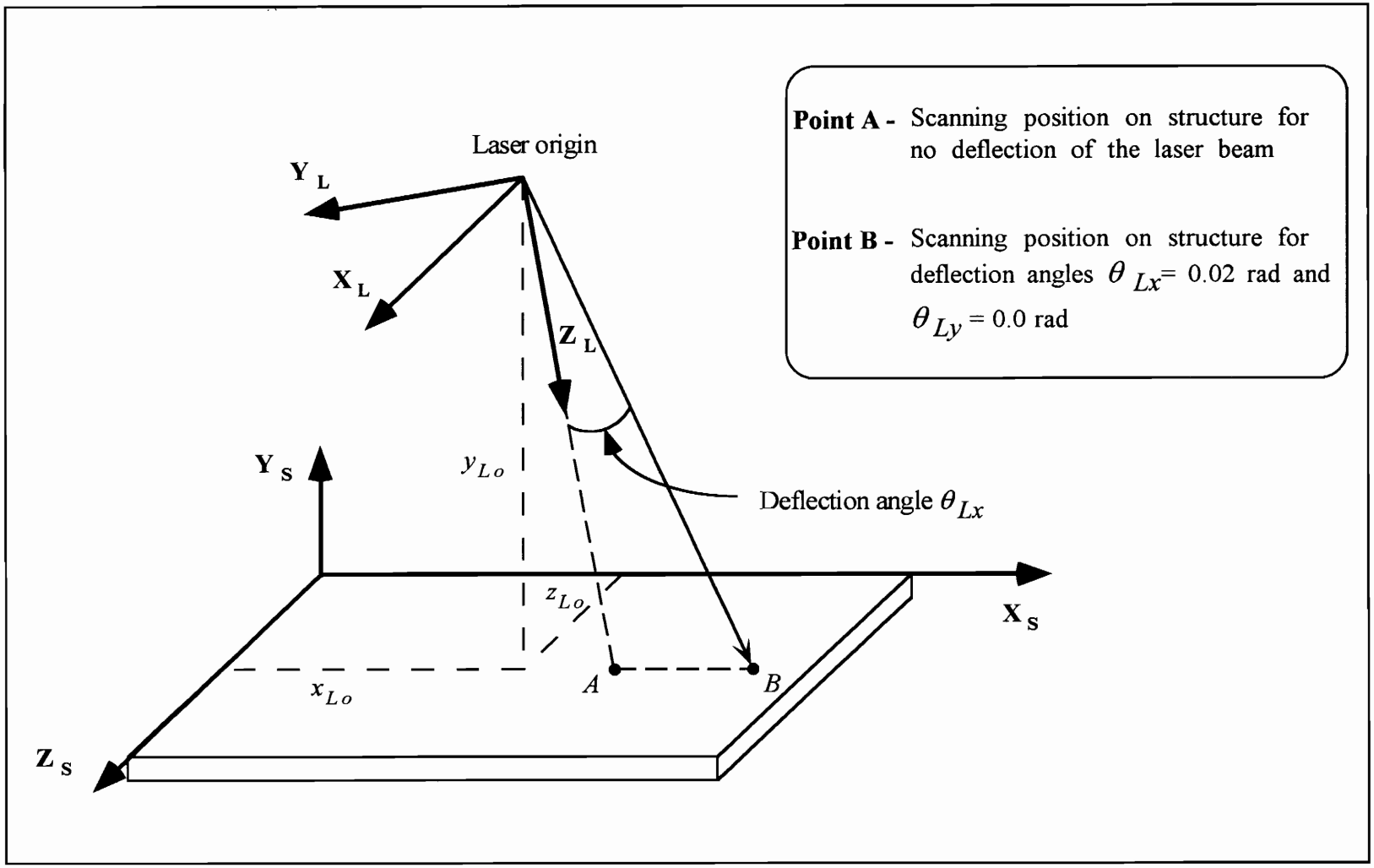

Figure 6.5: Experimental setup for the test case

The orientation of the laser will be chosen such that the x-axis of the laser will be aligned with the z-axis of the structure. Furthermore, the z- and y-axes of the laser will be orientated as to respectively make a 0.05 radians angle with the negative y- and x-axes of the structure. The orientation will be specified by means of the two vectors, $\overline{Laser_x}$ and $\overline{Laser_z}$, along the x- and z-axes of the laser coordinate system respectively. These vectors have the laser origin as origin and may be written as:

$$\overline{Laser_x} = \{12, 100, 10\} \qquad \overline{Laser_z} = \{0.3751, 0, 0.25\}$$

The laser beam will be deflected by the two angles, θ_{Lx} and θ_{Ly}.

$$\theta_{Lx} = 0.02 \quad \text{rad} \qquad \theta_{Ly} = 0.00 \quad \text{rad}$$

These angles are chosen as to avoid the so-called pincushion effect, which is inherent to the process of mapping the inside surface of a sphere (unit vector in spherical coordinate system) to a flat surface (scanning position of the laser beam on the structure). When mapping the inside surface of a sphere to a flat surface the shape of the surface being mapped is distorted. This distortion of the surface means that the scanning position is influenced by both deflection angles. The pincushion effect can be illustrated by setting the angle between the z- and y-axes of the laser and the negative y- and x-axes of the structure equal to zero (*Figure 6.5*). The pincushion effect is more prominent at larger deflection angles and in order to amplify the effect, large deflection angles (well beyond the range of the laser) will be considered. A 5 by 5 meter square plate with the laser positioned 2.5 meters directly above the center point will be evaluated. This setup will result in maximum deflection angles of $\pm\pi/4$ rad. θ_{Lx} is now varied between $-\pi/4$ and $\pi/4$ radians, while first keeping θ_{Ly} constant at -0.7 and then at 0.7 radians respectively. The process will then be repeated by varying θ_{Ly} while setting θ_{Lx} equal to -0.7 and 0.7 radians. The four lines obtained through this process is shown in *Figure 6.6*. The curved shapes of the vertical lines in *Figure 6.6* is known as the pincushion effect.

By avoiding the pincushion effect, it is possible to verify the scanning position obtained from the Ray-Patch intersection formulation by means of simple geometrical relationships.

Lastly, the convention of defining the structural coordinate system with the top surface of the structure in the x-z plane at $y = 0$, will be used.

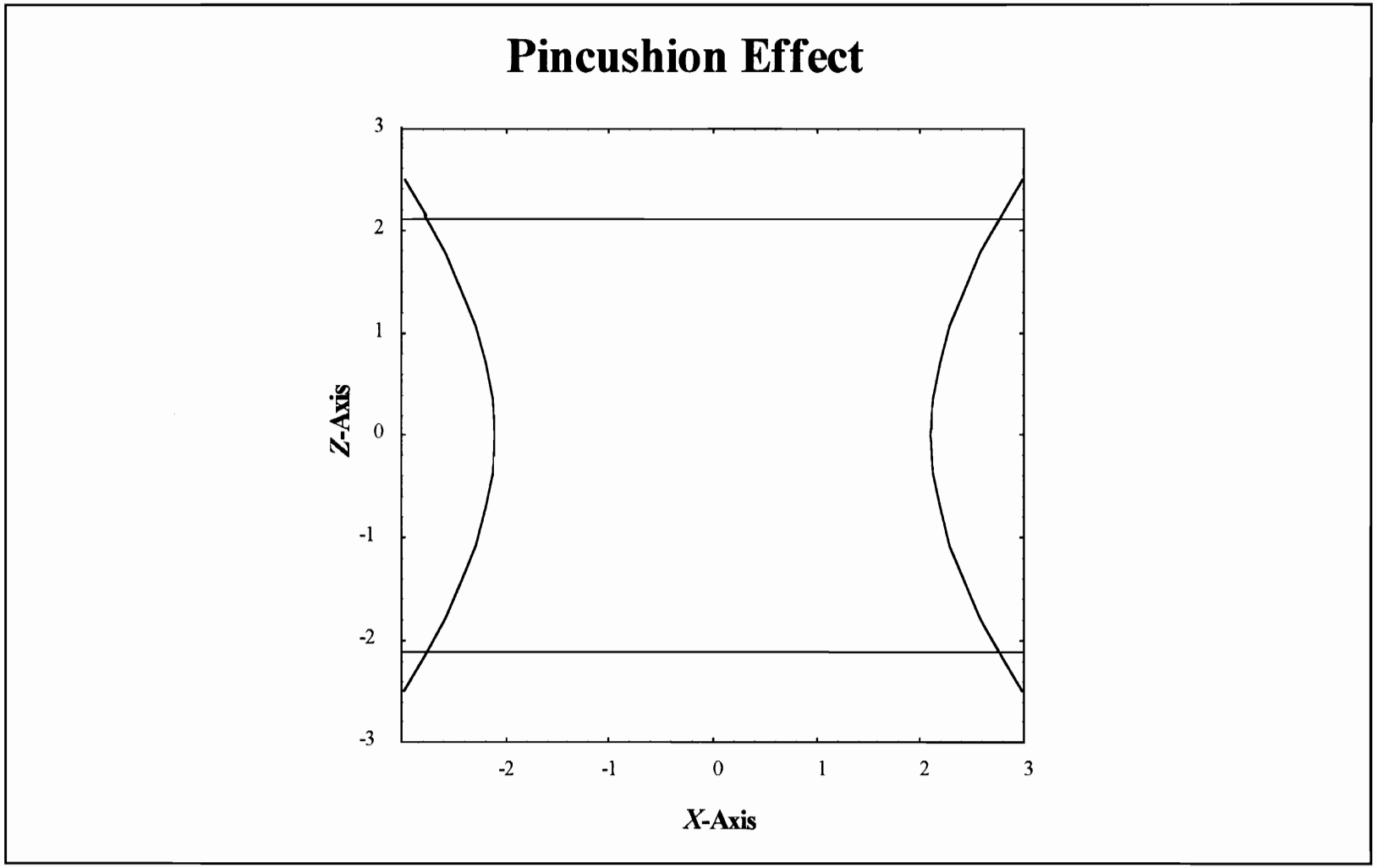

Figure 6.6: Pincushion effect

6.5.2 Computation of Ray-Patch intersection in terms of the spatial position of the laser

Equation 6.10 will be used to transform a unit vector along the laser beam from the spherical laser coordinate system to the rectangular laser coordinate system. The obtained transformation matrix may be written as:

$$\mathbf{T}_S = \begin{bmatrix} 0 \\ -0.019998 \\ 0.9998 \end{bmatrix} \quad \text{. . . (6.23)}$$

By taking the cross product of the two normalized vectors describing the orientation of the laser ($\overline{Laser_x}$ and $\overline{Laser_y}$), unit vectors of the axes of the laser coordinate system along the three axes of the structural coordinate system are obtained, as:

$$\hat{e}_x = \{0 \quad , 0 \quad , 0\}$$

$$\hat{e}_y = \{-0.99875 \quad , -0.04998 \quad , 0\}$$

$$\hat{e}_z = \{0.04998 \quad , -0.99875 \quad , 0\}$$

By making use of *Equation 6.11* the transformation matrix between the laser and structural rectangular coordinate systems may be written directly from these unit vectors (which also represent the direction cosines of the respective axes) as:

$$\mathbf{T}_R = \begin{bmatrix} 0 & 0 & 1 \\ -0.99875 & -0.04998 & 0 \\ 0.04998 & -0.99875 & 0 \end{bmatrix} \quad \text{. . . (6.24)}$$

The scanning position may then be solved from *Equation 6.13 through 6.16* where:

$$\mathbf{r}_{ScanningPosition} = \{x_{Lo} + \eta_x \cdot t, y_{Lo} + \eta_y \cdot t, z_{Lo} + \eta_z \cdot t\}$$

with:

$$\mathbf{R}_o = \{x_{Lo}, y_{Lo}, z_{Lo}\} = \{0.25, 2.5, 0.25\} \quad [\text{m}]$$

$$\mathbf{R}_d = \{\eta_x, \eta_y, \eta_z\} = \mathbf{T}_R^T \cdot \mathbf{T}_S = \{0.0699428, -0.997551, 0\}$$

$$\vec{N} = \{0, 1, 0\}$$

$$t = -\frac{(\vec{N} \cdot \mathbf{R}_o + D)}{\vec{N} \cdot \mathbf{R}_d} = 0.00246 \cdot y_{Lo} = 2.50614$$

. . . **(6.25)**

From *Equation 6.25* the scanning position may be solved as:

$$\mathbf{r}_{SP} = \{x_{Lo} + 0.0701146 \cdot y_{Lo}, 0, z_{Lo}\}$$

$$= \{0.425286, 0, 0.25\} \quad [\text{m}]$$

. . . **(6.26)**

The scanning position of the laser beam on the structure may also be calculated from the orientation and deflection angles of the laser and the laser beam respectively by making use of simple geometrical relationships. The results obtained by making use of the geometrical relationships, will be used to verify the results obtained from the Ray-Patch intersection formulation. The geometrical relationships and the corresponding results may be summarized as:

$$\mathbf{r}_{SP} = \{0.25 + 2.5 \cdot Tan(0.05 + 0.02), 0, 0.25\}$$

$$= \{0.425286, 0, 0.25\} \quad [\text{m}]$$

These results are exactly equal to the results obtained in *Equation 6.27*, thus verifying the result obtained from the Ray-Patch intersection formulation.

6.5.3 Computation of Ray-Patch intersection in terms of the spatial orientation of the laser

Since the procedure is the same for rotations about all three axes of the laser rectangular coordinate system, the test case will be evaluated only for rotations about the *x*-axis as a representative case. The test case will be evaluated for the specific rotation:

$$\delta_x = 0.01 \quad \text{rad}$$

The temporary rectangular matrix for rotations about the *x*-axis may be written from *Equation 6.17* as:

$$\mathbf{A}_x = \begin{bmatrix} 1 & 0 & 0 \\ 0 & Cos(\delta_x) & -Sin(\delta_x) \\ 0 & Sin(\delta_x) & Cos(\delta_x) \end{bmatrix}$$

From *Equation 6.18*, the new transformation matrix may be written as

$$\overline{\mathbf{T}}_R = \mathbf{T}_R \cdot \mathbf{A}^T$$

where the matrix $\mathbf{T}_R$ is the same transformation matrix of *Equation 6.24*, yielding (for $\delta_x = 0.01$ rad):

$$\overline{\mathbf{T}}_R = \begin{bmatrix} 0 & 0 & 1 \\ -0.99875 \cdot Cos(\delta_x) + 0.0499792 \cdot Sin(\delta_x) & -0.0499792 \cdot Cos(\delta_x) - 0.99875 \cdot Sin(\delta_x) & 0 \\ 0.0499792 \cdot Cos(\delta_x) + 0.99875 \cdot Sin(\delta_x) & -0.99875 \cdot Cos(\delta_x) + 0.0499792 \cdot Sin(\delta_x) & 0 \end{bmatrix}$$

$$= \begin{bmatrix} 0 & 0 & 1 \\ -0.998201 & -0.059964 & 0 \\ 0.059964 & -0.998201 & 0 \end{bmatrix}$$

. . . **(6.27)**

The spherical-to-rectangular transformation matrix, $\mathbf{T}_S$, is the same matrix as the matrix of *Equation 6.23* and may be written as:

$$\mathbf{T}_S = \begin{bmatrix} 0 \\ -0.019998 \\ 0.9998 \end{bmatrix}$$

From *Equation 6.19 through 6.22* and $\mathbf{T}_S$, the scanning position may be solved to obtain (once again for $\delta_x = 0.01$ rad)

$$\mathbf{r}_{SP} = \{x_{Lo} + \eta_x \cdot t, y_{Lo} + \eta_y \cdot t, z_{Lo} + \eta_z \cdot t\}$$

with

$$\mathbf{R}_o = \{x_{Lo}, y_{Lo}, z_{Lo}\} = \{0.25, 2.5, 0.25\} \quad [\text{m}]$$

$$\mathbf{R}_d = \{\eta_x, \eta_y, \eta_z\}^T = \mathbf{T}_R^T \cdot \mathbf{A}_x \cdot \mathbf{T}_S$$

$$= \begin{Bmatrix} 0.0699428 \cdot Cos(\delta_x) + 0.0699428 \cdot Sin(\delta_x) \\ -0.997551 \cdot Cos(\delta_x) + 0.0699428 \cdot Sin(\delta_x) \\ 0 \end{Bmatrix} = \begin{Bmatrix} 0.0799147 \\ -0.996802 \\ 0 \end{Bmatrix}$$

$$\vec{N} = \{0, 1, 0\}$$

$$t = -\frac{\vec{N} \cdot \mathbf{R}_o}{\vec{N} \cdot \mathbf{R}_d} = \frac{-2.5}{-0.997551 \cdot Cos(\delta_x) + 0.0699428 \cdot Sin(\delta_x)} = 2.50802 \qquad \textbf{. . . (6.28)}$$

yielding the scanning position as:

$$\mathbf{r}_{SP} = \{0.25 - \frac{2.5 \cdot (0.06994 \cdot Cos(\delta_x) + 0.997551 \cdot Sin(\delta_x))}{-0.997551 \cdot Cos(\delta_x) + 0.06994 \cdot Sin(\delta_x)}, 0, 0.25\}$$

$$= \{0.45042776, 0, 0.25\} \qquad \textbf{. . . (6.29)}$$

As in *Section 6.5.2*, the result obtained from the Ray-Patch intersection formulation may be verified by results obtained from simple geometrical relationships by calculating the scanning position as:

$$\mathbf{r}_{SP} = \{0.25 + 2.5 \cdot Tan(0.05 + 0.02 + 0.01), 0, 0.25\}$$

$$= \{0.4504278, 0, 0.25\}$$

As before, both results are exactly the same, showing the validity of the Ray-Patch intersection formulation.

Chapter 7

Sensitivity of the error function with respect to the spatial position and orientation of the laser

The Ray-Patch intersection formulation will be used to find the scanning position of the laser beam on the structure in terms of the spatial variables of the laser. Together with the finite element formulation and basis functions, the sensitivities of the error function with respect to the spatial variables of the laser may be evaluated. Only bi-linear surface patches will be considered and the approach will be derived for plate elements only. Once the approach is established for the two-dimensional plate element formulation, it is a much simpler task to simplify it to the one-dimensional beam formulation.

7.1 Fundamentals of the approach

The influence on the accuracy of a model, obtained through ESDM, due to changes in the position and orientation of the laser will be evaluated. This will be accomplished by writing the sensitivities in terms of their partial derivatives. The finite element basis functions as well as the Ray-Patch intersection formulation will be used in the evaluation of these partial derivatives.

7.1.1 Underlying motivation and fundamental philosophy for the approach

The sensitivity of the error function with respect to the spatial position and orientation of the laser must be evaluated. The ESDM error function, consistent with a finite element formulation, is given by *Equation 3.20* and is restated here as:

$$error_i = v_{xi} \cdot \eta_{xi} + v_{yi} \cdot \eta_{yi} + v_{zi} \cdot \eta_{zi} - \tilde{V}_{Li} \qquad \text{. . . (7.1)}$$

The unknown velocity field as well as the direction cosine terms contained in *Equation 7.1*, are dependent on a number of variables. This dependency may be shown by writing the individual terms in their functional form. The generalized functional relationships for the velocity terms may then be expressed as

$$v_{xi} = f_1(\omega, x_i, y_i, z_i) \quad v_{yi} = g_1(\omega, x_i, y_i, z_i) \quad v_{zi} = h_1(\omega, x_i, y_i, z_i) \qquad \text{. . . (7.2)}$$

showing the dependency of the velocity on the excitation frequency as well as on the location within the structure.

The direction cosines are, in turn, dependent on the spatial position and orientation of the laser as well as on the scanning position of the laser beam on the surface of the structure. These functional relationships for the direction cosines may be written as:

$$\eta_{xi} = f_2(x_{Lo}, y_{Lo}, z_{Lo}, x_i, y_i, z_i)$$

$$\eta_{yi} = g_2(x_{Lo}, y_{Lo}, z_{Lo}, x_i, y_i, z_i)$$

$$\eta_{zi} = h_2(x_{Lo}, y_{Lo}, z_{Lo}, x_i, y_i, z_i) \qquad \text{. . . (7.3)}$$

The components of the scanning position of the laser beam on the surface of the structure (x_i ,y_i and z_i), contained in the functional relationships of both *Equations 7.2 and 7.3*, are also dependent on a number of variables, including the spatial variables of the laser. If the components of the scanning position are expressed in functional form, the following relationships are obtained:

$$x_i = f_3\left(x_{Lo}, y_{Lo}, z_{Lo}, \overline{Laser_x}, \overline{Laser_z}, \theta_{Lx}, \theta_{Ly}, \text{Surface Representation}\right)$$

$$y_i = g_3\left(x_{Lo}, y_{Lo}, z_{Lo}, \overline{Laser_x}, \overline{Laser_z}, \theta_{Lx}, \theta_{Ly}, \text{Surface Representation}\right)$$

$$z_i = h_3\left(x_{Lo}, y_{Lo}, z_{Lo}, \overline{Laser_x}, \overline{Laser_z}, \theta_{Lx}, \theta_{Ly}, \text{Surface Representation}\right)$$

. . . **(7.4)**

The vectors $\overline{Laser_x}$ and $\overline{Laser_z}$ are used to represent the orientation of the laser head relative to the structural coordinate system. In *Equation 7.4* the two orthogonal vectors along the x and z axes of the three dimensional rectangular laser coordinate system are used, but any two of the three vectors defining the axes of the laser coordinate system may be used.

As shown in *Equation 7.4*, the scanning position is also a function of the method used to represent the surface. In this research, only bi-linear surface patches will be considered. This defines the functional relationships of *Equation 7.4* since the scanning position is no longer dependent on the method used, as long as it is capable of representing planar surfaces.

From the above functional relationships, it is clear that both the velocity components as well as the direction cosines are dependent on the spatial variables of the laser. Furthermore, in order to evaluate the derivatives of the error function with respect to the spatial variables of the laser, it will be necessary to find explicit functional relationships for the components of the scanning position in terms of the spatial variables.

7.1.2 Method of solving the problem.

The method of solving the problem consists of four basic steps. These steps may in turn be summarized conceptually as:

1. Find a numerical approximation of the geometry of the structure by making use of the finite element formulation
2. Expand the sensitivities of the error function with respect to the spatial variables of the laser into their partial derivatives

3. Find the scanning position of the laser beam on the structure in terms of the spatial variables of the laser by making use of coordinate transformations and the Ray-Patch intersection formulation (*Chapter 6*)
4. Solve the partial derivatives of *Step 2* in order to obtain a solution of the sensitivity of the error function with respect to the spatial variables of the laser

7.2 Resulting formulation

The mathematical formulation used to achieve the goals of this second part of the research, will now be developed. This includes the expansion of the sensitivity of the error function into its partial derivatives, the evaluation of these partial derivatives as well as the Ray-Patch intersection formulation.

7.2.1 Goals and criteria used to evaluate the success of the method

The goal of this second part of the thesis, as stated in *Chapter 1*, is to evaluate the sensitivity of the accuracy of a model, obtained from the ESDM formulation, to the spatial variables of position and orientation of the laser.

Specifically, the first-order sensitivities of the error function with respect to the spatial position and orientation of the laser will be evaluated. These sensitivities must be obtained by means of an analytical evaluation of the derivatives involved. This will be accomplished by making use of the finite element formulation and basis functions as well as the Ray-Patch intersection formulation.

7.2.2 Fundamental assumptions or limitations to be applied to the method

The only limitation of the work presented in this thesis, is the assumption that only flat, straight-sided plate elements will be considered. This will enable the use of a sub-parametric formulation of the elements, yielding a bi-linear representation of the surface. However, the method is, in general, naturally extendible to general three-dimensional surfaces.

7.2.3 Mathematical formulation

Differentiating the error function, *Equation 7.1*, with respect to a spatial variable of the laser, say χ, yields *Equation 7.5* as follows:

$$\frac{\partial(error_i)}{\partial\chi} = \left(\frac{\partial v_{xi}}{\partial\chi}\cdot\eta_{xi} + v_{xi}\cdot\frac{\partial\eta_{xi}}{\partial\chi}\right) + \left(\frac{\partial v_{yi}}{\partial\chi}\cdot\eta_{yi} + v_{yi}\cdot\frac{\partial\eta_{yi}}{\partial\chi}\right) + \left(\frac{\partial v_{zi}}{\partial\chi}\cdot\eta_{zi} + v_{zi}\cdot\frac{\partial\eta_{zi}}{\partial\chi}\right) \quad \text{. . . (7.5)}$$

The values of the direction cosines, contained in *Equation 7.5*, depend on the spatial position of the laser and the scanning position of the laser beam on the structure. The equations yielding the three direction cosines may be summarized as:

$$\eta_{xi} = \frac{\sqrt{(x_{Lo} - x_i)^2}}{\sqrt{(x_{Lo} - x_i)^2 + (y_{Lo} - y_i)^2 + (z_{Lo} - z_i)^2}}$$

$$\eta_{yi} = \frac{\sqrt{(y_{Lo} - y_i)^2}}{\sqrt{(x_{Lo} - x_i)^2 + (y_{Lo} - y_i)^2 + (z_{Lo} - z_i)^2}}$$

$$\eta_{zi} = \frac{\sqrt{(z_{Lo} - z_i)^2}}{\sqrt{(x_{Lo} - x_i)^2 + (y_{Lo} - y_i)^2 + (z_{Lo} - z_i)^2}} \quad \text{. . . (7.6)}$$

In *Chapter 3* it was shown that the velocity components contained in *Equation 7.5*, may be written as a function of the dynamic displacement response vector and the forcing frequency. Within the finite element formulation, the dynamic displacement field for a single direction over a single element is given in *Equation 7.7*.

$$v_{xi} = \omega\sum_{j=1}^{n}\left(\overline{u}_{xj}\cdot N_j(\xi_i, \eta_i)\right) \quad \text{. . . (7.7)}$$

The derivatives of the direction cosines with respect to the spatial variables of the laser yields fifteen non-zero derivatives to be evaluated. Evaluation of the scanning position in terms of the spatial variables of the laser, by making use of the Ray-Patch intersection formulation (*Chapter 6*), enables the calculation of these derivatives. These derivatives may be summarized as:

$$\frac{\partial \eta_{xi}}{\partial \chi_{Lo}} = \frac{\partial}{\partial \chi_{Lo}}(\eta_{xi}) \qquad \frac{\partial \eta_{yi}}{\partial \chi_{Lo}} = \frac{\partial}{\partial \chi_{Lo}}(\eta_{yi}) \qquad \frac{\partial \eta_{zi}}{\partial \chi_{Lo}} = \frac{\partial}{\partial \chi_{Lo}}(\eta_{zi})$$

$$\frac{\partial \eta_{xi}}{\partial z_{Lo}} = \frac{\partial}{\partial z_{Lo}}(\eta_{xi}) \qquad \frac{\partial \eta_{yi}}{\partial z_{Lo}} = \frac{\partial}{\partial z_{Lo}}(\eta_{yi}) \qquad \frac{\partial \eta_{zi}}{\partial z_{Lo}} = \frac{\partial}{\partial z_{Lo}}(\eta_{zi})$$

$$\frac{\partial \eta_{xi}}{\partial \delta_{x}} = \frac{\partial}{\partial \delta_{x}}(\eta_{xi}) \qquad \frac{\partial \eta_{yi}}{\partial \delta_{x}} = \frac{\partial}{\partial \delta_{x}}(\eta_{yi}) \qquad \frac{\partial \eta_{zi}}{\partial \delta_{x}} = \frac{\partial}{\partial \delta_{x}}(\eta_{zi})$$

$$\frac{\partial \eta_{xi}}{\partial \delta_{y}} = \frac{\partial}{\partial \delta_{y}}(\eta_{xi}) \qquad \frac{\partial \eta_{yi}}{\partial \delta_{y}} = \frac{\partial}{\partial \delta_{y}}(\eta_{yi}) \qquad \frac{\partial \eta_{zi}}{\partial \delta_{y}} = \frac{\partial}{\partial \delta_{y}}(\eta_{zi})$$

$$\frac{\partial \eta_{xi}}{\partial \delta_{z}} = \frac{\partial}{\partial \delta_{z}}(\eta_{xi}) \qquad \frac{\partial \eta_{yi}}{\partial \delta_{z}} = \frac{\partial}{\partial \delta_{z}}(\eta_{yi}) \qquad \frac{\partial \eta_{zi}}{\partial \delta_{z}} = \frac{\partial}{\partial \delta_{z}}(\eta_{zi})$$

. . . **(7.8)**

The only terms of *Equation 7.5* that remain to be evaluated, are the derivatives of the velocity components with respect to the spatial variables of the laser. By taking the finite element formulation and local coordinates of the elements into account, the derivatives of the components of the velocity vector may be further expanded into it's partial derivatives. This expansion will be done by making use of the chain rule of differentiation, which yields *Equation 7.9* for the *x*-component of the velocity vector, as follows:

$$\frac{\partial v_{xi}}{\partial \chi} = \frac{\partial v_{xi}}{\partial \xi}\left(\frac{\partial \xi}{\partial x_i}\cdot\frac{\partial x_i}{\partial \chi} + \frac{\partial \xi}{\partial y_i}\cdot\frac{\partial y_i}{\partial \chi} + \frac{\partial \xi}{\partial z_i}\cdot\frac{\partial z_i}{\partial \chi}\right)$$

$$+\frac{\partial v_{xi}}{\partial \eta}\left(\frac{\partial \eta}{\partial x_i}\cdot\frac{\partial x_i}{\partial \chi} + \frac{\partial \eta}{\partial y_i}\cdot\frac{\partial y_i}{\partial \chi} + \frac{\partial \eta}{\partial z_i}\cdot\frac{\partial z_i}{\partial \chi}\right)$$

. . . **(7.9)**

Similar expressions may be derived for the *y*- and *z*-components of the velocity vector, yielding a total of fifteen different partial derivatives to be evaluated. These partial derivatives may be divided into three general groups as follows:

7.2.3.1 Partial derivatives of the velocity components with respect to the local coordinates of the element

This group consists of six partial derivatives, which may be summarized as:

$$\frac{\partial v_{xi}}{\partial \xi} \quad \frac{\partial v_{xi}}{\partial \eta} \quad \frac{\partial v_{yi}}{\partial \xi} \quad \frac{\partial v_{yi}}{\partial \eta} \quad \frac{\partial v_{zi}}{\partial \xi} \quad \frac{\partial v_{zi}}{\partial \eta}$$

. . . **(7.10)**

When the velocity components are obtained from the displacement field as shown in *Equation 7.7*, the partial derivatives of the velocity components with respect to the local coordinates of the element may be written (for the *x*-component of the velocity vector) as:

$$\frac{\partial v_{xi}}{\partial \xi} = \omega\sum_{j=1}^{n}\left(\bar{u}_{xj}\cdot\frac{dN_j(\xi_i,\eta_i)}{d\xi}\right) \qquad \frac{\partial v_{xi}}{\partial \eta} = \omega\sum_{j=1}^{n}\left(\bar{u}_{xj}\cdot\frac{dN_j(\xi_i,\eta_i)}{d\eta}\right)$$

. . . **(7.11)**

Similar expressions may be written for the *y*- and *z*-components of the velocity vector. For the plate element used in this research, there is a total of twenty shape functions and *n* (*Equation 7.11*) is, thus, equal to 20.

The shape functions are explicit polynomial functions of the local coordinates and the derivatives of the shape functions with respect to the local coordinates of the element may, thus, be calculated from *Equations 4.26 and 4.33* for the plane-stress and the Kirchoff plate elements respectively. Upon evaluation of these derivatives, *Equation 7.11* may be written as shown in *Equation 7.12* for the shape functions of the plane stress element.

$$\frac{\partial v_{xi}}{\partial \xi} = \omega \cdot \begin{Bmatrix} u_{x1} & u_{x2} & u_{x3} & u_{x4} \end{Bmatrix} \cdot \begin{Bmatrix} (\eta - 1) \\ -\eta \\ \eta \\ (1 - \eta) \end{Bmatrix}$$

$$\frac{\partial v_{xi}}{\partial \eta} = \omega \cdot \begin{Bmatrix} u_{x1} & u_{x2} & u_{x3} & u_{x4} \end{Bmatrix} \cdot \begin{Bmatrix} (\xi - 1) \\ (1 - \xi) \\ \xi \\ -\xi \end{Bmatrix}$$

. . . **(7.12)**

Similar relationships may be obtained for the shape functions of the Kirchoff plate element.

7.2.3.2 Partial derivatives of the local coordinates of the elements with respect to the scanning position

This group of partial derivatives also consists of six terms which may be written as:

$$\frac{\partial \xi}{\partial x_i} \quad \frac{\partial \eta}{\partial x_i} \qquad \frac{\partial \xi}{\partial y_i} \quad \frac{\partial \eta}{\partial y_i} \qquad \frac{\partial \xi}{\partial z_i} \quad \frac{\partial \eta}{\partial z_i}$$

. . . **(7.13)**

In this thesis, the derivatives of the local coordinate system with respect to the y-component of the scanning position will always be equal to zero. This is due to the fact that the y-coordinate of the surface of the structure is always a constant for a flat surface and the local coordinates of the scanning position is, thus, independent of the y-coordinate

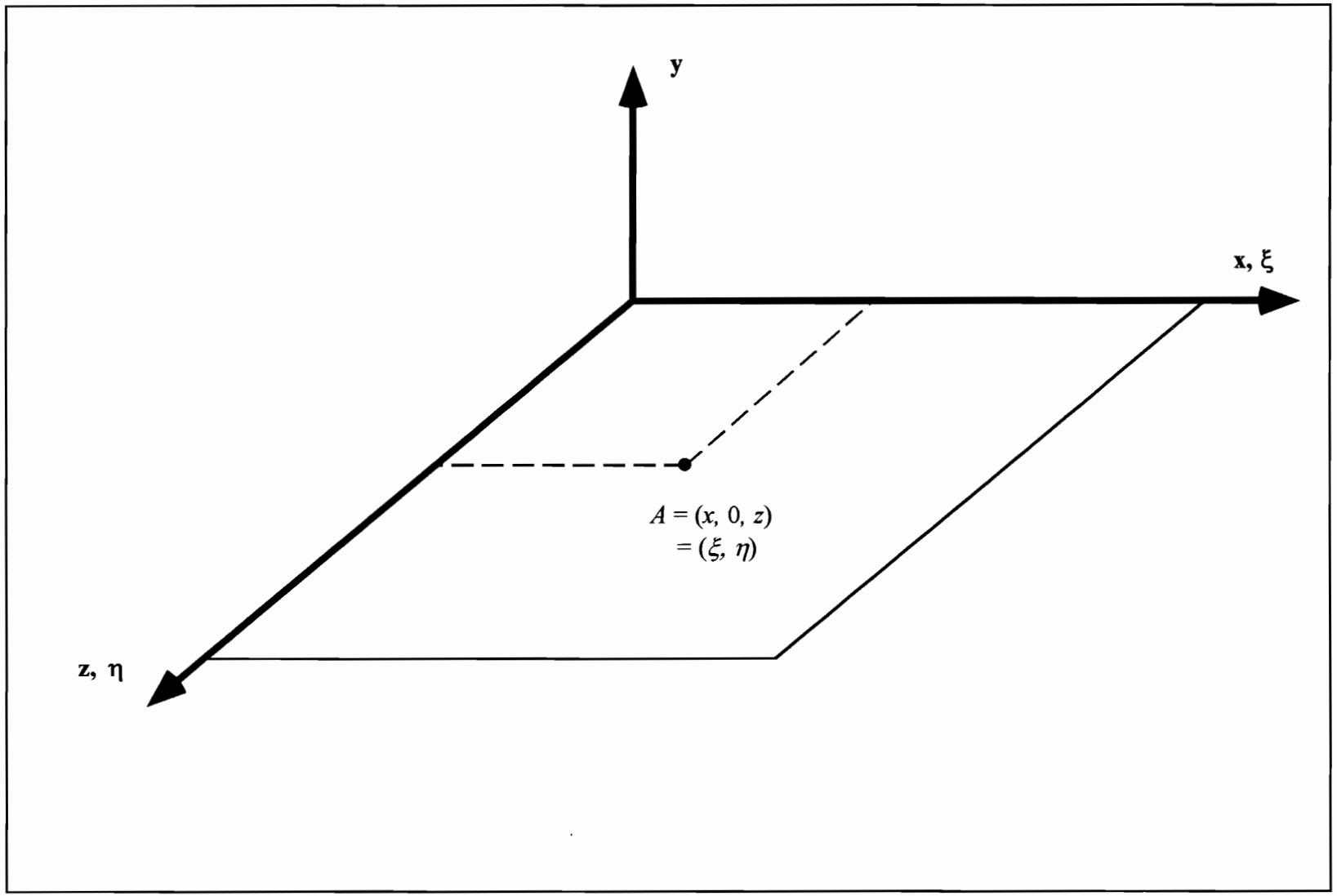

Figure 7.1: Dependence on the local coordinates (ξ, η) of any point, A, in a planar surface

of the surface. This independence of the local coordinates with respect to the *y*-coordinate of the surface is shown schematically in *Figure 7.1*.

Taking into account the fact that the *y*-coordinate of the surface of the structure will be a constant, the surface of the structure may be represented by a function containing the *x* and *z*-components, say $\phi(x,z)$. The derivatives of this function with respect to the local coordinates may be written as shown in *Equation 7.14* by making use of the chain rule of differentiation (Reddy 1993):

$$\frac{\partial \phi}{\partial \xi} = \frac{\partial \phi}{\partial x}\frac{\partial x}{\partial \xi} + \frac{\partial \phi}{\partial z}\frac{\partial z}{\partial \xi} \qquad \frac{\partial \phi}{\partial \eta} = \frac{\partial \phi}{\partial x}\frac{\partial x}{\partial \eta} + \frac{\partial \phi}{\partial z}\frac{\partial z}{\partial \eta} \qquad \text{. . . (7.14)}$$

Equation 7.14 may be written in matrix form as:

$$\begin{Bmatrix} \frac{\partial \phi}{\partial \xi} \\ \frac{\partial \phi}{\partial \eta} \end{Bmatrix} = \mathbf{J} \cdot \begin{Bmatrix} \frac{\partial \phi}{\partial x} \\ \frac{\partial \phi}{\partial z} \end{Bmatrix} \quad \text{where} \quad \mathbf{J} = \begin{bmatrix} \frac{\partial x}{\partial \xi} & \frac{\partial z}{\partial \xi} \\ \frac{\partial x}{\partial \eta} & \frac{\partial z}{\partial \eta} \end{bmatrix} \qquad \text{. . . (7.15)}$$

The matrix **J** is called the Jacobian matrix of the transformation.

The relationship between the global coordinates (*x* and *z*) and the local coordinates (ξ and η) of the surface of the structure will be obtained by making use of a sub-parametric formulation (*Equation 7.16*). A sub-parametric formulation is one where the shape functions used to interpolate the geometry is of a lower order than the shape functions used to interpolate the response of the structure. The sub-parametric formulation used, will represent the geometry of the flat, straight-sided plate elements by means of the bi-linear Lagranian shape functions of the plane-stress element (*Equation 4.26*) as follows:

$$x_i = \sum_{j=1}^{4} \left(\bar{x}_j . N_j(\xi_i, \eta_i) \right) \qquad z_i = \sum_{j=1}^{4} \left(\bar{z}_j . N_j(\xi_i, \eta_i) \right) \qquad \text{. . . (7.16)}$$

The derivatives with respect to the global coordinates may then be written as:

$$\frac{\partial \phi}{\partial x} = \frac{\partial \phi}{\partial \xi}\frac{\partial \xi}{\partial x} + \frac{\partial \phi}{\partial \eta}\frac{\partial \eta}{\partial x} \qquad \frac{\partial \phi}{\partial z} = \frac{\partial \phi}{\partial \xi}\frac{\partial \xi}{\partial z} + \frac{\partial \phi}{\partial \eta}\frac{\partial \eta}{\partial z}$$

. . . **(7.17)**

With the matrix form given by:

$$\begin{Bmatrix} \frac{\partial \phi}{\partial x} \\ \frac{\partial \phi}{\partial z} \end{Bmatrix} = \Gamma \cdot \begin{Bmatrix} \frac{\partial \phi}{\partial \xi} \\ \frac{\partial \phi}{\partial \eta} \end{Bmatrix} \qquad \text{where} \quad \Gamma = \begin{bmatrix} \frac{\partial \xi}{\partial x_i} & \frac{\partial \eta}{\partial x_i} \\ \frac{\partial \xi}{\partial z_i} & \frac{\partial \eta}{\partial z_i} \end{bmatrix}$$

. . . **(7.18)**

If *Equation 7.15* is pre-multiplied on both sides by the inverse of the Jacobian matrix *Equation 7.19* is obtained:

$$\begin{Bmatrix} \frac{\partial \phi}{\partial x} \\ \frac{\partial \phi}{\partial z} \end{Bmatrix} = \mathbf{J}^{-1} \cdot \begin{Bmatrix} \frac{\partial \phi}{\partial \xi} \\ \frac{\partial \phi}{\partial \eta} \end{Bmatrix} \quad \text{where} \quad \mathbf{J}^{-1} = \frac{1}{Det|\mathbf{J}|}\begin{bmatrix} J_{22} & -J_{12} \\ -J_{21} & J_{11} \end{bmatrix}$$

. . . **(7.19)**

Thus, from *Equations 7.18 and 7.19*, the derivatives of the local coordinates with respect to the scanning position may then be written as:

$$\frac{\partial \xi}{\partial x_i} = \frac{1}{Det|\mathbf{J}|}\frac{\partial z_i}{\partial \eta} \qquad \frac{\partial \eta}{\partial x_i} = -\frac{1}{Det|\mathbf{J}|}\frac{\partial z_i}{\partial \xi}$$

$$\frac{\partial \xi}{\partial z_i} = -\frac{1}{Det|\mathbf{J}|}\frac{\partial x_i}{\partial \eta} \qquad \frac{\partial \eta}{\partial z_i} = \frac{1}{Det|\mathbf{J}|}\frac{\partial x_i}{\partial \xi}$$

. . . **(7.20)**

7.2.3.3 Partial derivatives of the scanning position with respect to the spatial variables of the laser

This group of partial derivatives consists of three terms which may be written as:

$$\frac{\partial x_i}{\partial \chi} \qquad \frac{\partial y_i}{\partial \chi} \qquad \frac{\partial z_i}{\partial \chi} \qquad \text{. . . (7.21)}$$

The variable χ denotes any of the spatial variables of the laser. These partial derivatives may be calculated once the scanning position of the laser beam on the surface of the structure is known as a function of the spatial variables of the laser. This will be accomplished by using the Ray-Patch intersection formulation as developed in *Chapter 6*. The sensitivity of x_i with respect to ∂x_{Lo} and $\partial \delta_x$ will be shown as representative cases.

From *Equation 6.13*, the x component of the scanning position may be written as:

$$x_i = x_{Lo} + \eta_x \cdot t$$

where the direction cosines are defined in terms of transformation matrices as

$$\{\eta_x, \eta_y, \eta_z\} = \mathbf{T}_R^T \cdot \mathbf{T}_s$$

for the position variables of the laser (*Equation 6.15*) and as

$$\{\eta_x, \eta_y, \eta_z\} = \mathbf{T}_R^T \cdot \mathbf{A}_x \cdot \mathbf{T}_s$$

for the orientation variables of the laser (*Equation 6.21*).

From *Chapter 6*, the parametric variable, t, and the position and orientation of the laser is defined as (*Equations 6.14 and 6.15*):

$$t = -\frac{(\vec{N} \cdot \mathbf{R}_o + D)}{\vec{N} \cdot \mathbf{R}_d}$$

$$\mathbf{R}_o = \{x_{Lo}, y_{Lo}, z_{Lo}\} \qquad \mathbf{R}_d = \{\eta_x, \eta_y, \eta_z\}$$

From the previous parametric relationships for the scanning position, it will be noted that the direction cosines of the laser beam are independent of the spatial position of the laser, and the spatial position of the laser is independent of the spatial orientation of the laser. The derivative of the x component of the scanning position with respect to the spatial variables, ∂x_{Lo} and $\partial \delta_x$, may then be written as:

$$\frac{\partial x_i}{\partial x_{Lo}} = 1 + \frac{\partial \eta_x}{\partial x_{Lo}} \cdot t + \eta_x \cdot \frac{\partial t}{\partial x_{Lo}}$$

$$= 1 + \eta_x \cdot \left(- \frac{\vec{N} \cdot \{1, 0, 0\}}{\vec{N} \cdot \mathbf{R}_d} \right) \quad \text{. . . (7.22)}$$

$$\frac{\partial x_i}{\partial \delta_x} = \frac{\partial x_{Lo}}{\partial \delta_x} + \frac{\partial \eta_x}{\partial \delta_x} \cdot t + \eta_x \cdot \frac{\partial t}{\partial \delta_x}$$

$$= \frac{\partial \eta_x}{\partial \delta_x} \cdot t + \eta_x \cdot \left(\frac{\vec{N} \cdot \mathbf{R}_o}{\left(\vec{N} \cdot \mathbf{R}_d \right)^2} \right) \cdot \left(\vec{N} \cdot \left\{ \frac{\partial \eta_x}{\partial \delta_x}, \frac{\partial \eta_y}{\partial \delta_x}, \frac{\partial \eta_z}{\partial \delta_x} \right\} \right) \quad \text{. . . (7.23)}$$

7.3 Test case

The same setup as used in the test case of *Chapter 6* will be used to evaluate the sensitivities of the error function with respect to the spatial position and orientation of the laser for a specific scanning position. The setup consists of a 0.5 by 0.5 square plate modeled by one element and is shown schematically in *Figure 7.2*. From *Chapter 6* the setup of the test case may be summarized as follows:

Position of the laser: The laser will be positioned 2.5 meters above the center point of the plate, with the coordinates of the laser origin as:

$$\{ x_{Lo},\ y_{Lo},\ z_{Lo} \} = \{0.25, 2.5, 0.25\} \quad [\text{m}]$$

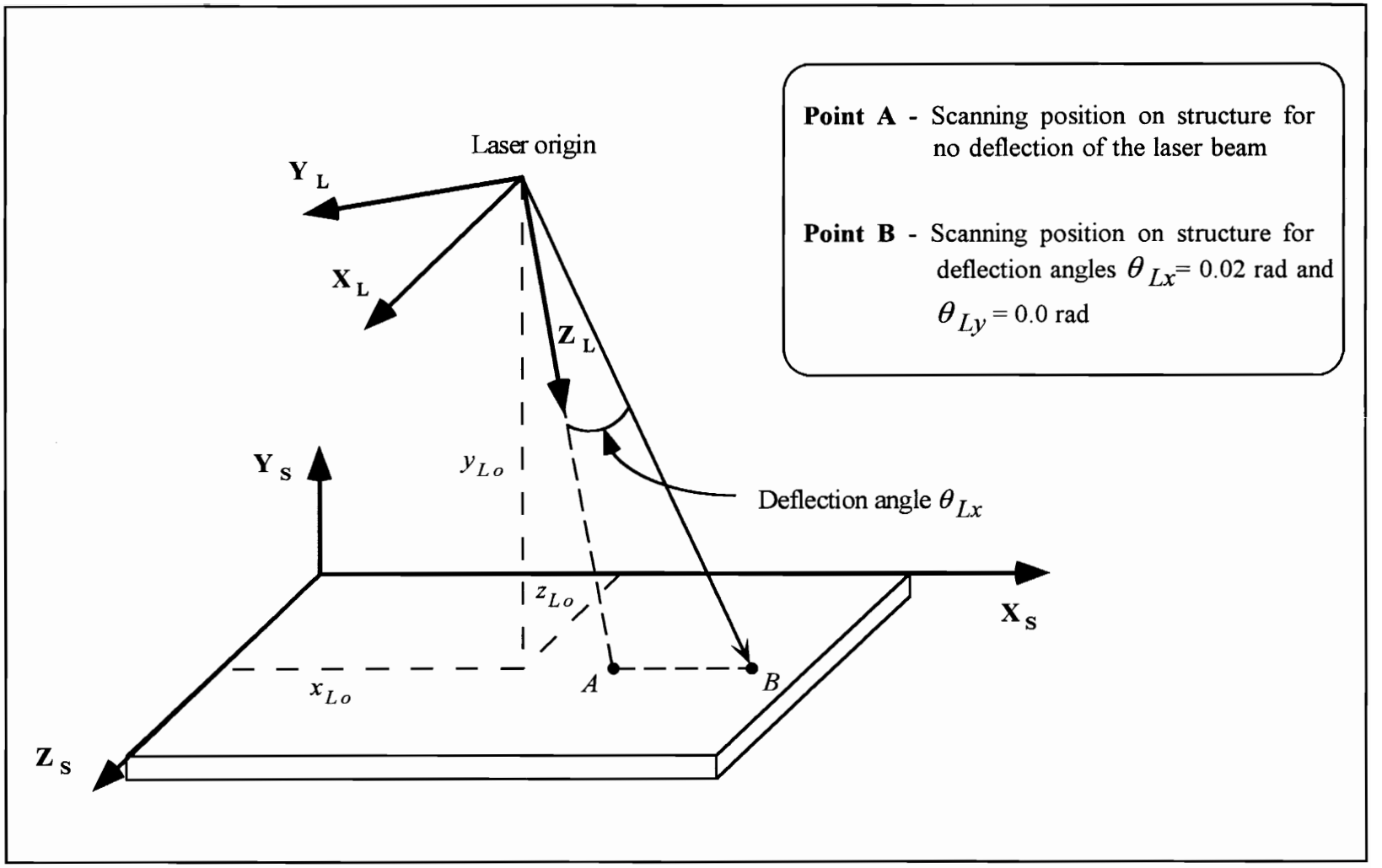

Figure 7.2: Experimental setup for the test case

Orientation vectors: The orientation will be specified by means of the two vectors along the *x*- and the *z*-axes of the laser coordinate system. These vectors have the laser origin as origin and may be written as:

$$\overline{Laser_x} = \{5, 2.5, 0.25\} \qquad \overline{Laser_z} = \{0.3751, 0, 0.25\}$$

Deflection angles: The two deflection angles of the laser beam may be written as:

$$\theta_{Lx} = 0.02 \quad \text{rad} \qquad \theta_{Ly} = 0.00 \quad \text{rad}$$

Furthermore, in order to find a numerical solution to *Equation 7.5*, a displacement field will be assumed over the domain of the element. This displacement field will be obtained from the exact solution of the differential equation describing the transverse dynamic displacement response of a cantilevered beam excited by a transverse, harmonic forcing function at the free end. This differential equation is shown in *Equation 4.40*, and will be solved exactly the same way as in *Chapter 4*, but with a total length of 0.5 m. Rotations about the *z*-axis of the element will be zero from this model, while rotations about the *x*-axis may be obtained from evaluation of the derivative with respect to the *x*-axis. As in *Chapter 4*, the parameters of the harmonic forcing function is given by

$$f_0 = 5 \quad \text{N}$$

$$\omega = 0.1 \quad \text{rad/s}$$

yielding the following response (although the plate elements also yield axial displacements at the top and bottom surfaces of the structure, these velocities are a factor of 10^3 smaller than the transverse displacements for this setup and will, thus, be ignored):

$$Dof = \{u_1, v_1, w_1, \theta_{x1}, \theta_{z1}, u_2, v_2, w_2, \theta_{x2}, \theta_{z2}, u_3, v_3, w_3, \theta_{x3}, \theta_{z3}, u_4, v_4, w_4, \theta_{x4}, \theta_{z4}\}$$

$$
\begin{aligned}
Dof = \{ & 0, & 0, & 0, & 0, \\
& 0, & 0, & 0, & 0, \\
& 0.663754E\text{-}3, & 0, & -0.00196128, & 0, \\
& 0.663754E\text{-}3, & 0, & -0.00196128, & 0\}
\end{aligned}
$$

The velocity field may be obtained from the displacement field by making use of *Equation 7.7*, and the interpolation functions for the plate element defined in *Equations 4.26 and 4.33* yielding:

$$v_x = v_z = 0.0$$

$$v_y = 0.101062E-3 \cdot \xi^2 - 0.0346868E-3 \cdot \xi^3$$

. . . (7.24)

Lastly, the relationship between the x-z and the ξ-η coordinates may be evaluated from *Equation 7.16*. In general, this relationship is non-linear and a root finder is needed in order to solve for the local coordinates (ξ-η) in terms of the global coordinates (x-z). However, for the specific case at hand, where a square plate along the x- and z-axes of the structure is considered, the relationships between the local and global coordinates are obtained as:

$$x = 0.5 \cdot \xi \qquad y = 0.5 \cdot \eta$$

$$\xi = 2 \cdot x \qquad \eta = 2 \cdot y$$

. . . (7.25)

The sensitivity of the error function with respect to the spatial variables of the laser may now be calculated from *Equation 7.5*, which reduces to the form shown in *Equation 7.26* for the specific test case. The simplification of *Equation 7.5* is due to the fact that the velocities in the x and z directions are equal to zero.

$$\frac{d(error_i)}{d\chi} = \left(\frac{dv_{yi}}{d\chi} \cdot \eta_{yi} + v_{yi} \cdot \frac{d\eta_{yi}}{d\chi} \right)$$

. . . **(7.26)**

7.3.1 Sensitivity of the error function with respect to the spatial position of the laser

From *Equation 6.26*, the scanning position for the test case, with no variation in the orientation of the laser, is known as:

$$\mathbf{r}_{SP} = \{x_{Lo} + 0.0701146 \cdot y_{Lo}, 0, z_{Lo}\}$$

$$= \{0.425286, 0, 0.25\} \quad [\text{m}]$$

. . . **(7.27)**

With the value of the scanning position known, the numeric values of the local coordinates, the direction cosines as well as the velocity field at the specific scanning position may be evaluated as follows:

Local coordinates (From *Equation 7.25*)**:**

$$\xi = 0.850572 \qquad \eta = 0.5$$

Direction cosines (From *Equation 7.6*)**:**

$$\eta_x = 0.0699428 \qquad \eta_y = 0.997551 \qquad \eta_z = 0.0$$

Velocity field (From *Equation 7.24*)**:**

$$v_y = 0.05177054\text{E}-3 \quad \text{m.s}^{-1}$$

With the direction cosines and the velocity field known, the next step is to obtain the value of the derivative of the velocity component with respect to the spatial position of the laser. This derivative will be obtained from *Equation 7.9* , which reduces to

Equation 7.28 for the specific test case. This simplification of *Equation 7.9* is due to the fact that the velocity field is a function of the local coordinate ξ only (*Equation 7.24*) and the $\frac{\partial v_{yi}}{\partial \eta}$ term is, thus, equal to zero. Furthermore, the local coordinate ξ is only a function of x (*Equation 7.25*) and the $\frac{\partial \xi}{\partial y_i}$ and $\frac{\partial \xi}{\partial z_i}$ terms are thus equal to zero.

$$\frac{\partial v_{yi}}{\partial \chi} = \frac{\partial v_{yi}}{\partial \xi} \cdot \frac{\partial \xi}{\partial x_i} \cdot \frac{\partial x_i}{\partial \chi}$$

. . . **(7.28)**

For the specific test case, the terms of *Equation 7.28* may be evaluated from *Equations 7.24, 7.25 and 7.27* to obtain:

$$\begin{aligned} \frac{\partial v_{yi}}{\partial \xi} \cdot \frac{\partial \xi}{\partial x_i} &= (0.202124\text{E}-3 \cdot \xi - 0.10406\text{E}-3 \cdot \xi^2) \cdot (2) \\ &= 0.404249\text{E}-3 \cdot \xi - 0.208121\text{E}-3 \cdot \xi^2 \end{aligned}$$

. . . **(7.29)**

and

$$\frac{\partial x_i}{\partial x_{Lo}} = 1 \qquad \frac{\partial x_i}{\partial y_{Lo}} = 0.0701146 \qquad \frac{\partial x_i}{\partial z_{Lo}} = 0$$

. . . **(7.30)**

The derivative of the direction cosines with respect to the spatial position of the laser were calculated from *Equation 7.8*. All the values were calculated to be equal to zero, and in general, when flat surfaces are considered this will always be the case. This is due to the fact that, when flat surfaces are considered, changes in the spatial position of the laser only shifts the scanning position of the laser beam on the structure without having an influence on the direction of the laser beam (*Figure 7.3*).

The sensitivities of the error function with respect to the spatial position of the laser may, thus, be calculated to be:

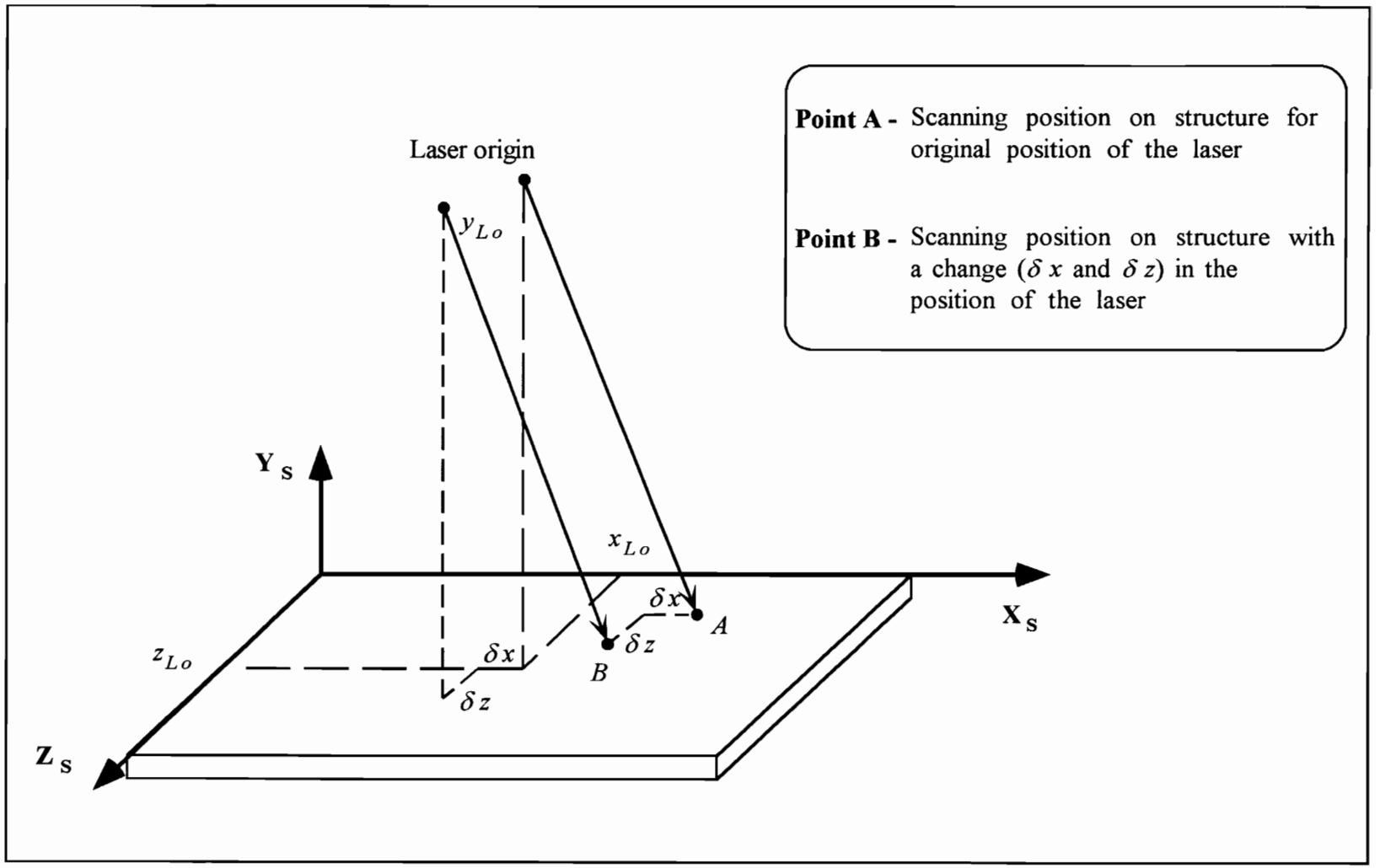

Figure 7.3: Effect on scanning position due to a change in the position of the laser.

$$\frac{\partial(error)}{\partial x_{Lo}} = \frac{\partial v_y}{\partial x_{Lo}} \cdot \eta_y = \left(0.404249E-3 \cdot \xi - 0.208121E-3 \cdot \xi^2\right)\Big|_{\xi=0.850572} \cdot (1) \cdot (0.997551)$$

$$= 0.19279969\text{E-}3$$

$$\frac{\partial(error)}{\partial y_{Lo}} = \frac{\partial v_y}{\partial y_{Lo}} \cdot \eta_y = 0.013518073E-3$$

$$\frac{\partial(error)}{\partial z_{Lo}} = \frac{\partial v_y}{\partial z_{Lo}} \cdot \eta_y = 0$$

. . . **(7.31)**

The obtained results may be used to form an approximation to the change in the velocity components due to a change in the position of the laser. This approximation will be obtained by forming a first-order Taylor series expansion of the velocity components about a specific point. The Taylor series expansion will be performed on the velocity components and not the error function, due to the fact that the $\widetilde{V}_{Li}$ term in *Equation 7.1* is not known.

This approximation will be used to validate the results by comparing the results obtained from the approximation to the exact results obtained from *Equation 7.28*. The procedure yields a valid test of $\frac{\partial(error)}{\partial \chi}$ due to the fact that the η_y term, the only difference between $\frac{\partial(error)}{\partial \chi}$ and $\frac{\partial v_y}{\partial \chi}$, are easy to calculate and may be checked by hand.

For changes in the velocity component due to changes in the *x*-coordinate of the laser, this procedure yields:

$$\Delta v_{yi} = \Delta x_{Lo} \cdot \frac{\partial(error)}{\partial x_{Lo}}$$

. . . **(7.32)**

For a 10% change in the *x*-coordinate of the laser, *Equation 7.33* predicts a change in the velocity component of:

$$\Delta v_{yi} = (0.025)\cdot(0.19279969\text{E}-3) = 4.81999225\text{E}-6 \quad \text{m.s}^{-1}$$

The actual change may be evaluated by finding the new scanning position from *Equation 7.27*, the new local coordinates from *Equation 7.25* and finally the new value of the velocity component from *Equation 7.24*. These values may be summarized as

$$x_i = 0.275 \text{ m} \qquad z_i = 0.450286 \text{ m} \qquad \xi = 0.900572$$

$$v_{yi} = 0.0566294\text{E}-3 \quad \text{m.s}^{-1}$$

yielding:

$$\Delta v_{yi} = (0.0566294\text{E}-3)-(0.05177054\text{E}-3) = 4.85884967\text{E}-6 \quad \text{m.s}^{-1}$$

The difference between the results obtained from *Equation 7.32* and the actual results is only 0.8%, showing the accuracy of the obtained sensitivity.

7.3.2 Sensitivity of the error function with respect to the spatial orientation of the laser

The sensitivity of the error function with respect to the spatial orientation of the laser will be evaluated for the same scanning position considered in *Section 7.3.1*. As a representative case, rotations about the x-axis of the laser will be considered. From *Chapter 6, Equation 6.29*, the scanning position of the specific test case may be written in terms of rotations about the x-axis of the laser as:

$$\mathbf{r}_{ScanningPosition} = \{0.25 - \frac{2.5\cdot\left(0.06994\cdot Cos(\delta_x)+0.997551\cdot Sin(\delta_x)\right)}{-0.997551\cdot Cos(\delta_x)+0.06994\cdot Sin(\delta_x)}, 0, 0.25\} \quad \text{. . . (7.33)}$$

With no variation in the orientation of the laser δ_X will be equal to zero and the numeric values of the local coordinates, the direction cosines and the velocity field for the scanning position may be obtained as in *Section 7.3.1* as:

Local coordinates (From *Equation 7.25*):

$$\xi = 0.850572 \qquad \eta = 0.5$$

Direction cosines (From *Equation 7.6*):

$$\eta_x = 0.0699428 \qquad \eta_y = 0.997551 \qquad \eta_z = 0.0$$

Velocity field (From *Equation 7.24*):

$$v_y = 0.05177054\text{E}-3 \quad \text{m.s}^{-1}$$

The value of the derivative of the velocity component with respect to the rotation about the *x*-axis of the laser may be written from *Equation 7.28* as

$$\frac{\partial v_{yi}}{\partial \delta_x} = \frac{\partial v_{yi}}{\partial \xi} \cdot \frac{\partial \xi}{\partial x_i} \cdot \frac{\partial x_i}{\partial \delta_x}$$

with $\frac{\partial v_{yi}}{\partial \xi} \cdot \frac{\partial \xi}{\partial x_i}$ known from *Equation 7.29*.

The derivative of the scanning position with respect to a rotation about the *x*-axis of the laser can now be evaluated from *Equation 7.33* to obtain:

$$\frac{\partial x_i}{\partial \delta_x} = 2.5 + \frac{0.0122901 \cdot \left(Cos(\delta_x) + 14.2624 \cdot Sin(\delta_x)\right)^2}{\left(Cos(\delta_x) - 0.0701146 \cdot Sin(\delta_x)\right)^2} \qquad \text{. . . (7.34)}$$

Furthermore, from *Equation 7.6*, the direction cosine of the laser beam with respect to the *y*-axis, may be written in terms of the rotation about the *x*-axis as:

$$\eta_y = 0.997551 \cdot \left(Cos(\delta_x) - 0.0701146 \cdot Sin(\delta_x)\right) \qquad \text{. . . (7.35)}$$

The derivative of the direction cosine with respect to the rotation about the *x*-axis of the laser may then be calculated from *Equation 7.35* to obtain:

$$\frac{\partial \eta_y}{\partial \delta_x} = 0.997551 \cdot \left(-0.0701146 \cdot Cos(\delta_x) - Sin(\delta_x)\right)$$

. . . **(7.36)**

Finally, the sensitivity of the error function with respect to the rotation about the *x*-axis of the laser may be obtained from *Equation 7.26*, making use of the values for η_{yi} and v_{yi} as well as of *Equations 7.34 and 7.36*. The result is shown in *Equation 7.37* as:

$$\frac{\partial(error)}{\partial \delta_x} = \left(\frac{\partial v_{yi}}{\partial \delta_x} \cdot \eta_{yi} + v_{yi} \cdot \frac{\partial \eta_{yi}}{\partial \delta_x}\right)$$

$$= \left(2.5 + \frac{0.0122901 \cdot \left(Cos(\delta_x) + 14.2624 \cdot Sin(\delta_x)\right)^2}{\left(Cos(\delta_x) - 0.0701146 \cdot Sin(\delta_x)\right)^2}\right) \cdot \left(0.404249\text{E}-3 \cdot \xi - 0.208121\text{E}-3 \cdot \xi^2\right) \cdot \left(0.997551\right)$$

$$+ \left(0.05177054\text{E}-3\right) \cdot \left(0.997551 \cdot \left(-0.0701146 \cdot Cos(\delta_x) - Sin(\delta_x)\right)\right)$$

. . . **(7.37)**

The results will be tested in the same way as was done in *Section 7.3.1*, with the Taylor series expansions of $\frac{dv_{yi}}{d\delta_x}$ and $\frac{d\eta_{yi}}{d\delta_x}$ given by:

$$\Delta v_{yi} = \Delta \delta_x \cdot \frac{\partial(v_{yi})}{\partial \delta_x} \qquad \Delta \eta_{yi} = \Delta \delta_x \cdot \frac{\partial(\eta_{yi})}{\partial \delta_x}$$

. . . **(7.38)**

For a rotation of 0.01 rad, *Equation 7.38* would predict changes in the values of the velocity component and the direction cosine of:

$$\Delta v_{yi} = (0.01) \cdot (2.5160685) \cdot (19527129\text{E}-4)$$

$$= 4.91315942\text{E}-6 \quad \text{m.s}^{-1}$$

$$\Delta\eta_{yi} = (0.01)\cdot(-0.079914694)$$

$$= -0.7991469\text{E}-3 \quad \text{rad}$$

The actual changes may be evaluated by finding the new scanning position from *Equation 7.33*, the new local coordinates from *Equation 7.25*, the new value of the velocity component from *Equation 7.24* and lastly the new value of the direction cosine from *Equation 7.35*. These values may be summarized as

$$x_i = 0.25 \text{ m} \quad z_i = 0.4504278 \text{ m} \quad \xi = 0.9008556$$

$$v_{yi} = 0.056657074\text{E}-3 \quad \text{m.s}^{-1}$$

yielding:

$$\Delta v_{yi} = (0.056657074\text{E}-3)-(0.0517705357\text{E}-3) = 4.8865384458\text{E}-6 \quad \text{m.s}^{-1}$$

and

$$\Delta\eta_{yi} = (0.996802)-(0.997551) = -0.74929\text{E}-3 \quad \text{rad}$$

The difference between the approximate results obtained from *Equation 7.38* and the actual results is only 0.5% for the velocity components and 6.7% for the direction cosines, showing the accuracy of the obtained sensitivity. The larger difference for the direction cosines suggests that the function for the direction cosines is more non-linear than for the velocities. The linear approximation would thus deviate from the exact solution if δ_x is taken to be too large.

Chapter 8
Results obtained from the research

The sensitivity of the error function with respect to the elastic boundary conditions and the spatial variables of the laser will be calculated for a stainless steel beam. The same beam will be considered in both cases, but different boundary and loading conditions will be applied and different finite element models will be considered.

8.1 Example problem statement

The same structure will be considered in both the calculation of the sensitivity of the error function with respect to the elastic boundary conditions as well as with respect to the spatial variables of the laser. Also, the laser will be located at the same position and orientated the same way for both cases. The structure and the position and orientation of the laser may be summarized as follows:

8.1.1 Beam structure used

A beam structure made of 304 Stainless steel will be used. The geometry and material properties of the beam may be summarized as follows:

Dimensions:	Length	=	1.3716	m
	Width	=	0.0762	m
	Thickness	=	0.00635	m
Material:	ν	=	0.27	
	E	=	196	GPa
	ρ	=	7905	kg/m^3

. . . **(8.1)**

The different loading and boundary conditions, as well as the different finite element models used, will be discussed in detail in the applicable sections.

8.1.2 Position and orientation of the laser

The laser will be positioned 4 meters directly above the midpoint of the beam. The laser will be orientated in such a way that the x-axis is precisely aligned with the positive z-axis of the structure, the y-axis with the negative x-axis of the structure and the z-axis with the negative y-axis of the structure. This position and orientation of the laser is shown schematically when the two example problems are discussed in more detail.

The position of the laser (in the structural coordinate system) may, thus, be written as:

$$\{x_{Lo}, y_{Lo}, z_{Lo}\} = \{0.6858, 4, 0.0381\} \quad [\text{m}] \qquad \text{. . . (8.2)}$$

The vertical height of 4 meters was chosen to ensure that the deflection angle necessary to deflect the laser beam in such a way as to scan the complete structure, falls within the maximum range of the laser. The maximum deflection angle obtainable by the laser is ± 12.5° (0.2182 radians). For this test case the range of the deflection angles necessary to scan the complete surface of the structure may be summarized as:

$$\theta_{Lx} \in [-0.169799, 0.169799] \text{ rad} \qquad \theta_{Ly} \in [-0.00952471, 0.00952471] \text{ rad} \qquad \text{. . . (8.3)}$$

For the specific test case the two vectors along the x and z-axes of the laser may be written as:

$$\overline{Laser_x} = \{0.6858, 4, 0.05\} \quad [\text{m}] \qquad \overline{Laser_z} = \{0.6858, 0, 0.0381\} \quad [\text{m}] \qquad \text{. . . (8.4)}$$

These vectors have the same origin as the laser.

8.2 Sensitivity analysis of the error function with respect to the elastic boundary conditions of the finite element model

The sensitivity of the ESDM error function with respect to the elastic boundary conditions of the finite element model will be evaluated. By making use of first beam and then plate elements, two different finite element models of the beam structure will be constructed.

8.2.1 Simulated experimental setup

The simulated experimental setup consists of the structure, the boundary and loading conditions and the position and orientation of the laser. The structure as well as the position and orientation of the laser are summarized in *Equations 8.1, 8.2 and 8.4*, while the boundary and loading conditions will be stated in this section.

The beam will be subjected to elastic boundary conditions. The boundary conditions at the left end of the beam will be evaluated as if the beam was supported by a circular aluminum rod. The boundary conditions on the right end will be evaluated as if the beam was suspended from a bungi cord (*Figure 8.1* gives a schematic representation of the setup).

The dimensions and properties of the aluminum rod used to support the beam at the left end, will be taken as:

Dimensions:	Length	=	0.3	m
	Diameter	=	0.01	m
Material:	E	=	69	GPa

. . . **(8.5)**

By making use of the beam equations for a cantilevered beam (Cook and Young 1986) the stiffnesses for the elastic boundary conditions may be evaluated to be (consistent with the degrees of freedom of the beam):

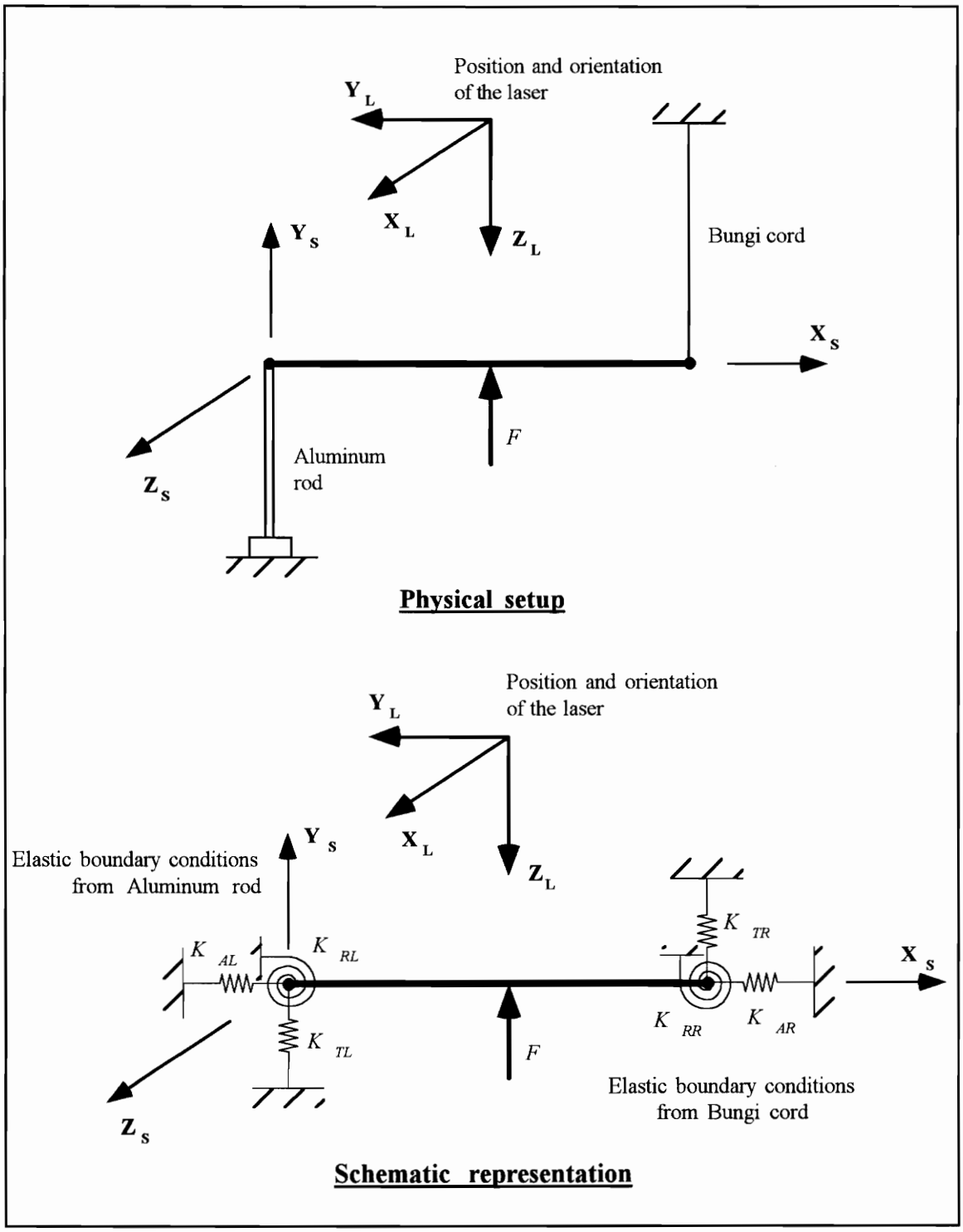

Figure 8.1: Experimental setup used for calculating the first- and second-order derivatives of the ESDM error function with respect to elastic boundary conditions

$$K_{axial} = \frac{3EI}{L^3} = 3.763\ 3662\text{x}10^3 \text{ N/m}$$

$$K_{transverse} = \frac{AE}{L} = 18.064\ 158\text{x}10^6 \text{ N/m}$$

$$K_{rotational} = \frac{2EI}{L^2} = 752.67324 \text{ N.m/rad}$$

. . . **(8.6)**

Lindholm and West (1994) obtained experimental values for the axial, rotational and transverse stiffnesses of the bungi cord. The values obtained are for a specific experimental setup and depend on the setup considered. Since the experimental setup of the example problem considered in this chapter is different from the setup used by Lindholm and West (1994), the bungi cord stiffness values will be different. Although it is realized that the stiffness values of the bungi cord for this example problem will be different from those obtained by Lindholm and West (1994), the values as obtained by Lindholm and West (1994) will be used as representative values for the bungi cord stiffnesses. These values may be summarized (once again consistent with the degrees of freedom of the beam) as:

$$K_{axial} = 210.2 \text{ N/m}$$

$$K_{transverse} = 1120.8 \text{ N/m}$$

$$K_{rotational} = 12.5 \text{ N.m/rad}$$

. . . **(8.7)**

The variables representing the elastic boundary stiffnesses at the left- and right-end points of the beam will be represented by

$$K_{AL} \quad K_{TL} \quad K_{RL} \quad K_{AR} \quad K_{TR} \quad K_{RR}$$

. . . **(8.8)**

where the first letter of the subscript represent the appropriate degree of freedom (Axial, Transverse or Rotational) and the second letter represent the specific end point (Left or Right). These variables are also shown in *Figure 8.1*.

The beam will be excited by a harmonic forcing function, applied at the midpoint of the beam. The magnitude and frequency of the forcing function may be summarized as:

$$F(x,t) = f_0 Sin(\omega t)$$

with:

$$f_0 = 5 \text{ N} \qquad \omega = 0.1 \text{ rad/s} \qquad \text{. . . (8.9)}$$

8.2.2 Example problem development

Two different numerical models were constructed for the beam. The first was a one-dimensional model, using beam elements while the second was a two-dimensional model, using plate elements. Models consisting of 4, 8, 16 and 32 elements were considered. The results obtained from the 16 element model were found to be well converged and will be stated in this chapter as a representative case.

Mathematically, the only difference between the two models lay in the values and dimensions of their respective stiffness and mass matrices which, in turn, result in different pseudo-dynamic stiffness matrices. The calculation of the response and the sensitivities for each model will, thus, be exactly the same except for the fact that different pseudo-dynamic stiffness matrices must be used.

First- and second-order derivatives of the error function with respect to boundary condition parameters were calculated for each model and the calculation of these derivatives as well as the formation of the required sensitivities will now be discussed separately.

8.2.2.1 First-order sensitivity of the error function with respect to the elastic boundary conditions of the numerical model

In *Chapter 5* it was shown how the first-order sensitivities of the error function with respect to the elastic boundary conditions of the finite element model may be

evaluated. From *Equation 5.12* the sensitivities may be obtained from the forcing frequency, the first-order derivatives of the dynamic displacement response with respect to the specific boundary condition being considered and the direction cosines of the laser beam.

The dynamic displacement response with respect to the elastic boundary conditions will be evaluated from the direct method of differentiation (*Equation 5.10*). The dynamic displacement response, necessary to evaluate *Equation 5.10*, will be obtained from a frequency response analysis as shown in *Equations 5.6 and 5.7*.

8.2.2.2 Second-order sensitivity of the error function with respect to the elastic boundary conditions of the numerical model

The second-order sensitivity of the error function with respect to the elastic boundary conditions may be calculated from *Equation 5.4*. Once again the equation is written in terms of the forcing frequency, the second-order derivatives of the dynamic displacement response with respect to the specific boundary conditions being considered and the direction cosines of the laser beam.

The second-order derivatives of the dynamic displacement response with respect to the elastic boundary conditions under consideration will also be obtained from the direct method of differentiation (*Equation 5.11*). As before the dynamic displacement response, needed to evaluate *Equation 5.11*, will be calculated from the frequency response analysis shown in *Equations 5.6 and 5.7*.

8.2.3 Discussion of the results of the example problem in general and their implications

As stated in the problem statement, a stainless steel beam with a vertical excitation force in the center will be considered. The beam will first be modeled using beam elements and then by using plate elements. The beam elements will yield only vertical displacements while the plate elements will yield vertical as well as small horizontal displacements due to the rotation of the beam. However, these horizontal displacements will be neglected due to the fact that they are much smaller (at least by an order of 10^3 in magnitude) than the vertical displacements, resulting in insignificantly small sensitivities.

Due to the fact that only the vertical displacements will be non-zero, the equations necessary to calculate the first- and second-order sensitivities (*Equations 5.3 and 5.4* respectively) will reduce to *Equations 8.10 and 8.11* as follows:

$$\frac{\partial(error)_i}{\partial\chi} = \omega \cdot \frac{\partial u_{yi}}{\partial\chi} \cdot \eta_{yi} \qquad \text{. . . (8.10)}$$

$$\frac{\partial^2(error)_i}{\partial\chi\partial\gamma} = \omega \cdot \frac{\partial^2 u_{yi}}{\partial\chi\partial\gamma} \cdot \eta_{yi} \qquad \text{. . . (8.11)}$$

The equations yielding the first- and second-order derivatives of the dynamic displacement response with respect to the elastic boundary conditions, as well as the equation yielding the direction cosines of the laser beam, reduce to:

$$\frac{\partial u_{yi}}{\partial\chi} = \mathbf{D}^{-1}\left(-\frac{\partial \mathbf{D}}{\partial\chi} \cdot u_{yi}\right) \qquad \text{. . . (8.12)}$$

$$\frac{\partial^2 u_{yi}}{\partial\chi\partial\gamma} = \mathbf{D}^{-1}\left(-\frac{\partial^2 \mathbf{D}}{\partial\chi\partial\gamma} \cdot u_{yi} - \frac{\partial \mathbf{D}}{\partial\chi} \cdot \frac{\partial u_{yi}}{\partial\gamma} - \frac{\partial \mathbf{D}}{\partial\gamma} \cdot \frac{\partial u_{yi}}{\partial\chi}\right) \qquad \text{. . . (8.13)}$$

with the direction cosines given by *Equation 8.14*:

$$\eta_{yi} = \frac{\sqrt{(y_{Lo} - y_i)^2}}{\sqrt{(x_{Lo} - x_i)^2 + (y_{Lo} - y_i)^2 + (z_{Lo} - z_i)^2}} \qquad \text{. . . (8.14)}$$

There are six first-order sensitivities and thirty six second-order sensitivities, of which twenty one are unique, that needs to be evaluated. The derivatives with respect to the axial stiffnesses of the boundary conditions will all be equal to zero due to the fact that

there is no dynamic response in the axial direction. This will reduce the number of unique, non-zero, sensitivities to four first-order and ten second-order sensitivities.

8.2.3.1 Significance of the obtained sensitivities of the error function with respect to the elastic boundary conditions

Some of the sensitivities of the error equation with respect to the boundary condition parameters obtained were very small. In order to define a cut-off point for which the influence of the specific parameter on the error function could be assumed negligible, the following approach was followed.

The magnitude of the influence of a sensitivity on the error function is determined both by the magnitude of the sensitivity and the magnitude of the parameter. In order to quantify the influence on the error function, a quadratic approximation of the error function about a specific point will be obtained from a Taylor-series expansion. From this approximation, the change in the error function due to a change in the parameter may be written as:

$$\Delta(error) = \Delta\chi \cdot \frac{\partial(error)}{\partial\chi} + \Delta\gamma \cdot \frac{\partial(error)}{\partial\gamma} + \frac{1}{2} \cdot \Delta\chi^2 \cdot \frac{\partial^2(error)}{\partial\chi^2} + \frac{1}{2} \cdot \Delta\chi \cdot \Delta\gamma \cdot \frac{\partial^2(error)}{\partial\chi\partial\gamma} + \frac{1}{2} \cdot \Delta\gamma^2 \cdot \frac{\partial^2(error)}{\partial\gamma^2}$$

. . . (8.15)

The minimum value for which the error function can be determined accurately is 1×10^{-5}. This value is determined by the floating point accuracy of the measuring instrument. A cut-off point will be defined as one for which a 50% change in a variable, causes a maximum change in the appropriate term on the right hand side of *Equation 8.15* of less than 1×10^{-8}. Any term larger than 1×10^{-8} will be considered to have a significant influence on the error function. The cut-off point may then be written as:

$$\left| \Delta\chi \cdot \frac{\partial(error)}{\partial\chi} \right| \leq 10^{-8} \qquad \left| \Delta\gamma \cdot \frac{\partial(error)}{\partial\gamma} \right| \leq 10^{-8}$$

. . . (8.15)

for the first-order sensitivities and:

$$\left|\frac{1}{2}\cdot\Delta\chi^2\cdot\frac{\partial^2(error)}{\partial\chi^2}\right|\le 10^{-8} \qquad \left|\frac{1}{2}\cdot\Delta\chi\cdot\gamma\cdot\frac{\partial^2(error)}{\partial\chi\partial\gamma}\right|\le 10^{-8}$$

$$\left|\frac{1}{2}\cdot\Delta\gamma^2\cdot\frac{\partial^2(error)}{\partial\gamma^2}\right|\le 10^{-8}$$

. . . **(8.16)**

for the second-order sensitivities.

From the above method, only three of the first-order derivatives and six of the second-order derivatives were found to be significant. These significant values, for a 50% change in the magnitude of the appropriate parameters, are shown in *Table 8.1*.

Also shown in *Table 8.1* is the change in the error function expressed as a percentage of the maximum velocity value of the response (0.00015 $m.s^{-1}$). It is important to note that the sensitivities are problem dependent. Also the frequency and amplitude of the excitation plays an important role in the magnitude of the sensitivities.

8.2.3.2 Dynamic displacement response

The dynamic displacement response of the beam is shown in *Figure 8.2*. This is the result obtained from the plate-element model. The beam elements yielded a similar result, with a mean difference in the nodal point displacement values of less than 0.02%. The mean difference between the two models was calculated by taking the average value of the difference in the results at each node point, expressed as a percentage with respect to the value as calculated by the plate element model.

$$diff = \left(\frac{w_{(plate)i} - w_{(beam)i}}{w_{(plate)i}}\right)\times 100$$

Table 8.1: Significant values of the sensitivities for a 50% change in the magnitude of the parameters

Sensitivity	Change in Error function [m.s^{-1}]	% of maximum dynamic velocity response
$\Delta K_{RL} \cdot \frac{\partial(error)}{\partial K_{RL}}\Big\|_{max}$	79.5893 10^{-6}	53.1
$\Delta K_{TR} \cdot \frac{\partial(error)}{\partial K_{TR}}\Big\|_{max}$	64.0019 10^{-6}	42.7
$\Delta K_{RR} \cdot \frac{\partial(error)}{\partial K_{RR}}\Big\|_{max}$	17.162 10^{-9}	0.01
$\frac{1}{2} \cdot \Delta K_{RL} \cdot \Delta K_{RL} \cdot \frac{\partial(error)}{\partial K_{RL} \partial K_{RL}}\Big\|_{max}$	0.11730 10^{-3}	78.2
$\frac{1}{2} \cdot \Delta K_{RL} \cdot \Delta K_{TR} \cdot \frac{\partial(error)}{\partial K_{RL} \partial K_{TR}}\Big\|_{max}$	20.7005 10^{-6}	13.8
$\frac{1}{2} \cdot \Delta K_{RL} \cdot \Delta K_{RR} \cdot \frac{\partial(error)}{\partial K_{RL} \partial K_{RR}}\Big\|_{max}$	5.53835 10^{-9}	0.004
$\frac{1}{2} \cdot \Delta K_{TR} \cdot \Delta K_{TR} \cdot \frac{\partial(error)}{\partial K_{TR} \partial K_{TR}}\Big\|_{max}$	27.1136 10^{-6}	18.1
$\frac{1}{2} \cdot \Delta K_{TR} \cdot \Delta K_{RR} \cdot \frac{\partial(error)}{\partial K_{TR} \partial K_{RR}}\Big\|_{max}$	0.12676 10^{-6}	0.01

8.2.3.3 Results for the first-order sensitivity of the error function with respect to the elastic boundary conditions of the numerical model

As stated earlier, there are only four non-zero values to be calculated. Of these four values only three have a significance on the error function (*Table 8.1*) and these are shown graphically in *Figures 8.3, 8.4 and 8.5*. The graphs show the magnitude of the sensitivity of the error function with respect to the elastic boundary condition over the length of the beam.

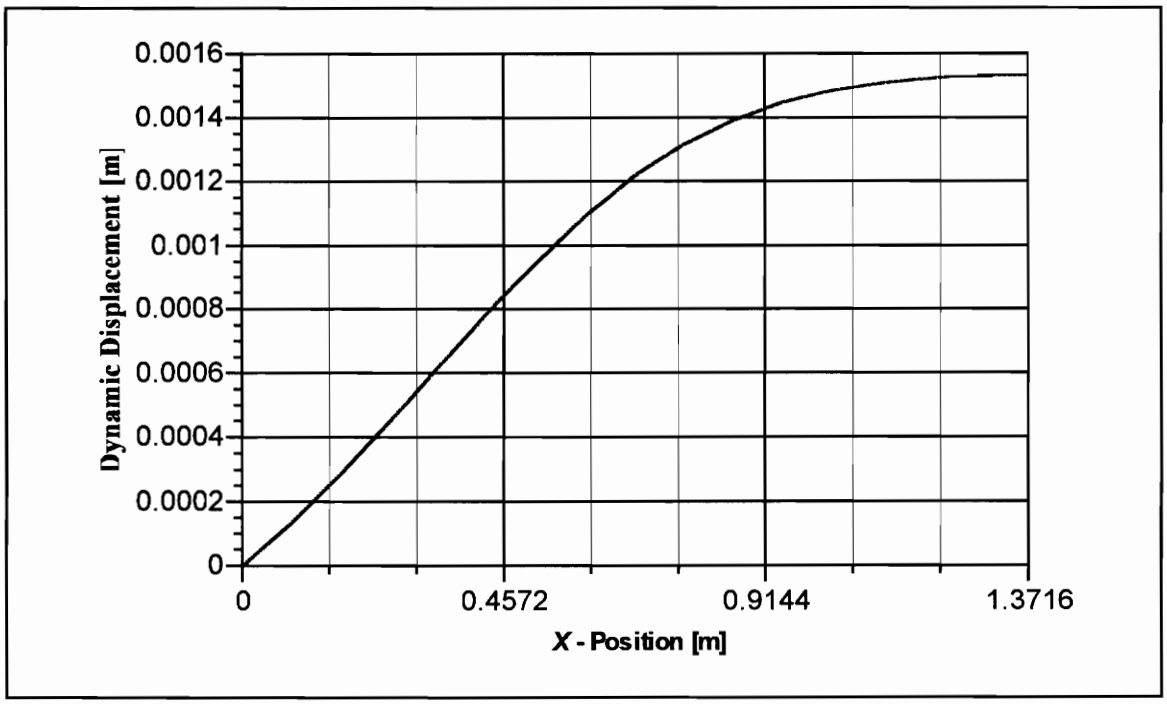

Figure 8.2: Dynamic Displacement response - Plate model

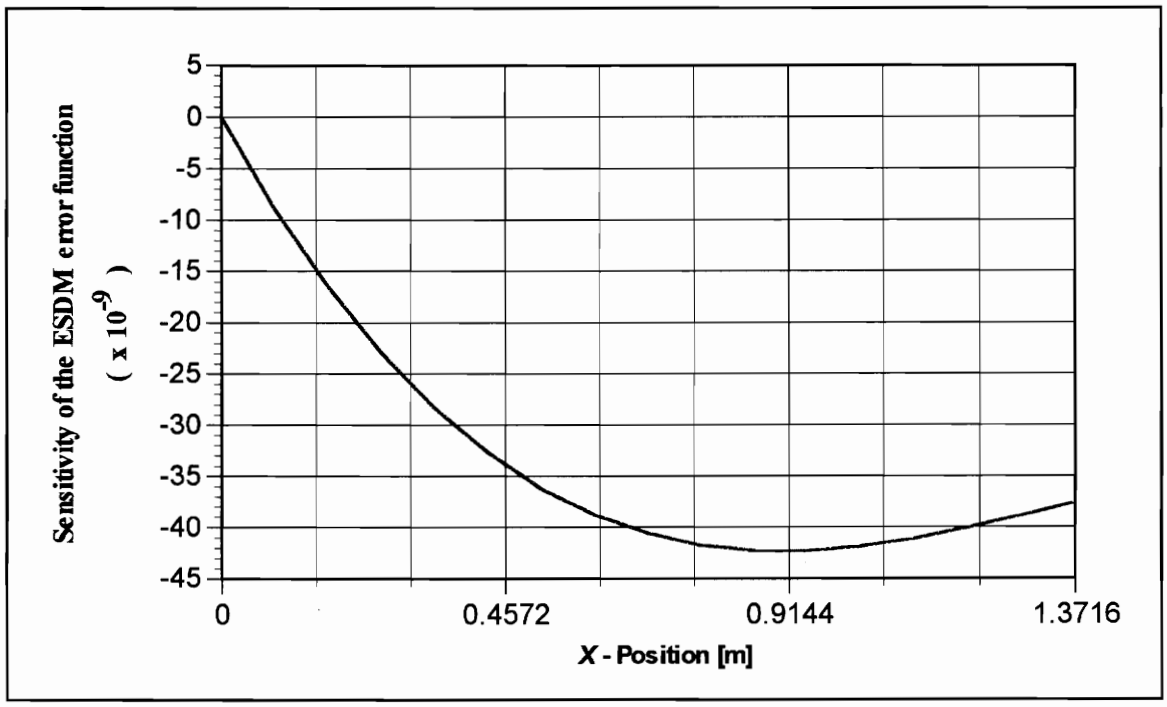

Figure 8.3: Sensitivity of the error function with respect to the elastic stiffness variable K_{RL}

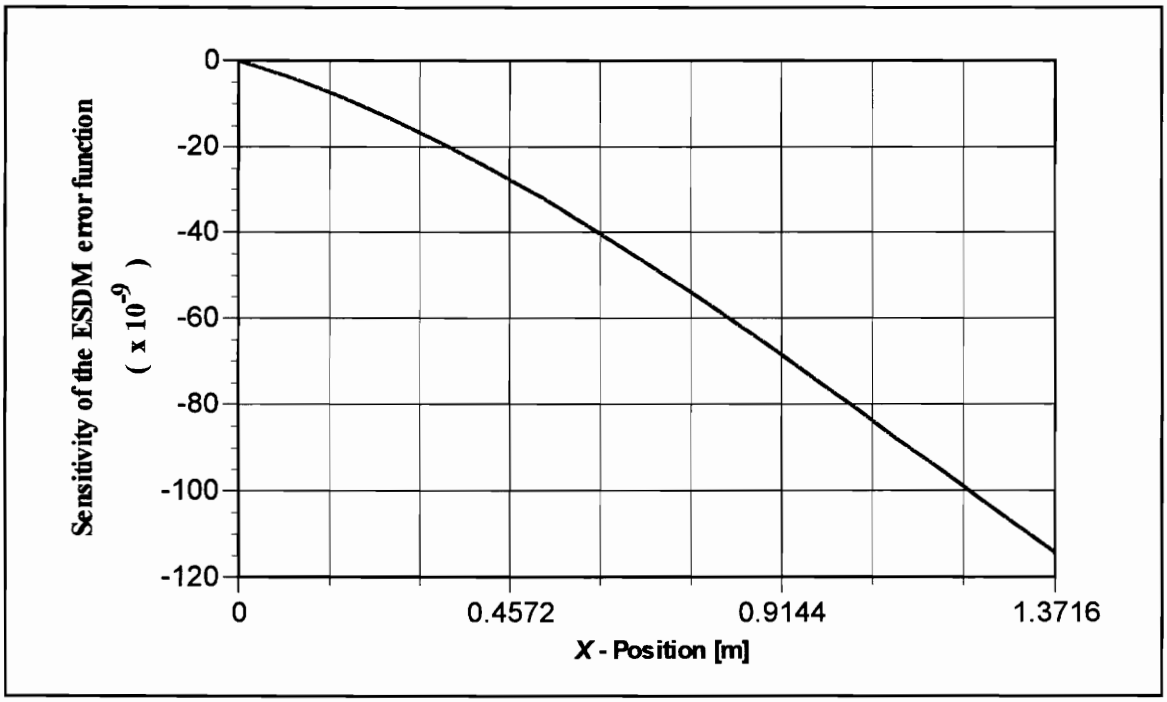

Figure 8.4: Sensitivity of the error function with respect to the elastic stiffness variable K_{TR}

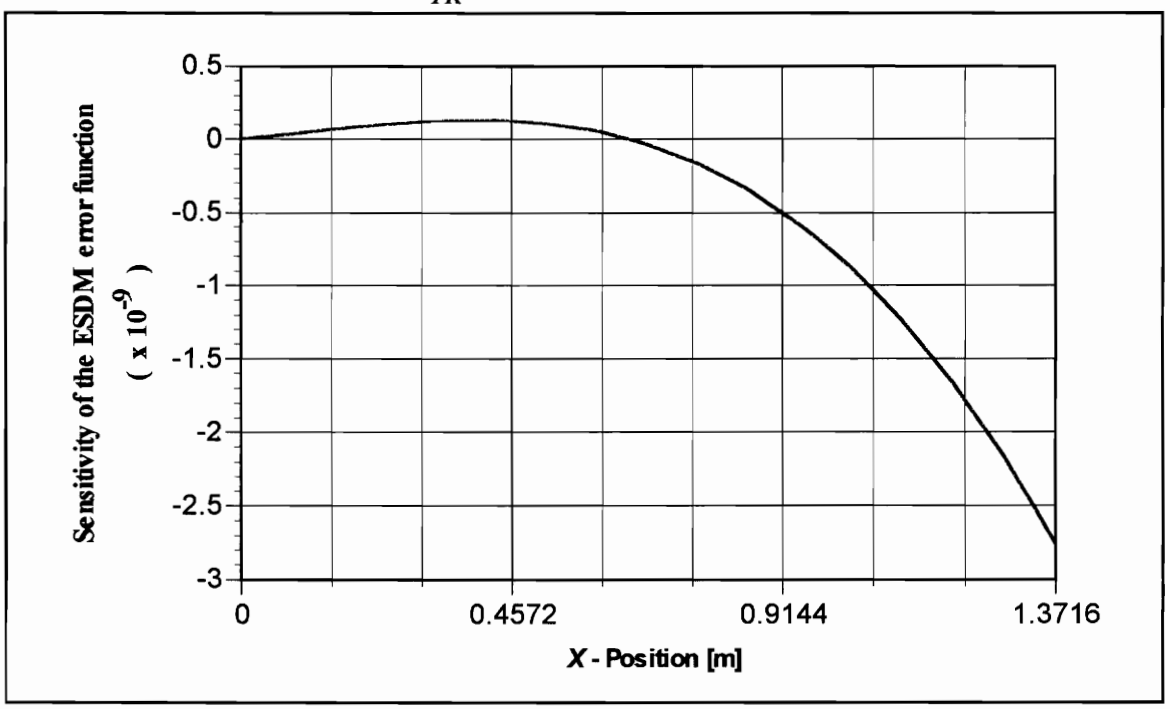

Figure 8.5: Sensitivity of the error function with respect to the elastic stiffness variable K_{RR}

The maximum value of the mean difference in the nodal point values obtained from the beam and plate element models was found to be less than 0.01%, and only the values obtained from the plate element model are, thus, shown.

8.2.3.4 Results for the second-order sensitivity of the error function with respect to the elastic boundary conditions of the numerical model

Of the ten non-zero, unique sensitivities, only five were found to have a significant influence on the error function (*Table 8.1*). These sensitivities are shown in *Figures 8.6 through 8.10*. Once again the graphs shown the magnitude of the sensitivity of the error function with respect to the elastic boundary condition over the length of the beam.

As before, only the results obtained from the plate element model are shown due to the fact that the results obtained from the two models are essentially the same.

8.2.3.5 General discussion of the results and their implications

The results obtained for the displacement response of the beam, are exactly as expected. That is, the displacement at the left end is essentially equal to zero due to the relatively high axial stiffness of the aluminum rod. The slope is not equal to zero at x=0 due to the relative low rotational stiffness of the support. At the right end the displacement is almost equal to the maximum displacement, but the influence of the axial stiffness of the bungi cord is clearly shown by the flattening of the displacement curve in this region.

8.2.3.5.1 First-order sensitivities

All the first-order sensitivities show the general non-linear trend that an increase in the value of the specific stiffness constant will cause a decrease in the value of the error function.

Furthermore, due to the dependency of the sensitivities on the velocity field, all the sensitivities have a value of zero at x=0. The magnitude of the sensitivities also depends on the position along the length of the beam. The elastic boundary conditions have the biggest influence on the error function at the right end point of the beam.

Lastly, as shown in *Table 8.1*, it was found that the rotational and transverse

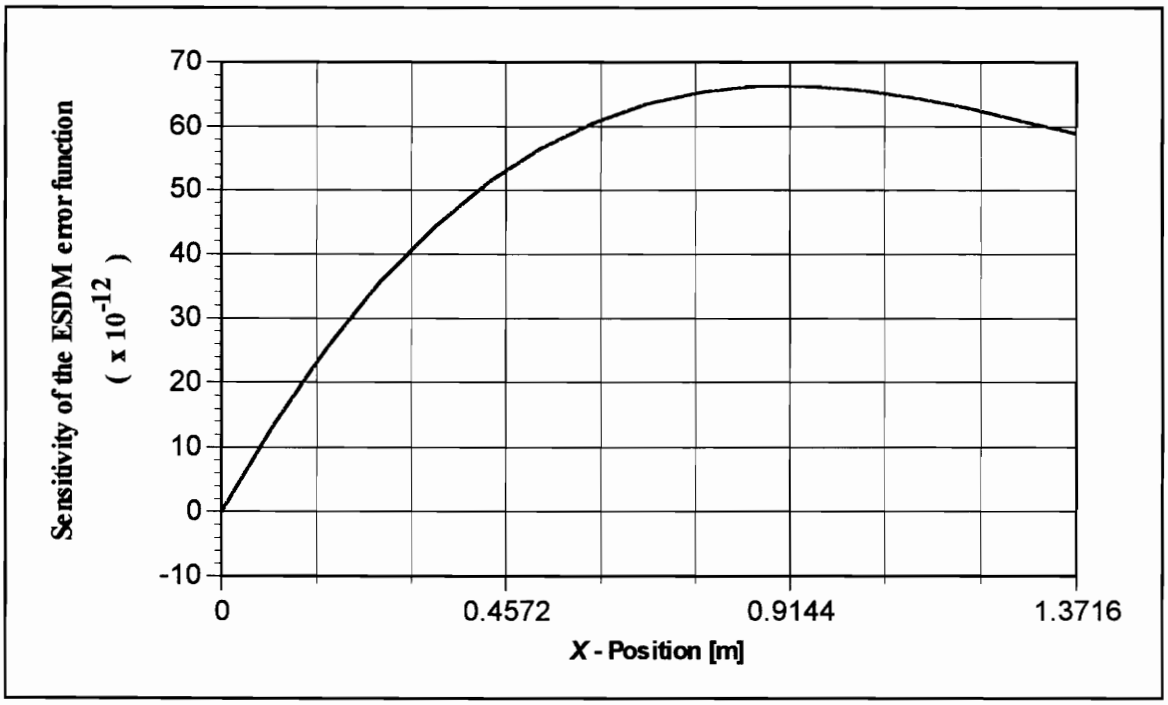

Figure 8.6: Second-order sensitivity of the error function with respect to the elastic stiffness variable K_{RL}

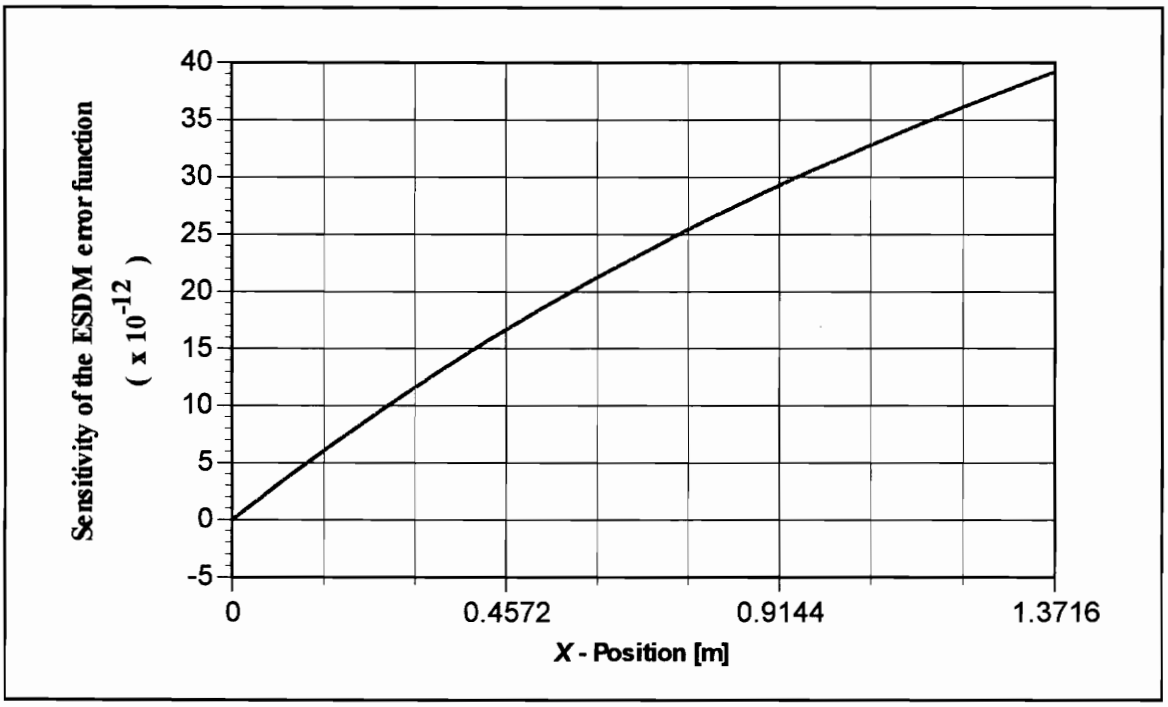

Figure 8.7: Second-order sensitivity of the error function with respect to the elastic stiffness variables K_{RL} and K_{TR}

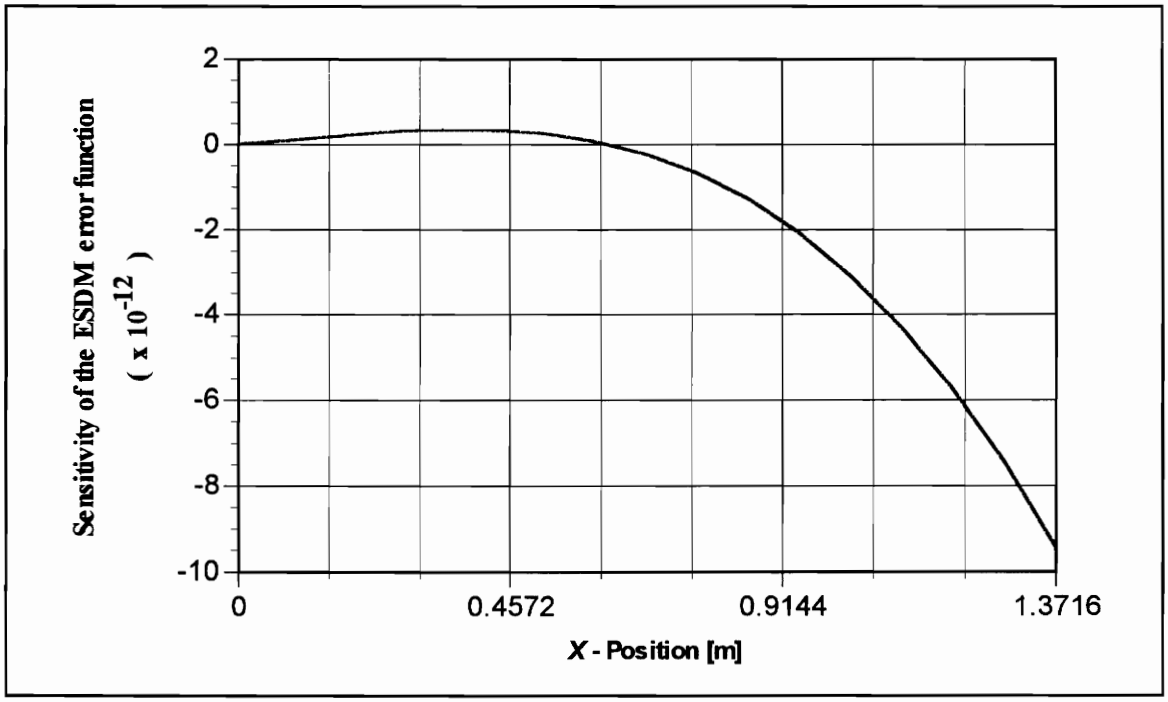

Figure 8.8: Second-order sensitivity of the error function with respect to the elastic stiffness variables K_{RL} and K_{RR}

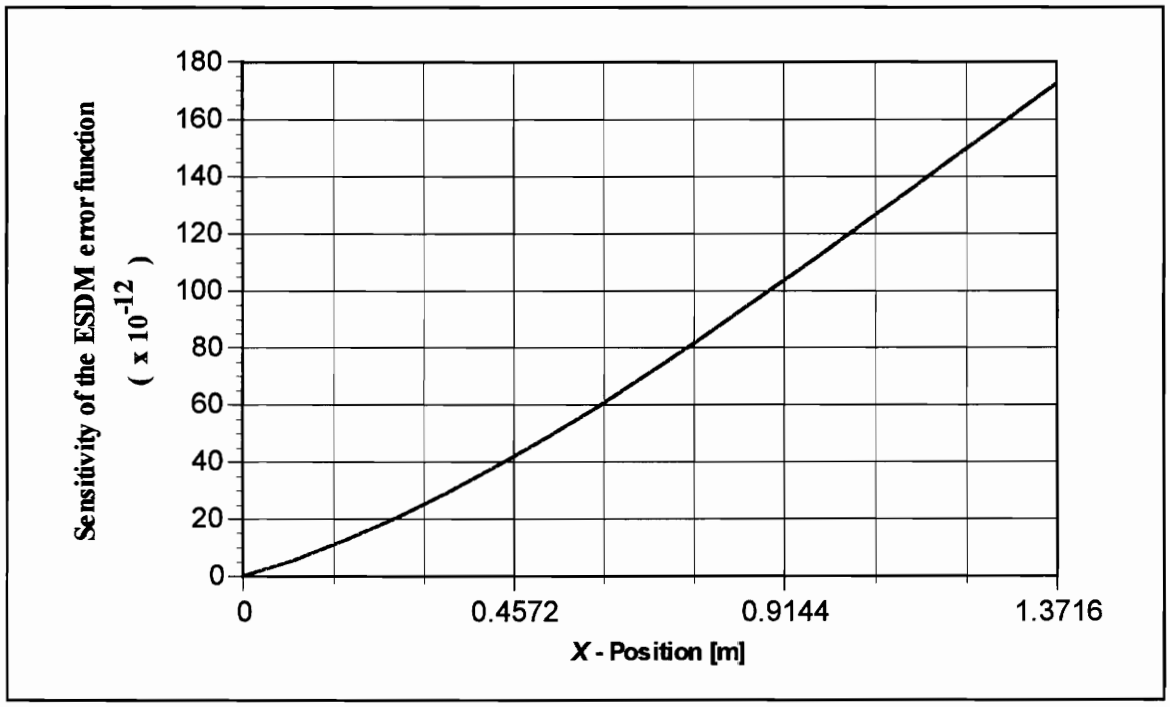

Figure 8.9: Second-order sensitivity of the error function with respect to the elastic stiffness variable K_{TR}

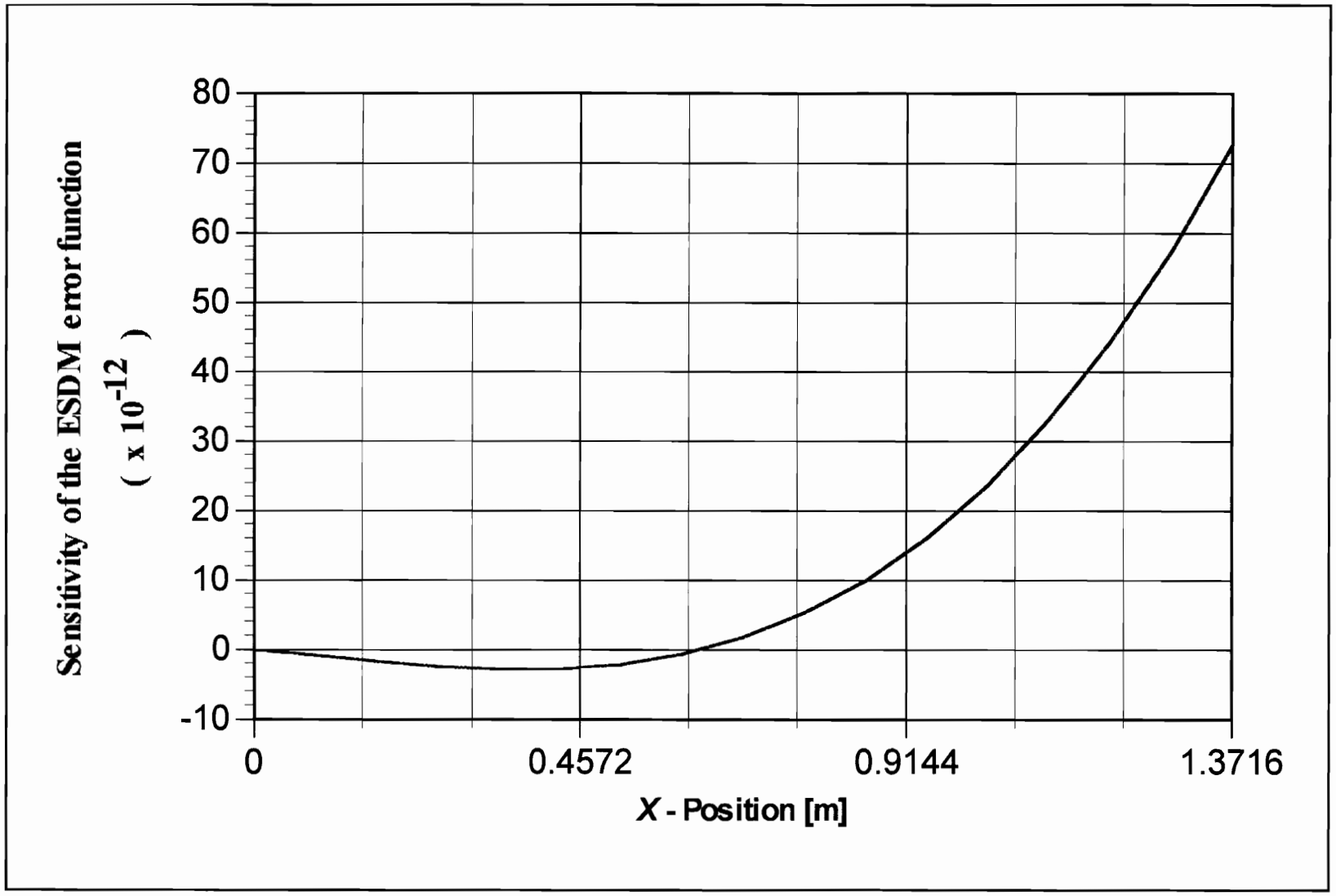

Figure 8.10: Second-order sensitivity of the error function with respect to the elastic stiffness variables K_{TR} and K_{RR}

stiffness at the left end have the biggest influence on the error function. However, the sensitivity with respect to the rotational stiffness at the right-end point of the beam is relatively small compared to the maximum velocity over the beam. This has several consequences. If one is to try to update this finite element model using velocity data, this sensitivity is well below the noise floor of the instrument, making it impossible to disguise between the noise and the error.

8.2.3.5.2 Second-order sensitivities

The two different shapes, as seen in the graphs of the first-order sensitivities (*Figures 8.3 through 8.5*), are reflected in the results obtained for the second-order sensitivities. The absolute magnitude of the results are however, as expected, much smaller than that obtained for the first-order sensitivities.

As shown in *Table 8.1*, the second-order sensitivity with the largest influence on the error function is the second-order sensitivity with respect to the rotational stiffness at the left end.

8.2.4 Discussion of results on example problem in terms of the goals

8.2.4.1 Positive aspects

Analytical expressions for the sensitivities of the error function with respect to the elastic boundary conditions could be found. The goals for this part of the research were, thus, met. Apart from the goals being met, there were quite a few other positive aspects of the results obtained, of which the most important may be summarized as follows:

1. The sensitivity of the error function with respect to any other model parameter (for example the sensitivity of the error function with respect to the Young's modulus of the material) can be calculated from exactly the same formulation used
2. Good correlation between the beam element and the plate element models were obtained

3. One can use the sensitivity information to update finite element methods.
4. The sensitivity information can be used to estimate the precision of the measurements required to update the candidate finite element models.

8.2.4.2 Negative aspects

The only negative aspect of the approach used, is the fact that only periodic loading conditions can be used. This is not really a problem due to the fact that most loading conditions may be written as a periodic function by means of a Fourier series expansion.

8.3 Sensitivity of the error function with respect to the spatial variables of the laser

The structure of *Section 8.1* will be used once again. The numerical model for this part of the calculations will differ somewhat from the previous models. Only a plate element model will be considered and the structure will be modeled by one element only. The simulated experimental setup used may be summarized as follows:

8.3.1 Simulated experimental setup

The simulated experimental setup is shown schematically in *Figure 8.11* and consists of the boundary and loading conditions and the constants of the numerical model.

8.3.1.1 Boundary and loading conditions

The boundary conditions imposed on the beam will not be of an elastic nature. A cantilevered beam (similar to the beam studied in *Chapter 7*) will be used. The beam will be rigidly fixed at the left end and will be free at the right end.

Furthermore, the beam will be subjected to a harmonic forcing function applied at the right end of the beam. The magnitude and frequency of the excitation force may be summarized as follows:

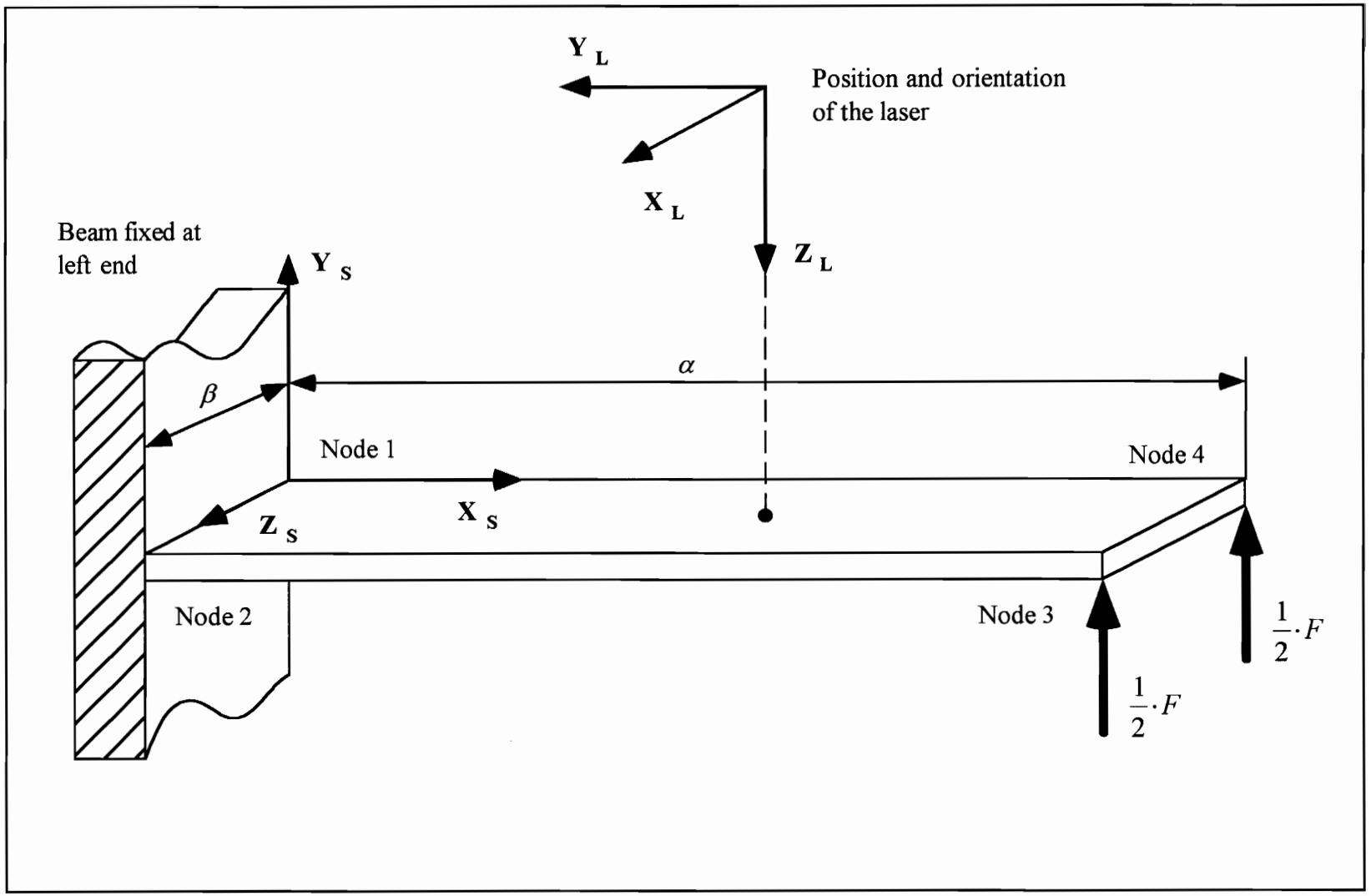

Figure 8.11: Experimental setup used to calculate the sensitivities of the ESDM error function with respect to the spatial position and orientation of the laser

$$F(x,t) = f_0 Sin(\omega t)$$

with:

f_0 = 5 N at the right end point and zero everywhere else

$$\omega = 0.1 \text{ rad/s}$$

. . . **(8.18)**

8.3.1.2 Numerical model

The structure will be modeled by one plate element (*Figure 8.11*) with the node point coordinates and element constants given by:

Node 1 = (0, 0, 0) Node 2 = (0, 0, 0.0762)
Node 3 = (1.3716, 0, 0.0762) Node 4 = (1.3716, 0, 0)

α = 1.3716 m β = 0.0762 m

. . . **(8.19)**

8.3.1.3 Displacement field

The specified excitation force will be incorporated into the model by obtaining the displacement field at the four node points of the single plate element used to model the beam. The displacement field due to the specific forcing function will be evaluated from the closed-form solution as was done in the example problem of *Chapter 7*, but for an element with a total length of 1.3716 m.

The prescribed displacements at the node points of the plate element were calculated to be:

$$u_1 = u_2 = u_3 = u_4 = v_1 = v_2 = w_1 = w_2 = w_3 = w_4 = 0$$

$$v_3 = v_4 = 0.0134895 \text{ m}$$

. . . **(8.20)**

The first derivative of the exact solution with respect to the x-direction give the values for the rotation θ_x at the node points as follows:

$$\theta_{x1} = \theta_{x2} = 0$$

$$\theta_{x3} = \theta_{x4} = -0.0147589 \quad \text{rad}$$

. . . **(8.21)**

The first derivative of the exact solution with respect to the z-direction give the values for the rotation θ_z at the node points as follows:

$$\theta_{z1} = \theta_{z2} = \theta_{z3} = \theta_{z4} = 0$$

. . . **(8.22)**

If the Hermitic shape functions of the plate element are used to interpolate the displacement along the length of the beam, the solution obtained at any position of the beam is very close to the value obtained from the exact solution. The maximum percent difference between the closed-form solution and the solution obtained from the interpolation along the length of the beam was found to be less than 0.5%. The interpolation obtained from the specified shape functions for one element will, thus, give a good approximation of the exact solution for this specific setup. This approximation was checked for accuracy so that convergence of the mesh would be less of an issue.

8.3.2 Example problem development

The derivative of the error function with respect to the spatial variables are given by *Equation 7.5*. In order to evaluate the sensitivity of the error function with respect to the spatial variables, it is necessary to evaluate the partial derivatives as shown in *Equations 7.8 and 7.9*. The calculation of these derivatives will now be discussed.

8.3.2.1 Partial derivatives of the velocity components with respect to the local coordinates of the elements

These derivatives may be written as a combination of the forcing frequency and the

displacement components as shown in *Equation 7.11*. Since the beam will only have a velocity component in the *y*-direction (due to the specific prescribed forcing function), the values of the velocity components and their derivatives with respect to the local coordinates may be summarized as follows:

$$v_{xi} = v_{zi} = 0$$

$$\frac{\partial v_{xi}}{\partial \xi} = \frac{\partial v_{zi}}{\partial \eta} = \frac{\partial v_{xi}}{\partial \xi} = \frac{\partial v_{zi}}{\partial \eta} = 0$$

$$v_{yi} = \omega \cdot \left(u_{y3} \cdot N_7 + \theta_{x3} \cdot N_9 + u_{y4} \cdot N_{10} + \theta_{x4} \cdot N_{12} \right)$$

$$\frac{\partial v_{yi}}{\partial \xi} = \omega \cdot \left(u_{y3} \cdot \frac{\partial N_7}{\partial \xi} + \theta_{x3} \cdot \frac{\partial N_9}{\partial \xi} + u_{y4} \cdot \frac{\partial N_{10}}{\partial \xi} + \theta_{x4} \cdot \frac{\partial N_{12}}{\partial \xi} \right)$$

$$\frac{\partial v_{yi}}{\partial \eta} = \omega \cdot \left(u_{y3} \cdot \frac{\partial N_7}{\partial \eta} + \theta_{x3} \cdot \frac{\partial N_9}{\partial \eta} + u_{y4} \cdot \frac{\partial N_{10}}{\partial \eta} + \theta_{x4} \cdot \frac{\partial N_{12}}{\partial \eta} \right)$$

where:

$$\frac{\partial N_7}{\partial \xi} = \eta(-1 + 3\eta - 2\eta^2 + 6\xi - 6\xi^2) \qquad \frac{\partial N_9}{\partial \xi} = \alpha\eta(2 - 3\xi)\xi$$

$$\frac{\partial N_{10}}{\partial \xi} = (-1 + \eta)(-\eta + 2\eta^2 - 6\xi + 6\xi^2) \qquad \frac{\partial N_{12}}{\partial \xi} = \alpha(-1 + \eta)\xi(-2 + 3\xi)$$

$$\frac{\partial N_7}{\partial \eta} = \xi(-1 + 6\eta - 6\eta^2 + 3\xi - 2\xi^2) \qquad \frac{\partial N_9}{\partial \xi} = \alpha(1 - \xi)\xi^2$$

$$\frac{\partial N_{10}}{\partial \eta} = \xi(-1 - 6\eta + 6\eta^2 - 3\xi + 2\xi^2) \qquad \frac{\partial N_{12}}{\partial \xi} = \alpha(-1 + \xi)\xi^2$$

. . . (8.23)

Upon evaluation, the derivative of the velocity component with respect to the local coordinates of the elements, were found to be:

$$\frac{\partial v_{yi}}{\partial \xi} = 0.00202252 \cdot \xi - 0.000673569 \cdot \xi^2 \qquad \frac{\partial v_{yi}}{\partial \eta} = 0$$

. . . **(8.24)**

8.3.2.2 Partial derivatives of the local coordinates of the elements with respect to the scanning position

The derivatives of the local coordinates with respect to the scanning position may be calculated from the inverse of the Jacobian matrix as shown in *Equation 7.20*. The bi-linear shape functions of the four noded element, as shown in *Equation 4.26*, will be used to form the Jacobian matrix. This sub-parametric formulation of the elements may be used since only flat, straight-sided elements will be considered.

The derivatives were calculated to be:

$$\frac{\partial \xi}{\partial x_i} = \frac{1}{1.3716} \qquad \frac{\partial \xi}{\partial z_i} = 0$$

$$\frac{\partial \eta}{\partial x_i} = 0 \qquad \frac{\partial \eta}{\partial z_i} = \frac{1}{0.0762}$$

. . . **(8.25)**

8.3.2.3 Partial derivatives of the scanning position and the direction cosines with respect to the spatial variables

These derivatives may be calculated exactly in the same way as shown for the test case of *Chapter 7*. The only difference being that the scanning position must now be evaluated at a number of points, scanning the surface of the beam, instead of only one point. The transformation matrix between the spherical and rectangular laser coordinates must be evaluated at every scanning position from *Equation 6.13* while the transformation between the rectangular laser and structural coordinate systems is given by *Equation 8.26* for the specific example problem being considered:

$$\begin{Bmatrix} x_i \\ y_i \\ z_i \end{Bmatrix} = \begin{bmatrix} 0 & 0 & 1 \\ -1 & 0 & 0 \\ 0 & -1 & 0 \end{bmatrix}^T \begin{Bmatrix} x_{Li} \\ y_{Li} \\ z_{Li} \end{Bmatrix}$$

. . . **(8.26)**

8.3.3 Discussion of the results on the example problem in general and their implications

In order to evaluate the sensitivity of the error function with respect to the spatial variables of the laser, it is necessary to evaluate *Equation 7.5*. As shown in *Section 8.3.2.1*, most of the terms contained in *Equation 7.5* are zero, reducing the equation to:

$$\frac{\partial (error)_i}{\partial \chi} = \frac{\partial v_{yi}}{\partial \chi} \cdot \eta_{yi} + v_{yi} \cdot \frac{\partial \eta_{yi}}{\partial \chi}$$

. . . **(8.27)**

where

$$\frac{\partial v_{yi}}{\partial \chi} = \frac{\partial v_{yi}}{\partial \xi_i} \cdot \frac{\partial \xi_i}{\partial x_i} \cdot \frac{\partial x_i}{\partial \chi}$$

. . . **(8.28)**

$$\eta_{yi} = \frac{\sqrt{(y_{Lo} - y_i)^2}}{\sqrt{(x_{Lo} - x_i)^2 + (y_{Lo} - y_i)^2 + (z_{Lo} - z_i)^2}}$$

. . . **(8.29)**

$$v_{yi} = \omega \sum_{j=1}^{20} \left(\overline{u}_{yi} \cdot N_j(\xi, \eta) \right)$$

. . . **(8.30)**

Equation 8.27 yields the sensitivity of the error function with respect to changes in the spatial variables of the laser. These changes will cause a shift in the scanning position of the laser beam on the structure, causing the error function to be evaluated at a different

position than measured by the laser. This error in the error function due to inaccuracies in the spatial variables which will be illustrated by the following example. Let the original scanning position, assuming no errors in the spatial variables of the laser, be represented by

$$\{x_i, y_i, z_i\}_{old} = \{x_{i(old)}, y_{i(old)}, z_{i(old)}\} \quad \text{. . . (8.31)}$$

and the new scanning position, due to errors in the spatial variables of the laser, by:

$$\{x_i, y_i, z_i\}_{new} = \{x_{i(new)}, y_{i(new)}, z_{i(new)}\} \quad \text{. . . (8.32)}$$

The error functions for the original and the new scanning position may then be written as:

$$(error_i)_{old} = v_{xi(old)} \cdot \eta_{xi(old)} + v_{yi(old)} \cdot \eta_{yi(old)} + v_{zi(old)} \cdot \eta_{zi(old)} - \tilde{V}_{Li(old)} \quad \text{. . . (8.33)}$$

$$(error_i)_{new} = v_{xi(old)} \cdot \eta_{xi(old)} + v_{yi(old)} \cdot \eta_{yi(old)} + v_{zi(old)} \cdot \eta_{zi(old)} - \tilde{V}_{Li(new)} \quad \text{. . . (8.34)}$$

A first-order Taylor-series expansion of the error in the error function due to inaccuracies in the spatial variables of the laser (*Equation 8.34* minus *Equation 8.33*), may now be calculated from *Equation 8.27*, yielding a first-order approximation of the error as::

$$\Delta(error)_i = \Delta\chi \cdot \left(\frac{d(error)_i}{d\chi} \right) \quad \text{. . . (8.35)}$$

8.3.3.1 Results for the sensitivity of the error function with respect to the spatial position of the laser

The sensitivity of the error function with respect to the spatial position of the laser will be calculated from *Equation 8.27*. As stated in the test case of *Chapter 7*, the derivatives of the direction cosines with respect to the spatial position of the laser will always be zero when considering flat surfaces. The same result is valid for this example problem and it is, thus, only necessary to evaluate the $\frac{\partial v_{yi}}{\partial \chi}$ and η_{yi} terms in order to obtain the required sensitivities.

Figure 8.12 shows the values for the sensitivity of the error function with respect to the *x*-position of the laser while *Figure 8.13* shows the sensitivity with respect to the *y*-position of the laser. These graphs show the values of the sensitivities over the whole surface of the beam, where the surface is mapped to a square region.

The sensitivity of the error function with respect to the *z*-position of the laser was calculated to be exactly equal to zero everywhere. This is due to the fact that the velocity profile is assumed to be independent of the *z*-coordinate of the structure for this specific example problem.

8.3.3.2 Results for the sensitivity of the error function with respect to the spatial orientation of the laser

The sensitivity of the error function with respect to the spatial orientation of the laser will also be calculated from *Equation 8.27*. This time, however, the sensitivities of the direction cosines with respect to the spatial variables of the laser, will be non-zero and the $\frac{\partial v_{yi}}{\partial \chi}$, η_{yi}, v_{Syi} and $\frac{\partial \eta_{yi}}{\partial \chi}$ terms must be evaluated.

Figure 8.14 gives the sensitivity with respect to the spatial orientation about the *x*-axis of the laser, *Figure 8.15* gives the sensitivity with respect to the orientation about the *y*-axis of the laser and *Figure 8.16* gives the sensitivity with respect to the orientation about the *z*-axis of the laser. As was done in *Chapter 7*, variations in the orientation of the laser will be represented by rotations about the axes of the laser, represented by the variables δ_x, δ_y and δ_z. The results shown were calculated for δ_x, δ_y and δ_z equal to zero, representing the case of small rotations about the *x*, *y* and *z* axes of the laser.

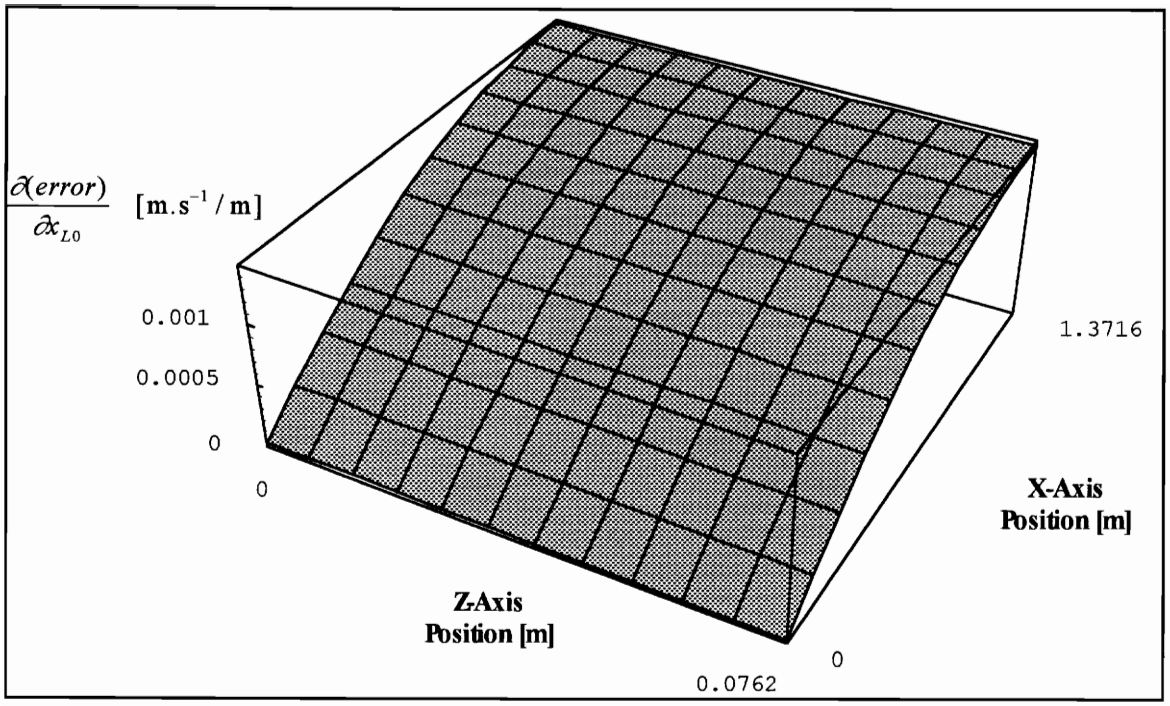

Figure 8.12: Sensitivity of the error function with respect to the spatial position variable, x_{Lo}, of the laser

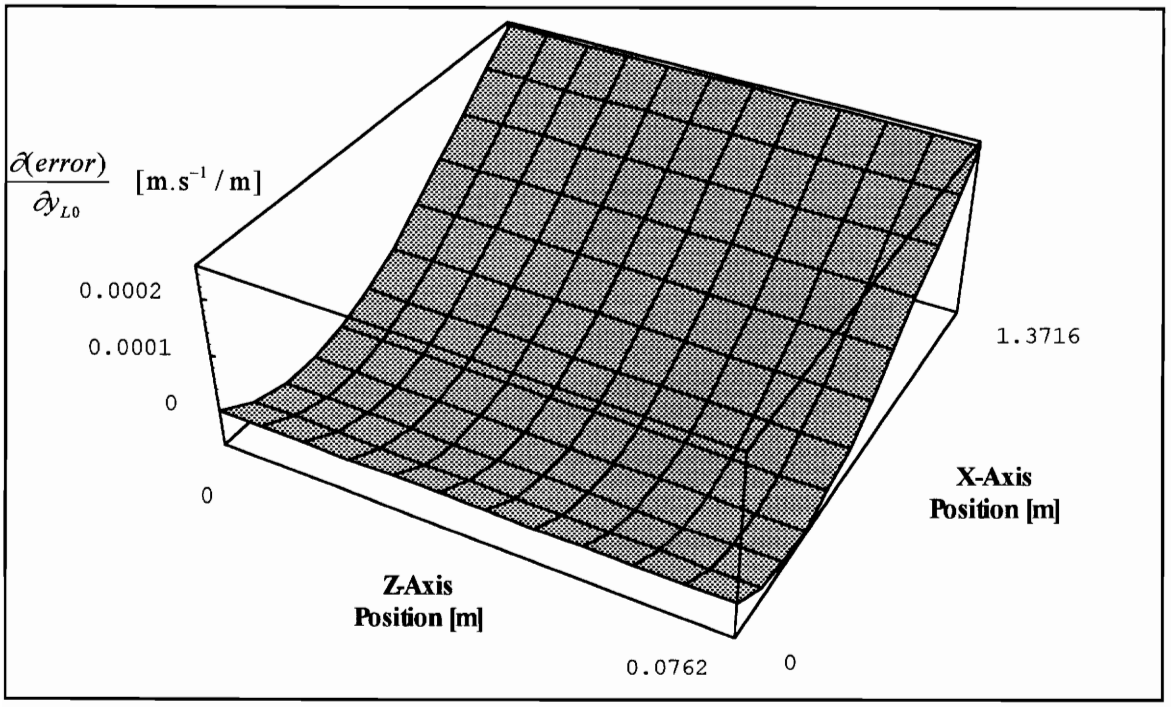

Figure 8.13: Sensitivity of the error function with respect to the spatial position variable, y_{Lo}, of the laser

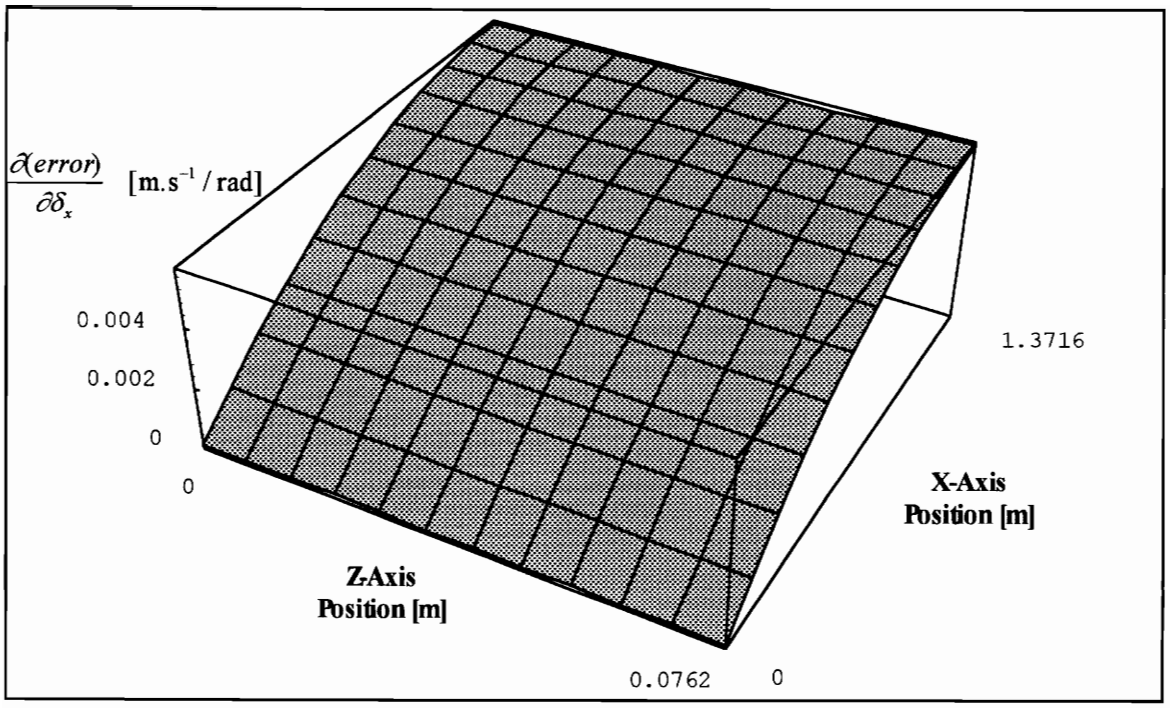

Figure 8.14: Sensitivity of the error function with respect to the spatial orientation variable, δ_x, of the laser

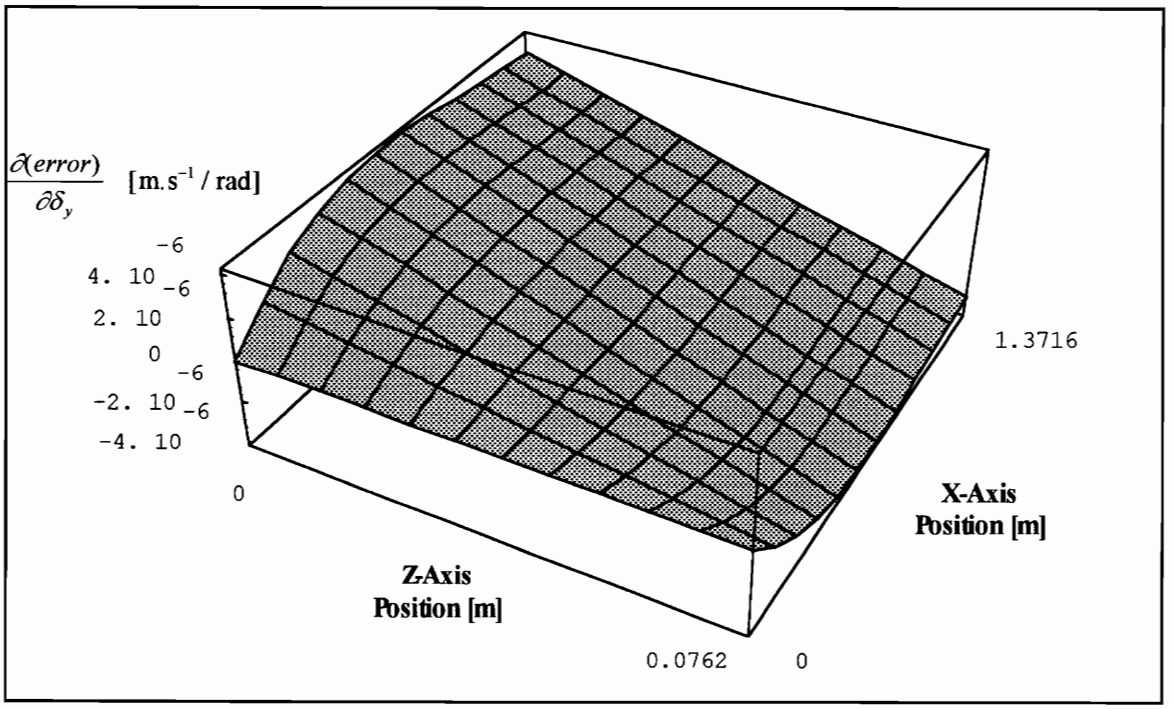

Figure 8.15: Sensitivity of the error function with respect to the spatial orientation variable, δy, of the laser

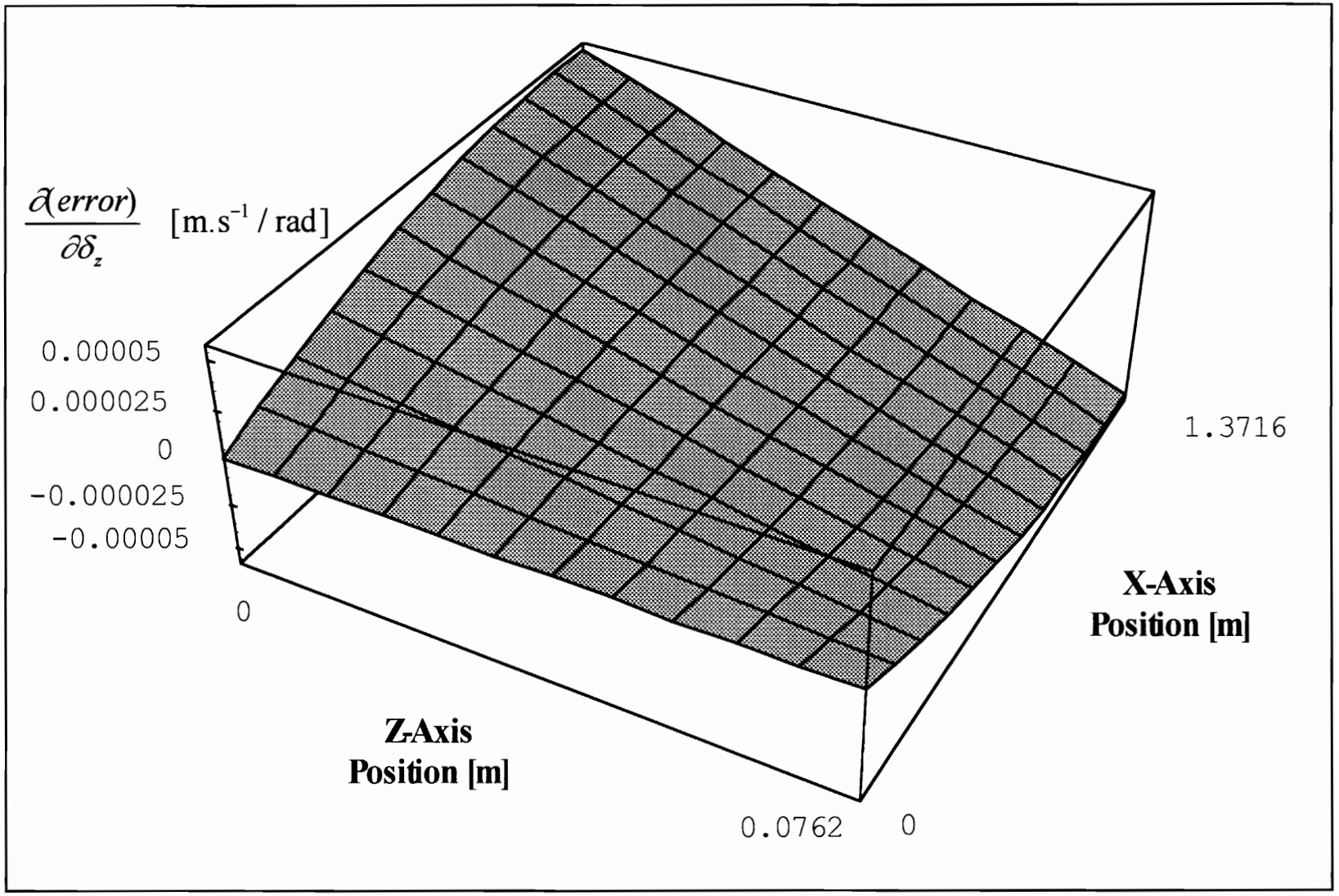

Figure 8.16: Sensitivity of the error function with respect to the spatial orientation variable, δ_z, of the laser

8.3.3.3 General discussion of the results and their implications

Of the six sensitivities of the error function with respect to the spatial position and orientation of the laser, five were found to be non-zero for the given case.

8.3.3.3.1 Sensitivity with respect to the spatial position of the laser

The sensitivities of the error function with respect to the spatial position of the laser are shown in *Figures 8.12 and 8.13*. These graphs are constant for a specific z-value. This is due to the fact that there is no variation in the velocity profile in the z-direction. Also the graphs have the general trend that they start out from zero and increase along the x-axis of the beam. This is due to the boundary condition dependency of the dynamic displacement response profile for the specific problem.

Furthermore, the sensitivity of the error function with respect to the z-position of the laser was found to be zero. This is also due to the fact that there is no variation in the velocity profile in the z-direction.

8.3.3.3.2 Sensitivity with respect to the spatial orientation of the laser

These sensitivities are shown in *Figures 8.14, 8.15 and 8.16*. Once again the graphs show the general trend of starting out with a zero value and increasing along the x-axis of the beam.

For small rotations about the x-axis of the laser, the sensitivity is constant along the z-axis of the structure. For small rotations about the y and z-axes, the sensitivities are no longer constant about the z-axis.

The maximum sensitivity with respect to small rotations about the x-axis is at least two orders of magnitude larger than that corresponding values for sensitivities with respect to small rotations about the y and z-axes.

8.3.4 Second example problem

Since the laser may be placed at infinitely many positions, each with a different influence on the sensitivities of the error function with respect to the spatial variables of the laser, it is impossible to generate results for all possibilities. In order to try and cover a

wider range of possible scanning positions, a second example problem is considered. The first problem gave the best-case scenario, with the laser directly above the center of the plate and the z-axis of the laser pointing directly downwards (*Figure 8.11*).

The working range of the laser is such that the z-axis of the laser may be orientated as to form a minimum angle of 10° with the surface of the structure, representing a worst-case scenario. The second test case will consider the same structure as the first test case (*Section 8.3.1*), but the laser will now be orientated in such a way that the z-axis make a 10° angle will the surface of the structure. This change in position and orientation of the laser will be accomplished by modifying the position and orientation of the first example problem (*Section 8.1.2*). The laser will be moved a positive distance in the x-direction of the structure and will be rotated about it's own x-axis in such a way that the z-axis of the laser will still point to the center point of the plate (*Figure 8.17*).

The new position and orientation vectors of the laser will then be:

$$\{x_{Lo}, y_{Lo}, z_{Lo}\} = \{23.37093, 4, 0.0381\} \quad [\text{m}] \qquad \text{. . . } \mathbf{(8.36)}$$

and

$$\overline{Laser_x} = \{23.37093, 4, 0.05\} \quad [\text{m}] \quad \overline{Laser_z} = \{0.6858, 0, 0.0381\} \quad [\text{m}] \qquad \text{. . . } \mathbf{(8.37)}$$

For the position and orientation of *Equations 8.36 and 8.37*, the range of the deflection angles, necessary to scan the surface of the structure, are given by:

$$\theta_{Lx} \in [-0.169799, 0.169799] \text{ rad} \qquad \theta_{Ly} \in [-0.00952471, 0.00952471] \text{ rad} \qquad \text{. . . } \mathbf{(8.38)}$$

As stated earlier the rest of the example problem setup (i.e. structure, boundary and loading conditions) will be the same as was considered in the first example problem (*Section 8.3.1*). Also, the example problem development will involve the same steps as for the first example problem, as discussed in *Section 8.3.2*. The details will, thus, be omitted and only the obtained results will be shown.

8.3.4.1 Results for the sensitivity of the error function with respect to the spatial position of the laser

As in the first example problem, only the sensitivities with respect to the x- and y-position of the laser were found to be non-negative. The two graphs are shown in *Figures 8.18 and 8.19* respectively.

The sensitivity of the error function with respect to the x-position of the laser shows the same trend as for the first test case, but the magnitude of the sensitivity were found to be smaller. For the first example problem the maximum value were found to be 0.0015 $m.s^{-1}/m$ while the maximum value for the second problem were found to be 0.0003 $m.s^{-1}/m$.

The sensitivity of the error function with respect to the y-position of the laser not only had a different magnitude, but also followed a different trend than was observed for the first example problem. The difference in the shape of the graphs is due to the large change in the values of the direction cosines of the laser beam with respect to the y-axis of the structure. The maximum value for the first problem was found to be 0.00025 $m.s^{-1}/m$ and for the second problem it was 0.0015 $m.s^{-1}/m$.

The maximum sensitivities for both problems are summarized in *Table 8.2*. *Table 8.3* summarize the magnitude of the error due to a 10% change in all the variables representing the spatial position of the laser, expressed as a percentage of the maximum velocity of the structure (0.00134895 $m.s^{-1}$).

From *Table 8.3* it is clear that an error in the x-coordinate of the spatial position of the laser have a bigger influence on the error function than a similar error in the y-coordinate of the spatial position of the laser for this particular case.

8.3.4.2 Results for the sensitivity of the error function with respect to the spatial orientation of the laser

All the graphs showed the same trends compared to the graphs of the first example problem, but with changes in the magnitude of the sensitivities. The results of the sensitivity of the error function with respect to δ_x, δ_y and δ_z are shown in *Figures 8.20, 8.21 and 8.22* respectively.

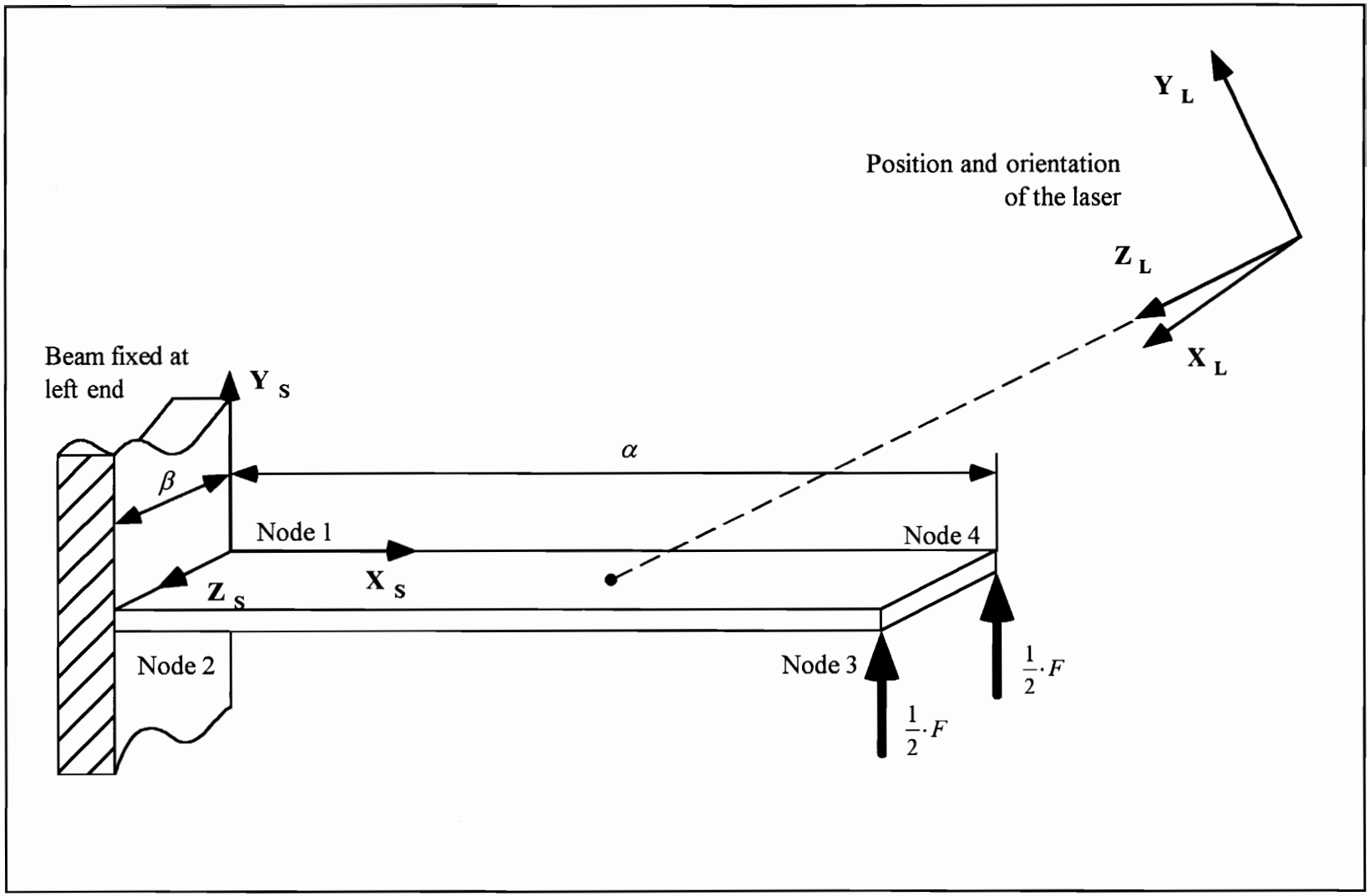

Figure 8.17: Experimental setup of the second example problem used to calculate the sensitivities of the ESDM error function with respect to the spatial position and orientation of the laser

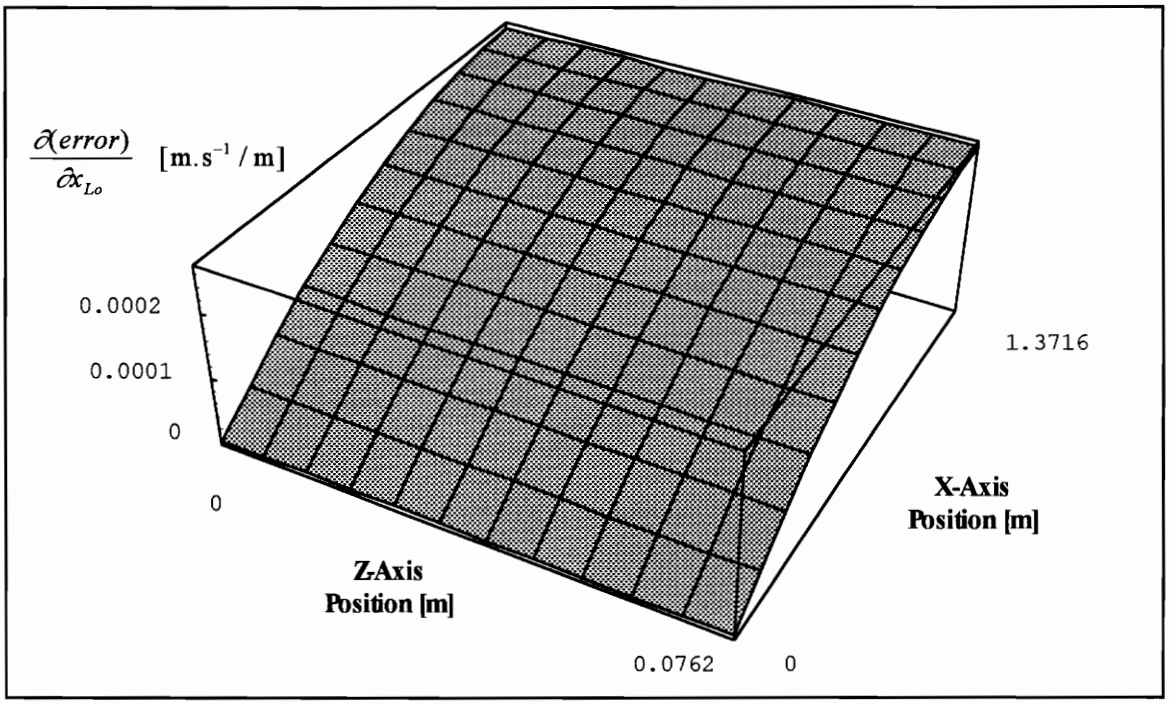

Figure 8.18: Sensitivity of the error function with respect to the spatial position variable, x_{Lo}, of the laser

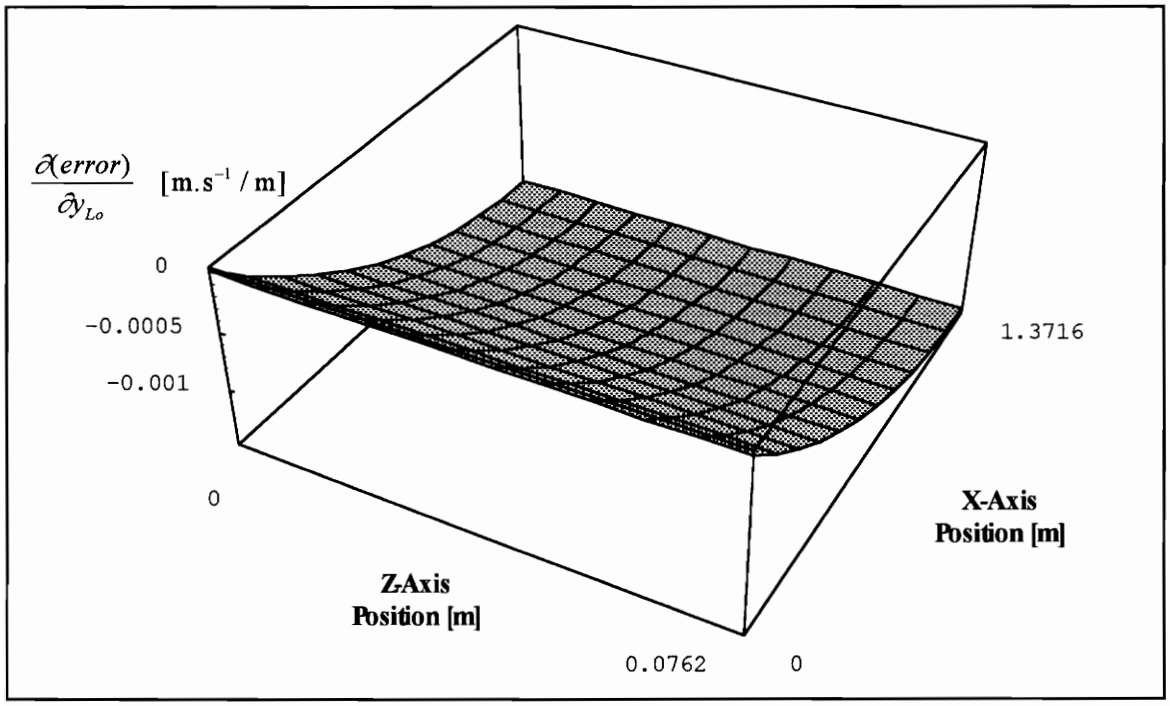

Figure 8.19: Sensitivity of the error function with respect to the spatial position variable, y_{Lo}, of the laser

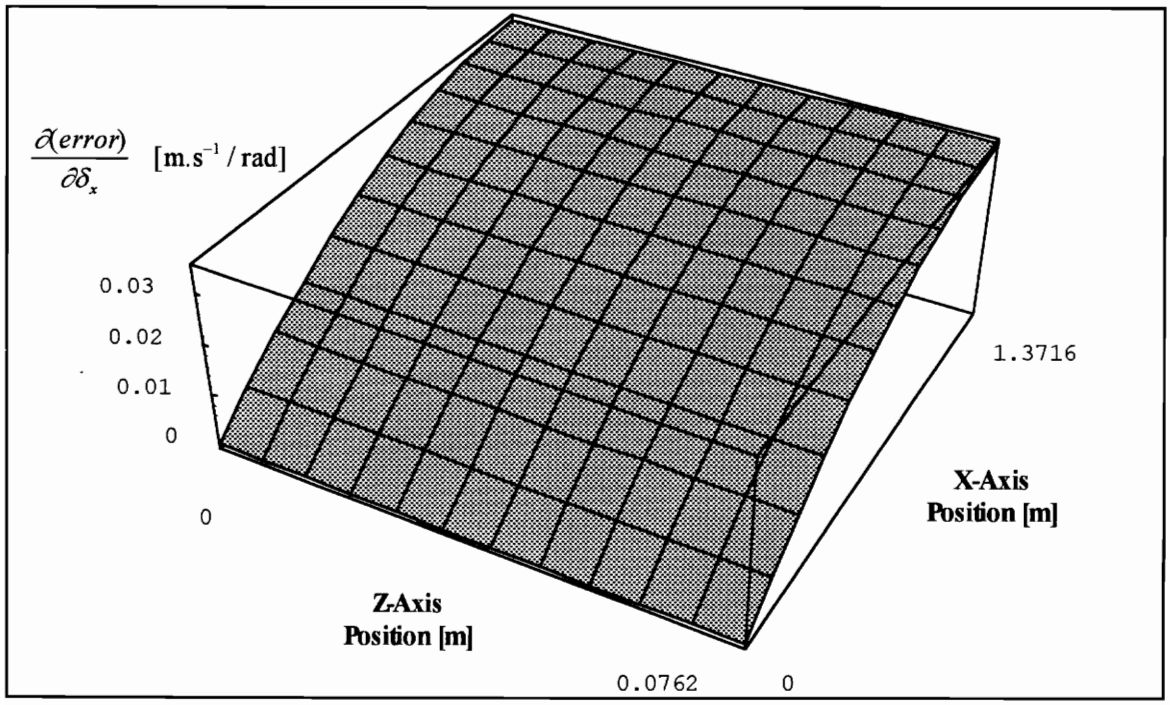

Figure 8.20: Sensitivity of the error function with respect to the spatial orientation variable, δ_x, of the laser

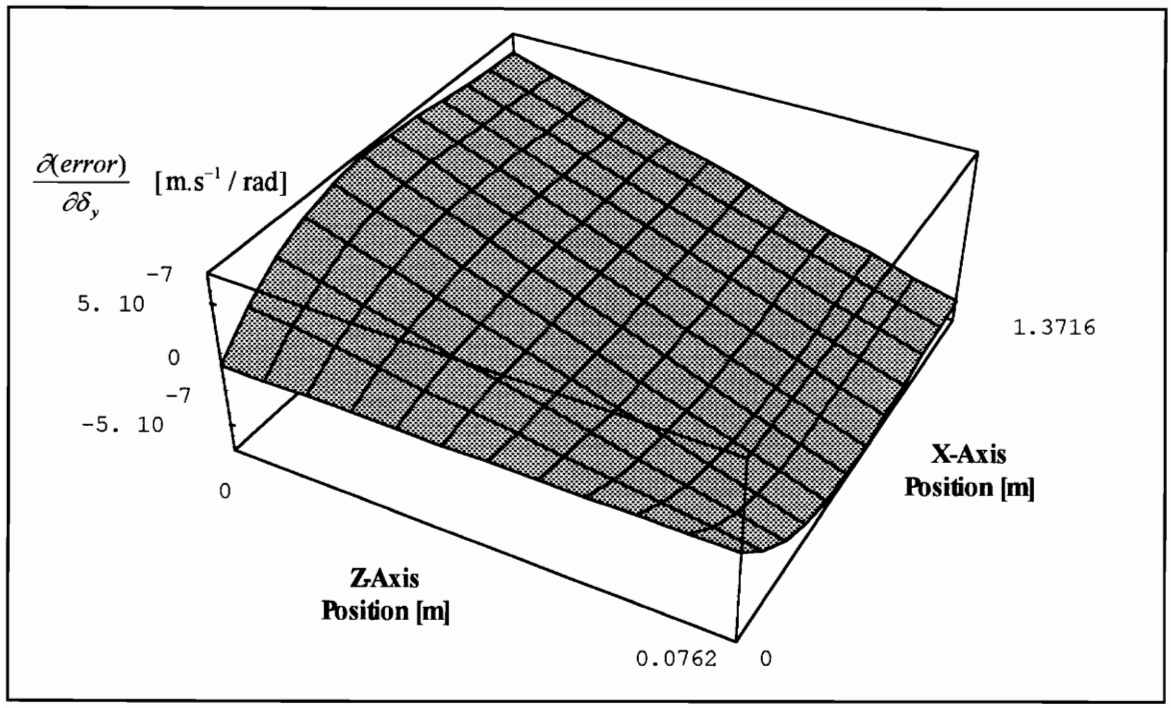

Figure 8.21: Sensitivity of the error function with respect to the spatial orientation variable, δy, of the laser

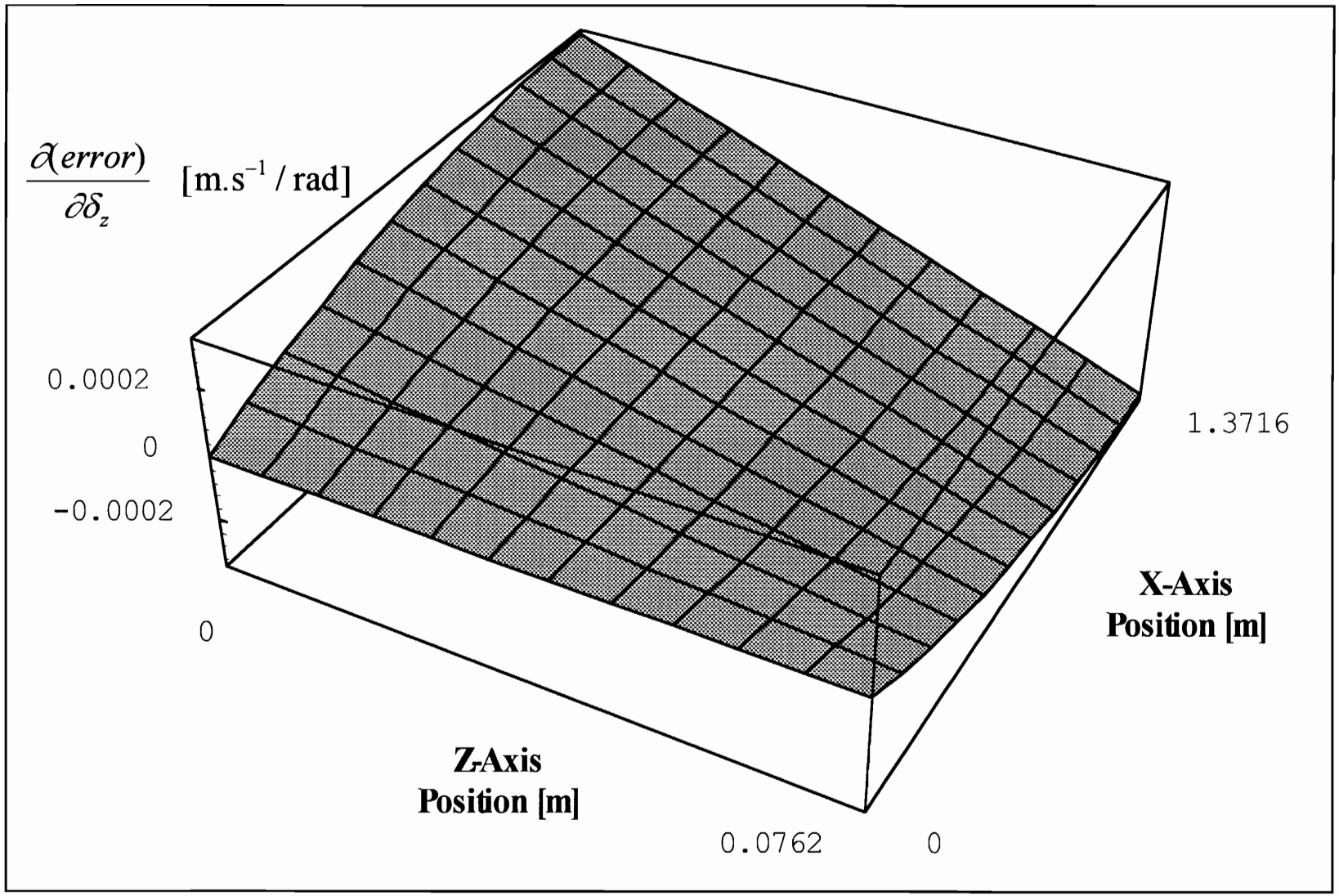

Figure 8.22: Sensitivity of the error function with respect to the spatial orientation variable, δ_z, of the laser

It was found that the error function is more sensitive to changes in the values of δ_x and δ_z for the position and orientation of the laser for the second example problem compared to the first problem. The maximum values of the two test cases are summarized in *Table 8.2*.

Table 8.3 summarize the magnitude of the error due to a 10% change in the maximum total deflection angle of the laser (10% of 0.35 radians), expressed as a percentage of the maximum velocity of the structure (0.00134895 $m.s^{-1}$).

From *Table 8.3* it is clear that the error function were less sensitive to changes in δ_y but more sensitive to changes in δ_x and δ_z for the second example problem compared to the results obtained from the first problem.

Table 8.2: Maximum values of the sensitivities of the error function with respect to changes in the position and orientation of the laser (first and second example problems)

Sensitivity of the error function with respect to:	**First Example Problem Position [$m.s^{-1}/m$] Orientation [$m.s^{-1}/rad$]**	**Second Example Problem Position [$m.s^{-1}/m$] Orientation [$m.s^{-1}/rad$]**
x_{Lo}	0.0015	0.0003
y_{Lo}	0.00025	-0.0015
z_{Lo}	0	0
δ_x	0.004	0.03
δ_y	4E-6	5E-7
δ_z	0.00005	0.0002

Table 8.3: Error expressed as a percentage of the maximum velocity value due to a 10% error in the position and a 0.035 rad error in the orientation of the laser (these values hold for all spatial variables)

Sensitivity of the error function with respect to:	% of maximum velocity Example Problem 1	% of maximum velocity Example Problem 2
x_{Lo}	2.8	51.9
y_{Lo}	7.4	-44.5
z_{Lo}	0	0
δ_x	10.4	77.8
δ_y	0.01	0.001
δ_z	0.13	0.52

8.3.5 Discussion of results on the example problem in terms of the goals

8.3.5.1 Positive aspects

It was possible to find analytical forms for the sensitivity of the error function with respect to all the spatial variables of the laser. The procedure for calculating these sensitivities were also programmed in the mathematical software package Mathematica (Version 2.2). These programs were developed in such a way that it can be used interactively by the user.

8.3.5.2 Negative aspects

The problem is set up for flat elements only. This is not such a big problem as curved surfaces may be modeled by a larger number of smaller elements.

Chapter 9
Summary, Conclusions and Recommendations

A summary of the work with conclusions and recommendations for future work will be given in this chapter.

9.1 Summary of the research

The work covered by this research may be divided into two parts:

1. Calculation of the sensitivity of the ESDM error function with respect to finite element model parameters. Boundary condition model parameters were used as the subject of this study.
2. Calculation of the sensitivity of the error function with respect to the spatial position and orientation of the laser

9.1.1 Sensitivity of the error function with respect to the elastic boundary conditions of the finite element model

A test case where the sensitivity of the error function with respect to elastic boundary conditions were evaluated, was considered. A theoretical beam structure, excited by a transverse harmonic forcing function in the center and subjected to different elastic boundary conditions at each end point, was examined.

The geometry of the structure was modeled mathematically by means of the finite element method. Two models were constructed, one using beam elements and the other using plate elements. The dynamic response of these finite element models was solved by means of a frequency response analysis resulting in a pseudo-dynamic stiffness matrix formulation. This formulation made it possible to use the direct method of differentiation

in order to calculate both the first- and second-order partial derivatives needed to form the required sensitivities.

9.1.2 Sensitivity of the error function with respect to the spatial position and orientation of the laser

The Ray-Patch intersection formulation, together with two coordinate transformations was used to solve the scanning position of the laser beam on the structure in terms of the spatial variables (position and orientation) of the laser. With the scanning position known as a function of the spatial variables of the laser, the error function could be written in terms of the same variables. Using the error function, known in terms of the spatial variables of the laser, the sensitivity of the error function with respect to these spatial variables could be calculated. The general form of the sensitivity of the error function with respect to the spatial variables of the laser was developed. In general, the sensitivity is a function of the representation of the geometry as well as the candidate finite element models and the dynamic response representation.
The sensitivities were successfully evaluated by examining a theoretical cantilevered beam structure with a transverse forcing function at the free end. For this test case, fixed boundary conditions and only one element were used. The solution, given the single element, was shown to be accurate.

9.2 Conclusions regarding the approach in solving the problem

From *Chapter 1*, the goals of the research may be summarized as:

1. *Evaluate the error sensitivity of the ESDM formulation to finite element model parameters*
2. *Evaluate the error sensitivity of the ESDM formulation to the spatial variables of position and orientation of the laser*

Furthermore, the hypothesis statement, may be restated as:

By calculation of the gradients of the error function with respect to model parameters of the finite element model, as well as with respect to the spatial variables of the laser, the influence of these variables on the accuracy of the obtained model may be evaluated.

Both the goals and the hypothesis statement of the research, as stated above, were satisfied. That is, it was possible to obtain the influence of finite element model parameters and the spatial variables of the laser on the ESDM error function, by calculating analytical gradients of the error function with respect to these variables.

The formulations developed were shown to be valid by making use of Taylor-series expansions.

Analytical forms for the sensitivity of the error function with respect to the elastic boundary conditions as well as for the sensitivity of the error function with respect to the spatial position and orientation of the laser could be found. The two different approaches used in each part of the research will now be discussed separately.

9.2.1 Sensitivity of the error function with respect to the elastic boundary conditions of the finite element model

The use of the finite element method was an essential part in finding the required sensitivities of the error function. The method made it possible to:

1. Model a structure with any arbitrary shape, loading and support conditions
2. Use different elements (for example beam and plate elements) in order to create models of different geometrical or response complexity
3. Use a frequency response analysis, yielding a pseudo-dynamic stiffness matrix formulation, for solving the dynamic response of the structure
4. Use the direct method of differentiation for calculation of the first- and second-order derivatives needed to form the required sensitivities

The frequency response analysis used was very effective. Not only could the dynamic response be found without the calculation of any eigenvector or eigenvalue, but the results were very accurate compared to the closed form solution (*Chapter 4*).

The impact of the formulation developed and the results obtained may be summarized as follows:

1. The results may be used to update finite element models
2. The results give insight in how to acquire data - especially with respect to the required noise levels
3. First- and second-order sensitivities could be obtained
4. Exact values of the sensitivities, based on the finite element model used, were obtained
5. The formulation is extendible to other elements
6. The formulation is applicable to damping and/or mass models
7. The formulation allows the calculation of the error sensitivity with respect to other model parameters (e.g. Young's modulus, Moment of inertia, etc.)

9.2.2 Sensitivity of the error function with respect to the spatial position and orientation of the laser

A parametric representation of the three-dimensional geometry and the Ray-Patch intersection formulation were used. This notation made it possible to use the Ray-Patch intersection formulation together with two coordinate transformations in order to write the error function in terms of the spatial variables of the laser. The main advantage of using the parametric notation is the fact that it simplifies the mathematical representation of the three dimensional geometry and the resulting intersection problem greatly.

The derivatives of the error function with respect to the spatial variables were calculated by expanding the function into it's partial derivatives, by means of the chain rule of differentiation. The calculation of these partial derivatives is almost trivial once the error function is known in terms of the spatial variables. All the partial derivatives were calculated by making use of the Mathematica (Version 2.2) software package.

The impact of the formulation developed and the results obtained may be summarized as follows:

1. The results give a better understanding of the impact of the spatial error on the accuracy of the ESDM model

2. The results make it possible to separate the spatial part of the total error
3. The results give a better understanding of the effects of registration of the laser
4. From the formulation developed it is clear that the evaluation of the error sensitivity with respect to the spatial variables of the laser is extremely important for curved surfaces

9.3 Recommendations for future work

This research developed an element of technology within the ESDM framework. As such it is, thus, almost certain that future work will be conducted in the same area. Some suggestions regarding this future work are mentioned in the following paragraphs.

Since this research was the first step in determining the required sensitivities, the work done was purely of a theoretical nature. It is, thus, necessary to expand upon this research by performing experimental work in order to verify the correctness of the theoretical results obtained.

The example problem used for obtaining the sensitivity of the error function with respect to the finite element model parameters made used of a forcing frequency of 0.1 Hz. It is realized that this frequency is low compared to the natural frequencies of the structure and more tests, spanning a wider range of frequencies should be evaluated. The formulation developed for obtaining the sensitivities of the error function with respect to the finite element model parameters is general in nature and should be expanded to include:

1. Damping and mass of the boundary conditions
2. Viscous and structural damping models
3. Error sensitivity with respect to other model parameters (e.g. Young's modulus, Moment of inertia, etc.)

The procedure for the calculation of the sensitivities of the error function with respect to the spatial variables of the laser was developed for flat surfaces only. This

procedure should be expanded to include the representation of generalized curved surfaces. This may be done by representing the arbitrary curvature of the surface by means of B-Splines or a similar geometric modeling approach.

Lastly, all the procedures were developed by making use of the Mathematica (Version 2.2) software package. This software is ideally suited for the development of new procedures, due to the fact that both symbolic notation as well as numerical values may be used. It has, however, the disadvantage of being time consuming when executing large problems. In order to make the procedures more useful, it is strongly recommended that more efficient source code are developed in a scientific programming language like FORTRAN or C. This will be especially useful when applying the procedures to structures with more degrees of freedom. These new source code could easily be verified with the existing Mathematica procedures for smaller systems.

REFERENCES

Arora, J.S. Introduction to Optimum Design. New York: McGraw-Hill, Inc., 1989.

Bartels, I.H., Beatty, J.C., and Barsky, B.A. An Introduction to Splines for Use in Computer Graphics and Geometric Modeling. Los Altos, California: Morgan Kaufmann Publishers, Inc., 1987.

Burden, R.L. and Faires, J.D. Numerical Analysis. 4th ed. Boston: PWS-KENT Publishing Company, 1989.

Clough, R.W. and Penzien, J. Dynamics of Structures. New York: McGraw-Hill, Inc., 1975.

Cook, R.D., Malkus. D.S. and Plesha, M.E. Concepts and Applications of Finite Element Analysis. 3d ed. New York: John Wiley & Sons, Inc., 1989.

Cook, R.D. and Young, W.C. Advanced Mechanics of Materials. New York: Macmillan Publishing Company, 1985.

Ellis, E. and Gulick, D. Calculus with Analytic Geometry. 3d ed. New York: Harcourt Brace Jonanovich, Publishers, 1986.

Glassner, A.S. An Introduction to Ray Tracing. London: Academic Press, 1989.

Haftka, R.T. and Gürdal, Z. Elements of Structural Optimization. 3d ed. Boston: Kluwer Academic Publishers, 1993

Haug, E.J., Choi, K.K. and Komkov, V. Design Sensitivity Analysis of Structural Systems. London: Academic Press, 1986.

Lindholm, B.E. and West, R.L. Determination of Suspension Effects by Direct Experiments and Comparisons to an Analytical Model, accepted by *12th International Modal Analysis Conference,* IMAC-XII, January 31-February 3, 1994, Honolulu, Hawaii, pp. 262-268.

Mathematica Enhanced Version 2.2 for Windows, Champaign, Illinois: Wolfram Research, Inc. 1993.

McCallion, H. Vibration of Linear Mechanical Systems. New York: John Wiley & Sons, 1973.

Meirovitch, L. Elements of Vibration Analysis. 2d ed. New York. McGraw-Hill, Inc., 1986.

Montgomery, D.E. Modeling and Visualization of Laser-Based Three-Dimensional Experimental Spatial Dynamic Response PhD. diss., Blacksburg, VA Virginia Polytechnic Institute and State University, 1994.

Ott, R.L. An Introduction to Statistical Methods and Data Analysis. 4th ed. Belmont, California: Duxbury Press, 1993.

Reddy, J.N. An Introduction to the Finite Element Method. 2d ed. New York. McGraw-Hill, Inc., 1993.

Wolfram, W. Mathematica: A System for Doing Mathematics by Computer. 2d ed. Redwood City, California: Addison-Wesley Publishing Co., 1991.

Zienkiewicz, O.C. and Taylor, R.L. The Finite Element Method. 4th ed. New York. McGraw-Hill, Inc., 1989.

Zill, D.G. Calculus. 3d ed. Boston: PWS-KENT Publishing Company, 1992.

APPENDIX A

MATHEMATICA SUBROUTINES FOR OBTAINING THE SENSITIVITY OF THE ERROR FUNCTION WITH RESPECT TO THE ELASTIC BOUNDARY CONDITIONS OF THE FINITE ELEMENT MODEL USING THE BEAM ELEMENT MODEL WITH THREE DEGREES OF FREEDOM PER NODE

```
(*****************************************************************************)
(*        Package of Mathematica subroutines for obtaining the sensitivity of *)
(*      the error function with respect to the elastic boundary stiffness variables for *)
(*    the modified beam element with three degrees of freedom per node, used in the research *)
(*                                                                           *)
(*                          DEVELOPED BY:  Gerhardus Venter                  *)
(*                                         1994 - 1995                       *)
(*                                         Copyright © 1995                  *)
(*                                                                           *)
(*****************************************************************************)
(*  SUBROUTINES:                                                             *)
(*****************************************************************************)
(*        AssembleMatrix          Subroutine to assemble element matrices into the global *)
(*                                matrix consistent with the direct method   *)
(*                                                                           *)
(*        Input/Output Variables  Description                                *)
(*        dof                     Degrees of freedom in the global matrix    *)
(*        ke                      Element matrix                             *)
(*        kg                      Global matrix                              *)
(*****************************************************************************)
(*        MassMatrixBeam          Subroutine yielding the mass matrix of the modified beam*)
(*                                element used with three degrees of freedom per node *)
(*                                                                           *)
(*        Input/Output Variables  Description                                *)
(*        rho                     Mass density of the material               *)
(*        a                       Cross sectional area of the element        *)
(*        l                       Length of the element                      *)
(*****************************************************************************)
(*        BoundaryStiffnessBeam   Subroutine yielding the boundary condition model *)
(*                                consisting of the elastic boundary conditions *)
(*                                                                           *)
(*        Input/Output Variables  Description                                *)
(*        Ka                      Axial stiffness of the boundary            *)
(*        Kt                      Tangential stiffness of the boundary       *)
(*        Kr                      Rotational stiffness of the boundary       *)
(*****************************************************************************)
(*        StiffnessMatrixBeam     Subroutine yielding the element stiffness matrix for the *)
(*                                modified beam element used with three degrees of freedom *)
(*                                per node                                   *)
(*                                                                           *)
(*        Input/Output Variables  Description                                *)
(*        e                       Young's Modulus of the material            *)
(*        i                       Moment of inertia about bending axis       *)
(*        a                       Cross sectional area of the element        *)
(*        l                       Length of the element                      *)
(*****************************************************************************)
(*        DynamicStiffnessBeam    Subroutine yielding the pseudo-dynamic stiffness matrix *)
(*                                for the structure from the global stiffness, mass and *)
(*                                damping matrices                           *)
(*                                                                           *)
```

```
(*          Input/Output Variables      Description                                  *)
(*          StiffnessMatrixBeam         Global stiffness matrix of the beam          *)
(*          MassMatrixBeam              Global mass matrix of the beam               *)
(*          DampingMatrixBeam           Global damping matrix of the beam            *)
(*          w                           Forcing frequency                            *)
(*****************************************************************************)

AssembleMatrix[dof_, ke_, kg_ ] :=  Module[{i, j, kgp = kg, le = Length[ke]},
Table[ kgp[[ dof[[i]],dof[[j]] ]] += ke[[i,j]], {i, 1, le}, {j, 1, le} ];
kgp     ]

MassMatrixBeam[rho_, a_, l_] :=
        rho*a*l*{  {1/2,  0,  0,  0,  0,  0},
                   {0,  1/2,  0,  0,  0,  0},
                   {0,  0,  0,  0,  0,  0},
                   {0,  0,  0,  1/2,  0,  0},
                   {0,  0,  0,  0,  1/2,  0},
                   {0,  0,  0,  0,  0,  0}}

BoundaryStiffnessBeam[Ka_,Kt_,Kr_] :=
        {{Ka,  0,  0},
         {0,  Kt,  0},
         {0,  0,  Kr}}

StiffnessMatrixBeam[e_, i_, a_, l_] :=
        (e*i*   {{a*l^2/i,  0,  0,  -a*l^2/i,  0,  0},
                 {0,  12,  6*l,  0,  -12,  6*l},
                 {0,  6*l,  4*l^2,  0,  -6*l,  2*l^2},
                 {-a*l^2/i,  0,  0,  a*l^2/i,  0,  0},
                 {0,  -12,  -6*l,  0,  12,  -6*l},
                 {0,  6*l,  2*l^2,  0,  -6*l,  4*l^2}}    )/l^3

DynamicStiffnessBeam[
StiffnessMatrixBeam_List, MassMatrixBeam_List,DampingMatrixBeam_List, w_] :=
StiffnessMatrixBeam - w^2*MassMatrixBeam + (w*DampingMatrixBeam) I
```

APPENDIX B

MATHEMATICA SUBROUTINES FOR OBTAINING THE SENSITIVITY OF THE ERROR FUNCTION WITH RESPECT TO THE ELASTIC BOUNDARY CONDITIONS OF THE FINITE ELEMENT MODEL USING THE PLATE ELEMENT MODEL WITH TWENTY DEGREES OF FREEDOM PER NODE

```
(*************************************************************************************)
(*        Package of Mathematica subroutines for obtaining the sensitivity of        *)
(*      the error function with respect to the elastic boundary stiffness variables for *)
(*   the modified plate element with twenty degrees of freedom per node, used in the research *)
(*                                                                                   *)
(*                          DEVELOPED BY:  Gerhardus Venter                          *)
(*                                  1994 - 1995                                      *)
(*                                Copyright © 1995                                   *)
(*                                                                                   *)
(*************************************************************************************)
(*  SUBROUTINES:                                                                     *)
(*************************************************************************************)
(*        AssembleMatrix          Subroutine to assemble element matrices into the global *)
(*                                matrix consistent with the direct method           *)
(*                                                                                   *)
(*        Input/Output Variables  Description                                        *)
(*        dof                     Degrees of freedom in the global matrix            *)
(*        ke                      Element matrix                                     *)
(*        kg                      Global matrix                                      *)
(*************************************************************************************)
(*        PlateBoundaryStiff      Subroutine yielding the boundary condition model   *)
(*                                consisting of the elastic boundary conditions      *)
(*                                                                                   *)
(*        Input/Output Variables  Description                                        *)
(*        Kt                      Tangential boundary stiffness                      *)
(*        Kl                      Longitudinal boundary stiffness                    *)
(*        Kr                      Rotational boundary stiffness                      *)
(*************************************************************************************)
(*        MassMatrixPlate         Subroutine yielding the consistent mass matrix for the *)
(*                                modified plate element with twenty degrees of freedom *)
(*                                per node                                           *)
(*                                                                                   *)
(*        Input/Output Variables  Description                                        *)
(*        r                       Mass density of the material used                  *)
(*        a                       Element length in the x-direction                  *)
(*        b                       Element length in the y-direction                  *)
(*        t                       Thickness of the element                           *)
(*************************************************************************************)
(*        StiffnessMatrixPlate    Subroutine yielding the element stiffness matrix for the *)
(*                                modified plate  element used with twenty degrees of *)
(*                                freedom per node                                   *)
(*                                                                                   *)
(*        Input/Output Variables  Description                                        *)
(*        l                       Length of the element                              *)
(*        v                       Poisson's ratio                                    *)
(*        a                       Element length in the x-direction                  *)
(*        b                       Element length in the y-direction                  *)
(*        e                       Young's Modulus of the material                    *)
(*        t                       Thickness of the element                           *)
(*************************************************************************************)
(*        DynamicStiffnessPlate   Subroutine yielding the pseudo-dynamic stiffness matrix *)
(*                                for the structure from the global stiffness, mass and *)
(*                                damping matrices                                   *)
```

```
(*                                                                                *)
(*        Input/Output Variables      Description                                 *)
(*        StiffnessMatrixPlate        Global stiffness matrix of the plate        *)
(*        MassMatrixPlate             Global mass matrix of the plate             *)
(*        DampingMatrixPlate          Global damping matrix of the plate          *)
(*        w                           Forcing frequency                           *)
(**********************************************************************************)

AssembleMatrix[dof_, ke_, kg_ ] :=
Module[{i, j, kgp = kg, le = Length[ke]},
Table[ kgp[[ dof[[i]],dof[[j]] ]] += ke[[i,j]], {i, 1, le}, {j, 1, le} ];
kgp     ]

PlateBoundaryStiff[Kt_,Kl_,Kr_] :=
    {   {Kt, 0 , 0 , 0 , 0 , 0 , 0 , 0 , 0 , 0 },
        {0 , Kl, 0 , 0 , 0 , 0 , 0 , 0 , 0 , 0 },
        {0 , 0 , Kl, 0 , 0 , 0 , 0 , 0 , 0 , 0 },
        {0 , 0 , 0 , 0 , 0 , 0 , 0 , 0 , 0 , 0 },
        {0 , 0 , 0 , 0 , Kr, 0 , 0 , 0 , 0 , 0 },
        {0 , 0 , 0 , 0 , 0 , Kt, 0 , 0 , 0 , 0 },
        {0 , 0 , 0 , 0 , 0 , 0 , Kl, 0 , 0 , 0 },
        {0 , 0 , 0 , 0 , 0 , 0 , 0 , Kl, 0 , 0 },
        {0 , 0 , 0 , 0 , 0 , 0 , 0 , 0 , 0 , 0 },
        {0 , 0 , 0 , 0 , 0 , 0 , 0 , 0 , 0 , Kr}}

MassMatrixPlate[r_,a_,b_,t_] :=
{{(1727*a*b*r*t)/12600, 0, 0, (461*a*b^2*r*t)/25200, (-461*a^2*b*r*t)/25200, (613*a*b*r*t)/12600, 0,
        0, (-137*a*b^2*r*t)/12600, (-199*a^2*b*r*t)/25200, (197*a*b*r*t)/12600, 0, 0,
        (-29*a*b^2*r*t)/6300, (29*a^2*b*r*t)/6300, (613*a*b*r*t)/12600, 0, 0,
        (199*a*b^2*r*t)/25200, (137*a^2*b*r*t)/12600},
{0, (a*b*r*t)/9, 0, 0, 0, 0, (a*b*r*t)/18, 0, 0, 0, 0, (a*b*r*t)/36, 0, 0, 0, 0, (a*b*r*t)/18, 0, 0, 0},
{0, 0, (a*b*r*t)/9, 0, 0, 0, 0, (a*b*r*t)/18, 0, 0, 0, 0, (a*b*r*t)/36, 0, 0, 0, 0, (a*b*r*t)/18, 0, 0},
{(461*a*b^2*r*t)/25200, 0, 0, (a*b^3*r*t)/315, -(a^2*b^2*r*t)/400, (137*a*b^2*r*t)/12600, 0, 0,
        -(a*b^3*r*t)/420, -(a^2*b^2*r*t)/600, (29*a*b^2*r*t)/6300, 0, 0, -(a*b^3*r*t)/840,
        a^2*b^2*r*t)/900, (199*a*b^2*r*t)/25200, 0, 0, (a*b^3*r*t)/630, (a^2*b^2*r*t)/600},
{(-461*a^2*b*r*t)/25200, 0, 0, -(a^2*b^2*r*t)/400, (a^3*b*r*t)/315, (-199*a^2*b*r*t)/25200, 0, 0,
        (a^2*b^2*r*t)/600, (a^3*b*r*t)/630, (-29*a^2*b*r*t)/6300, 0, 0, (a^2*b^2*r*t)/900,
        -(a^3*b*r*t)/840, (-137*a^2*b*r*t)/12600, 0, 0, -(a^2*b^2*r*t)/600, -(a^3*b*r*t)/420},
{(613*a*b*r*t)/12600, 0, 0, (137*a*b^2*r*t)/12600, (-199*a^2*b*r*t)/25200, (1727*a*b*r*t)/12600, 0,
        0, (-461*a*b^2*r*t)/25200, (-461*a^2*b*r*t)/25200, (613*a*b*r*t)/12600, 0, 0,
        (-199*a*b^2*r*t)/25200, (137*a^2*b*r*t)/12600, (197*a*b*r*t)/12600, 0, 0,
        (29*a*b^2*r*t)/6300, (29*a^2*b*r*t)/6300},
{0, (a*b*r*t)/18, 0, 0, 0, 0, (a*b*r*t)/9, 0, 0, 0, 0, (a*b*r*t)/18, 0, 0, 0, 0, (a*b*r*t)/36, 0, 0, 0},
{0, 0, (a*b*r*t)/18, 0, 0, 0, 0, (a*b*r*t)/9, 0, 0, 0, 0, (a*b*r*t)/18, 0, 0, 0, 0, (a*b*r*t)/36, 0, 0},
{(-137*a*b^2*r*t)/12600, 0, 0, -(a*b^3*r*t)/420, (a^2*b^2*r*t)/600, (-461*a*b^2*r*t)/25200, 0, 0,
        (a*b^3*r*t)/315, (a^2*b^2*r*t)/400, (-199*a*b^2*r*t)/25200, 0, 0, (a*b^3*r*t)/630,
        -(a^2*b^2*r*t)/600, (-29*a*b^2*r*t)/6300, 0, 0, -(a*b^3*r*t)/840, -(a^2*b^2*r*t)/900},
{(-199*a^2*b*r*t)/25200, 0, 0, -(a^2*b^2*r*t)/600, (a^3*b*r*t)/630, (-461*a^2*b*r*t)/25200, 0, 0,
        (a^2*b^2*r*t)/400, (a^3*b*r*t)/315, (-137*a^2*b*r*t)/12600, 0, 0, (a^2*b^2*r*t)/600,
        -(a^3*b*r*t)/420, (-29*a^2*b*r*t)/6300, 0, 0, -(a^2*b^2*r*t)/900, -(a^3*b*r*t)/840},
```

```
{(197*a*b*r*t)/12600, 0, 0, (29*a*b^2*r*t)/6300, (-29*a^2*b*r*t)/6300, (613*a*b*r*t)/12600, 0, 0,
        (-199*a*b^2*r*t)/25200, (-137*a^2*b*r*t)/12600, (1727*a*b*r*t)/12600, 0, 0,
        (-461*a*b^2*r*t)/25200, (461*a^2*b*r*t)/25200, (613*a*b*r*t)/12600, 0,  0,
        (137*a*b^2*r*t)/12600, (199*a^2*b*r*t)/25200},
{0, (a*b*r*t)/36, 0, 0, 0, 0, (a*b*r*t)/18, 0, 0, 0, 0, (a*b*r*t)/9, 0, 0, 0, 0, (a*b*r*t)/18, 0, 0, 0},
{0, 0, (a*b*r*t)/36, 0, 0, 0, 0, (a*b*r*t)/18, 0, 0, 0, 0, (a*b*r*t)/9, 0, 0, 0, 0, (a*b*r*t)/18, 0, 0},
{(-29*a*b^2*r*t)/6300, 0, 0, -(a*b^3*r*t)/840, (a^2*b^2*r*t)/900, (-199*a*b^2*r*t)/25200, 0, 0,
        (a*b^3*r*t)/630, (a^2*b^2*r*t)/600, (-461*a*b^2*r*t)/25200, 0, 0, (a*b^3*r*t)/315,
        -(a^2*b^2*r*t)/400, (-137*a*b^2*r*t)/12600, 0, 0, -(a*b^3*r*t)/420, -(a^2*b^2*r*t)/600},
{(29*a^2*b*r*t)/6300, 0, 0, (a^2*b^2*r*t)/900, -(a^3*b*r*t)/840, (137*a^2*b*r*t)/12600, 0, 0,
        -(a^2*b^2*r*t)/600, -(a^3*b*r*t)/420, (461*a^2*b*r*t)/25200, 0, 0, -(a^2*b^2*r*t)/400,
        (a^3*b*r*t)/315, (199*a^2*b*r*t)/25200, 0, 0, (a^2*b^2*r*t)/600, (a^3*b*r*t)/630},
{(613*a*b*r*t)/12600, 0, 0, (199*a*b^2*r*t)/25200, (-137*a^2*b*r*t)/12600, (197*a*b*r*t)/12600, 0, 0,
        (-29*a*b^2*r*t)/6300, (-29*a^2*b*r*t)/6300, (613*a*b*r*t)/12600, 0, 0,
        (-137*a*b^2*r*t)/12600, (199*a^2*b*r*t)/25200, (1727*a*b*r*t)/12600, 0, 0,
        (461*a*b^2*r*t)/25200, (461*a^2*b*r*t)/25200},
{0, (a*b*r*t)/18, 0, 0, 0, 0, (a*b*r*t)/36, 0, 0, 0, 0, (a*b*r*t)/18, 0, 0, 0, 0, (a*b*r*t)/9, 0, 0, 0},
{0, 0, (a*b*r*t)/18, 0, 0, 0, 0, (a*b*r*t)/36, 0, 0, 0, 0, (a*b*r*t)/18, 0, 0, 0, 0, (a*b*r*t)/9, 0, 0},
{(199*a*b^2*r*t)/25200, 0, 0, (a*b^3*r*t)/630, -(a^2*b^2*r*t)/600, (29*a*b^2*r*t)/6300, 0, 0,
         -(a*b^3*r*t)/840, -(a^2*b^2*r*t)/900, (137*a*b^2*r*t)/12600, 0, 0, -(a*b^3*r*t)/420,
        (a^2*b^2*r*t)/600,  (461*a*b^2*r*t)/25200, 0, 0, (a*b^3*r*t)/315, (a^2*b^2*r*t)/400},
{(137*a^2*b*r*t)/12600, 0, 0, (a^2*b^2*r*t)/600, -(a^3*b*r*t)/420, (29*a^2*b*r*t)/6300, 0, 0,
        -(a^2*b^2*r*t)/900, -(a^3*b*r*t)/840, (199*a^2*b*r*t)/25200, 0, 0, -(a^2*b^2*r*t)/600,
        (a^3*b*r*t)/630, (461*a^2*b*r*t)/25200, 0, 0, (a^2*b^2*r*t)/400, (a^3*b*r*t)/315}}

StiffnessMatrixPlate[l_,v_,a_,b_,e_,t_] :=
{{(e*t^3*(4*(l^(-2) + l^2) + (14 - 4*v)/5))/(12*a*b*(1 - v^2)), 0, 0,
        (e*t^3*(2/l^2 + (1 + 4*v)/5))/(12*a*(1 - v^2)),
        -(e*t^3*(2*l^2 + (1 + 4*v)/5))/(12*b*(1 - v^2)),
        (e*t^3*(2*(-2/l^2 + l^2) + (-14 + 4*v)/5))/(12*a*b*(1 - v^2)), 0, 0,
        (e*t^3*(2/l^2 + (1 - v)/5))/(12*a*(1 - v^2)),
        (e*t^3*(-l^2 + (1 + 4*v)/5))/(12*b*(1 - v^2)),
        (e*t^3*(-2*(l^(-2) + l^2) + (14 - 4*v)/5))/(12*a*b*(1 - v^2)), 0, 0,
        (e*t^3*(l^(-2) + (-1 + v)/5))/(12*a*(1 - v^2)),
        (e*t^3*(-l^2 + (1 - v)/5))/(12*b*(1 - v^2)),
        (e*t^3*(-2*(-l^(-2) + 2*l^2) + (-14 + 4*v)/5))/(12*a*b*(1 - v^2)), 0, 0,
        (e*t^3*(l^(-2) + (-1 - 4*v)/5))/(12*a*(1 - v^2)),
        -(e*t^3*(2*l^2 + (1 - v)/5))/(12*b*(1 - v^2))},
{0, (e*t*(-a^2 - 2*b^2 + a^2*v))/(-6*a*b + 6*a*b*v^2), (e*t)/(8*(1 - v)),
        0, 0, 0, (e*t*(-a^2 + b^2 + a^2*v))/(6*a*b - 6*a*b*v^2),
        (e*t*(-1 + 3*v))/(8*(-1 + v^2)), 0, 0, 0,
        (e*t*(-a^2 - 2*b^2 + a^2*v))/(12*a*b - 12*a*b*v^2), (e*t)/(8*(-1 + v)),
        0, 0, 0, (e*t*(-a^2 + 4*b^2 + a^2*v))/(-12*a*b + 12*a*b*v^2),
        (e*t*(1 - 3*v))/(8*(-1 + v^2)), 0, 0},
{0, (e*t)/(8*(1 - v)), (e*t*(-2*a^2 - b^2 + b^2*v))/(-6*a*b + 6*a*b*v^2),
        0, 0, 0, (e*t*(1 - 3*v))/(8*(-1 + v^2)),
        (e*t*(4*a^2 - b^2 + b^2*v))/(-12*a*b + 12*a*b*v^2), 0, 0, 0,
        (e*t)/(8*(-1 + v)), (e*t*(-2*a^2 - b^2 + b^2*v))/(12*a*b - 12*a*b*v^2),
        0, 0, 0, (e*t*(-1 + 3*v))/(8*(-1 + v^2)),
        (e*t*(a^2 - b^2 + b^2*v))/(6*a*b - 6*a*b*v^2), 0, 0},
```

```
{(e*t^3*(2/l^2 + (1 + 4*v)/5))/(12*a*(1 - v^2)), 0, 0,
        (b*e*t^3*(4/(3*l^2) + (4*(1 - v))/15))/(12*a*(1 - v^2)),
        -(e*t^3*v)/(12*(1 - v^2)),
        -(e*t^3*(2/l^2 + (1 - v)/5))/(12*a*(1 - v^2)), 0, 0,
        (b*e*t^3*(2/(3*l^2) + (-1 + v)/15))/(12*a*(1 - v^2)), 0,
        (e*t^3*(-l^(-2) + (1 - v)/5))/(12*a*(1 - v^2)), 0, 0,
        (b*e*t^3*(1/(3*l^2) + (1 - v)/15))/(12*a*(1 - v^2)), 0,
        (e*t^3*(l^(-2) + (-1 - 4*v)/5))/(12*a*(1 - v^2)), 0, 0,
        (b*e*t^3*(2/(3*l^2) - (4*(1 - v))/15))/(12*a*(1 - v^2)), 0},
{-(e*t^3*(2*l^2 + (1 + 4*v)/5))/(12*b*(1 - v^2)), 0, 0,
        -(e*t^3*v)/(12*(1 - v^2)),
        (a*e*t^3*((4*l^2)/3 + (4*(1 - v))/15))/(12*b*(1 - v^2)),
        (e*t^3*(-l^2 + (1 + 4*v)/5))/(12*b*(1 - v^2)), 0, 0, 0,
        (a*e*t^3*((2*l^2)/3 - (4*(1 - v))/15))/(12*b*(1 - v^2)),
        (e*t^3*(l^2 + (-1 + v)/5))/(12*b*(1 - v^2)), 0, 0, 0,
        (a*e*t^3*(l^2/3 + (1 - v)/15))/(12*b*(1 - v^2)),
        (e*t^3*(2*l^2 + (1 - v)/5))/(12*b*(1 - v^2)), 0, 0, 0,
        (a*e*t^3*((2*l^2)/3 + (-1 + v)/15))/(12*b*(1 - v^2))},
{(e*t^3*(2*(-2/l^2 + l^2) + (-14 + 4*v)/5))/(12*a*b*(1 - v^2)), 0, 0,
        -(e*t^3*(2/l^2 + (1 - v)/5))/(12*a*(1 - v^2)),
        (e*t^3*(-l^2 + (1 + 4*v)/5))/(12*b*(1 - v^2)),
        (e*t^3*(4*(l^(-2) + l^2) + (14 - 4*v)/5))/(12*a*b*(1 - v^2)), 0, 0,
        -(e*t^3*(2/l^2 + (1 + 4*v)/5))/(12*a*(1 - v^2)),
        -(e*t^3*(2*l^2 + (1 + 4*v)/5))/(12*b*(1 - v^2)),
        (e*t^3*(-2*(-l^(-2) + 2*l^2) + (-14 + 4*v)/5))/(12*a*b*(1 - v^2)), 0, 0,
        (e*t^3*(-l^(-2) + (1 + 4*v)/5))/(12*a*(1 - v^2)),
        -(e*t^3*(2*l^2 + (1 - v)/5))/(12*b*(1 - v^2)),
        (e*t^3*(-2*(l^(-2) + l^2) + (14 - 4*v)/5))/(12*a*b*(1 - v^2)), 0, 0,
        (e*t^3*(-l^(-2) + (1 - v)/5))/(12*a*(1 - v^2)),
        (e*t^3*(-l^2 + (1 - v)/5))/(12*b*(1 - v^2))},
{0, (e*t*(-a^2 + b^2 + a^2*v))/(6*a*b - 6*a*b*v^2),
        (e*t*(1 - 3*v))/(8*(-1 + v^2)), 0, 0, 0,
        (e*t*(-a^2 - 2*b^2 + a^2*v))/(-6*a*b + 6*a*b*v^2), (e*t)/(8*(-1 + v)),
        0, 0, 0, (e*t*(-a^2 + 4*b^2 + a^2*v))/(-12*a*b + 12*a*b*v^2),
        (e*t*(-1 + 3*v))/(8*(-1 + v^2)), 0, 0, 0,
        (e*t*(-a^2 - 2*b^2 + a^2*v))/(12*a*b - 12*a*b*v^2), (e*t)/(8*(1 - v)), 0, 0},
{0, (e*t*(-1 + 3*v))/(8*(-1 + v^2)),
        (e*t*(4*a^2 - b^2 + b^2*v))/(-12*a*b + 12*a*b*v^2), 0, 0, 0,
        (e*t)/(8*(-1 + v)), (e*t*(-2*a^2 - b^2 + b^2*v))/(-6*a*b + 6*a*b*v^2),
        0, 0, 0, (e*t*(1 - 3*v))/(8*(-1 + v^2)),
        (e*t*(a^2 - b^2 + b^2*v))/(6*a*b - 6*a*b*v^2), 0, 0, 0,
        (e*t)/(8*(1 - v)), (e*t*(-2*a^2 - b^2 + b^2*v))/(12*a*b - 12*a*b*v^2), 0, 0},
{(e*t^3*(2/l^2 + (1 - v)/5))/(12*a*(1 - v^2)), 0, 0,
        (b*e*t^3*(2/(3*l^2) + (-1 + v)/15))/(12*a*(1 - v^2)), 0,
        (e*t^3*v)/(12*(1 - v^2)), (e*t^3*(-l^(-2) + (1 + 4*v)/5))/
        (12*a*(1 - v^2)), 0, 0, (b*e*t^3*(2/(3*l^2) - (4*(1 - v))/15))/
        (12*a*(1 - v^2)), 0, (e*t^3*(l^(-2) + (-1 + v)/5))/(12*a*(1 - v^2)), 0,
        0, (b*e*t^3*(1/(3*l^2) + (1 - v)/15))/(12*a*(1 - v^2)), 0},
```

```
{(e*t^3*(-l^2 + (1 + 4*v)/5))/(12*b*(1 - v^2)), 0, 0, 0,
        (a*e*t^3*((2*l^2)/3 - (4*(1 - v))/15))/(12*b*(1 - v^2)),
        -(e*t^3*(2*l^2 + (1 + 4*v)/5))/(12*b*(1 - v^2)), 0, 0,
        (e*t^3*v)/(12*(1 - v^2)), (a*e*t^3*((4*l^2)/3 + (4*(1 - v))/15))/
        (12*b*(1 - v^2)), (e*t^3*(2*l^2 + (1 - v)/5))/(12*b*(1 - v^2)), 0, 0,
        0, (a*e*t^3*((2*l^2)/3 + (-1 + v)/15))/(12*b*(1 - v^2)),
        (e*t^3*(l^2 + (-1 + v)/5))/(12*b*(1 - v^2)), 0, 0, 0,
        (a*e*t^3*(l^2/3 + (1 - v)/15))/(12*b*(1 - v^2))},
{(e*t^3*(-2*(l^(-2) + l^2) + (14 - 4*v)/5))/(12*a*b*(1 - v^2)), 0, 0,
        (e*t^3*(-l^(-2) + (1 - v)/5))/(12*a*(1 - v^2)),
        (e*t^3*(l^2 + (-1 + v)/5))/(12*b*(1 - v^2)),
        (e*t^3*(-2*(-l^(-2) + 2*l^2) + (-14 + 4*v)/5))/(12*a*b*(1 - v^2)), 0, 0,
        (e*t^3*(-l^(-2) + (1 + 4*v)/5))/(12*a*(1 - v^2)),
        (e*t^3*(2*l^2 + (1 - v)/5))/(12*b*(1 - v^2)),
        (e*t^3*(4*(l^(-2) + l^2) + (14 - 4*v)/5))/(12*a*b*(1 - v^2)), 0, 0,
        -(e*t^3*(2/l^2 + (1 + 4*v)/5))/(12*a*(1 - v^2)),
        (e*t^3*(2*l^2 + (1 + 4*v)/5))/(12*b*(1 - v^2)),
        (e*t^3*(2*(-2/l^2 + l^2) + (-14 + 4*v)/5))/(12*a*b*(1 - v^2)), 0, 0,
        -(e*t^3*(2/l^2 + (1 - v)/5))/(12*a*(1 - v^2)),
        (e*t^3*(l^2 + (-1 - 4*v)/5))/(12*b*(1 - v^2))},
{0, (e*t*(-a^2 - 2*b^2 + a^2*v))/(12*a*b - 12*a*b*v^2),
        (e*t)/(8*(-1 + v)), 0, 0, 0,
        (e*t*(-a^2 + 4*b^2 + a^2*v))/(-12*a*b + 12*a*b*v^2),
        (e*t*(1 - 3*v))/(8*(-1 + v^2)), 0, 0, 0,
        (e*t*(-a^2 - 2*b^2 + a^2*v))/(-6*a*b + 6*a*b*v^2), (e*t)/(8*(1 - v)), 0,
        0, 0, (e*t*(-a^2 + b^2 + a^2*v))/(6*a*b - 6*a*b*v^2),
        (e*t*(-1 + 3*v))/(8*(-1 + v^2)), 0, 0},
{0, (e*t)/(8*(-1 + v)), (e*t*(-2*a^2 - b^2 + b^2*v))/
        (12*a*b - 12*a*b*v^2), 0, 0, 0, (e*t*(-1 + 3*v))/(8*(-1 + v^2)),
        (e*t*(a^2 - b^2 + b^2*v))/(6*a*b - 6*a*b*v^2), 0, 0, 0,
        (e*t)/(8*(1 - v)), (e*t*(-2*a^2 - b^2 + b^2*v))/(-6*a*b + 6*a*b*v^2), 0,
        0, 0, (e*t*(1 - 3*v))/(8*(-1 + v^2)),
        (e*t*(4*a^2 - b^2 + b^2*v))/(-12*a*b + 12*a*b*v^2), 0, 0},
{(e*t^3*(l^(-2) + (-1 + v)/5))/(12*a*(1 - v^2)), 0, 0,
        (b*e*t^3*(1/(3*l^2) + (1 - v)/15))/(12*a*(1 - v^2)), 0,
        (e*t^3*(-l^(-2) + (1 + 4*v)/5))/(12*a*(1 - v^2)), 0, 0,
        (b*e*t^3*(2/(3*l^2) - (4*(1 - v))/15))/(12*a*(1 - v^2)), 0,
        -(e*t^3*(2/l^2 + (1 + 4*v)/5))/(12*a*(1 - v^2)), 0, 0,
        (b*e*t^3*(4/(3*l^2) + (4*(1 - v))/15))/(12*a*(1 - v^2)),
        -(e*t^3*v)/(12*(1 - v^2)), (e*t^3*(2/l^2 + (1 - v)/5))/(12*a*(1 - v^2)),
        0, 0, (b*e*t^3*(2/(3*l^2) + (-1 + v)/15))/(12*a*(1 - v^2)), 0},
{(e*t^3*(-l^2 + (1 - v)/5))/(12*b*(1 - v^2)), 0, 0, 0,
        (a*e*t^3*(l^2/3 + (1 - v)/15))/(12*b*(1 - v^2)),
        -(e*t^3*(2*l^2 + (1 - v)/5))/(12*b*(1 - v^2)), 0, 0, 0,
        (a*e*t^3*((2*l^2)/3 + (-1 + v)/15))/(12*b*(1 - v^2)),
        (e*t^3*(2*l^2 + (1 + 4*v)/5))/(12*b*(1 - v^2)), 0, 0,
        -(e*t^3*v)/(12*(1 - v^2)),
        (a*e*t^3*((4*l^2)/3 + (4*(1 - v))/15))/(12*b*(1 - v^2)),
        (e*t^3*(l^2 + (-1 - 4*v)/5))/(12*b*(1 - v^2)), 0, 0, 0,
        (a*e*t^3*((2*l^2)/3 - (4*(1 - v))/15))/(12*b*(1 - v^2))},
```

```
{(e*t^3*(-2*(-l^(-2) + 2*l^2) + (-14 + 4*v)/5))/(12*a*b*(1 - v^2)), 0, 0,
        (e*t^3*(l^(-2) + (-1 - 4*v)/5))/(12*a*(1 - v^2)),
        (e*t^3*(2*l^2 + (1 - v)/5))/(12*b*(1 - v^2)),
        (e*t^3*(-2*(l^(-2) + l^2) + (14 - 4*v)/5))/(12*a*b*(1 - v^2)), 0, 0,
        (e*t^3*(l^(-2) + (-1 + v)/5))/(12*a*(1 - v^2)),
        (e*t^3*(l^2 + (-1 + v)/5))/(12*b*(1 - v^2)),
        (e*t^3*(2*(-2/l^2 + l^2) + (-14 + 4*v)/5))/(12*a*b*(1 - v^2)), 0, 0,
        (e*t^3*(2/l^2 + (1 - v)/5))/(12*a*(1 - v^2)),
        (e*t^3*(l^2 + (-1 - 4*v)/5))/(12*b*(1 - v^2)),
        (e*t^3*(4*(l^(-2) + l^2) + (14 - 4*v)/5))/(12*a*b*(1 - v^2)), 0, 0,
        (e*t^3*(2/l^2 + (1 + 4*v)/5))/(12*a*(1 - v^2)),
        (e*t^3*(2*l^2 + (1 + 4*v)/5))/(12*b*(1 - v^2))},
{0, (e*t*(-a^2 + 4*b^2 + a^2*v))/(-12*a*b + 12*a*b*v^2),
        (e*t*(-1 + 3*v))/(8*(-1 + v^2)), 0, 0, 0,
        (e*t*(-a^2 - 2*b^2 + a^2*v))/(12*a*b - 12*a*b*v^2), (e*t)/(8*(1 - v)),
        0, 0, 0, (e*t*(-a^2 + b^2 + a^2*v))/(6*a*b - 6*a*b*v^2),
        (e*t*(1 - 3*v))/(8*(-1 + v^2)), 0, 0, 0,
        (e*t*(-a^2 - 2*b^2 + a^2*v))/(-6*a*b + 6*a*b*v^2), (e*t)/(8*(-1 + v)), 0, 0},
{0, (e*t*(1 - 3*v))/(8*(-1 + v^2)),
        (e*t*(a^2 - b^2 + b^2*v))/(6*a*b - 6*a*b*v^2), 0, 0, 0,
        (e*t)/(8*(1 - v)), (e*t*(-2*a^2 - b^2 + b^2*v))/(12*a*b - 12*a*b*v^2),
        0, 0, 0, (e*t*(-1 + 3*v))/(8*(-1 + v^2)),
        (e*t*(4*a^2 - b^2 + b^2*v))/(-12*a*b + 12*a*b*v^2), 0, 0, 0,
        (e*t)/(8*(-1 + v)), (e*t*(-2*a^2 - b^2 + b^2*v))/(-6*a*b + 6*a*b*v^2), 0, 0},
{(e*t^3*(l^(-2) + (-1 - 4*v)/5))/(12*a*(1 - v^2)), 0, 0,
        (b*e*t^3*(2/(3*l^2) - (4*(1 - v))/15))/(12*a*(1 - v^2)), 0,
        (e*t^3*(-l^(-2) + (1 - v)/5))/(12*a*(1 - v^2)), 0, 0,
        (b*e*t^3*(1/(3*l^2) + (1 - v)/15))/(12*a*(1 - v^2)), 0,
        -(e*t^3*(2/l^2 + (1 - v)/5))/(12*a*(1 - v^2)), 0, 0,
        (b*e*t^3*(2/(3*l^2) + (-1 + v)/15))/(12*a*(1 - v^2)), 0,
        (e*t^3*(2/l^2 + (1 + 4*v)/5))/(12*a*(1 - v^2)), 0, 0,
        (b*e*t^3*(4/(3*l^2) + (4*(1 - v))/15))/(12*a*(1 - v^2)),
        (e*t^3*v)/(12*(1 - v^2))},
{-(e*t^3*(2*l^2 + (1 - v)/5))/
        (12*b*(1 - v^2)), 0, 0, 0,
        (a*e*t^3*((2*l^2)/3 + (-1 + v)/15))/(12*b*(1 - v^2)),
        (e*t^3*(-l^2 + (1 - v)/5))/(12*b*(1 - v^2)), 0, 0, 0,
        (a*e*t^3*(l^2/3 + (1 - v)/15))/(12*b*(1 - v^2)),
        (e*t^3*(l^2 + (-1 - 4*v)/5))/(12*b*(1 - v^2)), 0, 0, 0,
        (a*e*t^3*((2*l^2)/3 - (4*(1 - v))/15))/(12*b*(1 - v^2)),
        (e*t^3*(2*l^2 + (1 + 4*v)/5))/(12*b*(1 - v^2)), 0, 0,
        (e*t^3*v)/(12*(1 - v^2)), (a*e*t^3*((4*l^2)/3 + (4*(1 - v))/15))/ (12*b*(1 - v^2))}}

DynamicStiffnessPlate
[StiffnessMatrixPlate_List, MassMatrixPlate_List, DampingMatrixPlate_List, w_] =
StiffnessMatrixPlate - w^2*MassMatrixPlate + (w*DampingMatrixPlate) I
```

APPENDIX C

MATHEMATICA SUBROUTINES FOR OBTAINING THE SENSITIVITY OF THE ERROR FUNCTION WITH RESPECT TO THE SPATIAL POSITION AND ORIENTATION OF THE LASER

```
(*****************************************************************************)
(*          Package of Mathematica subroutines for obtaining the sensitivity of *)
(*          the error function with respect to the spatial variables of the   *)
(*          laser using the modified plate element with twenty degrees        *)
(*          of freedom per node, used in the research                         *)
(*                                                                            *)
(*                    DEVELOPED BY:  Gerhardus Venter                         *)
(*                                   1994 - 1995                              *)
(*                                   Copyright © 1995                         *)
(*                                                                            *)
(*****************************************************************************)
(*  SUBROUTINES:                                                              *)
(*****************************************************************************)
(*      TwoVectorCross          Subroutine performing a cross product between two *)
(*                              vectors along two of the axes of the laser two obtain *)
(*                              the vector along the third axis               *)
(*                                                                            *)
(*      Input/Output Variables  Description                                   *)
(*      xl, yl, zl              Origin of the laser                           *)
(*      x1, y1, z1              Components of first vector                    *)
(*      x2, y2, z2              Components of second vector                   *)
(*****************************************************************************)
(*      SphericalToRectang      Subroutine yielding the transformation matrix between the*)
(*                              laser spherical and the laser rectangular coordinate *)
(*                              systems (for a unit vector)                   *)
(*                                                                            *)
(*      Input/Output Variables  Description                                   *)
(*      Tx                      Deflection angle of the laser beam about x-axis of the laser*)
(*      Ty                      Deflection angle of the laser beam about y-axis of the laser*)
(*****************************************************************************)
(*      Orientation             Subroutine yielding the transformation matrix between *)
(*                              the structural and laser rectangular coordinate systems *)
(*                                                                            *)
(*      Input/Output Variables  Description                                   *)
(*      ops                     12, 23, 31 according to the sequence in which the two *)
(*                              direction vectors of the laser axes system are specified *)
(*      xl, yl, zl              Origin of the laser                           *)
(*      zxl, zyl, zzl           Components of first vector                    *)
(*      xxl, xyl, xzl           Components of second vector                   *)
(*****************************************************************************)
(*      ScanPosition            Subroutine yielding the scanning position of the laser *)
(*                              beam on the surface of the structure in terms of the *)
(*                              spatial position of the laser                 *)
(*                                                                            *)
(*      Input/Output Variables  Description                                   *)
(*      xl, yl, zl              Origin of the laser                           *)
(*      Tx                      Deflection angle of the laser beam about x-axis of the laser*)
(*      Ty                      Deflection angle of the laser beam about y-axis of the laser*)
(*****************************************************************************)
```

```
(*          SpatialOrientation          Subroutine yielding the scanning position in terms of the *)
(*                                      spatial orientation of the laser                          *)
(*                                                                                                *)
(*          Input/Output Variables      Description                                               *)
(*          ops1                        Option specifying the axis about which to take rotations  *)
(*          ops2                        Option specifying the sequence of the two axes along the  *)
(*                                      laser axes system that is being prescribed                *)
(*          xl, yl, zl                  Origin of the laser                                       *)
(*          zxl, zyl, zzl               Components of first vector                                *)
(*          xxl, xyl, xzl               Components of second vector                               *)
(*          Tx                          Deflection angle of the laser beam about x-axis of the laser*)
(*          Ty                          Deflection angle of the laser beam about y-axis of the laser*)
(*************************************************************************************************)
(*          DirectionCosines            Subroutine yielding the direction cosines of the laser beam *)
(*                                      in terms of the spatial variables of the laser            *)
(*                                                                                                *)
(*          Input/Output Variables      Description                                               *)
(*          ops1                        Option specifying the axis about which to take rotations  *)
(*          ops2                        Option specifying the sequence of the two axes along the  *)
(*                                      laser axes system that is being prescribed                *)
(*          xl, yl, zl                  Origin of the laser                                       *)
(*          zxl, zyl, zzl               Components of first vector                                *)
(*          xxl, xyl, xzl               Components of second vector                               *)
(*          Tx                          Deflection angle of the laser beam about x-axis of the laser*)
(*          Ty                          Deflection angle of the laser beam about y-axis of the laser*)
(*************************************************************************************************)


TwoVectorCross[xl_,yl_,zl_,x1_,y1_,z1_,x2_,y2_,z2_] :=
        Module[{a1,a2,a3,b1,b2,b3,mat,cross,xx,yy,zz},

a1 = x1-xl;
a2 = y1-yl;
a3 = z1-zl;

b1 = x2-xl;
b2 = y2-yl;
b3 = z2-zl;

Vec1    = N[{a1,a2,a3}/Sqrt[a1^2+a2^2+a3^2]];
Vec2    = N[{b1,b2,b3}/Sqrt[b1^2+b2^2+b3^2]];

mat     = {{xx,yy,zz},Vec1,Vec2};
cross   = N[Det[mat]];
Vec3    = {     (cross/.{xx->1,yy->0,zz->0}),
                (cross/.{xx->0,yy->1,zz->0}),
                (cross/.{xx->0,yy->0,zz->1})}       ]
```

```
SphericalToRectang[Tx_,Ty_] := Module[{x,y,z},

x =     Cos[Tx] Sin[Ty];
y =     -Sin[Tx];
z =     Cos[Tx] Cos[Ty];
{x,y,z}         ]

Orientation[ops_,xl_,yl_,zl_,zxl_,zyl_,zzl_,xxl_,xyl_,xzl_] := Module[{},

DirCosAxes[xl,yl,zl,zxl,zyl,zzl,xxl,xyl,xzl];

If[ops == 12 ,{etax = Vec1 ,etay = Vec2 ,etaz = Vec3}];
If[ops == 23 ,{etax = Vec3 ,etay = Vec1 ,etaz = Vec2}];
If[ops == 31 ,{etax = Vec2 ,etay = Vec3 ,etaz = Vec1}];

{etax,etay,etaz}  ]

ScanPosition[xl_,yl_,zl_,Tx_,Ty_]:=Module[{trans,trans2,laser,ro,rd,pn,t},

trans           = {etax,etay,etaz};
trans2          = Transpose[trans];

laser           = Direct[Tx,Ty];
rd              = trans2.laser;
ro              = {xl,yl,zl};
pn              = {0,1,0};
t               = -(pn.ro)/(pn.rd);
ScanPos = ro + rd t         ]

SpatialOrientation[ops1_,ops2_,xl_,yl_,zl_,zxl_,zyl_,zzl_,xxl_,xyl_,xzl_,Tx_,Ty_] :=
Module[{san11,san22,san33,san44,trans},

(*Ops1 ->        1  - wrt Tx
                2  - wrt Ty
                3  - wrt Tz
 Ops2 ->        31 - z,x axes
                12 - x,y axes
                23 - y,z axes*)

Orientation[ops2,xl,yl,zl,zxl,zyl,zzl,xxl,xyl,xzl];
trans = {etax,etay,etaz};

If[ops1 == 1,
san11 = Simplify[Orientation[31,0,0,0,0,-Sin[te],Cos[te],1,0,0]]];
If[ops1 == 2,
san11 = Simplify[Orientation[12,0,0,0,Cos[te],0,-Sin[te],0,1,0]]];
If[ops1 == 3,
san11 = Simplify[Orientation[31,0,0,0,0,0,1,Cos[te], Sin[te],0]]];

san22 = san11.trans;
```

```
etax = san22[[ ]];
etay = san22[[ ]];
etaz = san22[[ ]];

san33 = ScanPosition[xl,yl,zl,Tx,Ty];
san44 = D[san33,te];

san5 = san44
san5                ]

DirectionCosires[ops1_,ops2_,xl_,yl_,zl_,zxl_,zyl_,zzl_,xxl_,xyl_,xzl_,Tx_,Ty_] :=
Module[{san11,san22,san33,san44,trans},

(*Ops1 ->        1  - wrt Tx
                2  - wrt Ty
                3  - wrt Tz
 Ops2 ->        31 - z,x axes
                12 - x,y axes
                23 - y,z axes*)

Orientation[ops2,xl,yl,zl,zxl,zyl,zzl,xxl,xyl,xzl];
trans = {etax,etay,etaz};

If[ops1 == 1,
san11 = Simplify[Orientation[31,0,0,0,0,-Sin[te],Cos[te],1,0,0]]];
If[ops1 == 2,
san11 = Simplify[Orientation[12,0,0,0,Cos[te],0,-Sin[te],0,1,0]]];
If[ops1 == 3,
san11 = Simplify[Orientation[31,0,0,0,0,0,1,Cos[te], Sin[te],0]]];

san22 = san11.trans;

etax = san22[[ ]];
etay = san22[[ ]];
etaz = san22[[ ]];

san33    = ScanPosition[xl,yl,zl,Tx,Ty];
temp     = Sqrt[yl^2+(xl-ScanPos[[1]])^2+(zl-ScanPos[[3]])^2];
dircosx  = Sqrt[(xl-ScanPos[[1]])^2]/temp;
dircosy  = Sqrt[yl^2]/temp;
dircosz  = Sqrt[(zl-ScanPos[[3]])^2]/temp;

dxte = D[dircosx,te];
dyte = D[dircosy,te];
dzte = D[dircosz,te];

san5 = {0,0,0}

san5[[1]] = dxte;
san5[[2]] = dyte;
san5[[3]] = dzte                ]
```

Vita

Gerhardus Venter was born in Bothaville, South Africa, on September 1, 1970. He received a Bachelor of Science degree in Mechanical Engineering from the University of Pretoria in 1992 and the Honors degree[1] in Mechanical Engineering from the same university in 1993. He also received the Rentmeester award for the best Honors student in the faculty of engineering at the University of Pretoria.

Mr. Venter enrolled in the Mechanical Engineering Department at Virginia Polytechnic Institute and State University in 1994 to pursue his graduate studies.

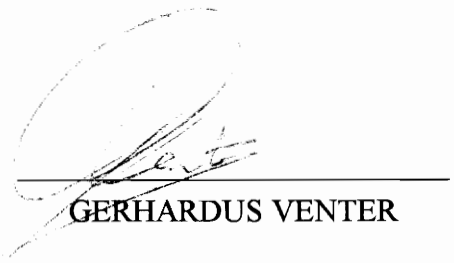

GERHARDUS VENTER

[1] Honors degree is a graduate degree consisting of eight graduate courses